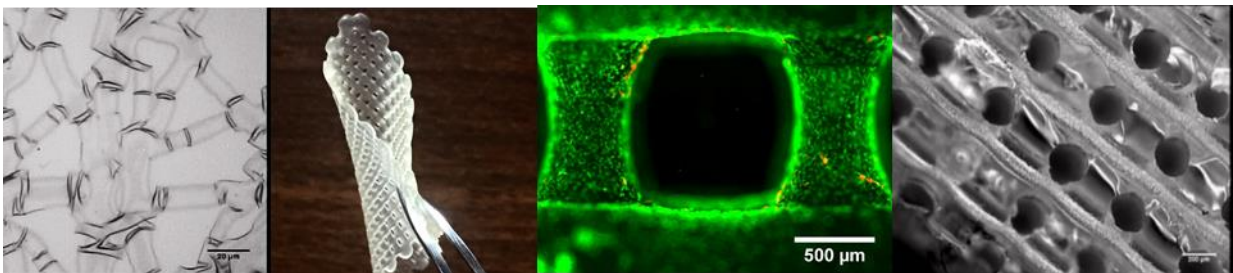# Intelligent Hydrogel Design: towards more Performing Hydrogel Processing

Annemie Houben

Supervisor(s): Prof. Dr. Peter Dubruel, Prof. Dr. Sandra Van Vlierberghe,
Dr. Hugues Van den Bergen

GHENT
UNIVERSITY

Table of Contents

Dankwoord - Acknowledgements

Een doctoraat is weg die je nooit alleen aflegt, daarom zijn er een hoop mensen die ik graag wil bedanken voor hun bijdrage gedurende de jaren. Binnen de PBM groep wil ik eerst en vooral mijn dankbaarheid uitdrukken voor mijn promotor prof. Peter Dubruel, om mij de mogelijkheid te geven aan dit doctoraat te beginnen, voor de begeleiding en voor de geboden kansen, en voor de praktische en professionele ondersteuning. Ook mijn co-promotor prof. Sandra Van Vlierberghe wil ik graag bedanken, voor de vele gesprekken (zowel wetenschappelijk als niet-wetenschappelijk), en voor het organiseren van een onderzoeksmogelijkheid aan de universiteit van Uppsala en UNS. Deze buitenlandse verblijven waren een erg verrijkende ervaringen, zowel op persoonlijk als professioneel vlak. Verder wil ik Peter en Sandra ook bedanken voor het grondige nalezen van dit werk, en alle andere publicaties en abstracts, en zo alles naar een hoger niveau te tillen. Ook Veerle Boterberg wil ik graag bedankten voor alle hulp met metingen, problemen met de apparatuur oplossen, de vele gezellige babbels en onze loopsessies tijdens de middagpauze.

I definitely want to thank all my PBM colleagues for the pleasant working atmosphere, all their help and all the scientific and not so scientific conversations. Special thanks to Lara, Jasper and Maxime. It has been great to work with friends that you have known for many years! Of course I also want to thank all my other colleagues throughout the years: Geert-Jan, Karolina, Arn, Birgit, Ine, Liesbeth, Joren, Stephanie, Annabelle, Esther, Diana G., Diana M., Myriam, Mahbub, Giuseppe, Evelien, Els, Adelaide and Tom (hope I am not forgetting anyone!). It was a pleasure working together, and I hope we will stay in touch and remain friends in the years to come! Furthermore, I would like to thank Nele, Aysu, Francesca and Oscar for contributing to this work! It was a pleasure guiding you all as thesis or Erasmus students, and I have been very lucky to work with such skilled and enthusiastic people! Good luck in your future careers!

Verder wil ik An Van Den Bulcke bedanken, voor de samenwerking aan het patent en het concepTT project. Ook wil ik ook Theo bedanken voor de hulp met reparaties aan de 3D-printers, pompen en andere toestellen, alsook zijn collega's van de centrale werkplaats.

Ook de samenwerking met Allnex was een enorm positieve, leerrijke en aangename ervaring. In de eerste plaats wil ik graag mijn co-promotor Hugues Van den Bergen bedanken voor het enthousiasme, de hulp en voor het delen van al zijn kennis. Dankzij hem zijn alle syntheses zeer vlot verlopen, wat vaak een struikelblok is bij vele doctoraten. Bij elke nieuwe stap in het werk stond hij steeds klaar met veel advies, tips en goede raad. Ook wil ik Dirk Bontinck bedanken, omdat dit doctoraat mede dankzij hem mogelijk was, en voor de aangename opvolgmeetings, zijn enthousiasme voor het project en de vele ideeën. Wie zeker ook een belangrijke rol heeft gespeeld in dit doctoraat is Patrice Roose. Dankzij zijn ongelofelijke kennis van de verschillende karaktarisatietechnieken, en zijn passie voor fysische chemie die hij steeds met veel hartstochtelijk deelt heb ik enorm veel bijgeleerd, en vanaf het begin een vlotte start gemaakt. Bedankt om steeds de tijd te nemen om mij alles uit te leggen, vaak meerdere keren, en er zo voor te zorgen dat ik steeds de motivatie had om dieper in

te gaan op de behaalde resultaten. Voor het uitvoeren van de syntheses wil ik zeker ook Lieven, Peter, Bastiaan, Ruben en de andere collega's bedanken voor de hulp bij de syntheses. In het karakterisatielabo wil ik ook Thierry zeker bedanken voor alle photo-DSC metingen, die een essentieel deel van dit werk uitmaken!

During my experiences abroad, I have gotten a lot of help from the supervisors and postdocs at Uppsala University: Prof. Tim Bowden, dr. Xi Lu, dr. Michael Palmer and dr. Anna Diez, and at UNSW: Prof. Penny Martens, Prof. Laura Poole-Warren and dr. Ulises Aregueta Robles. Thank you all for taking the time to learn me new techniques, and guide the experiments, and of course for all the pleasant social interactions!

Verder wil ik ook graag mijn vrienden, familie en ouders bedanken om steeds klaar te staan voor mij, zowel om de successen te vieren als om de moeilijke momenten door te komen. Het is een geruststellend gevoel te weten dat ik steeds bij jullie terecht kan. Ook Dries is de voorbije jaren een enorme steun geweest. Bedankt om dit doctoraat mogelijk te maken, voor je niet aflatende steun, voor je liefde en voor alles wat je voor mij gedaan hebt en elke dag opnieuw doet. Nu dit hoofdstuk in ons leven bijna is afgerond, kijk ik al uit naar het volgende! Eind dit jaar zal er zowel een phd als een baby in ons gezinnetje zijn. 2017 is het jaar van de grote veranderingen en er is niemand met wie ik deze liever zou willen meemaken.

Ik hoop dat de mensen die ik hier niet expliciet heb vernoemd, maar die ook hebben bijgedragen aan dit werk weten dat ik hen erg dankbaar ben voor de hulp!

Ten slotte wil ik ook graag mijn opa Robert Lampaert bedanken, die altijd ongelofelijk trots was op het feit dat ik aan het doctoreren was, maar jammer genoeg de verdediging niet meer zal meemaken. Hij was er ongetwijfeld graag bij geweest, en ik had er hem ook heel graag bij gehad. Daarom wil ik dit doctoraat graag opdragen aan hem.

Chapter 1: Introduction

Chapter 1: Introduction

Chapter 1: Introduction

1.1. Problem statement

To counter donor shortage when organ transplantation is required and to tackle commonly observed problems associated with prosthetic devices and transplanted organs (mismatch in mechanical properties or dimensions, infections, organ rejection)[2–4], tissue engineering has emerged in the biomedical field over the last four decades.[5] In tissue engineering, the aim is to develop biological substitutes to restore, maintain or improve tissue function.[3] In this field, hydrogels are of great interest, as their properties (soft, elastic behaviour, network structure and high water content) are quite similar to those of the extracellular matrix. [6–9]

However, hydrogels are difficult to process into complex, well-defined shapes.[8] To maintain their shape under *in vitro* and *in vivo* conditions (pH changes, mechanical effects, enzymatic degradation, calcification, adsorption, …)[10] hydrogels require chemical or physical crosslinking through for example photo-initiated free radical polymerization (chemical crosslinking)[11] or ionic bonds (physical crosslinking)[12,13]. Using the former approach, typically a photo-initiator generates radicals upon irradiation. These radicals initate the polymerization of reactive groups, such as acrylates or methacrylates resulting in network formation. These tunable crosslinked polymer networks can be created in a reproducible fashion, while maintaining temporal and spatial control over the reaction.[11]

One major drawback is that free radical polymerization relies on the mobility of the reactive groups and currently needs to be performed in solution or in the molten state. Therefore, the crosslinking method is generally incompatible with processing techniques which result in solid structures after processing including electrospinning and fused deposition modelling: the reactive groups in the processed structures posses insufficient mobility to allow for significant functional group conversion.[14,15] This makes hydrogels difficult to process into well-defined shapes, which is often highly important for their final application.[1,8,16]

1.2. Hydrogels in tissue engineering

1.2.1. Concept of tissue engineering

Over the course of history, mankind always had a desire to prolong life or increase life-quality.[3–5] Consequently, the treatment of large tissue defects and organ failure has always been a field of research with increasing interest.[17] Currently, the major treatment for organ/tissue failure consists of artificial substitutes (e.g. joints), non-living processed tissue (e.g. heart valves), or tissue taken from another site from the patients themselves or from a donor (transplantation).[5,18] However, problems typically arise using the latter approaches including scarcity of suitable donor organs (63.620 people were on the EU transplant waiting list in 2013)[19] and problems associated with intense immunosuppressive treatments (more susceptible to infections, increased risk of cardiovascular disease and cancer, strong side effects, noncompliance, …)[20–22]. Furthermore, prosthetic devices are often characterized by mismatched mechanics combined with wear and tear resulting in mechanical stresses exerted on the surrounding tissue and inflammation.[23] To tackle these problems, four decades ago "tissue engineering" (TE) emerged as an alternative approach in the biomedical field. The fundamental goal of tissue engineering has been defined by Langer and Vacanti as "*An interdisciplinary field that applies the principles from engineering and life sciences toward the development of biological substitutes that restore, maintain or improve tissue function.*"[3] It is a highly complex and interdisciplinary field combining engineering and life science principles.[8]

The extracellular matrix (ECM), which is the native environment of cells, consists of a complex mixture of structural and functional proteins and polysaccharides.[24] It provides support for the cells, and initiates a number of biochemical and biomechanical processes.[25,26] Of crucial importance in tissue engineering is the creation of 3D culture environments which mimic the ECM both in terms of (bio)mechanics as well as biological features to grow 3D tissue constructs starting from cells of the targeted tissue.[27–33] To this end, the cells are combined with so-called "scaffolds", developed from synthetic or natural materials, that should ideally guide cell growth towards the envisioned regenerated tissue in terms of architecture and cellular behaviour.[34,35] Non-toxic, often biodegradable building blocks are essential.[36] Consequently, healthy cells can gradually substitute the scaffold with natural ECM during biosynthesis.[36,37] ECM generation can be guided by the use of growth factors and/or interactions between the

cells and scaffold material (mechanical properties, chemical composition, hydrophilicity, …).[38,39]

Two distinct approaches can be distinguished to realize tissue engineering (Figure 1). In the first approach, artificial tissue is grown *in vitro* using cells from donor tissue (cell-based approach), which can be combined with a support system.[40] In the second approach, tissue is regenerated *in vivo* by guiding cell growth and function (cell-free approach), using growth factors or relying on the interactions between the cells and the biomaterial.[41] In both approaches, the scaffold plays a major role in the support and cultivation of cells. Using the cell-free method, it is important that the scaffold promotes cell migration to the scaffold and supports tissue regeneration to repopulate the scaffold by the host cells which are recruited from the surrounding tissue. When cells are seeded prior to implantation (i.e. in case of the cell-based method), the scaffold needs to be cell-instructive and should promote cell proliferation and differentiation when using stem cells. [40]
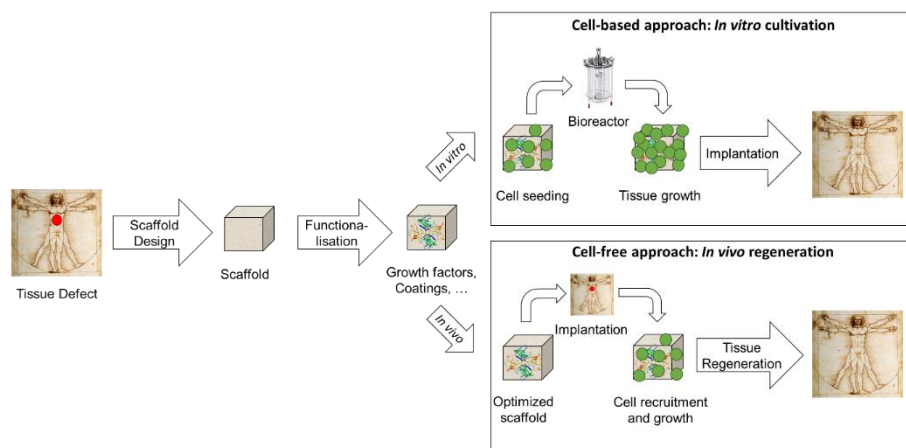
Figure 1: Scheme representing the different steps characteristic for the two approaches commonly applied in tissue engineering

Another way to classify approaches in tissue engineering is the top down approach, and the bottom up approach. In the former, a scaffold is used to support cell growth. Cells populate this scaffold, and create the extracellular matrix and microarchitecture, using growth factors, perfusion and/or mechanical stimulation. In the latter approach, no scaffold is used, but the cells are combined with bio-inks to enable tissue growth. The aim is to replicate the intricate microstructure of complex tissues, so often a modular approach is used where these structures are recreated on a microscale. Using a modular approach, the microstructures are combined to build larger complex tissues.[42] In this work, the scaffold-based top-down approach is used for all *in vitro*

tests. However, when the materials are further developed to allow for cell encapsulation, they can also be used in the bottom-up approach. To this end, the degradation time of the developed polymers will need to be modified to allow for faster degradation times (e.g. using degradable links or spacers).

When applying *in vitro* tissue cultivation prior to implantation, an alternative to cell seeding exists. Indeed, cells can be incorporated in the scaffold while processing (i.e. cell encapsulation: cells are mixed with the hydrogel solution prior to processing). Cells can be quite sensitive to the processing conditions; e.g. for a viability of HepG2-cells above 40%, the pressure needs to be below 40 psi (2.8 bar) and nozzle diameter above 150 μm [43]. Therefore, the seeding approach can be considered more straightforward from a technical point of view, as the absence of cells during processing reduces the processing limitations.[44–48] In contrast, cell encapsulation is beneficial as it can maximize cell content within the scaffold, results in a more homogeneous cell distribution (cell seeding can result in a reduced cell density in the center of the scaffold), and provides the possibility to encapsulate different cells into different zones of the scaffold.[40,49–57] This is highly relevant as tissues and organs often consist of distinct regions with different cell types.[58] To expand the cell population and to enable tissue development prior to implantation, a bioreactor is generally used.[59,60] The latter is a device in which biological and/or biochemical processes are manipulated through close control over environmental and operating conditions such as pH, temperature, pressure and nutrient and waste flow.[60] The use of tissues created by cultivation of cells onto scaffolds *in vitro* is not restricted to tissue regeneration applications, as cell-seeded scaffolds can also be utilized in other domains of regenerative medicine, such as external organ support devices[61] or model systems for pathological conditions in drug screening[62].

Generally, interconnected porous scaffolds are considered beneficial to facilitate diffusion-driven transport of oxygen, nutrients and waste towards and away from the cells respectively, as cells must be sufficiently close (100–200 μm) to oxygen and nutrient supply.[34,56,57,63] Additionally, the presence of an interconnected porous network improves the cell seeding and cell migration, resulting in homogenous cellular distributions throughout the scaffold compared to non-porous scaffolds, where the cells will only reside on the surface. To obtain this beneficial interconnective porosity, several techniques can be applied such as particle leaching and supercritical CO_2

treatment or processing techniques such as solid freeform fabrication (SFF) and electrospinning. [33,64,65]

1.2.2. Hydrogel scaffolds for tissue engineering purposes

Wichterle and Lim[66] were the first to report on hydrogels. In their work, they presented a hydrophilic gel based on poly(2-hydroxyethyl methacrylate) which could be used for biological purposes (e.g. to be applied as soft contact lenses). Ever since, there has been an increasing interest in hydrogels for biomedical and pharmaceutical purposes, with applications as wound dressings, biomedical coatings, tissue engineering constructs, contact lenses and drug delivery systems. [13,67–70]

Hydrogels can be defined as water-swollen, three-dimensional crosslinked networks. Depending on their composition, they can absorb up to thousands of times their dry weight.[8,9] The nature of the crosslinks is quite diverse and ranges from strong chemical crosslinks (covalent bonds), to physical links based on chain entanglements, ionic bonds, micro-crystalline zones, association bonds (e.g. hydrogen bonds) and van der Waals interactions or combinations thereof.[12,13] Hydrogels can be classified according to the origin of the constituting polymers (synthetic versus natural), their preparation method (homo- or copolymer-based hydrogels), their charge, their physical structure (amorphous versus semi-crystalline) or their crosslinking mechanism (permanent or reversible and chemical or physical). To permanently crosslink a hydrogel, radiation-induced polymerization (UV or visible light, gamma-rays, electron beam, …) is one of the more commonly applied mechanisms, as it offers both spatial and temporal control over the crosslinking.[11] In the category of reversible hydrogel materials, lower critical solution temperature (LCST) and upper critical solution temperature (UCST) behaviour can be distinguished. [71,72] Thermo-responsive hydrogels undergo a thermoreversible gelation above (cfr. LCST, e.g. Pluronic® F127 (T_{gel} = ± 20°C))[71] or below (UCST, e.g. gelatin(T_{gel} = ± 38°C))[72] a characteristic temperature.

Their characteristic soft, elastic behaviour (Young's modulus ranging from a few kPa to several MPa, and elongations up to 500%)[6,7] and high water uptake capacity, up to thousands of times their original dry weight[8,9], render hydrogels similar to the ECM, which explains their popularity to become used as tissue engineering constructs.[73–75] An important aspect when developing TE scaffolds is the required material biocompatibility. Two aspects can be distinguished in this respect including the surface

and the structural biocompatibility. Surface biocompatibility is associated with the chemical and physical characteristics of a material surface and is therefore strongly influenced by the material type and/or the application of coatings or other surface modification techniques.[76] Absorption or adsorption of biological molecules which regulate cell activities such as migration and adhesion, is typically also mediated by the surface chemistry.[77] The structural biocompatibility on the other hand is influenced by the scaffold architecture, both on a micro- (nm and µm sized features) as well as on macroscopic level (mm and cm sized features) and is obviously influenced by the processing method.[77]

Furthermore, the scaffold needs to provide structural integrity and define a space for the engineered tissue, guiding the restructuring process that occurs through proliferation of cells and ingrowth of host tissue.[78] Despite the importance of the outer scaffold geometry, one of the main disadvantages associated with the use of hydrogels is the difficulty to process them into pre-designed geometries.[8] Common applications of hydrogels include defect-filling scaffolds, soft tissue repair or matrices enabling drug and/or cell delivery.[79–81]

1.2.3. Polymers in tissue engineering

The majority of tissue engineering scaffolds is constructed from polymers, either from natural or synthetic origin. In addition to polymers, another important material category includes ceramics, which are mainly used for bone tissue engineering.[77] Often used ceramics include hydroxyapatite[82], β-tricalcium phosphate[83,84] and blends thereof.[85,86] Applying ceramics in solid freeform fabrication is quite challenging.[82] Therefore, these materials are often processed using indirect rapid prototyping. More information about the latter technique as well as the use of ceramic materials can be found in section 1.3.2.

The aim of the following paragraphs is to provide an overview of the most important material classes used for tissue engineering and biomedical applications, and to provide background information on materials mentioned and used throughout the work. As an important aspect of tissue engineering consists of the biocompatibility of the material, the biocompatibility of the selected materials is further evidenced by providing an overview of common biomedical applications of the selected materials, rather than solely focusing on their tissue engineering applications.

1.2.3.1. Overview and applications of synthetic polymers

The use of synthetic hydrogels for tissue engineering purposes can be considered advantageous as their synthesis is straightforward, scalable and reproducible, and the physical properties of final material are tuneable.[87–89] Their main drawback however is their lack of cell adhesion sites. To increase the cell-interactive properties of synthetic materials, modification or coating with biological molecules such as ECM proteins, peptide sequences and/or growth factors is a commonly used approach.[90–92] Alternatively, the bioactive properties can be enhanced via the fabrication of hydrogel composites by the integration of inorganic compounds (e.g. calcium phosphate or silicate-based) into the hydrogel.[89,93–97] In the following sections, an overview will be provided of the synthetic polymers commonly used in tissue engineering, and of those most relevant for this work. In addition, general material properties and common synthesis routes are discussed.

1.2.3.1.1. Urethane-based materials

Although polyurethanes have already been discovered in 1947 by Otto Bayer[98] and his co-workers, the first polyurethane applied for biomedical applications was only reported in 1967 by Boretos and Pierce[99] and commercialized by Ethicon Inc. as Biomer®. This segmented poly(ether)urethane was tested for a range of applications going from *in vivo* shunts, heart assist pumps and endotracheal tubes towards pacemaker wire insulation and chambers for the first artificial heart models.[100] The main advantage of urethane-based materials is their synthetic versatility, resulting in a broad range of products, covering thermoplastic elastomers to thermoset resins.[101,102] Polyurethanes are the fifth most used raw polymer based material in industrial production, and are quite interesting for biomedical applications as a result of their superior mechanical properties (tensile strength typically in the 6000-8000 psi (414-552 bar) range) [100], excellent flexibility (elongations from 400-700%)[100] and haemo- and tissue compatibility.[103–106] The (micro)phase separation[107] between hard, rigid segments and soft, flexible segments combined with the strong hydrogel bonds between the urethane linkages explains the exceptional mechanical properties of these materials.[108]

Figure 2: General synthesis scheme for a linear polyurethane based on a diol and a diisocyanate.

In a typical polyurethane synthesis, polyols such as polyethers, polyesters and diols are reacted with a diisocyanate (aromatic or aliphatic). In some cases, a low molecular weight chain extender is added. To catalyze the reaction, organometallics or tertiary amines are used, and often additives such as stabilizers or blowing agents (for foamed polyurethanes) are added. To create a linear polyurethane, a diol is reacted with a diisocyanate as depicted in Figure 2. Multifunctional polyols and/or multifunctional isocyanates are used to create branched or crosslinked structures. An overview of commonly used diisocyanates is shown in Figure 3.[100,109] Diphenylmethane diisocyanate (MDI) is an aromatic diisocyanate often used to synthesize PUs for biomedical applications, as it is used in two families of biomedical grade thermoplastic PUs: Pellethane™ and Vialon™. The main drawback of using aromatic diisocyanates is their inherent yellowing tendency, especially when exposed to UV-light (300-540 nm) due to the formation of chromophore groups as a result of oxidation reactions.[77] When targeting medical applications that require a transparent appearance, hydrogenated diphenylmethane diisocyanate (HMDI) has already been used as an aliphatic diisocyanate in Texoflex™, a non-yellowing, thermoplastic polyurethane.[110]
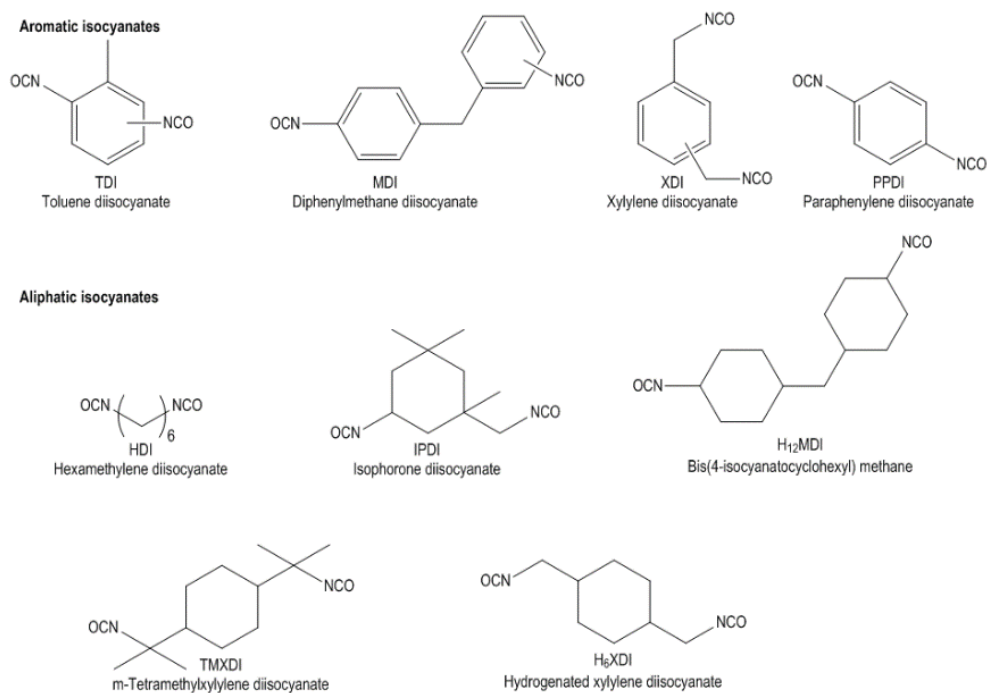
Figure 3: Overview of aromatic and aliphatic diisocyanates used in polyurethane synthesis.

To catalyze the reaction, tertiary amines and organometallic tin, lead and iron complexes are habitually used. As organotin compounds can be quite toxic, they need to be removed after the reaction.[111]

Applications of urethane-based materials in the biomedical industry are quite numerous, as depicted in Figure 4. In the following paragraphs, an overview of the most important applications is provided.
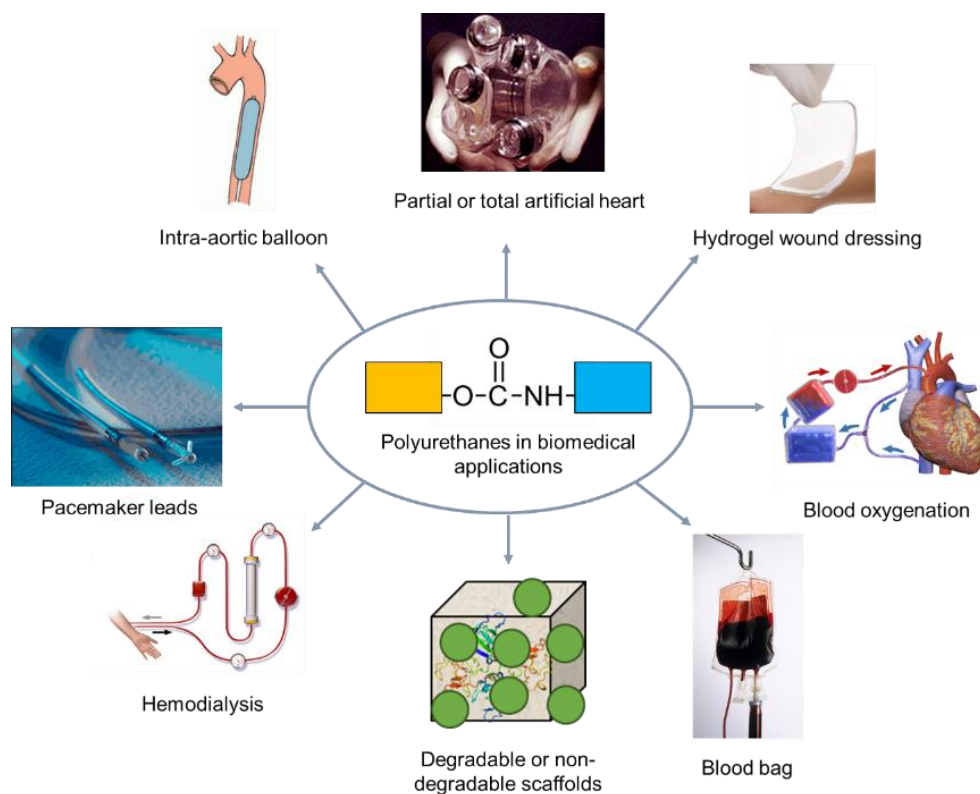
Figure 4: Overview of biomedical applications of polyurethanes

For cardiovascular applications, a range of commercially available polyurethanes have already been applied.[112] Cardiothane®, a thermoplastic, aromatic poly(ether urethane)-polydimethylsiloxane copolymer, is used in intra-aortic balloons for open-heart surgeries. To isolate pacemaker leads from the surrounding tissue, a thermoplastic polyurethane coating (Pellethane®) is applied as insulator. For the development of an artificial, implantable heart, poly(ether urethanes) and poly(carbonate urethanes) are extensively researched. [113–117] Biomer™, Tecoflex™, Avcothane™ and Biospan™ are other examples of commercially available polyurethanes in clinical use.

Polyurethanes are also used as a housing compound embedding hollow fiber membranes applied for haemodialysis. In addition, polyurethanes based on MDI, poly(propylene oxide) and various linear and cyclic aliphatic and aromatic diols have already been investigated as dialysis membranes. [118]

Artificial oxygenators provide oxygen and remove carbon dioxide from the blood and are applied as artificial lungs during cardiopulmonary surgery. Owing to their high haemocompatibility, polyurethanes are utilized as membranes, mostly in combination with other support materials. [100]

Due to their oxygen permeability and barrier properties, a range of polyurethanes are also applied in wound dressings. An ideal wound dressing accelerates the wound healing while minimizing scar formation. Typically, hydrogel materials are used as they absorb the wound exudate, generating a hydrated environment.[119,120] Examples of commercially available polyurethanes in wound healing include Opsite® CH, Tegaderm® Plus and Granuflex®.

Polyurethanes are attractive scaffold materials due to their tunability. Poly(ester urethanes) for example are often applied because their degradation profile can be adapted with respect to the desired application. When a slowly degrading or biostable material is desired, pol(ether urethane ureas) and poly(ether urethane dialkylsiloxanes) are well suited.[103,121–125]

1.2.3.1.2. Poly(α-esters)

Polyesters are thermoplastic polymers commonly used in applications for which biodegradability is desired (with the exception of poly(ethylene terephthalate) or PET, which is not biodegradable). These materials degrade through hydrolysis of the aliphatic ester linkages within their backbone. Because of the degradation time frame required for most biomedical applications, only aliphatic polyesters with short chains between the ester bonds are considered.[126] In the category of polyesters, the poly(α-hydroxy acid)s are extensively investigated to serve biomedical purposes. They are either synthesized through ring opening or condensation polymerization, depending whether a cyclic lactone monomer or the corresponding α-hydroxy acid monomer or derivatives thereof are used respectively.[127] As the latter mechanism leads to lower molecular weights, ring opening polymerization is the preferred route for applications that require a high molecular weight (e.g. to increase degradation time)[128] For biomaterials, polyesters based on lactide, glycolide and ε-caprolactone are mainly researched and applied.[129] The chemical structure of these monomers and their corresponding homopolymers are depicted in Figure 5.
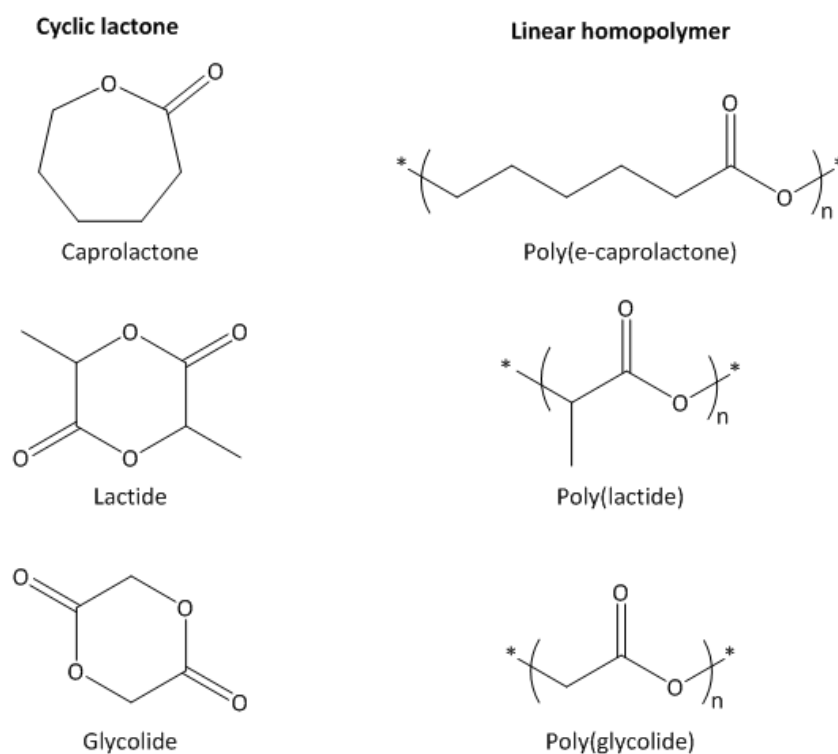
Figure 5: Common cyclic lactones and their corresponding homopolymers

Polyglycolide is one of the first degradable synthetic polymers investigated for biomedical applications. Due to its high degree of crystallinity (around 50%), it is characterized by a high Young's modulus (i.e. 12.5 GPa).[130] It is used in resorbable sutures and was the first FDA-approved polyester, known as Dexon®, in 1969. In addition, polyglycolide-based materials have already been investigated as tissue engineering scaffolds and as bone fixation devices.[131]

Another often applied polyester is polylactide. As lactide is a chiral molecule, poly(L-lactide) and poly(D-lactide) both exist as semi-crystalline polymers, while the polymerization of racemic (D,L)-lactide leads to an amorphous polymer. Because L-lactide occurs naturally, poly(L-lactide) or PLLA is applied most frequently. It has a lower degree of crystallinity (around 40%) compared to polyglycolide, which results in a modulus of approximately 4.8 GPa.[129] It is used in many orthopedic products as well as in suture fibers, blood vessel conduits and scaffolding materials for ligament replacement.[132,133] Due to the increased hydrophobicity compared to polyglycolide, it has a longer degradation time up to 5 years, depending on the degree of crystallinity and the molecular weight. In-vivo studies estimate a total degradation rate of over 3 years for *in vivo* degradation of high molecular weight PLA.[134] To decrease the degradation time, copolymers such as poly(L-lactide-co-glycolide) or PLGA and poly(L-

lactide-co-D,L-lactide) are often investigated and used for applications such as implant materials, sutures and skin replacement.[135]

As a result of the relatively low cost of the ε-caprolactone monomer, poly(ε-caprolactone) or PCL is frequently implemented in both biomedical as well as non-biomedical products. In addition, it dissolves in a wide range of organic solvents and is characterized by a low melting point (55-60°C) rendering it straightforward to process.[126] Crystallinity is around 50% (crystallized at room temperature).[134] It's mainly of interest for long-term applications as it degrades rather slowly over 2-3 years depending on the molecular weight and the degree of crystallinity. Again the degradation can be tuned by copolymerization, e.g. with DL-lactide or glycolide. It has a relatively low tensile modulus of approximately 23 MPa, but is highly flexible with an elongation at break of more than 700%.[136] Clinical applications include a long-term contraceptive device[130], meniscal tissue engineering[137] and bone tissue engineering[138]

1.2.3.1.3. Poly(ethylene glycol)-based materials

Poly(ethylene glycol) (PEG) or poly(ethylene oxide) (PEO) is heavily investigated as a biomaterial. It is a highly hydrophilic material and will therefore restrict and control the attachment of cells and proteins. As antibodies will have difficulties to attach, adverse immune responses to biomaterials can be decreased when using PEG/PEO.[139] If the molecular weight of the polymer exceeds 20,000 g/mol, the term PEO is used, while for lower molecular weights, PEG is applied. It is a viscous, colorless liquid at molecular weights below 1000 g/mol and forms a waxy solid at higher molecular weights. The most common synthesis mechanism uses ethylene oxide monomers which are initiated with water, ethylene glycol or ethylene glycol oligomers through an anionic initiation, which is associated with limited chain-transfer and termination, leading to a lower polydispersity compared to cationic polymerization.[140]
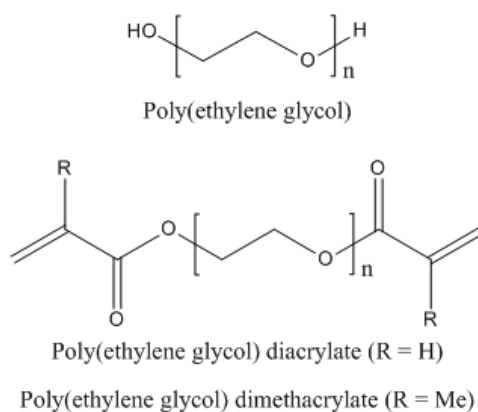
Figure 6: Chemical structures of poly(ethylene glycol) and poly(ethylene glycol) di(meth)acrylate

PEG can be easily modified to enable subsequent chemical crosslinking, for example by reaction of the terminal hydroxyl groups with acryloyl or methacryloyl chloride in the presence of trimethylamine.[141] Free radical polymerization is a crosslinking mechanism for (meth)acrylate-modified PEG and other (bio)polymers. Initiation mechanisms include thermal, redox and photo-initiation. The latter is advantageous as it offers both temporal and spatial control over the reaction, which will lead to a controlled reaction exotherm. The major drawback of photopolymerization is the limited penetration depth of the UV-light, which is a few millimeters depending on the refractive index of the material. Furthermore, it can be applied to create complex structures using lasers or photo-masks during polymerization.[142]

PEG-based materials have already been used for a range of applications including membranes for the encapsulation of islets of Langerhans[141,143,144], barriers to reduce intimal thickening after balloon angioplasty[145], matrices for encapsulation of chondrocytes, osteoblasts and mesenchymal stem cells[146–151], tissue engineering scaffolds[87] and for drug and peptide delivery.[152–155] Covalent attachment of PEG to active proteins (PEGylation technology) is another well-known application of PEG and has led to a number of FDA-approved compounds (e.g. PEGylated bovine adenosine deaminase (Adagen), PEGylated l-asparaginase (Oncaspar) and PEGylated products of interferon-alpha (IFN-alpha): peginterferon-2b (PegIntron) and peginterferon-2a (Pegasys)).[156–158]

However, over the last few years, a number of studies have shown that these PEGylated proteins can elicit an antibody response against PEG (anti-PEG).[156,159,160] In 22-25% of healthy blood donors, these PEG antibodies have already been detected.[161,162] This might reduce the therapeutic effect of PEG. Moreover, the

immunogenic response to PEG appears to be growing over the years, most likely due to the increased exposure to PEG present in cosmetics, pharmaceuticals and processed food products.[161] Polyoxazolines offer a valuable alternative, as their stealth behavior avoids antibody response.[163] Furthermore, as there is no frequent exposure to polyoxazolines in non-medical applications, the immunologic response to these polymers is not anticipated.

1.2.3.2. Natural polymers

Natural scaffolds are often constituted starting from ECM-components.[72] Two main categories can be distinguished including polysaccharide-based materials (e.g. hyaluronic acid, chondroitin sulfate, chitosan, alginate, cellulose, …) and protein-based materials (e.g. collagen, elastin, ….). The main advantage of natural polymers applied in TE is that they are inherently biocompatible and that they promote extracellular functions due to the numerous endogenous factors present (i.e. cell-specific peptide sequences such as RGD, IKVAV, …).[151,164,165] However, they result in complex and often ill-defined scaffolds in respect to the chemical composition, rendering it difficult to determine exactly which signals promote cell response. Moreover, in most cases their material properties cannot be manipulated easily, degradation is often too fast while they elicit an inherent batch to batch variability with respect to their mechanical, biological and chemical properties.[166]

1.2.3.2.1. Polysaccharides and derivatives

Polysaccharides consist of monosaccharide units connected by glycosidic linkages, with biological functions ranging from cell signaling to immune recognition.[126] Polysaccharides are a diverse class of biomaterials from human or non-human origin. An overview of the different polysaccharides is provided in Figure 7 and will be discussed in the upcoming paragraphs.

Polysaccharides of human origin

Polysaccharides of non-human origin
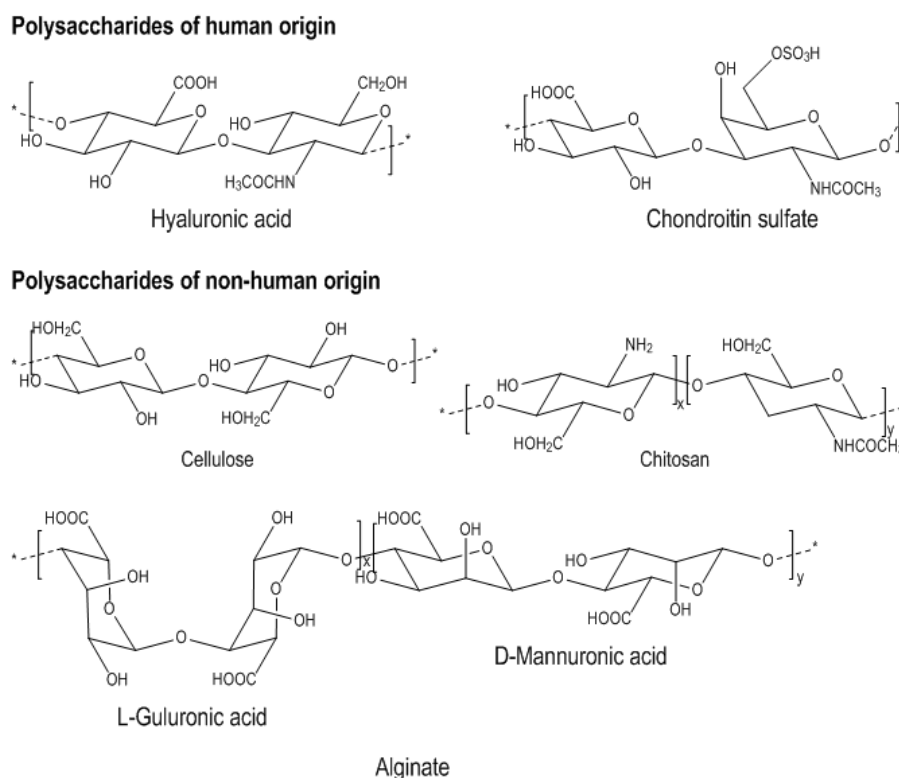
Figure 7: Chemical structure of common polysaccharides of human and non-human origin

Hyaluronic acid is a glycosaminoglycan consisting of alternating N-acetyl-D-glucosamine and glucuronic acid units. It can be found in most tissues in vertebrates and is not covalently bound to proteins, unlike other glycosaminoglycans. It is a major component of skin and plays a structural role in many other tissues as well.[167] In addition to being a structural component, it is actively involved in biological processes such as the modulation of cell migration and differentiation, the regulation of ECM organization and wound healing.[167,168] Modifications such as esterification have been explored and will influence the degradation rate.[169,170] Hyaluronic acid is heavily investigated for a range of applications such as synthetic bone grafts[171], injectable soft tissue fillers[172], synovial fluid substitutes[173] and to treat vascular diseases[174].

Chondroitin sulfate is the major component of aggrecan, which is found in the proteoglycans of articular cartilage. It increases the metabolic response of cartilage tissue and plays an important role in wound healing.[175,176] Chondroitin sulfate consists of a repeating N-acetyl galactosamine unit and sulfate-modified glucuronic acid.[177] Its main applications cover wound dressings[178] and scaffolds for cartilage tissue engineering.[179] Several mechanisms have already been explored to create crosslinked chondroitin sulfate, e.g.hydrazide and aldehyde modifications [180,181]

In addition to the polysaccharides found in the human body, three other types are extensively studied including chitosan, originating from crustacean skeletons, alginate which is a brown algae derivative and cellulose from green plants, algae and micro-organisms. Chitosan consists of β-(1-4)-linked D-glucosamine with random N-acetyl glucosamine pending groups. An often used crosslinking strategy to create hydrogels applies glutaraldehyde, while the crosslinking degree affects the degradation rate.[182] Tissue engineering applications involving the use of chitosan include the regeneration of cartilage, skin and bone.[183]

Alginate consists of β-(1-4)-linked D-mannuronic acid and α-L-guluronic acid monomers. In the presence of multivalent cations, it will form a physically crosslinked gel.[184] In addition, the carboxylic acid groups can be chemically modified to allow chemical crosslinking.[28] Applications of alginate include scaffold materials for bone regeneration.[185] Alginate and chitosan have already been investigated both separately as well as in combination as wound dressings and for drug and cell delivery.[186–189]

The last example, cellulose, is the most abundant organic biomaterial and consists of D-anhydroglucopyranose units.[190] The chemical modification of cellulose has mainly been performed on its hydroxyls groups. Modification reactions include esterification, etherification and oxidation and are mainly constrained by its limited solubility in organic solvents.[190] It is used for drug delivery applications,[191–194] to create stimuli-responsive hydrogels[195,196] and membranes[197]

1.2.3.2.2. Collagen and its derivatives.

The most abundant protein in the human body is collagen. It accounts for 25-35% of all proteins in animals and can be found in tendon, cartilage, bone and skin.[198,199] A single collagen chain (α-chain) forms an open helix structure and three single helical chains pack together in a tropocollagen right-handed triple helix.[200] Gelatin is a collagen derivative, obtained through acidic (gelatin A) or alkaline (gelatin B) hydrolysis. Typically, raw materials such as fish or pig skin, bovine hides and pig or bovine bones are used for the industrial production of gelatin.[201] As a result of the different hydrolysis mechanisms, the isoelectric points of gelatin A and gelatin B are different: gelatin A has a pH between 6 and 9, while gelatin B has a pH of 5. At physiological pH, gelatin A is positively charged while gelatin B has a negative charge. In addition, gelatin B shows an increased biocompatibility compared to gelatin A.[202]

Gelatin and collagen are often applied as ECM-mimicking tissue engineering material due to its non-immunogenic properties and the presence of RGD (arginine, glycine and aspartic acid) signaling sequences along its backbone which promote cell adhesion. In addition, it displays UCST behavior with a thermoreversible gel point around 38°C. Most applications require modifications to enable chemical crosslinking, as gelatin itself forms a very weak gel that dissolves at body temperature as a result of its UCST behaviour. Crosslinkable groups (e.g. photo-crosslinkable methacrylates) can be introduced by modifying the gelatin side chains such as lysine and hydroxylysine with methacrylamide.[203]

1.3. Development of porous scaffolds

1.3.1. Solid freeform fabrication

1.3.1.1. Advantages and drawbacks of the technique

SFF is a general term comprising all techniques that enable the production of structures via the sequential delivery of energy and/or materials according to a computer-aided design (CAD).[8] However, often other terms are applied to describe the same principle including additive manufacturing (AM), rapid prototyping (RP) and 3D printing (3DP).[8] Recently, an ISO/ASTM norm has been published regarding additive manufacturing nomenclature (ISO/ASTM 52900). This norm has been taken into account when selecting the appropriate terms for the different techniques. RP and AM can be considered general terms, whereas 3DP only refers to one subcategory based on the main technological concept.[8] These subcategories include irradiation-based systems, nozzle-based systems and printer-based systems.

Currently, SFF is considered as the "golden standard" for the generation of scaffolds due to its significant benefits over conventional porous scaffold production technologies. In conventional approaches the micro-architecture is mainly process-determined rather than design-driven and often requires extensive manual manipulation.[34,204] Furthermore, the obtained porosity is often random and poorly interconnected, resulting in limited transport of oxygen and nutrients.[63,205] In addition, industrially applied fabrication methods such as injection moulding or hot embossing, can never generate equally complex internal structures.[34] In contrast, SFF enables precise control over both macro- and microstructure with a high degree of reproducibility and homogeneity.[34,204,206,207] Additionally, the architecture of the

micropores can influence cellular behaviour.[207,208] As a result, SFF enables superior control over diffusion-driven transport, cell growth and differentiation.[35,36,208] Hence, the mechanical properties of the scaffolds can be tailored by design. Even gradient mechanical properties can be generated by combining different pore sizes/architectures within one single construct.[209,210] Moreover, the unique straightforward translation from CAD to CAM allows to tailor each implant to meet specific needs/designs often based on a 3D model obtained from medical imaging techniques.[211–214] Consequently, since the construction of each specific implant does not require the expensive production of robust moulds, patient specific implants become sufficiently cost-efficient for translation to the clinic.[214,215] In conclusion, SFF is the preferential technique to generate cost-efficient, patient-specific constructs closely mimicking the tissue defect based on medical imaging techniques.[34,86,211,212]

However, SFF techniques also exhibit certain limitations. For instance, the application of laser-based systems is limited to photo-polymerizable materials (e.g. Stereolithography, SLA or Two Photon Polymerization, 2PP) or highly controllable melting materials (Selective Laser Sintering, LS). In addition, unreacted monomers and photo-initiators applied in SLA can exhibit cytotoxicity.[34] Constructs generated via printing are often very brittle and mostly require a post-processing treatment to increase robustness.[8,216,217] As for nozzle-based systems, certain design limitations exist. For example, the resolution is inferior to printing and irradiation-based techniques. Also, certain shortcomings can be attributed to SFF techniques in general. First, each SFF technique is only suitable for the processing of a limited range of materials which exhibit the required properties. Secondly, resolution and architectural control are often highly dependent on applied material and SFF technique. Finally, successful SFF of novel materials frequently requires extensive and time-consuming optimization of processing parameters. [8,218,219] Therefore, compromises often have to be made in terms of resolution or material properties to generate suitable constructs.[56]

1.3.1.2.   Overview of the different methods

Most SFF techniques share a similar process flow. First, a 3D CAD design is generated which can be obtained from medical imaging or designed to meet specific needs. Next, it is sliced along the Z-axis into several consecutive '2D' layers. Finally, these consecutive layers are transferred to coordinates and fed to the SFF device, which processes them into a 3D construct in a layer-by-layer fashion. Some SFF techniques

have the possibility to operate outside of the conventional layer-by-layer methodology. This is for example the case with 2PP where a focussed spot can be scanned through a photo-crosslinkable solution in 3 dimensions. However, these also often apply layer-by-layer fabrication to decrease production times and simplify CAD processing.[220] An overview of the different categories of SFF techniques, including examples for each category, is presented in Figure 8 and the paragraphs below.
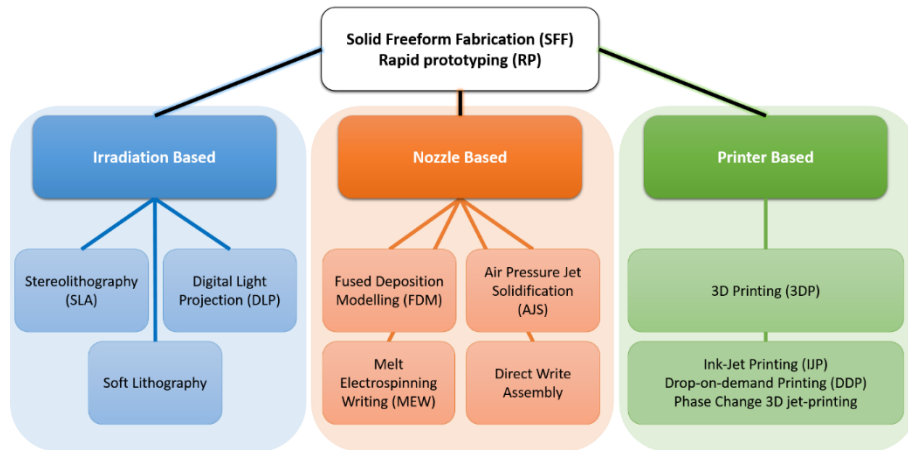
Figure 8:Overview and classification of currently applied template fabrication techniques for indirect Rapid Prototyping[8]

1.3.1.2.1. Irradiation-based systems

Irradiation-based systems deliver energy via radiation to transfer a CAD to a certain material. A distinction can be made based on the purpose of the applied irradiation between local photo-polymerization systems (e.g.. SL, 2PP) and sintering systems which apply heat to locally fuse particles together (i.e. LS). A similar approach is digital light projection (DLP) or microstereolithography (MSTL), where instead of laser irradiation, a UV lamp is used combined with a micromirror array. Every layer is converted into a pixelated image and transferred to the micromirror array (digital micromirror device, DMD) where every pixel corresponds to one micromirror. [221] Mirrors corresponding to areas which need to solidify reflect the UV light to the polymer solution, whereas the remaining mirrors reflect the light away.[222,223] Consequently, each layer is generated in one flash in contrast to processes exploiting the scanning of a laser beam, which makes the technique faster than conventional SL.[223] (Figure 9)
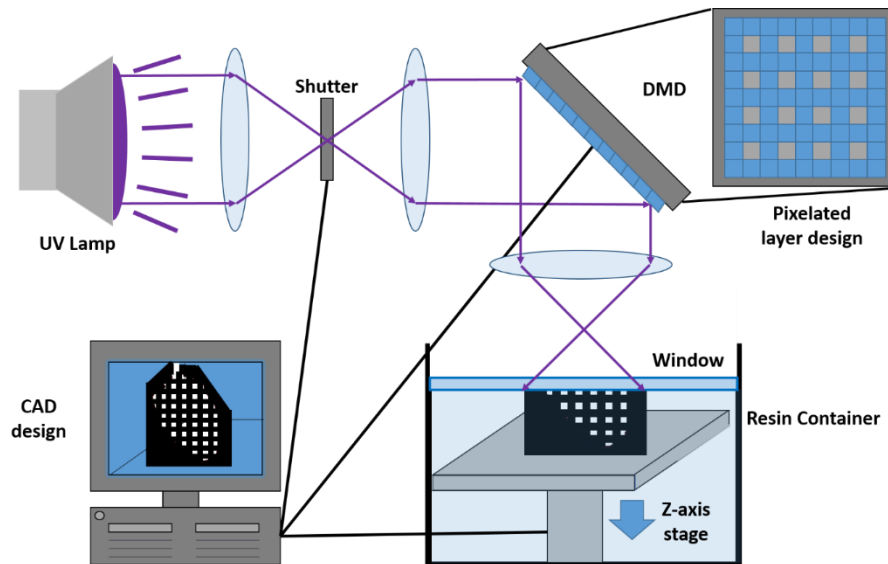
Figure 9: Digital light projection/microstereolithography principle.

Another irradiation-based technology is soft lithography. First, a pattern is generated via lithography on a robust photoresist. Next, poly(dimethylsiloxane) (PDMS) is "cast" onto the generated pattern, and the inverse pattern is transferred to the PDMS by hardening to generate a PDMS "stamp".[54] This soft "stamp" is then coated with the desired material followed by transfer of this material to a targeted surface, similar to conventional stamps coated with ink. The technique is referred to as soft lithography since lithography is applied as a master for a soft stamp material (PDMS). The technique cannot be considered a true SFF technique since only '2.5D' single-layer patterns are generated through this approach. However, by introducing several single-layer templates into the final material followed by template removal, 3D scaffolds can be obtained containing a stack of planar channels.[54]

1.3.1.2.2. Nozzle-based systems

Nozzle-based systems apply controlled X-Y movement of a material-depositing nozzle to generate each layer of the CAD. Increasing distance between the plotting head and plotting platform enables stacking of these layers to generate a 3D structure. A subcategorization can be performed based on the applied extrusion/dispensing mechanism.

The most straightforward nozzle-based technique is fused deposition modelling (FDM). The method uses a thermoplastic polymer filament which is fed by rollers through a heated nozzle which melts the polymer material just before deposition.[8,27,33,224] During deposition, the heat of the freshly deposited polymer softens the previous layer thereby

inducing interlayer attachment.[225] FDM can generate structures with strut diameters in the range of several 100 micrometers which is mainly controlled by nozzle diameter and extrusion rate.[225] The range of suitable materials for FDM remains limited since the materials have to be thermoplastic, exhibit suitable viscoelasticity and melting/solidification properties and have to be pre-processed into polymer filaments. For this technique, PLA is one of the most commonly applied materials.

A variation to FDM is air pressure jet solidification (AJS) which applies air pressure instead of rollers to force solutions or melts through a nozzle, thereby removing the need for preformed thermoplastic polymer filaments. In contrast with FDM, a larger range of materials can be applied including hydrogels, polymer/ceramic sludges, etc.[82,226,227] Similar to FDM, strut diameters can be obtained in the range of several 100 micrometers.[82]

Recently, the use of direct-write assembly was reported as a high-resolution variant of AJS. Via the combination of fine nozzle tips with fugitive inks, exhibiting specific viscoelastic properties, fine struts (down to 10 µm diameter) can be obtained by optimizing the pressure.[228,229] These properties have to enable ink deposition under high shear conditions combined with sufficient shape retention after structuring.[228,229] Therefore, sometimes the ink is photo-crosslinked during deposition to ensure sufficient mechanical integrity.[230] However, only a limited range of materials comply with these stringent viscoelastic properties, which is a restricting factor for many applications.[231]

Recently, a variation to nozzle based SFF techniques referred to as melt electrospinning writing (MEW) has been reported which applies the principles of melt electrospinning in combination with fluid dynamics to obtain ultra-narrow strut diameters typically in the range of 5 to 50 µm.[232,233]

1.3.1.2.3. Printer-based systems

3DP applies selective deposition of a liquid binder on a powder bed to selectively fuse powder particles together into a single layer of the CAD.[213,217,234,235] After completion of a layer, a roller distributes a new layer of powder onto the previous one and the process is repeated. Since infused powder acts as a support, complex 3D structures can be obtained with resolutions depending both on jet droplet and powder particle size, for iSFF resolutions in the range of 100 to 200 µm have been reported.[213,234,236]

When the complete structure is printed, unfused particles are blown away using pressurised air.[217] Often, the constructs are very brittle and require infiltration with a polymer solution (e.g. polyethylene glycol) or PEG) to reduce brittleness.[217] The material selection is limited, especially the use of synthetic degradable materials poses problems since organic solvents required for particle fusion dissolve most commercially available print nozzles.[213,234]

In addition to 3D printing, other printer-based techniques apply an inkjet nozzle to directly deposit droplets of a build-material (e.g. wax) by using piezoelectric actuation. This technique is referred to as inkjet printing (IJP), drop-on-demand printing (DDP) or phase change 3D jet-printing.[36,218,237] Upon impact, the droplets harden thereby forming beads which result in lines when adjacent beads overlap.[36,237] The method benefits from a high resolution as a consequence of the inkjet principle.[227] Often, two nozzles are applied to deposit two materials, being a build material to replicate the CAD and a support material to support overhanging struts during processing.[238] Application of a support material requires an additional support removal step by using a selective solvent before the final structure is obtained.[85,227,238,239] Additionally, some systems increase precision by milling away the top of each layer to a well-defined height before the next layer is deposited.[36,84–86,204,240] (Figure 10) Using this methodology, a layer height in the range of 10 to 20 µm can be obtained.[227]
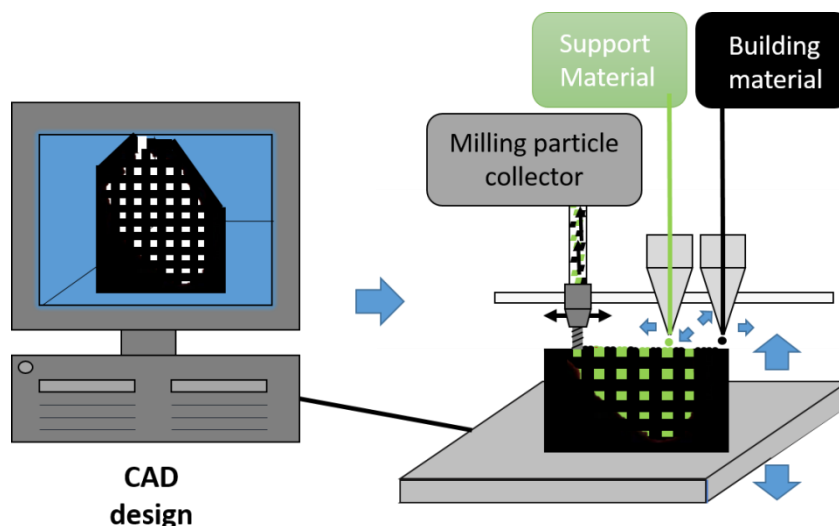
Figure 10: Principle of phase change 3D printing also referred to as drop on demand- or ink-jet printing principle.

A small variation to IJP can be considered as a hybrid between printer- and irradiation-based techniques. The technique is referred to as POLYJET™ and applies deposition

of photocurable droplets combined with immediate UV-curing, in this manner more robust structures are obtained in comparison to conventional IJP. Similar to IJP, the application of 2 nozzles enables the use of a support structure which can be selectively dissolved afterwards.[207,241]

1.3.2. Indirect Solid Freeform Fabrication

To overcome the limitations of conventional solid freeform fabrication techniques (limited material selection, brittleness and need for post treatment, low resolution and long optimization of new materials) [8,34,216–219] several research groups have been and are exploring a methodology which combines the benefits of SFF in terms of controlled, patient-specific design with the freedom of materials associated with conventional scaffold production techniques.[210,223,227,242] This approach applies a construct, generated via SFF techniques as a sacrificial mould or template for the final construct.[16] Therefore, the approach is referred to as "lost-mould technique", indirect solid freeform fabrication, indirect rapid prototyping (iSFF), indirect additive manufacturing or indirect 3D printing.[65,85,86,206,235] Here, the processing parameter requirements of the final scaffold material are of secondary importance, as a mould is generated using straightforward processing of well-established materials.[34,242] To generate the template, SFF techniques can be applied with superior resolution compared to direct SFF of the desired material.[227] By using high resolution techniques for template fabrication, for example SL, scaffolds with pore and strut sizes as low as 50 and 65 μm respectively can be obtained for materials unsuitable for direct fabrication using high resolution manufacturing methods.[38] Consequently, well-defined 3D scaffolds can be generated in a straightforward manner from materials previously identified as being "unprintable" due to thermomechanical properties that do not match the often strict temperature and pressure requirements for direct rapid prototyping.[37,82,85,213,219,238,239,243] Furthermore, less raw material is required since material consuming process optimization becomes superfluous. Additionally, only the volume of the final construct is required for scaffold production whereas most direct SFF techniques require excessive material amounts. For example, in SL, uncrosslinked material is washed away after shaping, in 3DP and LS unbound particles are blown away after structuring.[219] Additionally, iSFF allows a straightforward combination of different materials within one scaffold, including bioactive compounds. This is achieved either via blending of materials, or via the

creation of zones with different mechanical properties for specific tissue function (e.g. interface between soft and hard tissue).[219,238] Moreover, iSFF allows the creation of a hierarchical porosity in the final scaffold, since porous microstructures can be obtained inside the struts via conventionally applied techniques during or after casting.[35,65,82,205,219,223,234,235,237–239,242]

Consequently, iSFF has proven to circumvent hurdles commonly associated with direct SFF techniques and opens up unprecedented opportunities towards new scaffolding strategies[219] (sections 2.3. and 3). The combination of a large selection of SFF techniques with a vast variety of casting/template removal strategies results in a large range of diverse iSFF strategies. However, the generally applied methodology consists of three main steps[35–37]: (Figure 1)

1. Mould fabrication through SFF
2. Casting of the desired material + fixation of the final shape
3. Mould removal.

The design of the mould has to correspond to the inverse of the final construct.[213,242] Often this is accomplished *in silico* by generating an inverse 3D model.[210] In some cases SFF techniques already apply a secondary material during printing to act as a support for the final design, which can be selectively removed afterwards. Hence, selective removal of the construct material rather than support material and application of the support structure as mould for iSFF has been reported.[244] Consequently, the process of designing an inverse mould becomes redundant.[244,245] Another approach to avoid designing an inverse mould is to generate a first structure via SFF exhibiting the design of the final scaffold. This structure is then used as a sacrificial mould to generate the negative sacrificial mould for the final construct.[207,211,219,241]

To classify the range of approaches, a first categorization can be obtained by distinguishing between two main iSFF strategies. First, the combination of a sacrificial mould generated by SFF to control the macro-architecture (i.e. the external shape) of the final construct with conventional pore forming has been reported.[35,211,212,234,235,239,246] In the present paper, these methodologies will be referred to as external indirect rapid prototyping (eiSFF).[247] (Figure 11)
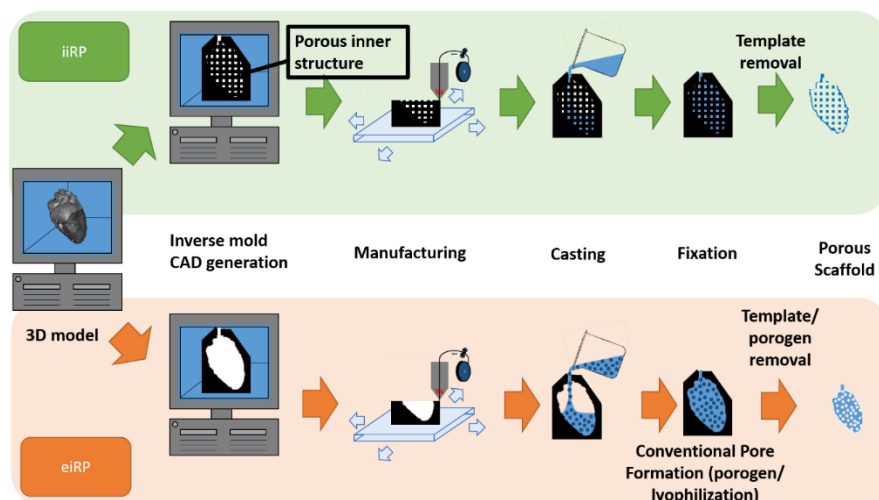
Figure 11: Comparison of the eiSFF and iiSFF approach

Secondly, the application of SFF templates has been targeted to obtain a controlled microporous structure into the final scaffold.[16,65,85,86,207,210,213,219,233,243] This methodology will be referred to as internal indirect rapid prototyping (iiSFF) (Figure 11). Sometimes conventional techniques are applied in combination with iiSFF to generate a hierarchical microporosity, resulting in the generation of porous struts which follow the morphology of the template.[204,213,219] Often also a combination of both approaches has been applied through which a desired outer contour is merged with well-defined inner architectures.[82,210,213,242]

1.3.2.1. Mould or Template fabrication process

1.3.2.1.1. Irradiation-based systems

In the category of irradiation based systems, to date only photo-polymerization techniques have been applied for iSFF. In this respect, the best known technique is SL where a laser beam is scanned across the surface of a photo-curable resin or (pre)polymer solution, thereby locally polymerizing the material. After solidification of a complete layer, the platform moves downwards for processing of the next layer. After multiple iterations, unpolymerized material is removed leaving behind the polymerized template.[30,210,248]

High resolution and precise architectural control render SL and DLP/MSTL ideal for complex porous templates suitable for iiSFF with high shape fidelity.[210,222,243,249] Currently, MSTL techniques enable generation of structures with (sub)-micron sized features.[214] However, since the applied mould is photo-crosslinked, template removal

becomes less straightforward. Consequently, the method is generally used to generate ceramic scaffolds which allow template removal via pyrolysis.[222,248]

1.3.2.1.2. Nozzle-based systems

As FDM is one of the most popular SFF techniques, several research groups have utilized this technology for the generation of controlled microstructures in iiSFF.[16,209,250,251] A key aspect is to select a filament material that can be selectively removed when using this method to create scaffolds for iSFF.

Another template fabrication technique is direct writing. Due to the limited range of materials compatible with this technique, it is more suitable for iiSFF than for direct SFF.[228,229,231] In a more specific example, the dynamic diameter control, generated by pressure variation, was exploited to create hierarchical vascular networks through iSFF.

Other nozzle-based techniques apply a piston for the deposition of material. In one specific iSFF example, a liquid hydrogel precursor is sucked into a capillary using a piston.[57] Next, physical gelation is induced into the capillary, followed by the deposition of the gel in a controlled area to obtain linear channels into a matrix of the final scaffold material with a diameter of 500 µm.[57]

A last nozzle-based technique used for template fabrication is MEW. Although the technique is very recent, it has already been applied to generate microchannels in a hydrogel structure via iiSFF.[233]

1.3.2.1.3. Printer-based systems

The limited material selection for 3DP-techniques in combination with the poor mechanical properties make the technique more attractive for iSFF than direct SFF if template removal is possible.[213,234] Therefore, Lee *et al.* used gelatin microparticles as a powder fused together with an aqueous solution to generate water-soluble templates.[213]

Another popular iSFF technique is IJP. Since the applied material in this technology is mainly limited to specific waxes which can easily be dissolved, the technique has proven to be very popular for iSFF as it combines high resolution with straightforward template removal.[83,85,226,240]

1.3.2.2. Casting methods

Following template generation, a casting step is performed to introduce the final scaffolding material. Since filling up the entire voids with the final scaffolding material can be difficult, several strategies have emerged in this respect. Applied methods include vacuum treatment, injection moulding and thermoforming.

Vacuum can be applied to remove all air bubbles from a solution during scaffold infiltration.[238] One strategy incorporates several templates into a solution of the final material followed by placing the entire container under vacuum.[16] In another approach a syringe filter has been cut in half to which the template was secured. Next, the filter and template were placed into a solution containing the final scaffold material followed by generating a vacuum using the plunger of the syringe thereby resulting in suction of the solution into the entire template.[240] (Figure 12)
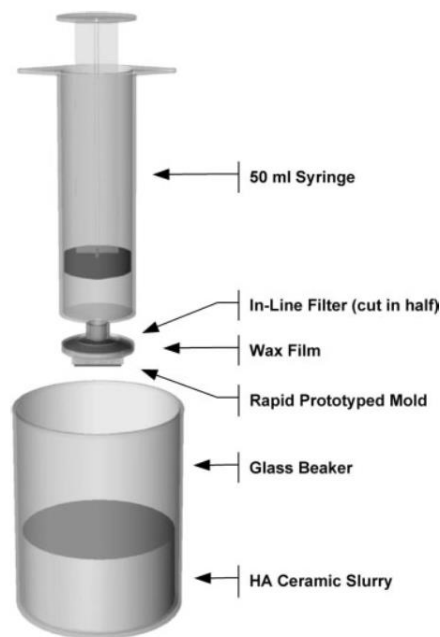
Figure 12: Casting via syringe-induced vacuum treatment. Reprinted from [240] with permission from Wiley.

If the viscoelastic properties of a melt allow straightforward material handling, pure polymer melts are directly injected into the mould via a syringe.[217,218] To this end, an extrusion chamber can be incorporated in the mould design. The chamber can be filled with a melt, followed by reproducible extrusion using a syringe plunjer.[218] (Figure 13)

After template removal, the remnants of the extrusion chamber have to be removed manually. [218]
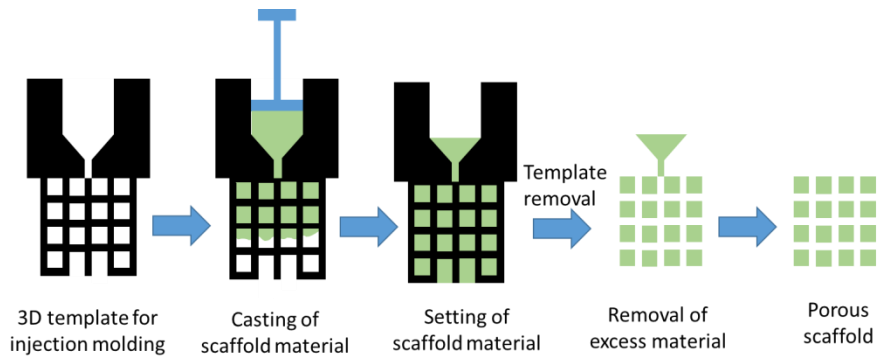
Figure 13: Principle of casting via injection moulding. In this approach the template contains a void for the final material before direct syringe injection.

Some research groups have already applied a design for the sacrificial mould which incorporates an inlet where a syringe can be attached and an outlet to remove excess material and air. (Figure 14) As a result, the final scaffold material can simply be injected into the mould, similar to injection moulding.[223,242] Consequently, scaffold generation is enabled in low tech environments (e.g. hospitals when it comes to scaffold production), if the templates are generated elsewhere.[242]
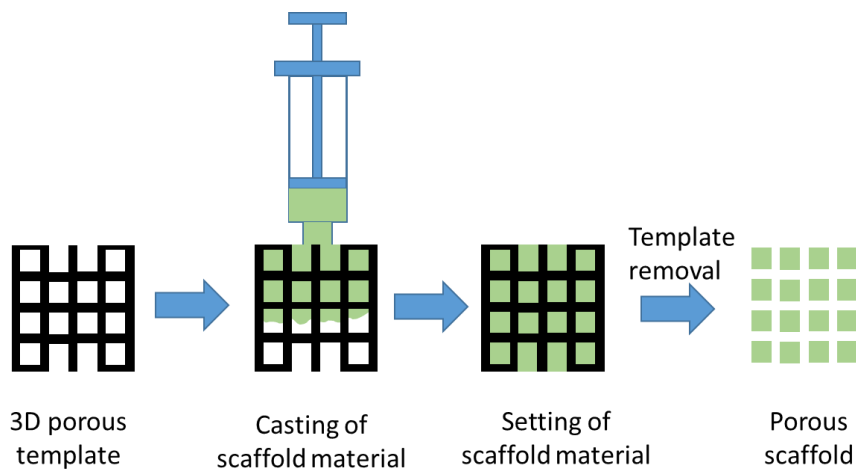
Figure 14:iSFF principle including direct syringe injection casting step. The template contains an inlet for the syringe and an outlet for removal of excess material.

As a final method, Sodian *et al.* have applied a technique where porous sheets of the scaffold material were heated, pressed against the negative mould and cooled to induce crystallization, thereby locking the final shape.[246,252] As a consequence, complete heart valves could be obtained from a single porous sheet with a controlled porosity without the need for suturing.[252]

1.3.2.3. Mould or template removal process

The final step in iSFF consists of template removal without damaging the final construct.[242] The absence of chemical interactions between template and scaffolding material facilitates this process. In addition, elasticity and swelling/shrinking behaviour of both the template and material should be taken into account. For instance, if brittle scaffolding materials are applied, swelling of the template during dissolution can result in stress-induced cracks and deformations arising in the final construct.[221] As a result, several techniques have arisen, including selective melting followed by evaporation, binder burnout and sintering, selective mould dissolution, selective mould degradation, and manual removal or aspiration.

If the template material exhibits a melting point below the thermal stability threshold of the scaffold material (e.g. wax and poly-(glycolic acid)/poly-(lactic acid) or PGA/PLA), the template can be removed by selectively melting the template.[219] To ensure complete template removal, a solvent can be applied to wash away any residue.[219] Sometimes melting alone is not sufficient for complete scaffold removal and often evaporation is necessary. In direct write assembly, the applied template material is often a fugitive ink. As a result, the template (vascular) structure can be removed by gentle heating to evaporate the ink.[228,229]

When ceramics are applied as a scaffolding material, organic templates can be removed by burnout or pyrolysis prior to sintering.[85,86,206,210,226,227,240,243,250,251] Pyrolysis followed by evaporation occurs when an organic material is heated to high temperatures (>400°C).[206,240] As a result, even unsolvable crosslinked networks generated by irradiation-based techniques can be removed.[206,222,249] As sintering at high temperatures is essential to remove the binder material applied for the ceramic slurry, template removal can occur without an additional step.[36]

Selective mould dissolution (SMD) is predominantly applied if the final scaffold material is a (synthetic) polymer. A prerequisite of the technique is the availability of a solvent which selectively dissolves the template material without influencing the scaffold material.[65,204,205,207,211,217–219,234,235,237–239,241,247] Therefore, the technique can be applied if the scaffold consists of crosslinked polymer networks which are unsoluble.[16] In addition, solvent mismatching systems can be an option (water versus organic solvents).[82,213] The method is often applied to remove wax templates generated via

DDP/IJP techniques.[83,84] Also, the removal of ceramic templates for the generation of scaffolds by using ceramic-specific solvents (e.g. RDO-APEX Engineering Products Corp) has been reported.[219]

SMD is one of the few template removal techniques suitable for cell encapsulation in iSFF. This can be accomplished when a water-soluble template (e.g. gelatin) is combined with a crosslinked hydrogel material containing cells (e.g. collagen).[54]

If the combination of high-resolution SL templates with thermally unstable scaffolding materials (e.g. (bio)polymers) is desired, pyrolysis and SMD are not possible for template removal.[221] Therefore, the solution can sometimes be found in creative chemistry. Liska *et al.* reported on the use of a hydrolysable crosslinkable material (using methacrylic anhydride as a crosslinker) for SL template generation. After casting, the mould was selectively removed via hydrolysis of the anhydride bonds using an alkaline solution.[221] Using this approach, high-resolution iiSFF and eiSFF scaffolds could be obtained from (PCL), poly(lactic-co-glycolic acid) (PLGA), poly-(L-lactic acid) (PLLA), chitosan, alginate and bone cement.[242]

Aspiration is a technique through which the template is removed from the final scaffolding material using a low vacuum pressure. It is clear that this method can only be applied for the removal of template fibers which do not show adhesion to the final scaffolding material.[57] The method can for instance be applied for the generation of blood vessels in labs on a chip (LoC) and organs on a chip.[57] Consequently, the technique is restricted to the generation of simple unbranched channels, which limit tissue engineering applications. However, these properties are often sufficient for LoC devices. The method can be considered as the least invasive template removal strategy.

SMD and aspiration have certain benefits over other scaffold removal methods, since they both allow the application of cell encapsulation via iSFF.[54,55,57] Furthermore, the sacrificial scaffolds can be produced elsewhere as a ready-to-go kit. Consequently, cellularized scaffolds can be obtained without the necessity of SFF knowhow and infrastructure. This feature increases the potential for rapid technology adoption and swift transfer to the clinic.[55] Consequently, iiSFF poses substantial benefits for the generation of vascular networks in comparison to direct SFF techniques.[55]

1.3.2.4. Overview of scaffold materials

A range of indirect scaffold materials have been described in literature to date including biopolymers, synthetic polymers, ceramics and composites. Many authors have highlighted the versatile nature of the iSFF technique by casting a selection of (bio)polymers and ceramics. [57,55,253] In addition to (bio)polymers and ceramics, the iSFF technique can also be used for the construction of porous metal implants, enabling cellular ingrowth.[236] Table 1 gives an overview of all iSFF approaches applied to date and contains information about the applied materials, the SFF technique, template material removal and the secondary pore creation strategy.

1.3.2.4.1. Biopolymers in indirect rapid prototyping

Extracellular matrix proteins are especially interesting for tissue engineering purposes, as they are inherently biocompatible, cell-interactive and do not result in toxic degradation products. However, they are often considered hard to process. Of considerable interest for tissue engineering purposes is collagen since it is the major constituent of the native human extracellular matrix.[54,65,237,254] Fabrication of micro channels in a collagen matrix using conventional SFF techniques has been limited to simple geometries, such as cylindrical tubes. To generate collagen scaffolds with complex microfluidic channels, a gelatin mould developed by stacking several patterned layers obtained via soft lithography has already been applied.[54] For some applications, the presence of micropores inside the scaffold can pose benefits with respect to diffusion-driven transport. When comparing critical point drying (CPD) and freeze drying for collagen scaffolds, CPD led to significantly higher shrinkage of the scaffold and could not result in a foam-like porous structure. Therefore, freeze drying is considered a more suitable technique for introducing microporosity in collagen scaffolds. [65]
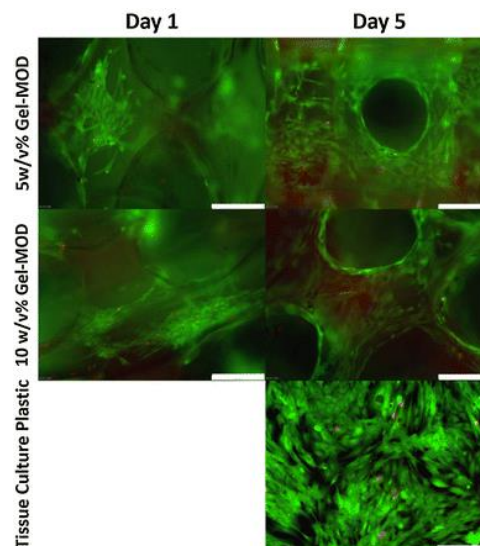
Figure 15: Live/dead fluorescence images obtained of the scaffolds seeded with human foreskin fibroblasts (HFF) for both types of scaffolds after 1 and 5 days of cell culture including control image on tissue culture plastic. (Scale bars represent 200 μm) Reprinted from source [16] With permission of Springer

Gelatin is a material derived from collagen either by acidic or alkaline hydrolysis. It has been combined with microspheres in an iSFF approach to create channelled, microporous scaffolds.[207] However, gelatin dissolves rapidly at physiological conditions and does not possess sufficiently high mechanical properties needed for many tissue engineering applications. Therefore, modification of the primary amine functions to obtain crosslinking functionalities (e.g. methacrylamides) is often performed.[12,16,72,255–257] Processing of low concentrations which are considered beneficial for cell viability via direct SFF becomes difficult.[56] However, in contrast to direct SFF, iSFF has enabled the construction of self-supporting scaffolds using polymer concentrations of 10 wt% and below (Figure 15).[16,57]

Another applied biomaterial is silk fibroin, a silk-derived, protein-based material which is of specific interest for the engineering of ligaments, bones and cartilages. It consists of amino-acids and is water insoluble, in contrast to gelatin. Conventional fabrication methods only allow limited control over the internal architecture. Therefore, Liu *et al* combined iSFF with freeze drying to develop silk fibroin tissue engineering scaffolds with macro-channels and micro-pores thereby enabling optimal cell infiltration.[239]

1.3.2.4.2. Synthetic polymers in indirect rapid prototyping

Due to their mechanical properties and biodegradability, polyesters are often applied for bone tissue engineering. These materials are often processed using fused deposition modelling. However, this method does not allow the creation of a secondary pore structure, for example by including porogens during the casting step. By using an

indirect approach, nanofibrous PLLA scaffolds, mimicking the morphological functions of type I collagen, can be generated by applying phase separation in dioxane.[212,247] Phase separation can be combined with paraffin microspheres to generate a tri-porous structure.[212] PCL is a biocompatible, semi-crystalline, slowly degrading polymer. It combines flexibility with robust mechanical properties, which makes it an attractive candidate for bone tissue engineering.[223,258,259] In addition, PCL has also been applied in eiSFF for the generation of a carotid artery. To this end, a dip coating process was combined with salt leaching to create a porous construct.[211] PLGA is another popular scaffold material for bone tissue engineering due to its robust mechanical properties. [235,260,261]
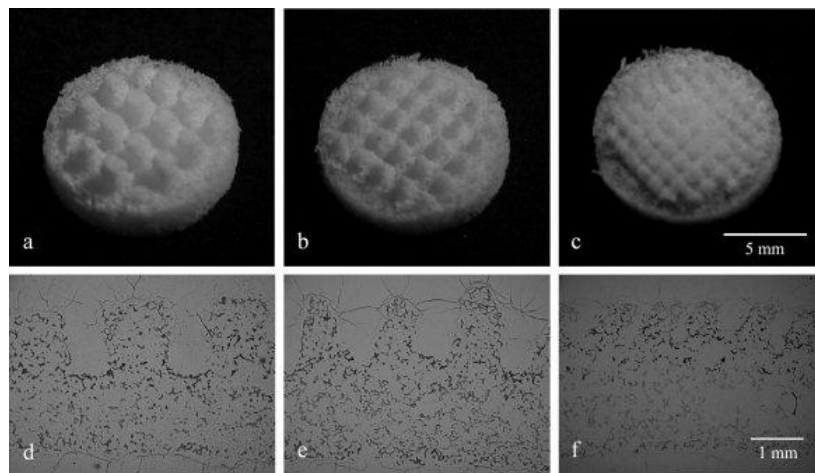
Figure 16: Figure 9: a-c, Macroscopic images of scaffolds with villi architecture with different dimensions. d-f, Cryosectional images. (left to right: 0.5,1,0.5 mm;0.5,1,1 mm; 1,1,1 mm; villus diameter; height; intervillus spacing respectively). Reprinted from source[235] with permission from Wiley Periodicals, Inc.

To demonstrate the obtainable resolution of iSFF, Lee *et al.* fabricated villi-shaped scaffolds and the effect of scaffold design on smooth muscle cell response was evaluated (Figure 16). A higher cell density was observed for scaffolds with smaller villi-features (0.5 mm vs 1 mm). This supports the hypothesis that a larger boundary surface area will better support mass transport.[235] Another polymer which has been applied for bone tissue engineering is poly(propylene fumarate) (PPF), an unsaturated linear polyester, which incorporates crosslinkable double bonds in its backbone. Furthermore, it has shown to support chondrocyte growth combined with matrix deposition. Rapid prototyping of unconventional polymers often requires tedious optimization of experimental processing parameters, which can be surpassed by using iSFF.

Poly-3-hydroxyoctanoate-co-3-hydroxyhexanoate and poly-4-hydroxybutyrate have been combined to create functional heart valves using the eiSFF approach, which allows the use of porogens [246,252] These materials are thermoplastic elastomers which are produced via a fermentation process.

Poly(2-oxazolines),a versatile material class with great potential for biological applications, have been applied in combination with MEW to generate a construct with microchannels.[233]

1.3.2.4.3. Ceramics in indirect rapid prototyping

Porous ceramics are generally applied as scaffolding materials for bone defects and spinal fusion applications. In this respect, iSFF is very appealing since any organic mould can be removed during sintering or pyrolysis, thereby elegantly combining two processing steps. In addition, direct rapid prototyping of ceramic slurries is challenging and often requires a long optimization process. For bone tissue engineering, calcium phosphate is most often used under the form of tricalcium phosphate (TCP), a calcium salt of phosphoric acid. This material is commercially available for its use in medical and dental applications. To fill the iSFF mould, TCP particles are combined with a binder solution to obtain a ceramic slurry. After casting, the binder (and mould) are removed via sintering.[83,84] To increase the scaffold potential, growth factors such as bone-morphogenic proteins (BMP) can be included in the scaffold post-sintering. Especially of interest is BMP-2, a bone matrix protein stimulating mesenchymal cell differentiation into chondrocytes and osteoblasts.[83]

A second important ceramic material for tissue engineering purposes is hydroxyapatite (HA), a calcium phosphate and major component of human bones and teeth. It has been studied extensively as bone graft material, since it enables the culture of many types of osteogenic and bone marrow cells. Implantation studies have already shown its ability to support ingrowth of bone into porous implants [37,39,41,49,56,74,80,105–108] (Figure 17). Often, a thermally crosslinked binder is used as a carrier for the HA particles, which can be removed during sintering.[15,206,210,222,243,262] However, if instead of a binder a self-setting solution is used, sintering is not required and growth factors such as BMP-2 can be included in the scaffold during fabrication.[82]
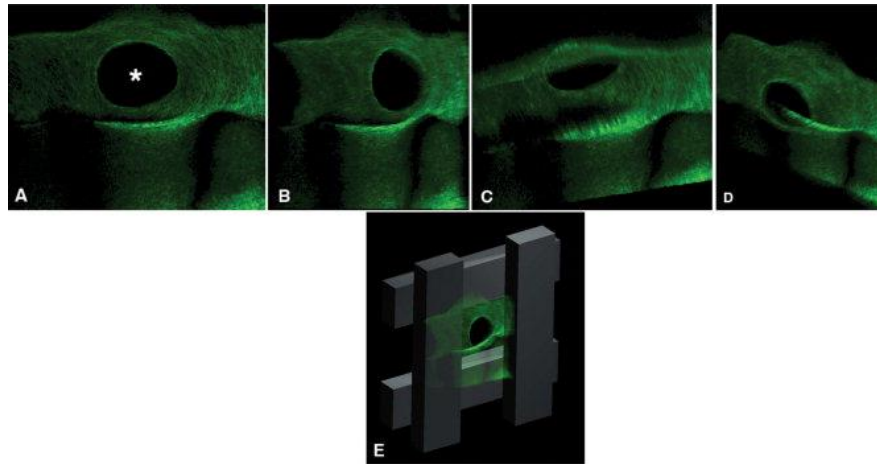
Figure 17: A-D, Confocal laser scanning microscope image of a cellular network grown on HA scaffold. E, Overlay of image B with a virtual drawing of the scaffold sector. Reprinted from source[262] with permission from Wiley Periodicals, Inc

When comparing HA and TCP or blends thereof as scaffold material, HA or HA/TCP blends prove to be superior to TCP in terms of cell viability, proliferation and osteogenic differentiation.[85,86] In addition to these conventional ceramic materials, alumina ceramic powders have also been investigated as scaffold materials.[250,251]

1.3.2.4.4. Composites and blends in indirect rapid prototyping

The casting process offers the possibility of creating biphasic and composite scaffolds which exhibit zones with different properties for structural tissue interface engineering. An interesting example is the combination of ceramic and polymer composites. Material-related properties such as flexibility of polyesters and toughness of ceramics can be combined as a composite or for the creation of discrete zones within the scaffold.[219] Inspired by natural bone, which is a composite of organic and inorganic compounds, Li *et al.* combined PLLA and chitosan with HA microspheres. PLLA is used for its high stability, while chitosan has a high biocompatibility. The addition of HA microspheres increases proliferation of pre-osteoblastic cells, resulting in an ideal scaffold for bone tissue engineering. (Figure 18).[238]
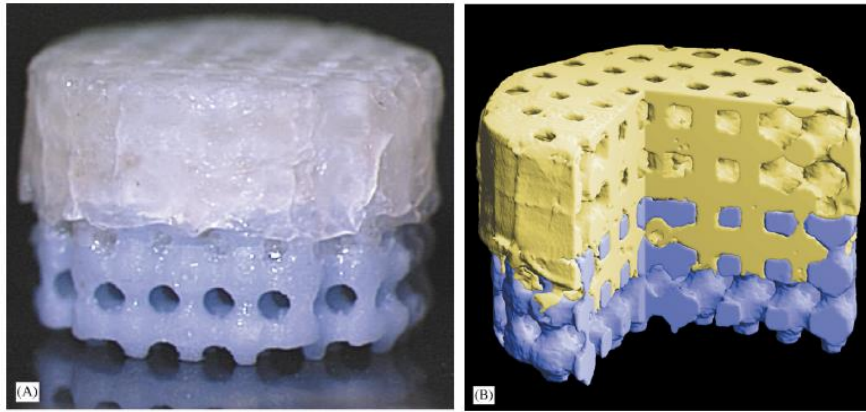
Figure 18: Biphasic PLA/HA ceramic scaffold (top, yellow: PLLA; bottom, blue: HA). Reprinted from source [238] with permission from Elsevier

By combining the synthetic polymer PPF, as described in paragraph 1.3.2.4.2 with β-TCP, an interesting composite can also obtained. In addition to its osteoconductivity, the mechanical properties of the material can increase during the early stages of degradation as a result of continued crosslinking and by complexation of the polymeric carboxylic acid groups with calcium ions.[263]

Besides biphasic scaffolds and blends, surface treatments can be applied to create multi-material scaffolds. For example, chitosan and PCL mandibular condyle shaped scaffolds were coated with apatite to increase osteoinductive properties.[213]

1.3.2.5. Applications of indirect solid freeform fabrication

Due to the versatile nature of the iSFF method, and the broad range of materials that can be applied, indirect scaffolds have been developed for different applications ranging from hard to soft tissues, tissue interfaces and the creation of vascular networks (Figure 19). By combining medical imaging with the 3D scaffold production methods, patient-specific and defect-specific tissue engineering implants can be developed. Furthermore, iSFF has been applied for the creation of microfluidic and vascular networks. However, since this topic is somewhat different from conventional tissue engineering it is discussed in a separate paragraph (1.3.2.5.3).

Figure 19: Applications of iSFF in the engineering of hard tissue, soft tissue and tissue interfaces

1.3.2.5.1. Hard tissue engineering using indirect rapid prototyping

The main advantage of iiSFF is its rigorous control in terms of scaffold architecture. As a result, the natural morphology of bone tissue including the complex internal microstructure with Volkman's and Haversian canals, can be carefully designed in the mould.[82]

Pore size and shape greatly influence the mechanical properties of a scaffold and tissue ingrowth. Increased porosity will lead to a better ingrowth, but will decrease the implant stiffness. Via design optimization, scaffold microstructures can be designed to match the mechanical properties of the target tissue, while maintaining sufficient porosity for tissue ingrowth.[210,243] In this respect, scaffolds with moduli and strength values in the range of human trabecular bone (compressive modulus of 10-900 MPa, yield stress of 0.2-14 MPa) could be generated using a casting method.[260]

In addition to the mechanical properties, pore shape can also influence cell growth. By choosing different pore shapes this influence can be assessed. Channel surface area and local curvature have been shown to strongly influence the tissue growth rate. Round channels result in uniform growth of MC3T3-E1 cells, while in polygonal pores,

tissue growth typically starts in the corners, whereas cells on the faces initially remained in a resting state. As a result, over time, round pores are obtained regardless of the initial pore shape.[208] (Figure 20). However, for identically shaped pores, with a size range of 350-800 µm, no significant effect on tissue ingrowth was observed in PCL even after 8 weeks of implantation.[259]
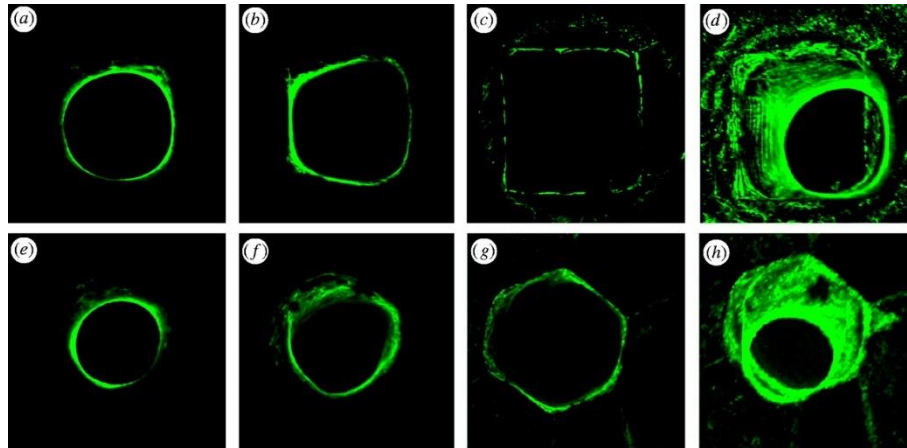
Figure 20: Tissue formation depending on pore structure. Because of different cellular growth rates of cells located in the corner or on the face of the pore, a final round shape is formed regardless of the initial pore morphology. Reprinted with permission from The Royal Society publishing[208].

Detsch *et al.* compared bone marrow stromal cell cultivation on hydroxyapatite scaffolds generated via a direct dispense plotting method and an iiSFF method. They observed that for the iiSFF scaffolds a higher differentiation of the bone marrow stromal cells into precursor osteoblasts occurred while the direct printed scaffold exhibited a higher proliferation rate. They concluded that both scaffold types were suitable for tissue culture.[226,227]

One of the targeted tissues to be regenerated using an iSFF approach is craniofacial tissue. Based on computed tomography (CT) or magnetic resonance imaging (MRI) scans the scaffold can closely mimic the architecture of the defect, for example the mandibular chondyle[253] or the zygoma[234]. Human digit bone was reconstructed by combining a phase separation technique with an eiSFF method including paraffin spheres.[212]

Aiming at cartilage tissue engineering an indirect PPF scaffold has been combined with a hyaluronic acid/collagen I hydrogel for cell delivery.[264] These scaffolds combined load bearing qualities with enhanced tissue regeneration. Both cubic and ellipsoid shaped pores resulted in good tissue infiltration without any significant difference.

Moore *et al.* developed a bio artificial graft for the repair of spinal cord injuries. Tailoring to the complex nature of these injuries they developed an implant active both at the molecular, the cellular and the tissue level. An implant closely mimicking the morphology of the human spinal cord was fabricated using PLLA. Due to its specific architecture the scaffold could be seeded with multiple cell types mirroring the anatomical tissue locations. Schwann-cell loaded scaffolds were implanted *in vivo* and promoted axon regeneration (Figure 21). [261]
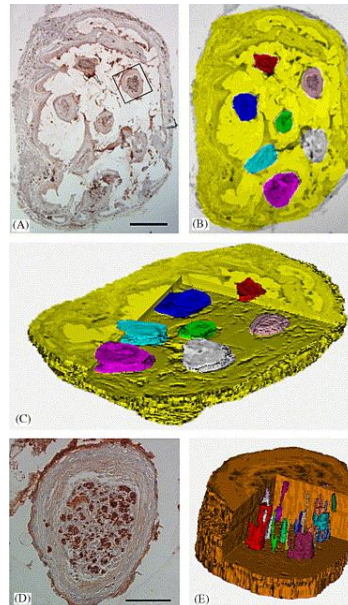
Figure 21: Histological images of tissue formed within the spinal cord scaffold, segmented axon bundles are clearly visible. Reprinted with permission from Elsevier[261]

1.3.2.5.2. Soft tissue engineering using indirect rapid prototyping

Using iSFF, complex structures with high resolutions can be achieved, which is demonstrated by printed scaffolds exhibiting a small villi architecture.[213,234,235]

Another complex tissue that has been generated using iSFF is the heart valve. The design needs to be both functional as well as physiologically correct and was obtained based on x-ray computed tomography. The designs included human pulmonary and aortic homografts and were based on moulds fabricated using stereolithography followed by thermoforming of porous PPF sheets to obtain the final structure.[246,252]

By combining eiSFF with dip coating and salt leaching, porous, patient-specific, bifurbicating blood vessels have been fabricated based on CT scans of a carotid artery (Figure 22) which exhibited a mechanical strength within the range of natural human

blood vessels (1-3 mPa). The biocompatibility of the scaffold was confirmed using human umbilical vein endothelial cells (HUVECs).[211]
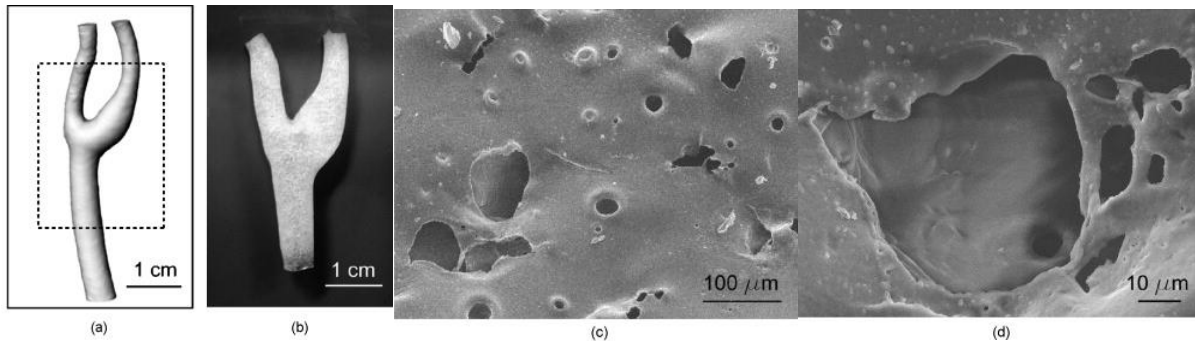
Figure 22: Bifurbicating carotid artery, reconstruction (a) and macroscopic image of the PCL scaffold (b). SEM images of the surface (c and d).Reprinted from source [211] with permission from Elsevier.

1.3.2.5.2.1. Indirect rapid prototyping as a solution for tissue interfaces

The treatment of periodontal diseases involves the formation of new cementum, periodontal ligament and alveolar bone. This challenging multi-tissue interface inspired the combination of a biphasic scaffold with PGA as periodontal ligament and PCL to engineer the bone compartment. A mould was developed to perfectly fit a human tooth dentin slice attached to the PGA region of the scaffold (Figure 23). [244,258]
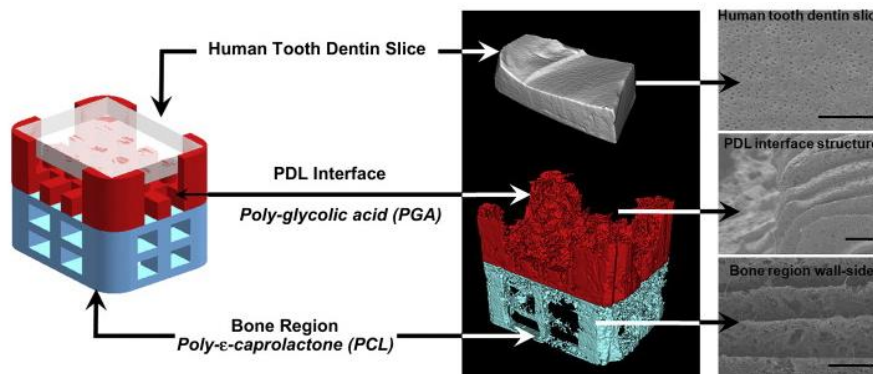
Figure 23: Polymer casted, hybrid scaffold for engineering the human periodontal tooth-ligament (PDL) interface. Left: 3D design, right: µ-CT images and 3D reconstruction. Scale bar is 50 µm. Reused from source[244] with permission from Elsevier.

1.3.2.5.3. Indirect templates for the formation of vascular networks

1.3.2.5.3.1. Vascularized tissue engineering constructs

Vascularization in tissue engineering constructs remains a key challenge as many different cell types need a constant supply of oxygen and nutrients. In the absence of blood vessels and capillaries, the thickness of most engineered tissues is limited to 100-200 µm.[265] This need is partially resolved by creating porous structures using

(direct) rapid prototyping techniques or other pore-creating methods. However, even with these porous scaffolds nutrient and oxygen supply is driven by passive diffusion. As a result, achieving cell densities close to physiological populations is extremely challenging since often necrotic areas are formed.[55] The use of sacrificial templates offers an elegant alternative to conventional porous structures via the generation of multiscale, vascular-like channels in engineered tissue, which enables active transport of nutrients and waste.

Natural vascularised tissues consist of three main components being the vascular lumen, the vascular wall lined with endothelial cells and a matrix of cells which surround the vascular channels. After removal of the vascular template the obtained channels can be perfused with endothelial cells to deposit a monolayer of cells. Consequently, hybrid cellularized scaffolds can be obtained exhibiting the presence of different cell types and a vascular network which closely mimics natural tissue.[54,55,57]

To enable template removal in the presence of encapsulated cells template materials have to be carefully selected taking into account a number of requirements. They cannot be cytotoxic and need to be removed under mild conditions without relying on cytotoxic organic solvents. Examples of these materials include agarose[57], gelatin[54] and carbohydrate-glass[55]. These can all be manually removed or dissolved by melting or dissolution in water or culture medium. An interesting approach to prevent leachables from entering into the matrix during template removal is the coating of vascular channels prior to casting. During selective dissolution this thin film prevents the leachables to enter the cell encapsulated hydrogel matrix while maintaining diffusion properties for biomolecules to the cells (Figure 24).
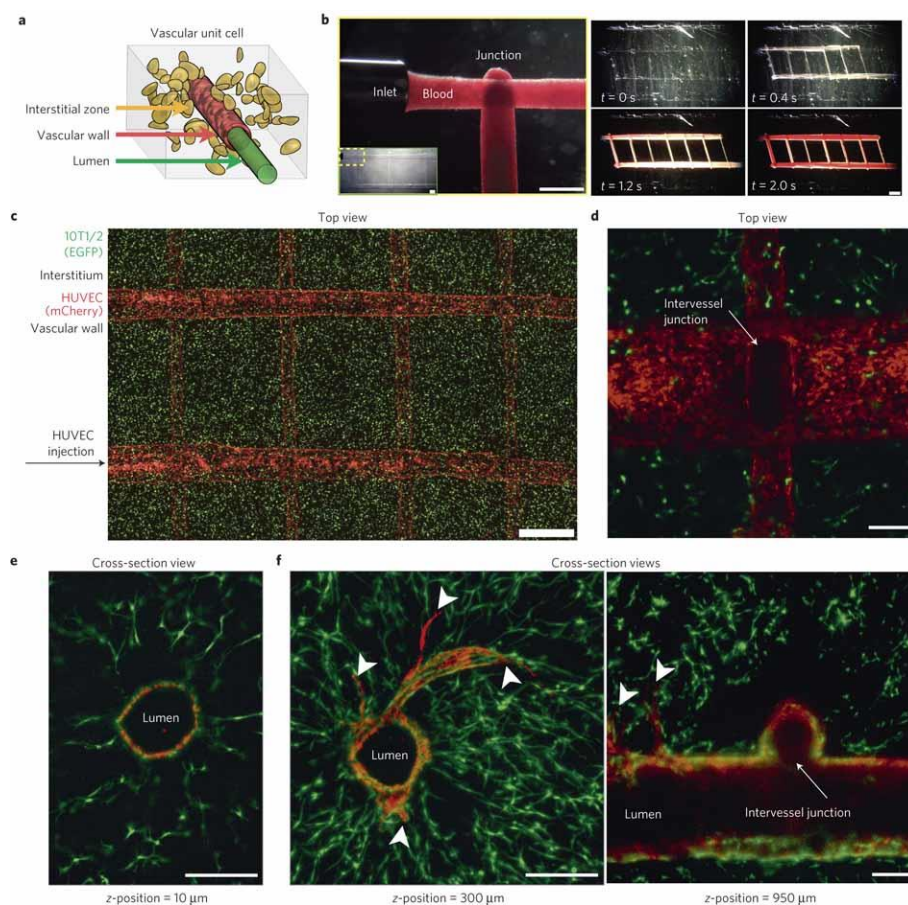
Figure 24: a, Vascular unit cell. b, Patterned vascular channels supporting human blood flow. Scale bars: 1 mm (left) 2 mm (right). C, Encapsulated 10T1/2 cells in a filbrin gel, seeded HUVECs expressing mCherry. d, Two intersecting channels demonstrating endothelisation. e, Cross-section of a representative channel after nine days in culture. f, Single and multicellular sprouts formed by endothelial cells (arrowheads) Reprinted with permission from Macmillan Publishers Ltd: Nature Materials[55], copyright (2012).

1.3.2.5.3.2. Microfluidics

Complex microfluidic channels are of interest for a range of applications in biotechnology, in sensors, lab on chips, organs on chips, chemical reactors and fluidic based computers. [228] They can be directly prototyped by (soft) lithography[266–268], laser ablation[269], deep proton writing[270], micro-milling[271] and ultra-precision diamond tooling[272]. Also, they can be produced at low cost in high volumes through replication techniques such as micro-injection moulding[273], hot embossing[274] or roll-to-roll printing[275] . However, with these techniques the creation of bifurcating true three-dimensional networks remains challenging. Direct writing with fugitive ink offers interesting perspectives in the creation of these microfluidic channels. For example, the creation of biomimetic vascular networks to study fluid transport efficiency has already been reported.[231]

Chapter 1: Introduction

Therriault et al. have used direct-write assembly with a fugitive ink to create channels with diameters ranging from 10-300 µm. An epoxy resin was cast and the ink was liquefied and removed forming a well-designed 3D epoxy network. By filling the channels with a photopolymerizable resin and selectively blocking some channels by using a filter before UV-curing, a tower network was created to perform 1D, 2D and 3D mixing experiments (*Figure 25*).
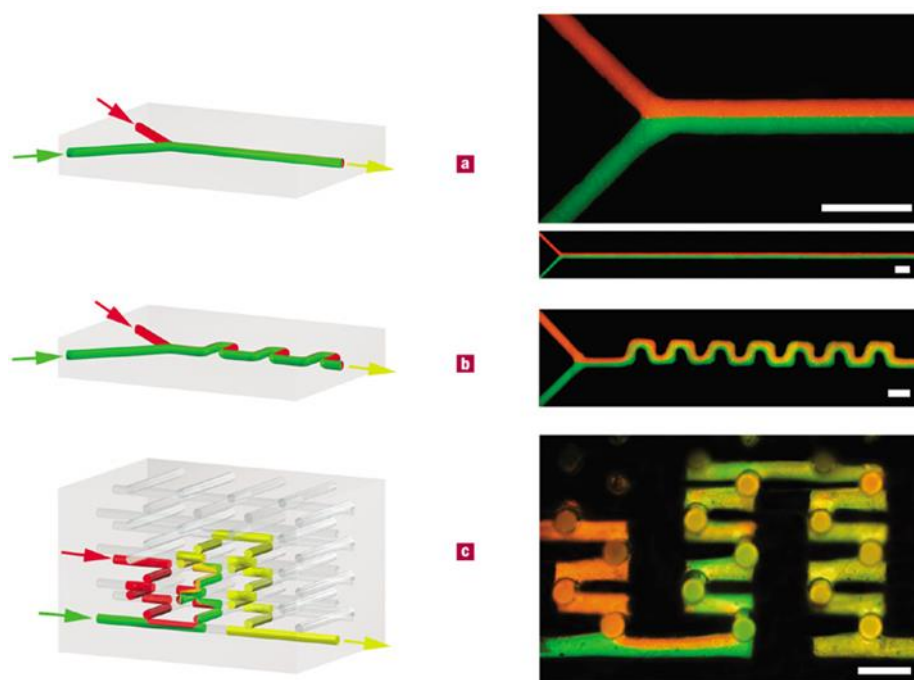
Figure 25: a-c, Schematic representations and fluorescent microscope images of 1D, 2D and 3D microfluidic mixing experiments. Arrows indicate flow direction. Reprinted with permission from Macmillan Publishers Ltd: Nature Materials[228], copyright (2003)

1.3.3. Electrospinning

Electrospinning is a method to create non-woven, porous fiber matrices which was discovered in the early 1930s.[76] More specifically, a polymer solution or melt is guided through a metal needle and a large voltage (1 – 30 kilovolt) is applied between the tip of the needle and the grounded collector plate. As a result, the pendant drop becomes charged leading to the formation of a Taylor cone. When the charge repulsion overcomes the surface tension, a polymer jet is ejected from the Taylor cone. While the jet travels to the collector plate, the solvent will evaporate thereby creating solid fibers with a nano- to microscale diameter. If this process is continued during a sufficient time span (2-30 min depending on the flow rate), a mat of electrospun fibers will be formed. The setup is depicted in Figure 26.
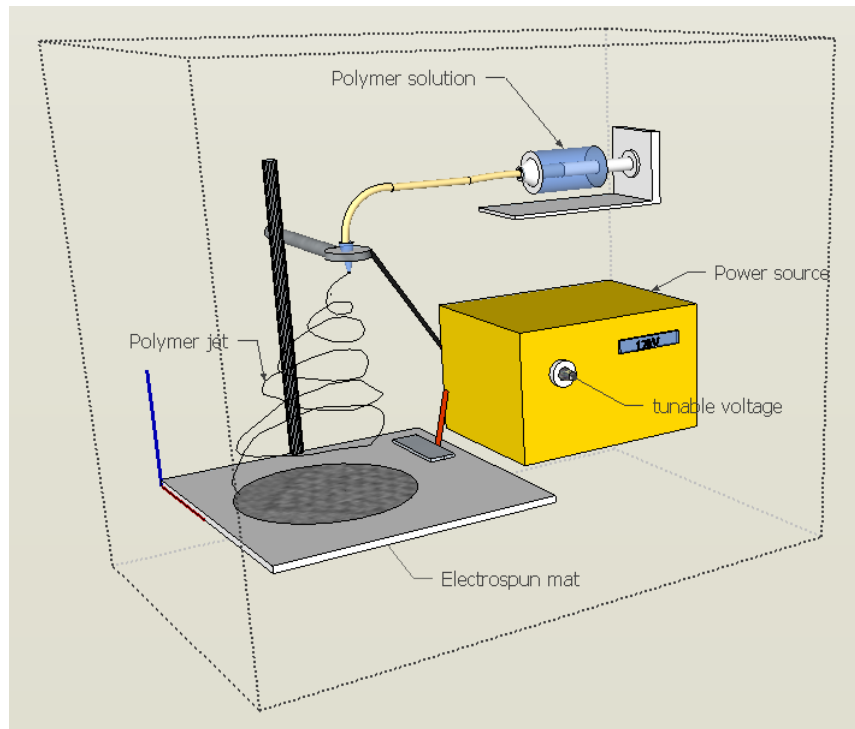
Figure 26: Electrospinning setup.

As a result of their micro- or nano-structure, the fibrous scaffolds possess a high surface to volume ratio, which provides the cells with more surface area for attachment. Their porous structure enables efficient transport of nutrients and metabolites throughout the scaffold. In addition, the random fiber structure mimics the protein fibers present in the ECM. This renders electrospun scaffolds ideal for a range of applications including bone[276], cartilage[277,278], vascular[279–282], neural[283–286] and bladder[287] tissue engineering. In addition, electrospun mats are highly investigated as wound bandages as their porosity enables gas exchange with the environment, while still offering a protective layer shielding the wound. In addition, the technique allows for the incorporation of antibiotic, antibacterial and other components promoting wound healing and preventing infection.[288–291]

1.3.4. Other pore creation techniques

In order to generate porous scaffolds, several other strategies than those mentioned above have been considered to date, such as critical point drying, freeze drying, porogen leaching, phase inversion, foaming and introducing gas forming agents

Critical point drying implies the exchange of an organic solvent with liquid CO_2 at room temperature at a controlled pressure. Next, the temperature is increased to 10° above the critical point of CO_2 which converts liquid CO_2 into gas, leaving behind a porous

network. The use of an organic solvent, often ethanol, is of crucial importance since liquid CO_2 is not miscible with water. The obtained pores are generally about 50 µm large.[65]

Freeze drying uses water (or another solvent) which is frozen to obtain ice crystals, followed by sublimation of these crystals. Consequently, empty pores are left with the morphological features of the ice crystals.[65,204,292,293] When the solvent is water, the mean pore diameter is typically in the range of 100-200 µm.[204]

In another approach, soluble salts or porogens can be incorporated into the scaffold material prior to casting. During template removal, the porogens are removed simultaneously, thereby leaving behind pores which exhibit the morphology and the size of the applied porogen.[207,213,223,234,235,242,246] Tan *et al.* have applied uniform microspheres as porogens and arranged them in the most closely packed conformation via ultrasonic treatment. Using this method, a reproducible porous interconnective network can be obtained.[207]

If a homogenous solution of two or more components (e.g. PCL in N-N-dimethylacetamide) exists at a certain temperature, sometimes phase separation between the components can occur during cooling. After precipitation, the solvent can be washed away, leaving behind a porous structure in the precipitated compound (e.g. poly-ε-(caprolactone) or PCL).[223,242,246,247] Under the right conditions (solvent system, cooling conditions), even nanofibrous structures can be generated which mimic the morphology of collagen fibers present in the ECM.[212,247]

Another technique which has been explored is foaming. By vigorously stirring certain scaffold materials including gelatin, viscous foams can be obtained. When the scaffold material is cast into the mould followed by immediate freezing to lock the shape, a highly microporous material is obtained with pores revealing a spherical morphology and uniform distribution. The pore size can be controlled by varying the stirring speed during foam generation.[241]

Another interesting approach to obtain micropores in a construct is the application of gas producing compounds. For example, when radical (photo-) polymerization is applied to lock the template shape into the final material, the use of azo-type initiators (e.g. VA-086) results in the generation of N_2 gas during activation. This results in the formation of micropores inside the final construct.[56]

1.4. Phd outline

In the present work, the aim was to explore different possibilities to circumvent the incompatibility of processing and crosslinking generally experienced with hydrogel building blocks. More specifically, in the second chapter, the development of a highly reactive hydrogel precursor was targeted to enable solid-state crosslinking thereby opening up unprecedented processing avenues. As the research was performed in close collaboration with an industrial partner (Allnex), the synthesis of the newly developed materials had to be readily translatable from lab-scale (mg to g range) to industrial scale (kg to ton range). As a result, the goal was to minimize the amount of synthesis and purification steps, and using industrially available reagents.

In this second chapter, the solid state reactive prepolymers will be characterised using a variety of different techniques ([1]H-Nuclear Magnetic resonance spectroscopy, infrared spectroscopy, Gel permeation chromatography, photo-differential scanning caloremetry (photo-DSC) and rheology). In addition, three different processing possibilites will be explored: extrusion-based solid freeform fabrication from melt, electrospinning and two-photon polymerization in the solid state. In a final part of the chapter, a preliminary investigation into potential of these materials for tissue engineering will be investigated by seeding different cell types onto the scaffolds obtained by solid freeform fabrication.

In the next chapter (chapter 3), the aim was to further characterise the prepolymers developed in chapter 2. Using different characterisation techniques, such as photo-DSC, rheology and UV-Vis spectrophotometry a deeper look into the origin and kinetics of the solid state reactivity can be obtained. Furthermore, by synthesizing a range of different polymers, the versatility of this approach can be explored. In a final part, a model was developed to investigate the significance of the different termination reaction occuring during the solid state reaction.

In addition, two more generally applicable hydrogel processing methods will be explored using the hydrogel precursors developed in this work. A first method, described in chapter 4, is indirect solid freeform fabriation, which applies conventional solid freeform fabrication techniques and materials to generate a template to be subsequently used to create scaffolds from a material of choice. With this technique, the drawbacks of conventional solid freeform fabrication, such as limited material

selection, brittleness and need for post treatment, low resolution and long optimization of new materials can be circumvented. [8,34,216–219]

For the second method, aqueous hydrogel solution that can be directly processed will be developed in chapter 5. Alltough many processing difficulties can be surpassed using a solid state reactive precursor, or by applying indirect rapid prototyping.. the composite material, described in Chapter 5, can be used as a solid freeform fabrication printing ink. The major advantage over the previously described methods is that this material could eventually be used to encapsulate cells during printing. To this end, the use of a silicate additive, inducing thixothropic behaviour and increasing the cellular response will be investigated in a second processing method to create a solid freeform fabrication ink suitable to generate 3D scaffolds for tissue engineering applications. The last chapter (chapter 6) will contain the major conclusions of the work and an outllook to future work.

1.5. References

1. Houben, A. *et al.* Indirect Rapid Prototyping: Opening Up Unprecedented Opportunities in Scaffold Design and Applications. *Ann. Biomed. Eng.* **45,** 1–26 (2016).

2. Rayes, N. *et al.* Causes of death after liver transplantation: an analysis of 41 cases in 382 patients. *Zentralbl. Chir.* **120,** 435–438 (1995).

3. Langer, R. & Vacanti, J. P. Tissue Engineering. *Science (80-.).* **260,** (1993).

4. Lanza, R., Langer, R. & Vacanti, J. P. *Principles of Tissue Engineering.* (Academic Press, 2013).

5. Vacanti, J. P. & Langer, R. Tissue engineering: the design and fabrication of living replacement devices for surgical reconstruction and transplantation. *Lancet* **354,** SI32-I34 (1999).

6. Hong, S. *et al.* 3D Printing of Highly Stretchable and Tough Hydrogels into Complex, Cellularized Structures. *Adv. Mater.* **27,** n/a-n/a (2015).

7. Bigi, A., Panzavolta, S. & Rubini, K. Relationship between triple-helix content and mechanical properties of gelatin films. *Biomaterials* **25,** 5675–5680 (2004).

8. Billiet, T. *et al.* A review of trends and limitations in hydrogel-rapid prototyping for tissue engineering. *Biomaterials* **33,** 6020–6041 (2012).

9. Zohuriaan-mehr, M. J. & Kabiri, K. Superabsorbent Polymer Materials: A review. *Iran. Polym. J.* **17,** 451–477 (2008).

10. Ratner, B. D. *Biomaterials Science: An Introduction to Materials in Medicine.* (2004).

11. Fisher, J. P., Dean, D., Engel, P. S. & Mikos, A. G. Photoinitiated Polymerization of Biomaterials. *Annu. Rev. Mater. Res.* **31,** 171–181 (2001).

12. Van Vlierberghe, S., Dubruel, P. & Schacht, E. Biopolymer-based hydrogels as scaffolds for tissue engineering applications: a review. *Biomacromolecules* **12,** 1387–408 (2011).

13. Slaughter, B. V, Khurshid, S. S., Fisher, O. Z., Khademhosseini, A. & Peppas, N. a. Hydrogels in regenerative medicine. *Adv. Mater.* **21,** 3307–3329 (2009).

14. Hutmacher, D. W. Biomaterials offer cancer research the third dimension. *Nat. Mater.* **9,** 90–93 (2010).

15. Hollister, S. J., Maddox, R. D. & Taboas, J. M. Optimal design and fabrication of scaffolds to mimic tissue properties and satisfy biological constraints. *Biomaterials* **23,** 4095–4103 (2002).

16. Van Hoorick, J. *et al.* Indirect additive manufacturing as an elegant tool for the production of self-supporting low density gelatin scaffolds. *J. Mater. Sci. Mater. Med.* **26,** 247 (2015).

17. Meyer, U. The History of Tissue Engineering and Regenerative Medicine in Perspective. *Fundam. Tissue Eng. Regen. Med.* 5–12 (2009). doi:10.1007/978-3-540-77755-7

18. Langer, R. S. & Vacanti, J. P. Tissue engineering: the challenges ahead. *Sci. Am.* **280,** 86–9 (1999).

19. Commission, E. *Journalist Workshop on Organ donation and transplantation: Recent Facts and Figures.* (2014).

20. de Geest, S., Abraham, I. & Dunbar-Jacob, J. Measuring Transplant Patients' Compliance with Immunosuppressive Therapy. *West. J. Nurs. Res.* **18,** 595–605 (1996).

21. Dantal, J. & Soulillou, J.-P. Immunosuppressive Drugs and the Risk of Cancer after Organ Transplantation. *N. Engl. J. Med.* **352,** 1371–1373 (2005).

22. Rifkind, D., Marchioro, T. L., Schneck, S. A. & Hill, R. B. Systemic fungal infections complicating renal transplantation and immunosuppressive therapy. *Am. J. Med.* **43,** 28–38 (1967).

23. Dillingham TR, A. R. Use and Satisfaction with Prosthetic Devices Among Persons with Trauma-Related Amputations: A Long- Term Outcome Study. *Am. J. Phys. Med. Rehabil.* **80,** 563–571 (2001).

24. Introduction, A. *Electrospinning and Nanofibers.*

25. Badylak, S. F. The extracellular matrix as a scaffold for tissue reconstruction. *Semin. Cell Dev. Biol.* **13,** 377–83 (2002).

26. Frantz, C., Stewart, K. M. & Weaver, V. M. The extracellular matrix at a glance. *J. Cell Sci.* **123,** (2010).

27. Landers, R. *et al.* Fabrication of soft tissue engineering scaffolds by means of rapid prototyping techniques. *journals Mater. Sci.* **37,** 3107–3116 (2002).

28. Graulus, G.-J. J. *et al.* Cross-linkable alginate-graft-gelatin copolymers for tissue engineering applications. *Eur. Polym. J.* **72,** 494–506 (2015).

29. Ovsianikov, A., Ostendorf, A. & Chichkov, B. N. Three-dimensional photofabrication with femtosecond lasers for applications in photonics and biomedicine. *Appl. Surf. Sci.* **253,** 6599–6602 (2007).

30. Melchels, F. P. W., Feijen, J. & Grijpma, D. W. A review on stereolithography and its applications in biomedical engineering. *Biomaterials* **31,** 6121–6130 (2010).

31. Ovsianikov, A. *et al.* Laser Fabrication of Three-Dimensional CAD Scaffolds from Photosensitive Gelatin for Applications in Tissue Engineering. *Biomacromolecules* **12,** 851–858 (2011).

32. Ovsianikov, A. *et al.* Laser Fabrication of 3D Gelatin Scaffolds for the Generation of Bioartificial Tissues. *Materials (Basel).* **4,** 288–299 (2011).

33. Woodfield, T. B. F. *et al.* Design of porous scaffolds for cartilage tissue engineering using a three-dimensional fiber-deposition technique. *Biomaterials* **25,** 4149–61 (2004).

34. Chia, H. N. & Wu, B. M. Recent advances in 3D printing of biomaterials. *J. Biol. Eng.* **9,** 4 (2015).

35. Liu, C. Z. *et al.* Novel 3D collagen scaffolds fabricated by indirect printing technique for tissue engineering. *J. Biomed. Mater. Res. B. Appl. Biomater.* **85,**

36. Liu, C. Z., Sachlos, E., Wahl, D. A., Han, Z. W. & Czernuszka, J. T. On the manufacturability of scaffold mould using a 3D printing technology. *Rapid Prototyp. J.* **13,** 163–174 (2007).

37. Maria, C. De, Acutis, A. De & Vozzi, G. *Indirect Rapid Prototyping for Tissue Engineering. Essentials of 3D Biofabrication and Translation* (Elsevier Inc.,

2015). doi:10.1016/B978-0-12-800972-7/00008-6

38. Burdick, J., Mason, M. & Hinman, A. Delivery of osteoinductive growth factors from degradable PEG hydrogels influences osteoblast differentiation and mineralization. *J. Control. Release* **83,** 53–63 (2002).

39. Chen, F.-M., Shelton, R. M., Jin, Y. & Chapple, I. L. C. Localized delivery of growth factors for periodontal tissue regeneration: Role, strategies, and perspectives. *Med. Res. Rev.* **29,** 472–513 (2009).

40. Nichol, J. W. *et al.* Cell-laden microengineered gelatin methacrylate hydrogels. *Biomaterials* **31,** 5536–44 (2010).

41. Strehin, I., Nahas, Z., Arora, K., Nguyen, T. & Elisseeff, J. A versatile pH sensitive chondroitin sulfate–PEG tissue adhesive and hydrogel. *Biomaterials* **31,** 2788–2797 (2010).

42. Nichol, J. W. & Khademhosseini, A. Modular tissue engineering: engineering biological tissues from the bottom up. *Soft Matter* **5,** 1312 (2009).

43. Chang, R., Nam, J. & Sun, W. Direct Cell Writing of 3D Microorgan for In Vitro Pharmacokinetic Model. *Tissue Eng. Part C Methods* **14,** 157–166 (2008).

44. Ma, P. X. Scaffolds for tissue fabrication. *Mater. Today* **7,** 30–40 (2004).

45. Butler, D. L., Shearn, J. T., Juncosa, N., Dressler, M. R. & Hunter, S. A. Functional tissue engineering parameters toward designing repair and replacement strategies. *Clin. Orthop. Relat. Res.* S190-9 (2004).

46. Peltola, S. M., Melchels, F. P. W., Grijpma, D. W. & Kellomäki, M. *A review of rapid prototyping techniques for tissue engineering purposes. Annals of medicine* **40,** (2008).

47. Yeong, W.-Y. Y. *et al.* Rapid prototyping in tissue engineering: challenges and potential. *Trends Biotechnol.* **22,** 643–652 (2004).

48. Sachlos, E. & Czernuszka, J. T. Making tissue engineering scaffolds work. Review: the application of solid freeform fabrication technology to the production of tissue engineering scaffolds. *Eur. Cell. Mater.* **5,** 29-39-40 (2003).

49. Hölzl, K. *et al.* Bioink properties before, during and after 3D bioprinting.

Biofabrication **8,** 32002 (2016).

50.   Markovic, M. *et al.* Hybrid Tissue Engineering Scaffolds by Combination of Three-Dimensional Printing and Cell Photoencapsulation. *J. Nanotechnol. Eng. Med.* **6,** 21004 (2015).

51.   Arcaute, K., Mann, B. K. & Wicker, R. B. Stereolithography of three-dimensional bioactive poly(ethylene glycol) constructs with encapsulated cells. *Ann. Biomed. Eng.* **34,** 1429–1441 (2006).

52.   Ovsianikov, A. *et al.* Laser photofabrication of cell-containing hydrogel constructs. *Langmuir* **30,** 3787–3794 (2014).

53.   Kang, K. H., Hockaday, L. a & Butcher, J. T. Quantitative optimization of solid freeform deposition of aqueous hydrogels. *Biofabrication* **5,** 35001 (2013).

54.   Golden, A. P. & Tien, J. Fabrication of microfluidic hydrogels using molded gelatin as a sacrificial element. *Lab Chip* **7,** 720 (2007).

55.   Miller, J. S. *et al.* Rapid casting of patterned vascular networks for perfusable engineered three-dimensional tissues. *Nat. Mater.* **11,** 768–774 (2012).

56.   Billiet, T., Gevaert, E., De Schryver, T., Cornelissen, M. & Dubruel, P. The 3D printing of gelatin methacrylamide cell-laden tissue-engineered constructs with high cell viability. *Biomaterials* **35,** 49–62 (2014).

57.   Bertassoni, L. E. *et al.* Hydrogel bioprinted microchannel networks for vascularization of tissue engineering constructs. *Lab Chip* **14,** 2202–2211 (2014).

58.   Kulig, K. M. & Vacanti, J. P. Hepatic tissue engineering. *Transpl. Immunol.* **12,** 303–310 (2004).

59.   Cukierman, E., Pankov, R., Stevens, D. R. & Yamada, K. M. Taking Cell-Matrix Adhesions to the Third Dimension. *Science (80-.).* **294,** 1708–1712 (2001).

60.   Martin, I., Wendt, D. & Heberer, M. The role of bioreactors in tissue engineering. *TRENDS Biotechnol.* **22,** 80–86 (2004).

61.   Mazariegos, G. V. *et al.* First Clinical Use of a Novel Bioartificial Liver Support System (BLSS)+. *Am. J. Transplant.* **2,** 260–266 (2002).

62.   Griffith, L. G. & Naughton, G. Tissue Engineering--Current Challenges and Expanding Opportunities. *Science (80-.).* **295,** 1009–1014 (2002).

63.   Park, S., Kim, G., Jeon, Y. C., Koh, Y. & Kim, W. 3D polycaprolactone scaffolds with controlled pore structure using a rapid prototyping system. *J. Mater. Sci. Mater. Med.* **20,** 229–234 (2009).

64.   Moroni, L., Schotel, R., Hamann, D., de Wijn, J. R. & van Blitterswijk, C. a. 3D Fiber-Deposited Electrospun Integrated Scaffolds Enhance Cartilage Tissue Formation. *Adv. Funct. Mater.* **18,** 53–60 (2008).

65.   Ho, Y.-C., Huang, F.-M. & Chang, Y.-C. Cytotoxicity of formaldehyde on human osteoblastic cells is related to intracellular glutathione levels. *J. Biomed. Mater. Res. B. Appl. Biomater.* **83,** 340–344 (2007).

66.   Wichterle, O. & Lim, D. Hydrophilic Gels for Biological Use. *Nature* **185,** 117–118 (1960).

67.   Hoffman, A. S. Hydrogels for biomedical applications. *Adv. Drug Deliv. Rev.* **54,** 3–12 (2002).

68.   Peppas, N. A., Bures, P., Leobandung, W. & Ichikawa, H. Hydrogels in pharmaceutical formulations. *Eur. J. Pharm. Biopharm.* **50,** 27–46 (2000).

69.   Jagur-Grodzinski, J. Polymeric gels and hydrogels for biomedical and pharmaceutical applications. *Polym. Adv. Technol.* **21,** 27–47

70.   Gupta, P., Vermani, K. & Garg, S. Hydrogels: from controlled release to pH-responsive drug delivery. *Drug Discov. Today* **7,** 569–579 (2002).

71.   Escobar-Chávez, J. J. *et al.* Applications of thermo-reversible pluronic F-127 gels in pharmaceutical formulations. *J Pharm Pharm. Sci* **9,** 339–358 (2006).

72.   Vlierberghe, S. Van, Schacht, E. & Dubruel, P. Reversible gelatin-based hydrogels: Finetuning of material properties. *Eur. Polym. J.* **47,** 1039–1047 (2011).

73.   Geckil, H., Xu, F., Zhang, X., Moon, S. & Demirci, U. Engineering hydrogels as extracellular matrix mimics. *Nanomedicine (Lond)* **5,** 469–484 (2010).

74.   Rowley, J. A., Madlambayan, G. & Mooney, D. J. Alginate hydrogels as

synthetic extracellular matrix materials. *Biomaterials* **20,** 45–53 (1999).

75.   Tibbitt, M. W. & Anseth, K. S. Hydrogels as extracellular matrix mimics for 3D cell culture. *Biotechnol. Bioeng.* **103,** 655–663 (2009).

76.   Li, W.-J. J., Laurencin, C. T., Caterson, E. J., Tuan, R. S. & Ko, F. K. Electrospun nanofibrous structure: a novel scaffold for tissue engineering. *J. Biomed. Mater. Res.* **60,** 613–621 (2002).

77.   Wintermantel, E. *et al.* Tissue engineering scaffolds using superstructures. *Biomaterials* **17,** 83–91 (1996).

78.   Fedorovich, N. E. *et al.* Evaluation of Photocrosslinked Lutrol Hydrogel for Tissue Printing Applications. *Biomacromolecules* **10,** 1689–1696 (2009).

79.   Gaharwar, A. K., Rivera, C. P., Wu, C. J., Schmidt, G. & Gaharwar Rivera ,C.P., Wu, C.-J., Schmidt, G., A. K. Transparent, elastomeric and tough hydrogels from poly(ethylene glycol) and silicate nanoparticles. *Acta Biomater.* **7,** 4139–4148 (2011).

80.   Anseth, K. S., Bowman, C. N. & Brannon-Peppas, L. Mechanical properties of hydrogels and their experimental determination. *Biomaterials* **17,** 1647–1657 (1996).

81.   Sun, J.-Y. *et al.* Highly stretchable and tough hydrogels. *Nature* **489,** 133–6 (2012).

82.   Chen, Z. Z. *et al.* Fabrication of artificial bioactive bone using rapid prototyping. *Rapid Prototyp. J.* **10,** 327–333 (2004).

83.   Chu, T.-M. G., Warden, S. J., Turner, C. H. & Stewart, R. L. Segmental bone regeneration using a load-bearing biodegradable carrier of bone morphogenetic protein-2. *Biomaterials* **28,** 459–67 (2007).

84.   Limpanuphap, S. & Derby, B. Manufacture of biomaterials by a novel printing process. *J. Mater. Sci. Mater. Med.* **13,** 1163–1166 (2002).

85.   Schumacher, M., Deisinger, U., Detsch, R. & Ziegler, G. Indirect rapid prototyping of biphasic calcium phosphate scaffolds as bone substitutes: influence of phase composition, macroporosity and pore geometry on

mechanical properties. *J. Mater. Sci. Mater. Med.* **21,** 3119–27 (2010).

86. Schumacher, M., Uhl, F., Detsch, R., Deisinger, U. & Ziegler, G. Static and dynamic cultivation of bone marrow stromal cells on biphasic calcium phosphate scaffolds derived from an indirect rapid prototyping technique. *J. Mater. Sci. Mater. Med.* **21,** 3039–48 (2010).

87. Drury Mooney, D.J., J. L., Drury, J. L. & Mooney, D. J. Hydrogels for tissue engineering: scaffold design variables and applications. *Biomaterials* **24,** 4337–4351 (2003).

88. Hoffman, A. S. Hydrogels for biomedical applications. *Adv. Drug Deliv. Rev.* **64,** 18–23 (2012).

89. Jia Kiick, K.L., X. Hybrid multicomponent hydrogels for tissue engineering. *Macromol. Biosci.* **9,** 140–156 (2009).

90. Bryant, S. J., Nicodemus, G. D. & Villanueva, I. Designing 3D Photopolymer Hydrogels to Regulate Biomechanical Cues and Tissue Growth for Cartilage Tissue Engineering. *Pharm. Res.* **25,** 2379–2386 (2008).

91. Rutz, A. L., Hyland, K. E., Jakus, A. E., Burghardt, W. R. & Shah, R. N. A Multimaterial Bioink Method for 3D Printing Tunable, Cell-Compatible Hydrogels. *Adv. Mater.* **27,** 1607–1614 (2015).

92. Whitaker, M. J., Quirk, R. A., Howdle, S. M. & Shakesheff, K. M. Growth factor release from tissue engineering scaffolds. *J. Pharm. Pharmacol.* **53,** 1427–1437 (2001).

93. Meenach Anderson, K.W., Hilt, J.Z., S. A. in *Safety of nanoparticles* 131–157 (Springer New York, 2009).

94. Seliktar, D. Extracellular stimulation in tissue engineering. *Ann. New York Acad. Sci.* **1047(1),** 386–394 (2005).

95. Gaharwar Peppas, N.A., Khademhosseini, A., A. K. Nanocomposite hydrogels for biomedical applications. *Biotechnol. Bioeng.* **111,** 441–453 (2014).

96. Schexnailder Gaharwar, A.K., Bartlett II, R.L., Seal, B.L., Schmidt, G., P. J. Tuning cell adhesion by incorporation of charged silicate nanoparticles as

cross-linkers to polyethylene oxide. *Macromol. Biosci.* **10,** 1416–1423 (2010).

97.	Zhu Marchant, R.E., J. Design properties of hydrogel tissue-engineering scaffolds. *Expert Rev. Med. Devices* **8,** 607–626 (2011).

98.	Bayer, O. Das Di-Isocyanat-Polyadditionsverfahren (Polyurethane). *Angew. Chemie* **59,** 257–272 (1947).

99.	Boretos, J. W. & Pierce, W. S. Segmented Polyurethane: A New Elastomer for Biomedical Applications. *Science (80-.).* **158,** (1967).

100.	Zdrahala, R. J. & Zdrahala, I. J. Biomedical Applications of Polyurethanes: A Review of Past Promises, Present Realities, and a Vibrant Future. *J. Biomater. Appl.* **14,** 67–90 (1999).

101.	Martin, D. J., Meijs, G. F., Gunatillake, P. A., McCarthy, S. J. & Renwick, G. M. The effect of average soft segment length on morphology and properties of a series of polyurethane elastomers. II. SAXS-DSC annealing study. *J. Appl. Polym. Sci.* **64,** 803–817 (1997).

102.	Kim, H. Do, Huh, J. H., Kim, E. Y. & Park, C. C. Comparison of properties of thermoplastic polyurethane elastomers with two different soft segments. *J. Appl. Polym. Sci.* **69,** 1349–1355 (1998).

103.	Santerre, J. P., Woodhouse, K., Laroche, G. & Labow, R. S. Understanding the biodegradation of polyurethanes : From classical implants to tissue engineering materials. **26,** 7457–7470 (2005).

104.	Han, D. K., Jeong, S. Y. & Kim, Y. H. Evaluation of blood compatibility of PEO grafted and heparin immobilized polyurethanes. *J. Biomed. Mater. Res.* **23,** 211–28 (1989).

105.	Zhang, C., Zhang, N. & Wen, X. Synthesis and characterization of biocompatible, degradable, light-curable, polyurethane-based elastic hydrogels. *J. Biomed. Mater. Res. A* **82,** 637–50 (2007).

106.	Zhang, L., Jeon, H. K., Malsam, J., Herrington, R. & Macosko, C. W. Substituting soybean oil-based polyol into polyurethane flexible foams. *Polymer (Guildf).* **48,** 6656–6667 (2007).

107. Kwei, T. K. Phase separation in segmented polyurethanes. *J. Appl. Polym. Sci.* **27,** 2891–2899 (1982).

108. Yilgor, E., Yilgor, I. & Yurtsever, E. Hydrogen bonding and polyurethane morphology. I. Quantum mechanical calculations of hydrogen bond energies and vibrational spectroscopy of model compounds. *Polymer (Guildf).* **43,** 6551–6559 (2002).

109. Delebecq, E., Pascault, J. & Boutevin, B. On the Versatility of Urethane: Urea Bonds/Reversibility , Blocked Isocyanate and Non-isocyanate Polyurethane. *Chem. Rev.* **113,** 80–118 (2013).

110. Szycher, M., Poirier, V. L. & Dempsey, D. No TitleSynthesis and fabrication of polyurethane elastomers for cardiac systems. in *Proceeding of the SPE 35th Annual Technical Conference Vol. 35* 743–747 (1977).

111. Tanzi, M. C. *et al.* Cytotoxicity of some catalysts commonly used in the synthesis of copolymers for biomedical use. *J. Mater. Sci. Mater. Med.* **5,** 393–396 (1994).

112. Vermette, P., Griesser, H. J., Laroche, G. & Guidoin, R. *Biomedical Applications of Polyurethanes*. (2001).

113. Slepian, M. J., Alemu, Y., Soares, J. S., G. Smith, R. & Einav, S. The Syncardia™ total artificial heart: in vivo, in vitro, and computational modeling studies. *J. Biomech.* **46,** 266–275 (2013).

114. Parker, M. S. *et al.* Total Artificial Heart Implantation: Clinical Indications, Expected Postoperative Imaging Findings, and Recognition of Complications. *Am. J. Roentgenol.* **202,** W191–W201 (2014).

115. Jansen, P., van Oeveren, W., Capel, A. & Carpentier, A. In vitro haemocompatibility of a novel bioprosthetic total artificial heart. *Eur. J. Cardiothorac. Surg.* **41,** e166-72 (2012).

116. Carpentier, A. *et al.* First clinical use of a bioprosthetic total artificial heart: report of two cases. *Lancet* **386,** 1556–1563 (2015).

117. Alves, M. H. *et al.* Degradable, click poly(vinyl alcohol) hydrogels: characterization of degradation and cellular compatibility. *Biomed. Mater.* **7,**

24106 (2012).

118. Lyman, D. J. & Loo, B. H. New synthetic membranes for dialysis. IV. A copolyether-urethane membrane system. *J. Biomed. Mater. Res.* **1,** 17–26 (1967).

119. Dyson, M., Young, S., Pendle, C. L., Webster, D. F. & Lang, S. M. Comparison of the Effects of Moist and Dry Conditions on Dermal Repair. *J. Invest. Dermatol.* **91,** 434–439 (1988).

120. Winter, G. D. Formation of the Scab and the Rate of Epithelization of Superficial Wounds in the Skin of the Young Domestic Pig. *Nature* **193,** 293–294 (1962).

121. Gorna, K. & Gogolewski, S. Biodegradable polyurethanes for implants. II. In vitro degradation and calcification of materials from poly(epsilon-caprolactone)-poly(ethylene oxide) diols and various chain extenders. *J. Biomed. Mater. Res.* **60,** 592–606 (2002).

122. Guelcher, S. A. Biodegradable polyurethanes: synthesis and applications in regenerative medicine. *Tissue Eng. Part B Rev.* **14,** 3–17 (2008).

123. Grad, S., Kupcsik, L., Gorna, K., Gogolewski, S. & Alini, M. The use of biodegradable polyurethane scaffolds for cartilage tissue engineering: potential and limitations. *Biomaterials* **24,** 5163–5171 (2003).

124. Guan, J., Fujimoto, K. L., Sacks, M. S. & Wagner, W. R. Preparation and characterization of highly porous, biodegradable polyurethane scaffolds for soft tissue applications. *Biomaterials* **26,** 3961–71 (2005).

125. Tanzi, M. C., Mantovani, D., Petrini, P., Guidoin, R. & Laroche, G. Chemical stability of polyether urethanes versus polycarbonate urethanes. *J. Biomed. Mater. Res.* **36,** 550–559 (1997).

126. Nair, L. S. & Laurencin, C. T. Biodegradable polymers as biomaterials. *Prog. Polym. Sci.* **32,** 762–798 (2007).

127. Okada, M. Chemical syntheses of biodegradable polymers. *Prog. Polym. Sci.* **27,** 87–133 (2002).

128. Edlund, U. & Albertsson, A.-C. Polyesters based on diacid monomers. *Adv. Drug Deliv. Rev.* **55,** 585–609 (2003).

129. Middleton, J. C. & Tipton, A. J. Synthetic biodegradable polymers as orthopedic devices. *Biomaterials* **21,** 2335–2346 (2000).

130. Nair, L. S. & Laurencin, C. T. in *Tissue Engineering I* 47–90 (Springer Berlin Heidelberg, 2005). doi:10.1007/b137240

131. Terasaka, S., Iwasaki, Y., Shinya, N. & Uchida, T. Fibrin Glue and Polyglycolic Acid Nonwoven Fabric as a Biocompatible Dural Substitute. *Oper. Neurosurg.* **58,** ONS-134-ONS-139 (2006).

132. Lu, H. H. *et al.* Anterior cruciate ligament regeneration using braided biodegradable scaffolds: in vitro optimization studies. *Biomaterials* **26,** 4805–4816 (2005).

133. Zilberman, M., Nelson, K. D. & Eberhart, R. C. Mechanical properties andin vitro degradation of bioresorbable fibers and expandable fiber-based stents. *J. Biomed. Mater. Res. Part B Appl. Biomater.* **74B,** 792–799 (2005).

134. Nguyen, Q. T., Hwang, Y., Chen, A. C., Varghese, S. & Sah, R. L. Cartilage-like mechanical properties of poly (ethylene glycol)-diacrylate hydrogels. *Biomaterials* **33,** 6682–6690 (2012).

135. Leinonen Sanna, Suokas Esa, Veiranto Minna, Törmälä Pertti, Waris Timo, A. N. Holding Power of Bioabsorbable Ciprofloxacin-Containing Self-reinforced Poly-L/DL-lactide 70/30 Bioactive Glass 13 Miniscrews in Human Cadaver Bone. *J. Craniofac. Surg.* **13,** 212–218 (2002).

136. Gunatillake, P., Mayadunne, R. & Adhikari, R. Recent developments in biodegradable synthetic polymers. *Biotechnol. Annu. Rev.* **12,** 301–347 (2006).

137. Chiari, C. *et al.* A tissue engineering approach to meniscus regeneration in a sheep model. *Osteoarthr. Cartil.* **14,** 1056–1065 (2006).

138. Mondrinos, M. J. *et al.* Porogen-based solid freeform fabrication of polycaprolactone – calcium phosphate scaffolds for tissue engineering. *Biomaterials* **27,** 4399–4408 (2006).

139. Cheung, H. Y., Lau, K. T., Lu, T. P. & Hui, D. A critical review on polymer-based bio-engineered materials for scaffold development. *Compos. Part B Eng.* **38,** 291–300 (2007).

140. Mori, Y. *et al.* A new antithrombogenic material with long polyethyleneoxide chains. *Trans. Am. Soc. Artif. Intern. Organs* **28,** 459–63 (1982).

141. Cruise, G. M., Scharp, D. S. & Hubbell, J. A. Characterization of permeability and network structure of interfacially photopolymerized poly(ethylene glycol) diacrylate hydrogels. *Biomaterials* **19,** 1287–94 (1998).

142. Ifkovits, J. L. & Burdick, J. A. Review: Photopolymerizable and Degradable Biomaterials for Tissue Engineering Applications. *Tissue Eng.* **13,** 2369–2385 (2007).

143. Cruise, G. M. *et al.* In vitro and in vivo performance of porcine islets encapsulated in interfacially photopolymerized poly(ethylene glycol) diacrylate membranes. *Cell Transplant.* **8,** 293–306

144. Cruise, G. M., Hegre, O. D., Scharp, D. S. & Hubbell, J. A. A sensitivity study of the key parameters in the interfacial photopolymerization of poly(ethylene glycol) diacrylate upon porcine islets. *Biotechnol. Bioeng.* **57,** 655–65 (1998).

145. West, J. L. & Hubbell, J. A. Separation of the arterial wall from blood contact using hydrogel barriers reduces intimal thickening after balloon injury in the rat: the roles of medial and luminal factors in arterial healing. *Proc. Natl. Acad. Sci. U. S. A.* **93,** 13188–93 (1996).

146. Bryant, S. J. & Anseth, K. S. The effects of scaffold thickness on tissue engineered cartilage in photocrosslinked poly(ethylene oxide) hydrogels. *Biomaterials* **22,** 619–626 (2001).

147. Elisseeff, J. *et al.* Transdermal photopolymerization of poly(ethylene oxide)-based injectable hydrogels for tissue-engineered cartilage. *Plast. Reconstr. Surg.* **104,** 1014–22 (1999).

148. Elisseeff, J. *et al.* Photoencapsulation of chondrocytes in poly(ethylene oxide)-based semi-interpenetrating networks. *J. Biomed. Mater. Res.* **51,** 164–71 (2000).

149. Elisseeff, J., McIntosh, W., Fu, K., Blunk, T. & Langer, R. Controlled-release of IGF-I and TGF-β1 in a photopolymerizing hydrogel for cartilage tissue engineering. *J. Orthop. Res.* **19,** 1098–1104 (2001).

150. Nuttelman, C. R., Tripodi, M. C. & Anseth, K. S. In vitro osteogenic differentiation of human mesenchymal stem cells photoencapsulated in PEG hydrogels. *J. Biomed. Mater. Res.* **68A,** 773–782 (2004).

151. Burdick, J. a. & Anseth, K. S. Photoencapsulation of osteoblasts in injectable RGD-modified PEG hydrogels for bone tissue engineering. *Biomaterials* **23,** 4315–4323 (2002).

152. Hill-West, J. Inhibition of thrombosis and intimal thickening by in situ photopolymerization of thin hydrogel barriers. *Proc. Natl. Acad. Sci. U. S. A.* **91,** 5967–5971 (1994).

153. West, J. & Hubbell, J. Photopolymerized hydrogel materials for drug delivery applications. *React. Polym.* (1995).

154. Burdick, J. A., Ward, M., Liang, E., Young, M. J. & Langer, R. Stimulation of neurite outgrowth by neurotrophins delivered from degradable hydrogels. *Biomaterials* **27,** 452–9 (2006).

155. PIANTINO, J., BURDICK, J., GOLDBERG, D., LANGER, R. & BENOWITZ, L. An injectable, biodegradable hydrogel for trophic factor delivery enhances axonal rewiring and improves performance after spinal cord injury. *Exp. Neurol.* **201,** 359–367 (2006).

156. Garay, R. P. & Labaune, J. P. Immunogenicity of Polyethylene Glycol (PEG). 104–107 (2011).

157. Jevševar, S., Kunstelj, M. & Porekar, V. G. PEGylation of therapeutic proteins. *Biotechnol. J.* **5,** 113–128 (2010).

158. Veronese, F. M. & Pasut, G. PEGylation, successful approach to drug delivery. *Drug Discov. Today* **10,** 1451–1458 (2005).

159. Ganson, N. J., Kelly, S. J., Scarlett, E., Sundy, J. S. & Hershfield, M. S. Control of hyperuricemia in subjects with refractory gout, and induction of antibody against poly(ethylene glycol) (PEG), in a phase I trial of subcutaneous

PEGylated urate oxidase. *Arthritis Res. Ther.* **8,** R12 (2006).

160. Hamad, I., Hunter, A. C., Szebeni, J. & Moghimi, S. M. Poly(ethylene glycol)s generate complement activation products in human serum through increased alternative pathway turnover and a MASP-2-dependent process. *Mol. Immunol.* **46,** 225–232 (2008).

161. Armstrong, J. K. *et al.* Antibody against poly(ethylene glycol) adversely affects PEG-asparaginase therapy in acute lymphoblastic leukemia patients. *Cancer* **110,** 103–111 (2007).

162. Garratty, G. Modulating the red cell membrane to produce universal/stealth donor red cells suitable for transfusion. *Vox Sang.* **0,** 071127145052003–??? (2007).

163. Hoogenboom, R. Poly(2-oxazoline)s: A Polymer Class with Numerous Potential Applications. *Angew. Chemie Int. Ed.* **48,** 7978–7994 (2009).

164. Hern, D. L. & Hubbell, J. A. Incorporation of adhesion peptides into nonadhesive hydrogels useful for tissue resurfacing. *J. Biomed. Mater. Res.* **39,** 266–76 (1998).

165. Marletta, G., Ciapetti, G., Satriano, C., Pagani, S. & Baldini, N. The effect of irradiation modification and RGD sequence adsorption on the response of human osteoblasts to polycaprolactone. *Biomaterials* **26,** 4793–4804 (2005).

166. Hunt, N. C. & Grover, L. M. Cell encapsulation using biopolymer gels for regenerative medicine. *Biotechnol. Lett.* **32,** 733–742 (2010).

167. Weigel, P. H., Hascall, V. C. & Tammi, M. Hyaluronan synthases. *J. Biol. Chem.* **272,** 13997–4000 (1997).

168. Brekke, J. H. & Thacker, K. in *An introduction to Biomaterials* (eds. Guelcher, S. A. & Hollinger, J.) 219–248 (Taylor & Francis Group, 2006).

169. Mori, M., Yamaguchi, M., Sumitomo, S. & Takai, Y. Hyaluronan-based Biomaterials in Tissue Engineering. *ACTA Histochem. Cytochem.* **37,** 1–5 (2004).

170. Lepidi, S. *et al.* Hyaluronan Biodegradable Scaffold for Small-caliber Artery

Grafting: Preliminary Results in an Animal Model. *Eur. J. Vasc. Endovasc. Surg.* **32,** 411–417 (2006).

171. Hunt, D. R., Jovanovic, S. A., Wikesjö, U. M. E., Wozney, J. M. & Bernard, G. W. Hyaluronan Supports Recombinant Human Bone Morphogenetic Protein-2 Induced Bone Reconstruction of Advanced Alveolar Ridge Defects in Dogs. A Pilot Study. *J. Periodontol.* **72,** 651–658 (2001).

172. Eppley, B. L. & Dadvand, B. Injectable Soft-Tissue Fillers: Clinical Overview. *Plast. Reconstr. Surg.* **118,** 98e–106e (2006).

173. Kato, Y., Nakamura, S. & Nishimura, M. Beneficial actions of hyaluronan (HA) on arthritic joints: Effects of molecular weight of HA on elasticity of cartilage matrix. *Biorheology* **43,** 347–354 (2006).

174. Volpi, N. Therapeutic Applications of Glycosaminoglycans. *Curr. Med. Chem.* **13,** 1799–1810 (2006).

175. Kosir, M. A., Quinn, C. C. V., Wang, W. & Tromp, G. Matrix Glycosaminoglycans in the Growth Phase of Fibroblasts: More of the Story in Wound Healing. *J. Surg. Res.* **92,** 45–52 (2000).

176. Chan, P. S., Caron, J. P., Rosa, G. J. M. & Orth, M. W. Glucosamine and chondroitin sulfate regulate gene expression and synthesis of nitric oxide and prostaglandin E2 in articular cartilage explants. *Osteoarthr. Cartil.* **13,** 387–394 (2005).

177. Silbert, J. E. & Sugumaran, G. Biosynthesis of Chondroitin/Dermatan Sulfate. *IUBMB Life (International Union Biochem. Mol. Biol. Life)* **54,** 177–186 (2002).

178. Gilbert, M. E. *et al.* Chondroitin Sulfate Hydrogel and Wound Healing in Rabbit Maxillary Sinus Mucosa. *Laryngoscope* **114,** 1406–1409 (2004).

179. van Susante, J. L. . *et al.* Linkage of chondroitin-sulfate to type I collagen scaffolds stimulates the bioactivity of seeded chondrocytes in vitro. *Biomaterials* **22,** 2359–2369 (2001).

180. Kirker, K. R., Luo, Y., Nielson, J. H., Shelby, J. & Prestwich, G. D. Glycosaminoglycan hydrogel films as bio-interactive dressings for wound healing. *Biomaterials* **23,** 3661–3671 (2002).

181. Bergman, K. *et al.* Injectable cell-free template for bone-tissue formation. *J. Biomed. Mater. Res. Part A* **91A,** 1111–1118 (2009).

182. Azab, A. K. *et al.* Crosslinked chitosan implants as potential degradable devices for brachytherapy: In vitro and in vivo analysis. *J. Control. Release* **111,** 281–289 (2006).

183. Shi, C. *et al.* Therapeutic Potential of Chitosan and Its Derivatives in Regenerative Medicine. *J. Surg. Res.* **133,** 185–192 (2006).

184. Klöck, G. *et al.* Biocompatibility of mannuronic acid-rich alginates. *Biomaterials* **18,** 707–713 (1997).

185. Simmons, C. A., Alsberg, E., Hsiong, S., Kim, W. J. & Mooney, D. J. Dual growth factor delivery and controlled scaffold degradation enhance in vivo bone formation by transplanted bone marrow stromal cells. *Bone* **35,** 562–569 (2004).

186. George, M. & Abraham, T. E. Polyionic hydrocolloids for the intestinal delivery of protein drugs: Alginate and chitosan — a review. *J. Control. Release* **114,** 1–14 (2006).

187. Baruch, L. & Machluf, M. Alginate–chitosan complex coacervation for cell encapsulation: Effect on mechanical properties and on long-term viability. *Biopolymers* **82,** 570–579 (2006).

188. Stone, C. A., Wright, H., Devaraj, V. S., Clarke, T. & Powell, R. Healing at skin graft donor sites dressed with chitosan. *Br. J. Plast. Surg.* **53,** 601–606 (2000).

189. Burkatovskaya, M. *et al.* Use of chitosan bandage to prevent fatal infections developing from highly contaminated wounds in mice. *Biomaterials* **27,** 4157–4164 (2006).

190. Qiu, X. & Hu, S. 'Smart' Materials Based on Cellulose: A Review of the Preparations, Properties, and Applications. *Materials (Basel).* **6,** 738–781 (2013).

191. Cheng, R., Feng, F., Meng, F., Deng, C. & Feijen, J. Glutathione-responsive nano-vehicles as a promising platform for targeted intracellular drug and gene delivery. *J. Control. Release* **152,** 2–12 (2011).

192. Delcea, M., Möhwald, H. & Skirtach, A. G. Stimuli-responsive LbL capsules and nanoshells for drug delivery. *Adv. Drug Deliv. Rev.* **63,** 730–747 (2011).

193. Manchun, S., Dass, C. R. & Sriamornsak, P. Targeted therapy for cancer using pH-responsive nanocarrier systems. *Life Sci.* **90,** 381–387 (2012).

194. Zhang, Q., Re Ko, N. & Kwon Oh, J. Recent advances in stimuli-responsive degradable block copolymer micelles: synthesis and controlled drug delivery applications. *Chem. Commun.* **48,** 7542 (2012).

195. Prabaharan, M. & Mano, J. F. Stimuli-Responsive Hydrogels Based on Polysaccharides Incorporated with Thermo-Responsive Polymers as Novel Biomaterials. *Macromol. Biosci.* **6,** 991–1008 (2006).

196. Sannino, A., Demitri, C. & Madaghiele, M. Biodegradable Cellulose-based Hydrogels: Design and Applications. *Materials (Basel).* **2,** 353–373 (2009).

197. Posey-Dowty, J. D. *et al.* Zero-order release formulations using a novel cellulose ester. *Cellulose* **14,** 73–83 (2006).

198. Gautam, S., Dinda, A. K. & Mishra, N. C. Fabrication and characterization of PCL/gelatin composite nanofibrous scaffold for tissue engineering applications by electrospinning method. *Mater. Sci. Eng. C. Mater. Biol. Appl.* **33,** 1228–35 (2013).

199. Gómez-Guillén, M. C., Giménez, B., López-Caballero, M. E. & Montero, M. P. Functional and bioactive properties of collagen and gelatin from alternative sources: A review. *Food Hydrocoll.* **25,** 1813–1827 (2011).

200. Brodsky, B. & Ramshaw, J. A. M. The collagen triple-helix structure. *Matrix Biol.* **15,** 545–554 (1997).

201. Djagny, V. B., Wang, Z. & Xu, S. Gelatin: a valuable protein for food and pharmaceutical industries: review. *Crit. Rev. Food Sci. Nutr.* **41,** 481–92 (2001).

202. Burdick, J. *Biomaterials for Tissue Engineering Applications: A Review of the Past and Future Trends.* (SpringerWienNewYork, 2010).

203. Van Den Bulcke, A. I. *et al.* Structural and Rheological Properties of

Methacrylamide Modified Gelatin Hydrogels. *Biomacromolecules* **1,** 31–38 (2000).

204. Manjubala, I. *et al.* Biomimetic mineral-organic composite scaffolds with controlled internal architecture. *J. Mater. Sci. Mater. Med.* **16,** 1111–9 (2005).

205. Sachlos, E., Reis, N., Ainsley, C., Derby, B. & Czernuszka, J. T. A process to make collagen scaffolds with an artificial circulatory system using rapid prototyping. *Mater. Res. Soc. Symp. Proc.* **758,** (2002).

206. Chu, T.-M. G. M. G., Halloran, J. W., Hollister, S. J. & Feinberg, S. E. Hydroxyapatite implants with designed internal architecture. *J. Mater. Sci. Mater. Med.* **12,** 471–478 (2001).

207. Tan, J. Y., Chua, C. K. & Leong, K. F. Fabrication of channeled scaffolds with ordered array of micro-pores through microsphere leaching and indirect Rapid Prototyping technique. 83–96 (2013). doi:10.1007/s10544-012-9690-3

208. Rumpler, M., Woesz, A., Dunlop, J. W. ., van Dongen, J. T. & Fratzl, P. The effect of geometry on three-dimensional tissue growth. *J. R. Soc. Interface* **5,** 1173–1180 (2008).

209. Hattiangadi, A. & Bandyopadhyay, A. Processing , Characterization and Modeling of Non-Random Porous Ceramic Structures. *Int. Solid Free. Fabr. Symp.* 319–326 (1999).

210. Hollister, S. J., Levy, R. a, Chu, T. M., Halloran, J. W. & Feinberg, S. E. An image-based approach for designing and manufacturing craniofacial scaffolds. *Int. J. Oral Maxillofac. Surg.* **29,** 67–71 (2000).

211. Uchida, T. *et al.* Development of biodegradable scaffolds based on patient-specific arterial configuration. *J. Biotechnol.* **133,** 213–8 (2008).

212. Wang, P., Hu, J. & Ma, P. X. The engineering of patient-specific, anatomically shaped, digits. *Biomaterials* **30,** 2735–40 (2009).

213. Lee, J.-Y., Choi, B., Wu, B. & Lee, M. Customized biomimetic scaffolds created by indirect three-dimensional printing for tissue engineering. *Biofabrication* **5,** (2013).

214. Skoog, S. a, Goering, P. L. & Narayan, R. J. Stereolithography in tissue engineering. *J. Mater. Sci. Mater. Med.* **25,** 845–856 (2013).

215. DeBeer, N. & Merwe, A. Van Der. Patient-specific intervertebral disc implants using rapid manufacturing technology. *Rapid Prototyp. J.* **19,** 126–139 (2013).

216. Lam, C. X. ., Mo, X. ., Teoh, S. . & Hutmacher, D. . Scaffold development using 3D printing with a starch-based polymer. *Mater. Sci. Eng. C* **20,** 49–56 (2002).

217. Lu, L. *et al.* Biocompatibility and biodegradation studies of PCL / b -TCP bone tissue scaffold fabricated by structural porogen method. *J. Mater. Sci. Mater. Med.* **23,** 2217–2226 (2012).

218. Mondrinos, M. J. *et al.* Porogen-based solid freeform fabrication of polycaprolactone-calcium phosphate scaffolds for tissue engineering. *Biomaterials* **27,** 4399–408 (2006).

219. Taboas, J. . M., Maddox, R. . D., Krebsbach, P. . H. & Hollister, S. . J. Indirect solid free form fabrication of local and global porous, biomimetic and composite 3D polymer-ceramic scaffolds. *Biomaterials* **24,** 181–194 (2003).

220. Torgersen, J. *et al.* Photo-sensitive hydrogels for three-dimensional laser microfabrication in the presence of whole organisms. *J. Biomed. Opt.* **17,** 105008 (2012).

221. Liska, R., Schwager, F., Maier, C., Cano-Vives, R. & Stampfl, J. Water-soluble photopolymers for rapid prototyping of cellular materials. *J. Appl. Polym. Sci.* **97,** 2286–2298 (2005).

222. Woesz, a. *et al.* Towards bone replacement materials from calcium phosphates via rapid prototyping and ceramic gelcasting. *Mater. Sci. Eng. C* **25,** 181–186 (2005).

223. Kang, H. W., Rhie, J.-W. W. & Cho, D. W. Development of a bi-pore scaffold using indirect solid freeform fabrication based on microstereolithography technology. *Microelectron. Eng.* **86,** 941–944 (2009).

224. Mäkitie, A. a *et al.* Novel additive manufactured scaffolds for tissue engineered trachea research. *Acta Otolaryngol.* **133,** 412–417 (2013).

225. Yang, S., Leong, K.-F., Zhaohui, D. & Chua, C. Review The Design of Scaffolds for Use in Tissue Engineering. Part II. Rapid Prototyping Techniques. *Tissue Eng.* **8,** 1–11 (2002).

226. Detsch, R., Uhl, F., Deisinger, U. & Ziegler, G. 3D-Cultivation of bone marrow stromal cells on hydroxyapatite scaffolds fabricated by dispense-plotting and negative mould technique. *J. Mater. Sci. Mater. Med.* **19,** 1491–1496 (2008).

227. Deisinger, U. *et al.* Fabrication of tailored hydroxyapatite scaffolds: Comparison between a direct and an indirect rapid prototyping technique. *Key Eng. Mater.* **361–363 II,** 915–918 (2008).

228. Therriault, D., White, S. R. & Lewis, J. a. Chaotic mixing in three-dimensional microvascular networks fabricated by direct-write assembly. *Nat. Mater.* **2,** 265–271 (2003).

229. Therriault, D., Shepherd, R. F., White, S. R. & Lewis, J. a. Fugitive inks for direct-write assembly of three-dimensional microvascular networks. *Adv. Mater.* **17,** 395–399 (2005).

230. Barry, R. A. *et al.* Direct-Write Assembly of 3D Hydrogel Scaffolds for Guided Cell Growth. *Adv. Mater.* **21,** 2407–2410 (2009).

231. Wu, W. *et al.* Direct-write assembly of biomimetic microvascular networks for efficient fluid transport. *Soft Matter* **6,** 739 (2010).

232. Brown, T. D., Dalton, P. D. & Hutmacher, D. W. Direct Writing By Way of Melt Electrospinning. *Adv. Mater.* **23,** 5651–5657 (2011).

233. Haigh, J. N. *et al.* Hierarchically Structured Porous Poly(2-oxazoline) Hydrogels. *Macromol. Rapid Commun.* n/a-n/a (2015). doi:10.1002/marc.201500495

234. Lee, M., Dunn, J. C. Y. & Wu, B. M. Scaffold fabrication by indirect three-dimensional printing. *Biomaterials* **26,** 4281–4289 (2005).

235. Lee, M., Wu, B. M. & Dunn, J. C. Y. Effect of scaffold architecture and pore size on smooth muscle cell growth. *J. Biomed. Mater. Res. Part A* **87A,** 1010–1016 (2008).

236. Melican, M. C. *et al.* Three-dimensional printing and porous metallic surfaces: a new orthopedic application. *J. Biomed. Mater. Res.* **55,** 194–202 (2001).

237. Sachlos, E., Reis, N., Ainsley, C., Derby, B. & Czernuszka, J. T. Novel collagen scaffolds with predefined internal morphology made by solid freeform fabrication. *Biomaterials* **24,** 1487–1497 (2003).

238. Li, L. H. *et al.* In vitro bioactivity of bioresorbable porous polymeric scaffolds incorporating hydroxyapatite microspheres. *Acta Biomater.* **6,** 2525–2531 (2010).

239. Liu, M. J. J., Chou, S. M., Chua, C. K., Tay, B. C. M. & Ng, B. K. The development of silk fibroin scaffolds using an indirect rapid prototyping approach: morphological analysis and cell growth monitoring by spectral-domain optical coherence tomography. *Med. Eng. Phys.* **35,** 253–62 (2013).

240. Wilson, C. E. *et al.* Design and fabrication of standardized hydroxyapatite scaffolds with a defined macro-architecture by rapid prototyping for bone-tissue-engineering research. *J. Biomed. Mater. Res. A* **68,** 1–10 (2003).

241. Tan, J. Y., Chua, C. K. & Leong, K. F. Indirect fabrication of gelatin scaffolds using rapid prototyping technology. *Virtual Phys. Prototyp.* **5,** 45–53 (2010).

242. Kang, H.-W. & Cho, D.-W. Development of an indirect stereolithography technology for scaffold fabrication with a wide range of biomaterial selectivity. *Tissue Eng. Part C. Methods* **18,** 719–29 (2012).

243. Chu, T. M. G., Orton, D. G., Hollister, S. J., Feinberg, S. E. & Halloran, J. W. Mechanical and in vivo performance of hydroxyapatite implants with controlled architectures. *Biomaterials* **23,** 1283–93 (2002).

244. Park, C. H. *et al.* Biomimetic hybrid scaffolds for engineering human tooth-ligament interfaces. *Biomaterials* **31,** 5945–5952 (2010).

245. Park, C. H. *et al.* Tissue engineering bone-ligament complexes using fiber-guiding scaffolds. *Biomaterials* **33,** 137–145 (2012).

246. Sodian, R. *et al.* Application of stereolithography for scaffold fabrication for tissue engineered heart valves. *Am. Soc. Artif. Intern. Organs J.* **48,** 12–16 (2002).

247. Chen, V. J., Smith, L. A. & Ma, P. X. Bone regeneration on computer-designed nano-fibrous scaffolds. **27,** 3973–3979 (2006).

248. Seol, Y.-J. J., Kim, J. Y., Park, E. K., Kim, S.-Y. Y. & Cho, D.-W. W. Fabrication of a hydroxyapatite scaffold for bone tissue regeneration using microstereolithography and molding technology. *Microelectron. Eng.* **86,** 1443–1446 (2009).

249. Chang, P.-C. *et al.* Bone tissue engineering with novel rhBMP2-PLLA composite scaffolds. *J. Biomed. Mater. Res. A* **81,** 771–780 (2007).

250. Bose, S., Darsell, J., Kintner, M., Hosick, H. & Bandyopadhyay, A. Pore size and pore volume effects on alumina and TCP ceramic scaffolds. *Mater. Sci. Eng. C* **23,** 479–486 (2003).

251. Bose, S., Suguira, S. & Bandyopadhyay, A. Processing of controlled porosity ceramic structures via fused deposition. *Scr. Mater.* **41,** 1009–1014 (1999).

252. Sodian, R. *et al.* Fabrication of a trileaflet heart valve scaffold from a polyhydroxyalkanoate biopolyester for use in tissue engineering. *Tissue Eng.* **6,** 183–8 (2000).

253. Hollister, S. *et al.* Engineering craniofacial scaffolds. *Orthod. Craniofac. Res.* **8,** 162–173 (2005).

254. Sachlos, E., Reis, N., Ainsley, C., Derby, B. & Czernuszka, J. T. A Process to Make Xollagen Scaffolds with an Artificial Circulatory System using Rapid Prototyping. in *Materials Research Society Symposium Proceedings, Vol 758* (2002).

255. VanDenBulcke, A. I. *et al.* Structural and Rheological Properties of Methacrylamide Modified Gelatin Hydrogels. *Biomacromolecules* **1,** 31–38 (2000).

256. Van Vlierberghe, S. *et al.* Hydrogel network formation revised: high-resolution magic angle spinning nuclear magnetic resonance as a powerful tool for measuring absolute hydrogel cross-link. *Appl. …* **64,** 1176–1180 (2010).

257. VanRie, J. *et al.* Cryogel-PCL combination scaffolds for bone tissue repair. *J. Mater. Sci. Mater. Med.* **26,** 5465 (2015).

258. Park, C. H. *et al.* Tissue engineering bone-ligament complexes using fi ber-guiding scaffolds. *Biomaterials* **33,** 137–145 (2012).

259. Mantila Roosa, S. M., Kemppainen, J. M., Moffitt, E. N., Krebsbach, P. H. & Hollister, S. J. The pore size of polycaprolactone scaffolds has limited influence on bone regeneration in an in vivo model. *J. Biomed. Mater. Res. - Part A* **92,** 359–368 (2010).

260. Saito, E. *et al.* Experimental and computational characterization of designed and fabricated 50:50 PLGA porous scaffolds for human trabecular bone applications. *J. Mater. Sci. Mater. Med.* **21,** 2371–83 (2010).

261. Moore, M. J. *et al.* Multiple-channel scaffolds to promote spinal cord axon regeneration. **27,** 419–429 (2006).

262. Rumpler, M. *et al.* Three-dimensional growth behavior of osteoblasts on biomimetic hydroxylapatite scaffolds. *J Biomed Mater Res* **81A,** 40–50 (2007).

263. Lin, C.-Y. *et al.* Functional Bone Engineering Using ex Vivi Gene THerapy and Topology-Optimized, Biodegradable Polymer Composite Scaffolds. *Tissue Eng.* **11,** 1589–1598 (2005).

264. Liao, E., Yaszemski, M., Krebsbach, P. & Hollister, S. Tissue-engineered cartilage constructs using composite hyaluronic acid/collagen I hydrogels and designed poly(propylene fumarate) scaffolds. *Tissue Eng.* **13,** 537–550 (2007).

265. Jain, R. K., Au, P., Tam, J., Duda, D. G. & Fukumura, D. Engineering vascularized tissue. *Nat. Biotechnol.* **23,** 821–3 (2005).

266. Liu, R. H. *et al.* Passive mixing in a three-dimensional serpentine microchannel. *J. Microelectromechanical Syst.* **9,** 190–197 (2000).

267. Higgins, J. M., Eddington, D. T., Bhatia, S. N. & Mahadevan, L. Sickle cell vasoocclusion and rescue in a microfluidic device. *Proc. Natl. Acad. Sci. U. S. A.* **104,** 20496–500 (2007).

268. Runyon, M. K., Johnson-Kerner, B. L., Kastrup, C. J., Van Ha, T. G. & Ismagilov, R. F. Propagation of blood clotting in the complex biochemical network of hemostasis is described by a simple mechanism. *J. Am. Chem. Soc.* **129,** 7014–5 (2007).

269. Lim, D., Kamotani, Y., Cho, B., Mazumder, J. & Takayama, S. Fabrication of microfluidic mixers and artificial vasculatures using a high-brightness diode-pumped Nd:YAG laser direct write method. *Lab Chip* **3,** 318–23 (2003).

270. Verschooten, T., Ottevaere, H., Vervaeke, M., Van Erps, J. & Thienpont, H. Proof-of-concept demonstration of a total internal reflection based module for fluorescence and absorbance detection using a 3D-printed syringe pump. *Proc. SPIE* **9130,** 91300E–91300E–11 (2014).

271. Grumann, M. *et al.* Sensitivity enhancement for colorimetric glucose assays on whole blood by on-chip beam-guidance. *Biomed. Microdevices* **8,** 209–214 (2006).

272. De Coster, D. *et al.* Free-Form Optics Enhanced Confocal Raman Spectroscopy for Optofluidic Lab-on-Chips. *IEEE J. Sel. Top. quantum Electron.* **21,** 2701108 (2015).

273. Gadegaard, N., Mosler, S. & Larsen, N. B. Biomimetic polymer nanostructures by injection molding. *Macromol. Mater. Eng.* **288,** 76–83 (2003).

274. De Coster, D. *et al.* Mass-manufacturable polymer microfluidic device for dual fiber optical trapping. *Opt. Express* **23,** 30991 (2015).

275. Vig, A. L. *et al.* Roll-to-roll fabricated lab-on-a-chip devices. *J. Micromechanics Microengineering* **21,** 35006 (2011).

276. Venugopal, J. R., Low, S., Choon, A. T., Kumar, a B. & Ramakrishna, S. Nanobioengineered electrospun composite nanofibers and osteoblasts for bone regeneration. *Artif. Organs* **32,** 388–397 (2008).

277. Li, W.-J. W.-J. *et al.* A three-dimensional nanofibrous scaffold for cartilage tissue engineering using human mesenchymal stem cells. *Biomaterials* **26,** 599–609 (2005).

278. Li, W.-J., Jiang, Y. J. & Tuan, R. S. Cell-nanofiber-based cartilage tissue engineering using improved cell seeding, growth factor, and bioreactor technologies. *Tissue Eng. Part A* **14,** 639–48 (2008).

279. Lee, S., Yoo, J. & Lim, G. In vitro evaluation of electrospun nanofiber scaffolds for vascular graft application. *J. Biomed. Mater. Res.* **83,** 999–1008 (2007).

280. Xu, C. Y., Inai, R., Kotaki, M. & Ramakrishna, S. Aligned biodegradable nanofibrous structure: a potential scaffold for blood vessel engineering. *Biomaterials* **25,** 877–886 (2004).

281. McMahon, R. E. *et al.* Hydrogel-electrospun mesh composites for coronary artery bypass grafts. *Tissue Eng. Part C* **17,** 451–461 (2011).

282. Detta, N. *et al.* Novel electrospun polyurethane/gelatin composite meshes for vascular grafts. *J. Mater. Sci. Mater. Med.* **21,** 1761–1769 (2010).

283. Koh, H. S., Yong, T., Chan, C. K. & Ramakrishna, S. Enhancement of neurite outgrowth using nano-structured scaffolds coupled with laminin. *Biomaterials* **29,** 3574–3582 (2008).

284. Prabhakaran, M. P. *et al.* Electrospun biocomposite nanofibrous scaffolds for neural tissue engineering. *Tissue Eng. Part A* **14,** 1787–1797 (2008).

285. Yang, F. *et al.* Fabrication of nano-structured porous PLLA scaffold intended for nerve tissue engineering. *Biomaterials* **25,** 1891–1900 (2004).

286. Ghasemi-Mobarakeh, L., Prabhakaran, M. P., Morshed, M., Nasr-Esfahani, M. H. & Ramakrishna, S. Electrospun poly(ε-caprolactone)/gelatin nanofibrous scaffolds for nerve tissue engineering. *Biomaterials* **29,** 4532–4539 (2008).

287. Baker, S. C. *et al.* Characterisation of electrospun polystyrene scaffolds for three-dimensional in vitro biological studies. *Biomaterials* **27,** 3136–3146 (2006).

288. Stubbe, B. & Compernolle, N. Biopolymer-based wound dressings: from film casting towards electrospinning. *2014 Annu. Meet.* (2014).

289. Ishihara, M. *et al.* Photocrosslinkable chitosan as a dressing for wound occlusion and accelerator in healing process. *Biomaterials* **23,** 833–840 (2002).

290. Khil, M.-S., Cha, D.-I., Kim, H.-Y., Kim, I.-S. & Bhattarai, N. Electrospun nanofibrous polyurethane membrane as wound dressing. *J. Biomed. Mater. Res.* **67B,** 675–679 (2003).

291. Rujitanaroj, P., Pimpha, N. & Supaphol, P. Wound-dressing materials with antibacterial activity from electrospun gelatin fiber mats containing silver

nanoparticles. *Polymer (Guildf).* **49,** 4723–4732 (2008).

292. Van Vlierberghe, S. *et al.* Toward modulating the architecture of hydrogel scaffolds: curtains versus channels. *J. Mater. Sci. Mater. Med.* **19,** 1459–1466 (2008).

293. Vlierberghe, S. Van *et al.* Porous gelatin hydrogels: 1. Cryogenic formation and structure analysis. *Biomacromolecules* **8,** 331–7 (2007).

Chapter 1: Introduction

Chapter 2:

Flexible Oligomer Spacers as Key to Solid-State Photopolymerization of Hydrogel Precursors

This chapter describes the synthesis and characterization of the solid state reactive materials developed. Parts of this chapter have been published as communication entitled "Flexible Oligomer Spacers as the Key to Solid-State Photopolymerization of Hydrogel Precursors" (Houben, A. et al. Flexible Oligomer Spacers as the Key to Solid-State Photopolymerization of Hydrogel Precursors. Mater. Today Chem. **4,** *84–89 (2017)).*[1]

Chapter 2: Flexible Oligomer Spacers as Key to Solid-State Photopolymerization of Hydrogel Precursors

2.1. Introduction

As mentioned in the previous chapter, photopolymerization is an attractive technique to create tunable crosslinked polymer networks as it offers temporal and spatial control over the reaction.[2,3] Furthermore, it is an energy-efficient process, as the polymerization can be initiated using low-energy UV irradiation. Therefore, this technique has been widely used to prepare crosslinked hydrogel networks starting from synthetic and natural polymers modified with photoreactive groups such as (meth)acrylates.[4–6] Synthetic hydrogels are especially appealing as they can be prepared in a controllable and reproducible way, which in turn results in tailored mechanical and swelling properties.[7]

Efficient crosslinking of conventional photoreactive hydrogel precursors relies on the mobility of the reactive groups and, hence, is typically addressed from the liquid state. To this end, solid precursors are processed from the melt at elevated temperature or after dissolution in a suitable solvent. However, this represents a limiting factor for many processing techniques (e.g. electrospinning, rapid prototyping, …) as these result in solid materials when processing is complete. This renders photocrosslinkable hydrogel materials hard to process into well-defined shapes with specific internal characteristics important towards their functional properties in e.g. biomedical applications. [8–12]

Herein, a model hydrogel precursor is introduced that overcomes this challenge using a prepolymer designed to enable successful crosslinking in the solid state. Not surprisingly, little has been reported on solid-state photopolymerization (SSPP) in literature as polymerization kinetics and functional group conversion are naturally expected to be inefficient. The few papers refer to monomer compounds (e.g. octadecyl (meth)acrylate),[13–15] but so far, solid-state photopolymerization of macromolecular precursors and the concurrent technological benefit have never been described to the best of our knowledge.

In the present approach, the hydrogel precursor is based on a polyethylene glycol (PEG) backbone which forms a semi-crystalline solid at room temperature. Photocrosslinking in the solid-state is promoted by the introduction of an oligomeric flexible spacer which separates the photoreactive acrylate groups from the immobilized

PEG backbone polymer. Though spacers have already been applied to introduce cell- and protein interactive moieties in hydrogels,[16–20] their use to provide motional freedom for reactivity enhancement has not been described to date.

2.2. Materials and Methods

2.2.1. Synthesis of model precursor

Prior to the synthesis of the precursors, Poly(ethylene glycol) (MW 2000 g mol^{-1}, Merck) (PEG$_{2000}$) was vacuum dried under a N$_2$ blanket in a double walled glass reactor equipped with a stirrer and connected to an oil bath heating system. Subsequently, the inhibitor 2,6-di-tert-butyl-4-methylphenol (BHT, Innochem GMBH) was added as a radical scavenger and phosphoric acid (H$_3$PO$_4$) was introduced to inhibit the reaction of the carboxyl groups present on the PEG (1.35 mmol g^{-1}). The synthesis of PEG2000-OEOAcr occurred through a two-step process (see Figure 1). In a first step, PEG was linked to isophorone diisocyanate (IPDI) in a 1:2 stoichiometric ratio. Reaction between the hydroxyl groups of PEG and the isocyanates at 65°C was catalyzed by addition of 300 ppm bismuth neodecanoate which is proceeded by an exotherm occurring in a temperature range of 80-90°C. The urethane formation reaction further continued at T = 80°C. A potentiometric back titration allowed to monitor the progress of the urethane formation reaction. If the expected quantity of NCO groups is higher than 10%, the sample weight should be around 0.2 g. If the expected quantity of NCO groups is less than 2%, the sample weight should be around 1 g. The sample is dissolved in 3 ml of a di-n-butylamine solution (64.5 g diluted to 1 L with N-methylpyrrolidone, NMP), and 50 ml of NMP is added. The excess of di-n-butylamine is titrated potentiometrically using a 0.1 M HCl solution. A degree of conversion for the acrylate groups of 50 % after the first reaction step was targeted, corresponding with an NCO-value of 3.44 %. When the NCO-value decreased below the theoretical value, the selected end group (monoacrylated oligo(ethylene oxide) (OEOAcr, MW 336 g mol^{-1}, GEO Specialty Chemicals), monoacrylated oligo(propylene oxide) (OPOAcr, MW 420 g mol^{-1}, GEO Specialty Chemicals), monoacrylated oligo(ϵ-caprolactone) (OClAcr, 334 g mol^{-1}, Allnex) or hydroxyethylacrylate (HEA, 24 g mol^{-1}, Allnex) was added dropwise under air atmosphere in the presence of 300 ppm bismuth neodecanoate. Next, the temperature was raised to 80°C. The reaction progress was monitored by measuring the NCO value via potentiometric titration. The reaction proceeded until the NCO value reached the theoretical value of 0.02 meq/g (value when half of the acrylate groups have reacted). After completion of the reaction, 500 ppm phenothiazine (PTZ, Sigma Aldrich) and 500 ppm triphenyl phosphite (TPP,

Sigma-Aldrich) were added as stabilizers and the reaction was completed by cooling to room temperature. Subsequently, the PEG2000-OEOAcr was filtered and transferred into a plastic container and stored at room temperature. Synthesis scale ranged from 100 g up to 5 kg.
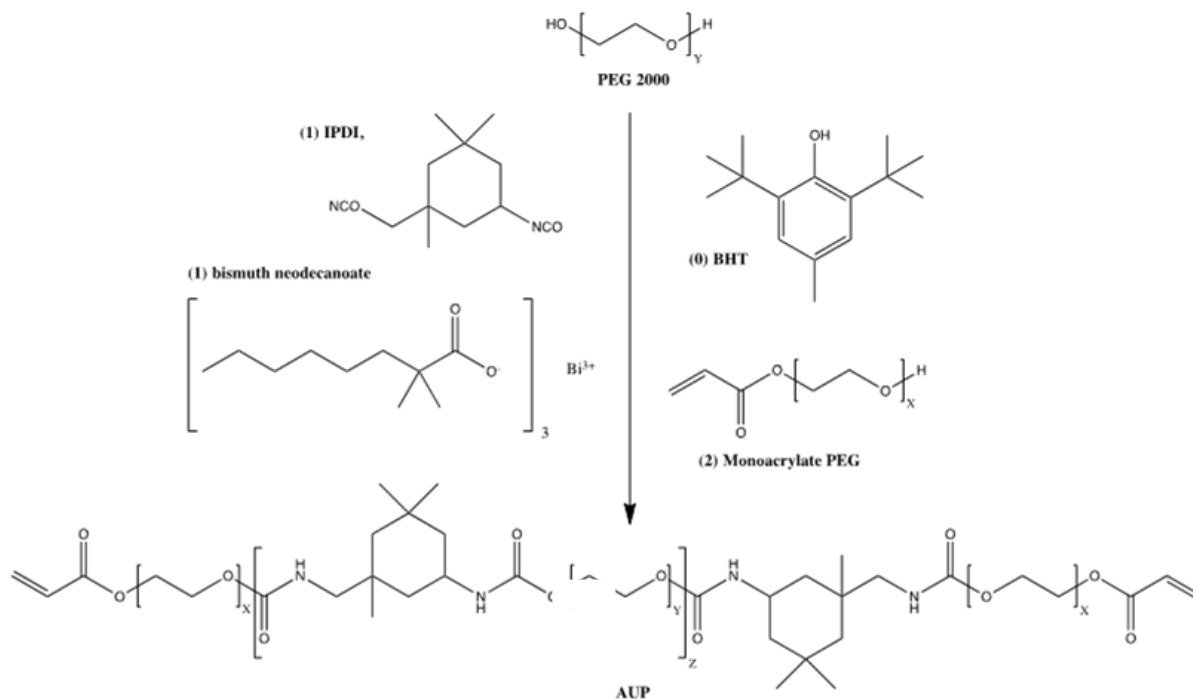
Figure 1: Synthesis scheme of the model precursor PEG$_{2000}$-OEOAcr

2.2.2. Gel permeation chromatography

The number average molecular weight (M_n), the weight average molecular weight (Mw) and the polydispersity (PDI) were determined by conventional gel permeation chromatography (GPC) using polystyrene standards EasyCal from Polymer Laboratories (weight average Mw range: 200 – 400.000 g/mol). The polymer (PEG$_{2000}$-OEOAcr), its starting materials PEG$_{2000}$, OEOAcr, IPDI and two PEG standards (MW 1000 and 4000 g/mol) where dissolved (1.0% wt/wt) in tetrahydrofuran (THF) containing 0.5% toluene as flow rate marker. Analysis was performed by liquid chromatography (Merck-Hitachi L7100) equipped with 3 PLGel Mixed-D LS polystyrene divinylbenzene GPC columns (300 mm X 7.5 mm, particle size 5 μm). The sample components were separated by the GPC columns based on their molecular size in solution and detected by a refractive index detector. Data were gathered and processed by Polymer Laboratories Cirrus GPC software.

2.2.3. Nuclear magnetic resonance spectroscopy

The ^{1}H-NMR spectrum of the hydrogel precursors was recorded on a Bruker Avance 500 MHz Spectrometer. Deuterated chloroform (CDCl$_3$) was used as solvent. The number of scans was 16, the acquisition time was set to 3.17 seconds and the relaxation delay was 1.0 second. Spectra were analyzed using the Spinworks software (version 2.5).

2.2.4. Infrared spectroscopy analysis

Fourier Transform infrared spectroscopy was performed on a Bio-Rad FT-IR spectrometer FTS 575C operating in Attenuated Total Reflection mode. A diamond crystal with ZnSe crystal lens was used, with a refractive index of 2.4 at 1000 cm^{-1}. Each spectrum is the result of 8 scans. The recorded spectra were analyzed using WIN-IR Pro software.

2.2.5. Differential photocalorimetry

DPC thermograms were recorded under nitrogen flow using a Mettler DSC823e with a Hamamatsu Lightningcure™ LC8 (L9588) unit.). Aluminum crucibles (20 μL) were used for the experiments. The light source was a medium-pressure mercury-xenon lamp with prominent emission lines at 298, 302, 313, 365, 405 and 435 nm. The irradiance level in the UV-A range was adjusted to 15 mW cm^{-2} at the position of the sample crucible. The sample mass was typically 3 to 4 mg. An open empty aluminum crucible was placed at the reference location and the DSC cell was closed with an UV-transparent quartz cover. Dry nitrogen was used as flow gas, unless mentioned otherwise (flow rate of 50 mL min^{-1}). In order to compensate for the heat flow generated by the light source, reference and sample sides of the DSC cell were illuminated simultaneously. However, imperfect balance still led to a differential in evolved heat. Hence, to obtain the net reaction exotherm, photopolymerization was completed in a first step and the background heat flow was determined during a second one. The two heat flow signals were subsequently subtracted. Prior to irradiation, the samples were annealed at 60°C for 1 min, then cooled at a rate of -5 °C min^{-1} to the crosslinking temperature (20 or 50°C). After 10 minutes at the selected temperature, the two UV-exposure cycles of 4 min were started. Maximum polymerization rate and double bond conversion were calculated according to literature procedures. [21,22]

2.2.6. Oscillatory photo-rheology

The photopolymerization process of the precursor solutions was studied at 21°C using an Anton Paar MCR 300 rheometer equipped with an EXFO novacure 2000 UV-A light (intensity 140 mW cm^{-2}) for sample irradiation from the bottom through a quartz plate. A parallel plate setup (ø 25 mm) was used. Frequency and strain sweeps were recorded to establish the linear visco-elastic range of the materials. A shear frequency of 1 Hz and an amplitude of 1 % were selected as they were well within this range. To study the effect of the network formation on the mechanical properties, the elastic shear modulus (G') was monitored over time (gap 0.35 mm). UV light was switched on after 60 s during 10 min, followed by a 60 s measurement period without UV exposure. The photopolymerization followed for different concentrations (10 wt%, 30 wt% and 70 wt%) with and without a photo-initiator 1-Hydroxycyclohexyl phenyl ketone (HCPK).

2.2.7. Determination of the gel fraction and swelling degree

Circular disks (thickness 2 mm, diameter 10 mm) were prepared from the appropriate solutions using glass plates covered by teflon release foil and separated by a silicon spacer. The precursor was dissolved in the appropriate amount of water, heated to 40°C to decrease dissolution time. For the sample cured in the solid state, the precursor was molten at 60 °C and left to cool overnight. The samples were exposed from both sides to UV-A light for 20 minutes (300-400 nm, 2×8 mW cm^{-2}). Samples were subsequently lyophilized (Christ alpha I-5) and weighed (w_{d0}). The mass was again determined after equilibrium swelling in double distilled water at room temperature (w_s). The final dry mass w_{df} was obtained after a second lyophilization step. The swelling ratio and the gel fraction were respectively calculated according to (w_s-w_{df})/w_{df} and w_{df}/w_{d0}.

2.2.8. Electrospinning

Electrospinning was performed using an in-house designed and developed device comprising a power supply (Glassman High Voltage, Inc, Model series EL50P00) capable of generating a potential between 0 and 50 kV and a 6 syringe motor driven pumping system (New Era Pump System, Inc, Model Multy-phase NE1600). For electrospinning experiments, an ideal composition was selected after optimization (as described in results and discussion) containing poly(ethylene glycol) (10^6 g/mol,

Sigma) (2 wt% concentration) dissolved in a 1:1 water/ethanol mixture, to which PEG$_{2000}$-OEOAcr was added (45 wt% concentration). A photo-initiator, Irgacure 2959 (BASF) (2 mol% relative to double bond concentration), was added to obtain maximal crosslinking (see the following chapter). The distance between the needle and the collector plate was 15 cm, the flow rate was set to 1.5 mL/h and the potential difference was 15 kV. The electrospun fiber mats were crosslinked by UV-A illumination during 20 minutes (300-400 nm) under N$_2$ atmosphere.

2.2.9. Fused deposition modeling

Fused deposition modeling was performed using the Bioscaffolder^{TM} system (System-Engineering, Hünxe, Germany) equipped with an extrusion head. PEG$_{2000}$-OEOAcr was printed onto a cooled platform (13°C). Optimal processing parameters where selected after optimization (as described in results and discussion): a printing temperature of 57°C, a needle diameter of 160 μm, XY plotting speed of 220 mm min^{-1}, Z plotting speed of 700 mm min^{-1}, layer thickness of 0.14 mm and a strut distance of 1 mm. The obtained scaffolds were subsequently cross-linked via UV-A curing (300-400 nm, 7,5 mW cm^{-2} from top and bottom, 20-60 min) and uncross-linked polymer was extracted in chloroform.

2.2.10. Gelatin methacrylamide coating

Gelatin-methacrylamide (GM) was prepared similar to a previously reported protocol. [12,23] In brief, 100 g gelatin B was dissolved in 1 l phosphate buffer (0.1 mmolar, pH = 7.4) at 40 °C. Under vigorous stirring, 3 equivalents of methacrylic anhydride, relative to the number of free primary amine functionalities in gelatin (38.5 mmol amines), were added. After 1h, the reaction was diluted with 1 l double distilled water followed by 24 hours dialysis (Spectra/Por 4, MWCO 12-14 kg/mol) at 40°C. Finally, the material was frozen at -20°C and lyophilized to obtain a dry solid. The degree of substitution (DS), being 93%, was determined using ^{1}H-NMR spectroscopy at 40 °C (D$_2$O, Bruker WH 500 MHz NMR spectrometer). The integrations of the characteristic signals of the methacrylamides at 5.75 and 5.51 ppm were compared to the Val, Leu and Ile reference signal present at 1.01 ppm as previously reported. [24] The obtained GM was applied as a coating by dissolving it in double-distilled water (1 wt% concentration) in the presence of 2 mol% Irgacure 2959 photo-initiator (BASF) relative to the

methacrylamides. Next, the hydrogel scaffolds were swollen overnight in this solution at 5°C, to minimize potential hydrolysis of gelatin. Next, the scaffolds were crosslinked with UV-A light (300-400 nm, 2 x 8 mW cm^{-2} from top and bottom) for 1h and any uncrosslinked gelatin was dissolved in double distilled water for 1h at 40°C. The samples were subsequently lyophilized.

2.2.11.   Two photon polymerization

The two-photon polymerization setup was used as described by Ovsianikov *et al.*[25] A high power femtosecond laser oscillator (MaiTai eHP DeepSee, Spectra-Physics, 800 nm, 60 fs, 90 MHz, <450 mW) was used and focused with a 32 × water-immersion microscope objective (Zeiss). For the positioning of the laser focus within the photosensitive resin, either a galvo scanner or a 3D piezo stage is applied. The CCD camera that is mounted behind a dichroic mirror is used for online monitoring of the 2PP process.

2.2.12.   Biological evaluation

Human adipose-tissue derived mesenchymal stem cells (ATMSC, P9, CryoSave) were cultured in DMEM GlutaMAX-1^{TM} supplemented with 10% fetal bovine serum. Mouse calvaria preosteoblast cells (MC3T3-E1, P14, ATCC) were cultured in alfa-minimal essential medium supplemented with 10% fetal bovine serum, 2 mM L-glutamine and 0.5 vol% penicillin-streptomycin (10^4 U mL^{-1}- 10^4 µg mL^{-1}). Scaffolds were incubated in serum-free culture medium and ATMSC (250 000 cells/40 µl) and MC3T3 (150 000 cells/40 µl) cells were seeded subsequently. After 3 hours, additional culture medium was added and the scaffolds were kept in culture (37°C, 5% CO_2) for 23 days. Calcein AM/propidium iodide staining was performed after 1, 7, 14 and 23 days to evaluate cell viability by fluorescence microscopy (Type U-RFL-T, Olympus).

2.3.   Results and Discussion

2.3.1. Synthesis and characterisation of the precursor

To investigate the unique solid state reactivity, a range of precursors with different spacer groups (OEO, OPO, OCl, HEA) and a PEG backbone (MW 2000 g/mol), were synthesized at kilogram-scale following a solvent-free, two-step synthesis process in conditions relevant for up-scaled (kg to ton scale) industrial manufacturing. [11,26] For all

precursors, the spacer group is attached to the backbone polymer using isophorone diisocyanate as depicted in Figure 1. The model compound, of which the molecular structure is shown in figure 2B, was the first polymer synthesized in the work and showed an excellent solid state reactivity. Therefore, no further optimization of the polymer structure was required.

A

B
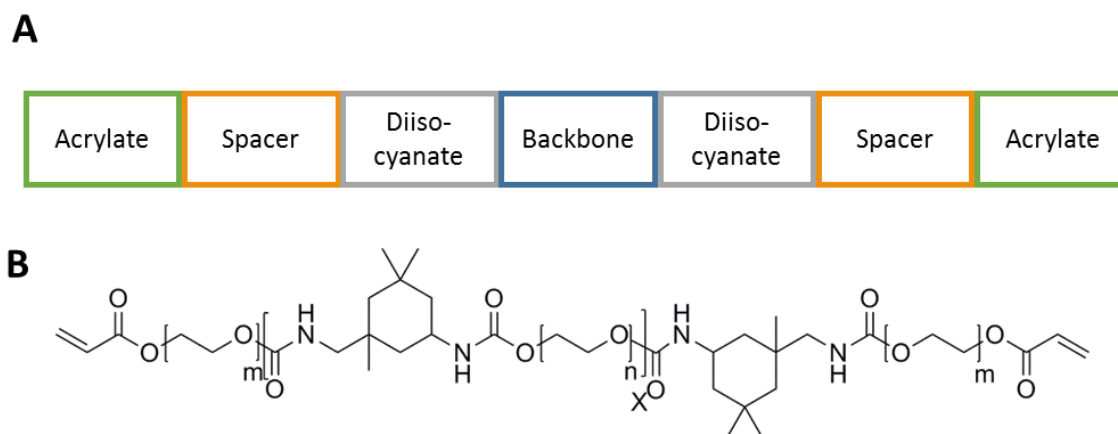
Figure 2. A: General structure of the solid state reactive polymers depicting the different building blocks. B: Model compound PEG$_{2000}$-OEOAcr used for characterization and processing (n = 40, m = 6, x = 1-3).

2.3.1.1.   ^{1}H-NMR spectroscopy of the model precursor

The 1H-NMR spectrum for the model precursor PEG2000-OEOAcr shown in Figure 2B with an oligo-ethylene oxide spacer (OEO) is provided in Figure 3. The signals from 0.85 to 1.9 ppm correspond to the methyl and cyclic methylene groups (g, h, i, k) of IPDI. The other protons of IPDI (e, j) can be observed at 2.9 and 3.25 ppm. Protons of the PEG-methyl in the spacer and backbone adjacent to the urethane (l' and d") can be found at 4.2 ppm, while the PEG-methyl protons next to the acrylate group (d') are detected at 4.3 ppm. The signal from the urethane protons (m) can be observed between 4.7 and 5.1 ppm while the peaks at 5.85, 6.15 and 6.4 ppm correspond to the acrylate protons (a, b, c). An oxa-Michael addition reaction can occur as a side reaction between the hydroxyl groups of unreacted PEG and the acrylates of PEG2000-OEOAcr 27,28 This is evidenced by the signal at 2.6 ppm (*) and will slightly reduce the acrylate concentration. The extend was determined by adding 3-nitroacetophenone as an internal standard, to determine the exact molar concentration of double bonds by comparing the peak of the internal standard and the signals assigned to the double bonds. The resulting value of 0.6256 mmol g^{-1} is in close correspondence to the

theoretical value of 0.6421 mmol g^{-1}, calculated based on the amount of monoacrylate PEG added during the synthesis (i.e. 0.80 mole monoacrylate PEG on a total mass of 1246 g). Therefore, it can be concluded that the oxa-Michael addition reaction does not lead to a significant reduction in double bond concentration, and can be considered a minor side reaction.
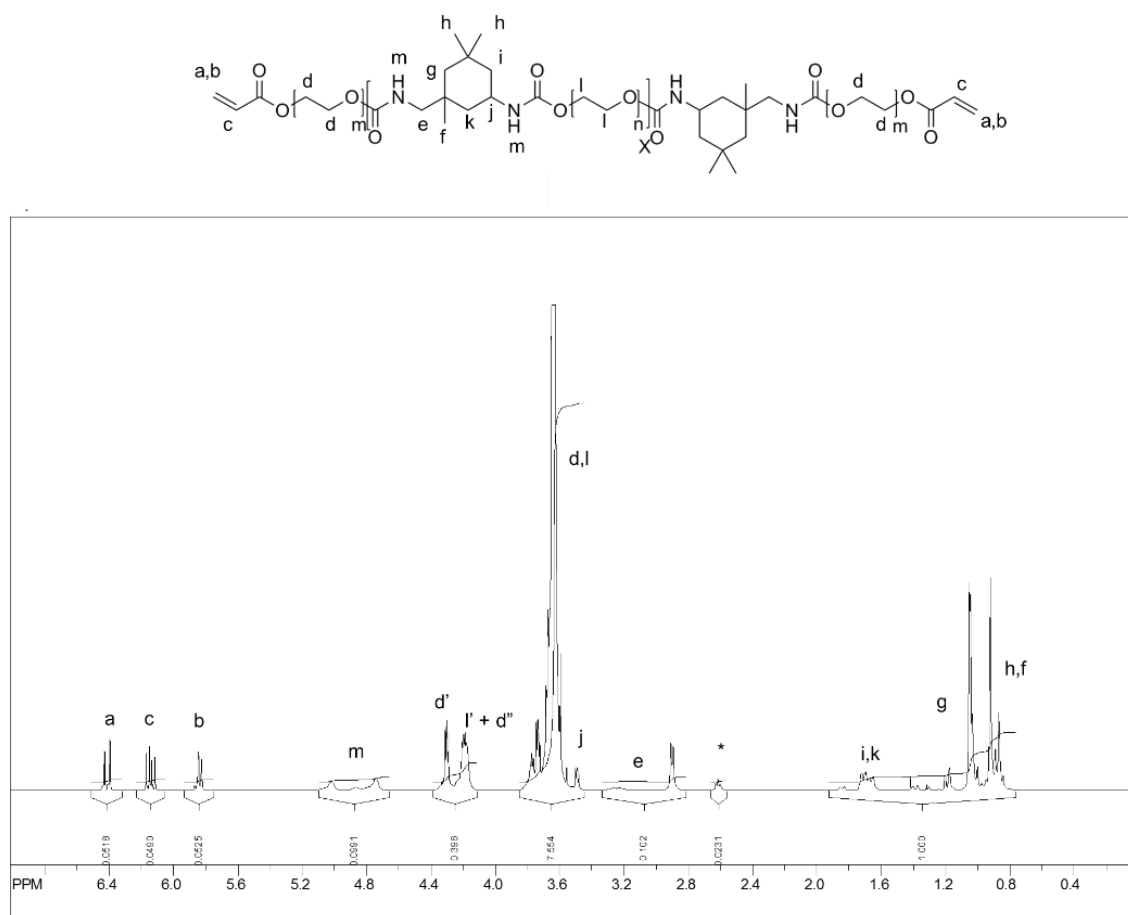
Figure 3: ^{1}H-NMR spectrum of the precursor

2.3.1.2. Gel permeation chromatography analysis of the precursor and reagents to assess the molecular weight and the composition

For polycondensations, the polydispersity is controlled by using stoichiometrically unbalanced reactants (i.e. using an excess of one of the reagents to control the molar mass) and by limiting the removal of the formed by-product.[29] However, this is not achievable in urethanisation reactions due to the impurity of the reagents (see below) and because in these reactions, no removable by-product is formed. Therefore, a controlled synthesis of polyurethanes is not straightforward.[30] To increase the control, a diisocyanate with a primary and secondary isocyanate group (e.g. IPDI) can be

combined with a selective catalyst (e.g. dibutyl tin dilaurate or bismuth neodecanoate) to obtained a more controlled two-step reaction.[26] GPC analysis revealed the final composition of the product: by comparing the chromatogram of PEG_{2000}-OEOAcr (black line) with the chromatograms of the raw materials (colored lines) in Figure 3, the different reaction products could be identified. Analysis of PEG standards (dotted lines) showed an excellent match between the measured molecular weight and the actual molecular weight. At position 1, a small fraction (1.6 mol%) of the diadduct of IPDI and PEG monoacrylate can be observed. This peak is quite broad due to the high molecular weight dispersity (3.8) of the PEG monoacrylate reagent shown in blue, caused by the variation of the number of ethylene oxide units, with an average value of 5. This low molecular weight product (number average MW is 1250 g mol^{-1}) can be considered as a by-product of the synthesis.[26] As a result, further purification steps (e.g. extraction) can be avoided what renders the precursor even more applicable and relevant towards industrial applications. The number of repeats of the PEG backbone, indicated by x in the molecular structure in Figure 1, is one for the peak at position 2, two for the peak at position 3 and three for the peak at position 4. While the aim of the synthesis was to obtain a polymer where the backbone repeats only once (z=1 in Figure 1), for some of the polymers the backbone will repeat multiple times. As explained higher, the urethanisation reaction is difficult to control. Here, PEG is reacted with IPDI, and because of the selectivity of the catalyst, only the primary isocyanate will react. However, as this selectivity is imperfect, for some of the IPDI molecules both diisocyanate groups will react, leading to the observed repeating backbone (1-3 repeats). The number average molecular weight was calculated to be 3800 g mol^{-1} and the weight average 6740 g mol^{-1}, which results in a polydispersity of 1.78.
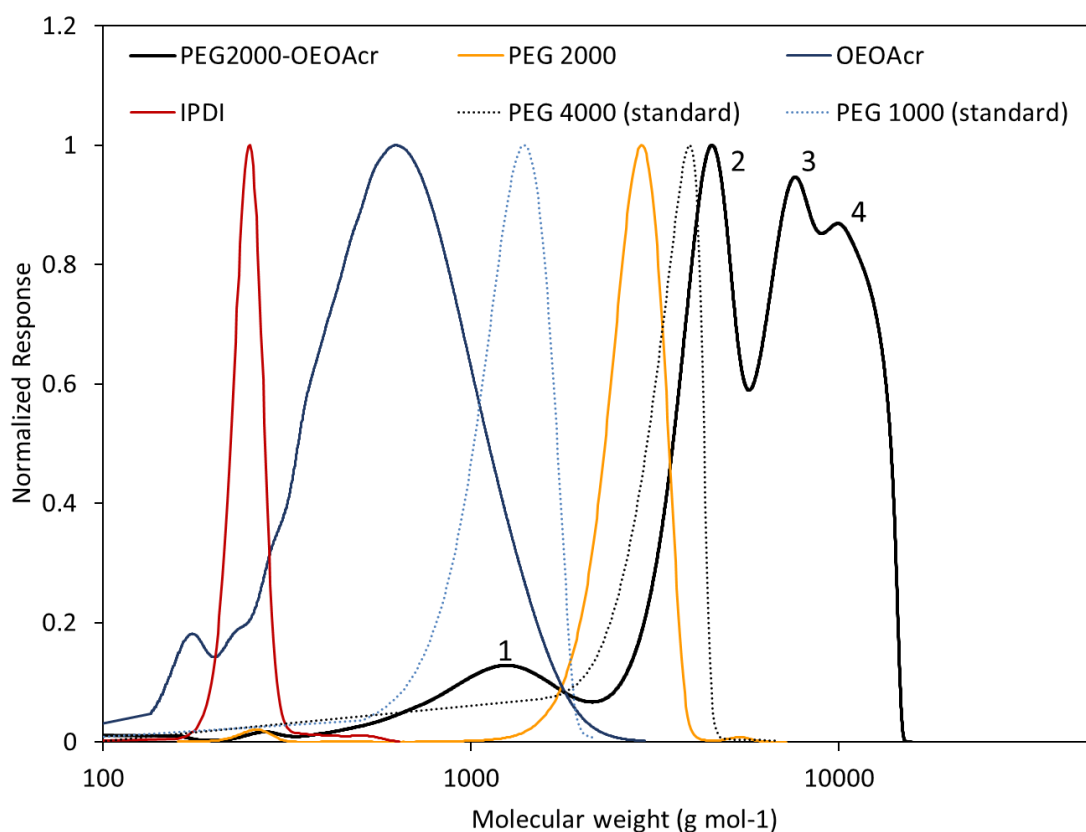
Figure 4: GPC chromatogram of the reagents used (PEG 2000, IPDI, PEG monoacrylate), the reaction product (PEG2000-OEOAcr) and 2 reference standards (PEG 1000 and PEG 4000)

2.3.1.3.   Infrared spectroscopy analysis of the precursor

Characteristic bands for the urethane groups[31] were observed in the ATR-FT-IR spectrum in Figure 5. including the stretching of NH groups (v_{N-H}) at 3331 cm^{-1}, the carbonyl stretch ($v_{C=O}$) at 1718 cm^{-1}, the amide II band (NH bending vibration) at 1530 cm^{-1}, the bending of C-H$_2$ (δ_{C-H2}) at 1466 cm^{-1}, the amide IV band at 1240 cm^{-1} and stretch bands of C-O-C at 1104 cm^{-1} and 1074 cm^{-1}. The acrylate terminal groups show characteristic vibrations at 810 cm^{-1}, 1410 cm^{-1} and 1640 cm^{-1}.
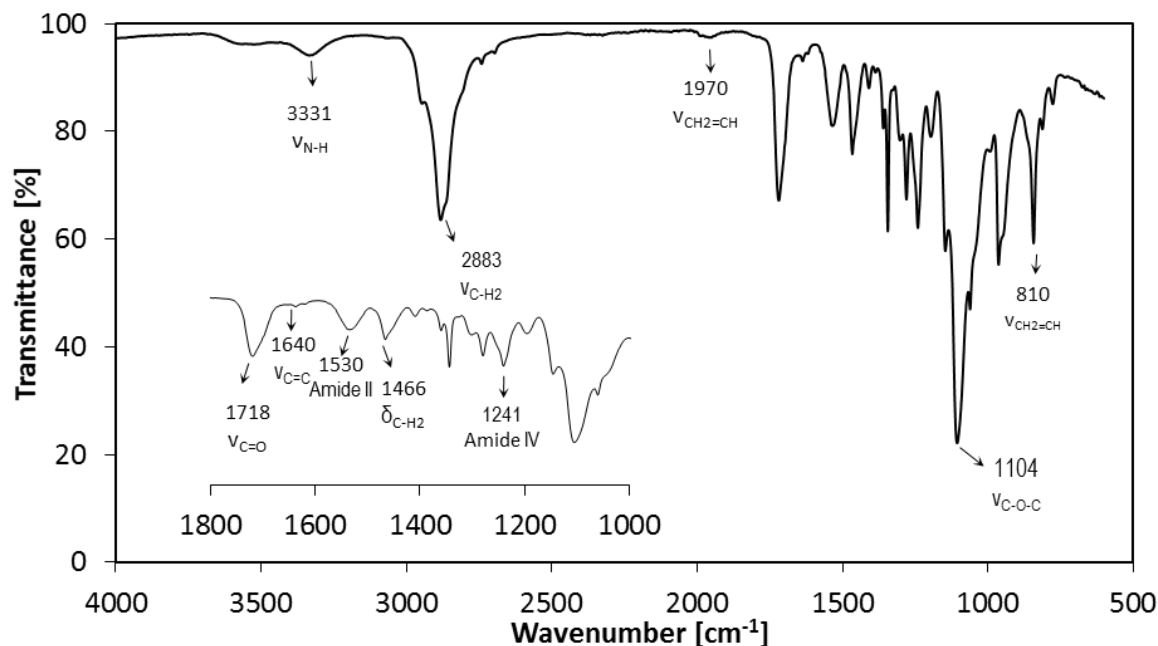
Figure 5: ATR-FT-IR spectrum of the precursor (PEG$_{2000}$-OEOAcr).

2.3.2. Investigation of the solid-state reactivity of the hydrogel precursors

Upon crystallization of the precursor , the backbone polymer forms crystalline domains segregating the acrylate groups into structured zones as depicted schematically in Figure 6. As further suggested by optical microscopy, the crystalline domains are seemingly aligned as long strings building-up lamellae in spherulitic structures. Although other attempts have been made to visualize this phase separation (i.e. IR surface mapping, AFM), their resolution was not sufficient to detect the different zones. It can be anticipated that in such an immobilized structure, the polymerization can merely propagate along the acrylate-enriched zones following a reactive diffusion mechanism provided that functional proximity and motional freedom is sufficient. By incorporating a flexible spacer, the resulting prepolymers exhibit excellent solid state photo-reactivity at room temperature and, surprisingly, even in the absence of a photo-initiator. Initiator-free polymerization avoids any potential toxic effects associated with the photo-initiator, eliminates pre-processing mixing steps as well as the need to find a photo-initiator suitable for the selected processing technique.[25,32,33] This auto-initiation will be investigated in more detail in the following chapter. The implemented strategy is here specifically demonstrated for a telechelic acrylated hydrogel precursor (Figure 2B) based on PEG with a molar mass of 2000 g mol-1 linked to a short oligoethylene oxide (OEO) spacer with an average ethoxylation degree of six.

- 🔵 Backbone
- 🟡 Spacer
- 🟢 Acrylate
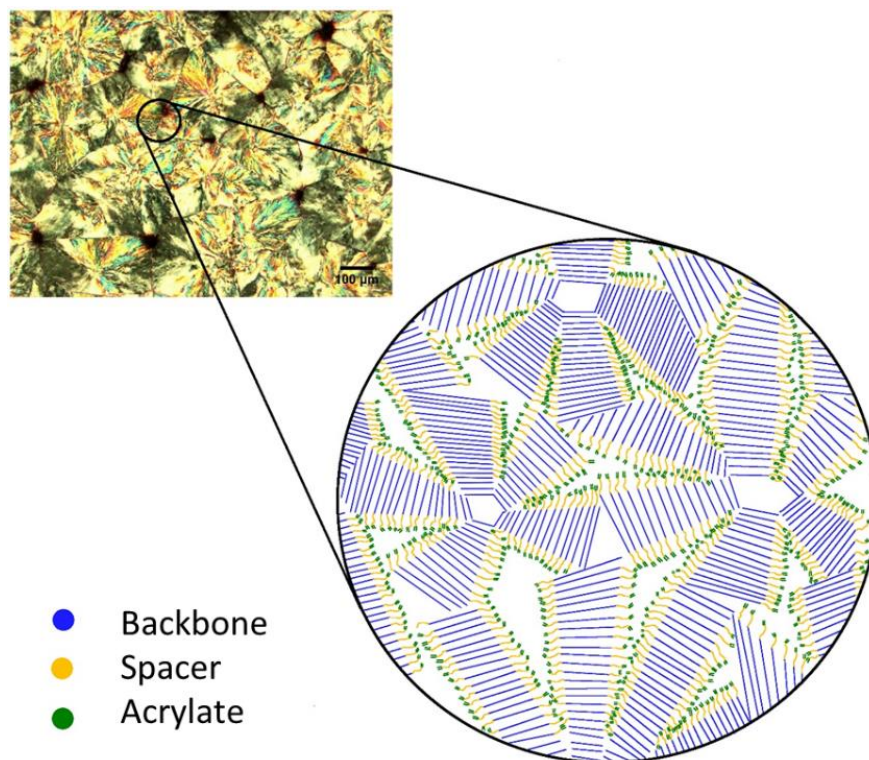
Figure 6: Optical microscopy image (scale bar 100 µm) and hypothetical drawing of the phase separation into PEG-rich, crystalline zones and acrylate-rich amorphous zones in the precursor solid state.

Figure 7 compares the initiator-free photopolymerization of the model prepolymer (PEO2000-OEOAcr) in the solid and the molten state as determined by differential photocalorimetry. The top curves show the reaction exotherms upon UV-exposure for which the maximum of the heat flow $h_{p,max}$ provides a good index for the reactivity. The lower panel of Figure 7 represents the double bond conversion (DBC) during photopolymerization with a final value close to 52% in both the solid and the molten state. This was calculated from the total heat released ΔH_p (J g^{-1}):

$$DBC\ (\%) = 100 \cdot \Delta H_p / (c_{acr} \cdot \Delta H_{0,p}) \qquad (1)$$

where $\Delta H_{0,p} = 77.6 \pm 1.1$ kJ mol^{-1} is the molar reaction enthalpy of acrylate double bonds and $c_{acr} = 0.626$ mmol g^{-1} is the concentration of acrylate double bonds of the model precursor estimated independently using proton NMR spectroscopy.[21,22] The maximum polymerization rate $r_{p,max}$ can be estimated after proper scaling of $h_{p,max}$ according to:

$$r_{p,max} = h_{p,max} / (c_{acr} \cdot \Delta H_{0,p}) \qquad (2)$$

Clearly, at the two temperatures the precursor exhibits significant polymerization in less than one minute but, remarkably, the reaction proceeds 2.5 times faster in the solid state as deducted from the $r_{p,max}$ values. An accelerating effect can be anticipated from the local concentration of acrylate groups in the periphery of the crystalline domains after solidification (cfr. Figure 6) as the rate of free radical polymerization is proportional to the double bond concentration. However, the immobilization of the precursor chains and the association of the double bonds must also significantly affect the reaction paths and the corresponding rate constants. For instance, propagation and termination controlled by translational diffusion of the growing polymer, typically resulting in the auto-acceleration step at early stage of the reaction in the liquid state, are completely inhibited in the solid-state. Reaction diffusion and monomolecular termination reactions (i.e. radical entrapment) are assumed to operate as the controlling mechanisms for propagation and termination in the solid-state reaction kinetics, as will be investigated in more detail in the following chapter.
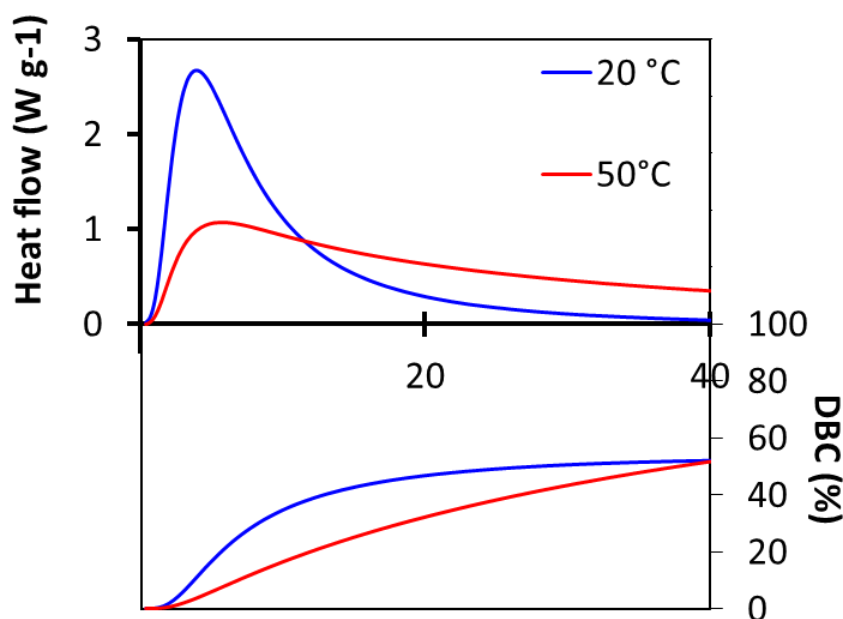
Figure 7: Heat flow profiles obtained by photocalorimetry (top) and double bond conversion (DBC, bottom) in the solid (20°C) and molten state (50°C) for PEG$_{2000}$-OEOAcr.

The importance of the nature of the spacer group on the polymerization kinetics in liquid and solid form is illustrated in Figure 8 where the maximum polymerization rate $r_{p,max}$ is compared for precursors with a short spacer of one ethylene oxide unit (PEG-HEAcr) and flexible oligomer spacers with an average of six propylene oxide units (PEG-OPOAcr), three ε-caprolactone units (PEG-OCLAcr) and six ethylene oxide units

104

(PEG-OEOAcrylate). In addition, this figure shows the versatility of this approach, as all polymers were reactive in the solid state. The various precursors are ranked according to a decreasing reactivity when photopolymerized in the melt without initiator. In the assumption of constant propagation in the early stage of the polymerization, the decrease of $r_{p,max}$ essentially reflects the decreasing ratio between initiation and termination. The auto-initiation process was investigated using photo-DSC as depicted in Figure 8. In a first step, the different building blocks of the polymer were irradiated separately, in the absence of a photo-initiator. Only in case of the monoacrylate-PEG, an exotherm was witnessed as a result of auto-initiation. To further investigate where exactly in this molecule the initiation takes place, smaller segments of this molecule (i.e. hydroxyethyl acrylate and acrylic acid) were irradiated as well. Interestingly, even in the case of acrylic acid, a strong peak (7.8 W g^{-1}) can be observed. Therefore, it can be concluded that the acrylate compound is the primary radical initiator showing a strong variation in efficiency depending on the chemical environment. [34,35]
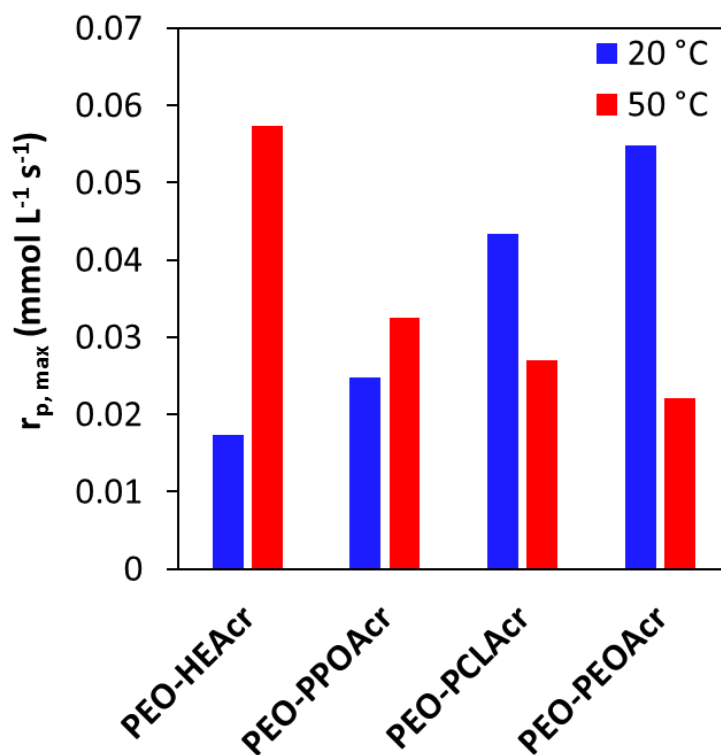
Figure 8: Maximal polymerization rate ($r_{p,max}$) for precursors with different oligomer spacers as studied by photo-DSC.

Termination on the other hand is influenced by viscosity and both factors are assumed to control the reported $r_{p,max}$ value.[2] In full contrast, the inversion of the trend for polymerization in the solid state now reveals a reactivity increase along the same series. This clearly demonstrates that the kinetic parameters are profoundly altered by the structural changes upon crystallization and that the spacing group has a prominent role. The polymerization rate increases with increasing spacer length, resulting in a local free volume gain.[36] Additionally, the rate also depends on the chemical nature of the spacer. The three selected spacers (OPOAcr, OClAcr and OEOAcr) contain flexible units according to polymer stiffness parameters such as Flory's characteristic ratio C_n, defined as the ratio of the mean square unperturbed end-to-end distance for a real chain to the value expected for an ideal (or freely jointed) chain with the same number of bonds. Recently, Kokubo and Vana reported very accurate C_n values for polyethylene oxide and polypropylene oxide, i.e. 3.96 and 5.76 respectively, quantifying the higher flexibility of the OEO spacer relative to the OPO one.[37] Reliable values could not be found for PCL but typical C_n values for polyesters are in the same range.[36]
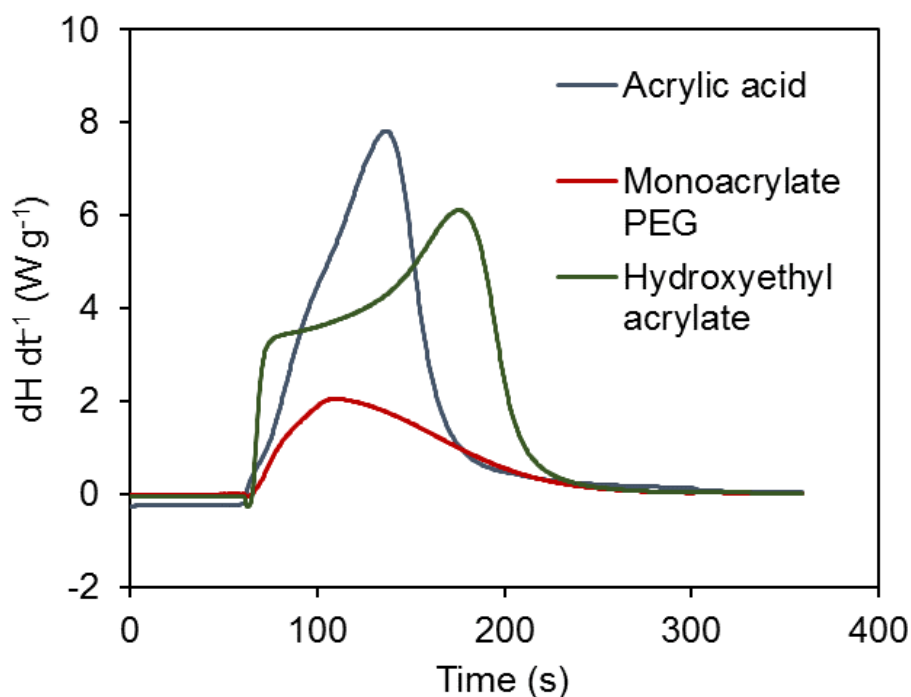
Figure 9: Photo-DSC thermograms of the different building blocks enabling the investigation of the auto-initiation process.

The model precursor (PEG-OEOAcr) is readily soluble in water up to 90 wt%. The aqueous solutions can be photopolymerized in the absence of a photo-initiator yielding high gel fractions close to 100% for precursor concentrations between 20 and 100 wt%, as depicted in Figure 10. Only at the lowest concentration (10 wt%) and when crosslinking in the solid state, the gel fraction slightly drops to respectively 88.9 ± 0.7 %.and 93.5 ± 1.2 %.
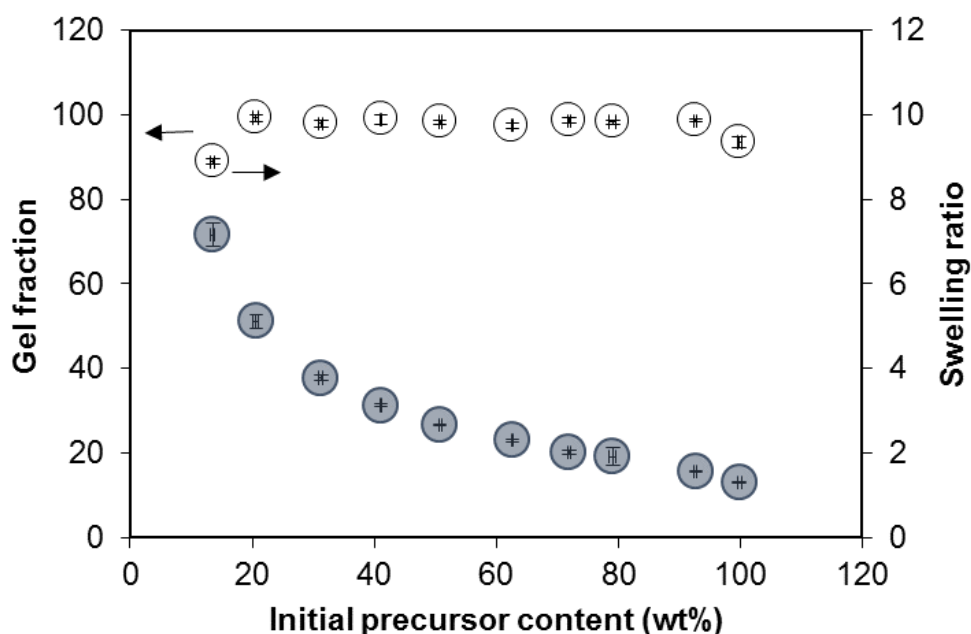
Figure 10: Swelling ratio and gel fraction results for PEG$_{2000}$-OEOAcr in concentrations in water varying from 10 to 100 wt% in the absence of a photo-initiator (n=3).

The photopolymerization process of different aqueous solutions of the hydrogel precursor was followed by oscillatory rheology in the linear viscoelastic regime. Figure 11 shows the build-up of the elastic shear modulus, *G'*, upon UV-exposure for the model precursor in the absence (dotted line) and in the presence (full line) of a photo-initiator, i.e. 1-hydroxycyclohexyl phenyl ketone (HCPK, 1.5 mol% relative to the acrylates present). As anticipated, the results reveal that the presence of a photo-initiator accelerates the network build-up, yet, with a negligible influence on the final moduli for concentrated (≥30 wt%) systems. In dilute conditions (<30 wt%), however, the final network exhibits a higher density of elastically active chains when polymerized with a photo-initiator as illustrated for the 10 wt% solution for which the final *G'* reaches 7.5 kPa compared to 5 kPa in initiator-free conditions. Similar values where obtained by Lin-Gibson *et al* for PEG dimethacrylates (MW 2000) g/mol, with a storage modulus for a 10 wt% concentration of 10 kPa.[38] In addition, there is a clear effect of the

concentration of the precursor on the rheological properties, both with and without a photo-initiator. Lower concentrations will result in a lower final storage modulus, which increases with increasing precursor concentration, up to 630 kPa for a 70 wt% concentration.
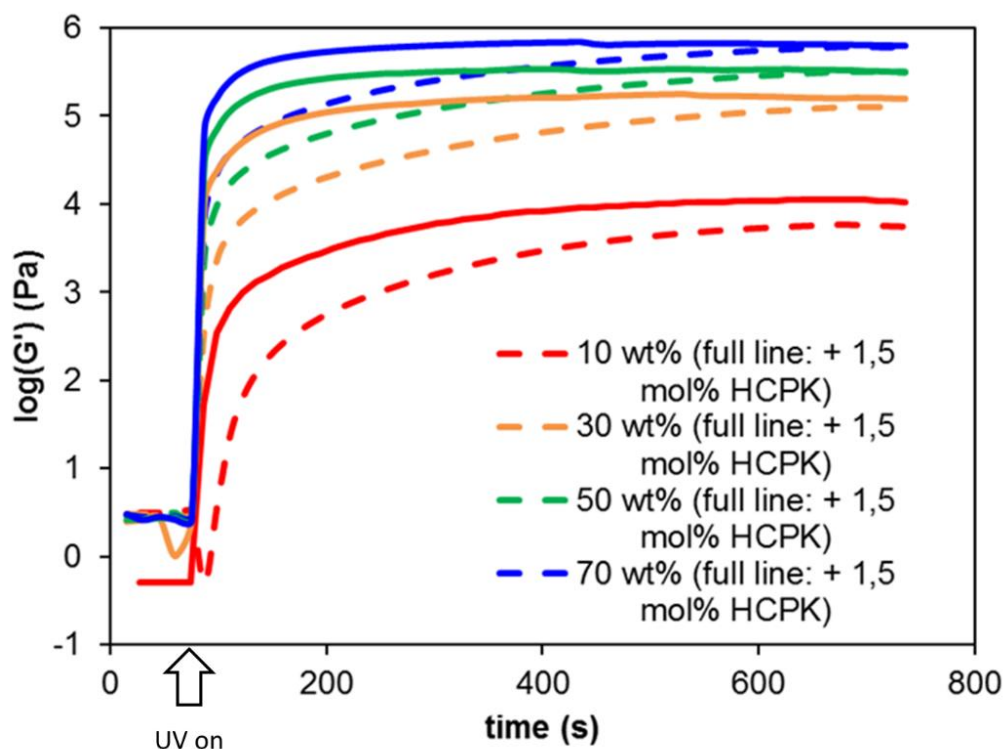
Figure 11: Storage moduli monitored by photo-rheology for different precursor contents, in the absence (dotted lines) and in the presence (solid lines) of a photo-initiator (1.5 mol% HCPK)

2.3.3. Investigation of the processing potential of the developed polymers

2.3.3.1. Electrospinning of the solid state reactive polymer

The exceptional solid state reactivity is particularly useful when dealing with polymer processing techniques for hydrogel applications. A first example is the manufacturing of a solid microfiber mat by electrospinning (Figure 12). Previously, fiber crosslinking using UV light has been attempted during formation, from the needle to the collector plate, when the solvent was still present. [39,40] However, substantial conversion levels were hard to achieve upon curing due to the short effective exposure time (i.e. < 1s). In contrast, with the solid-state reactive precursor, the fibers could be effectively crosslinked in a separate post-processing step following electrospinning.
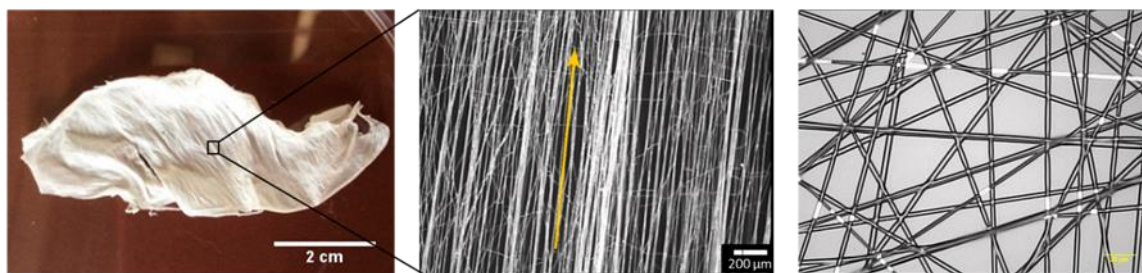
Figure 12: Dry electrospun fiber mat of the model precursor PEG$_{2000}$-OEOAcr deposited randomly right), or in an aligned fashion (middle).

To optimize the electrospinning process, a number of parameters can be varied, related to the composition of the electrospinning solution or to the electrospinning process. An overview of the evaluated parameters is provided in Table 1. For each parameter combination, the electrospinning process was evaluated visually (fiber formation, occurrence of drips, stable Taylor cone) and microscopically (fiber morphology and regularity, presence of beads, fiber size and variations in size). Some commonly observed fiber irregularities and defects, compared to regular fibers, are depicted in Figure 13. With regards to the solution, the PEG$_{2000}$-OEOAcr concentration was varied between 5 and 45 wt%. As the polymer has a relatively low molar mass (Mn of 3800 g mol^{-1}), the electrospinning process and fiber formation where not stable for the evaluated concentrations. Viscosity enhancement with high molar mass PEG (10^6 g mol^{-1}) was required to enable fiber formation. Due to its high molecular weight, this additive increases the amount of chain entanglements (should be a at least 2.5 entanglements/chain), resulting in stable fiber formation.[41] The concentration of the high molar mass PEG additive was varied between 1 and 9 wt%.
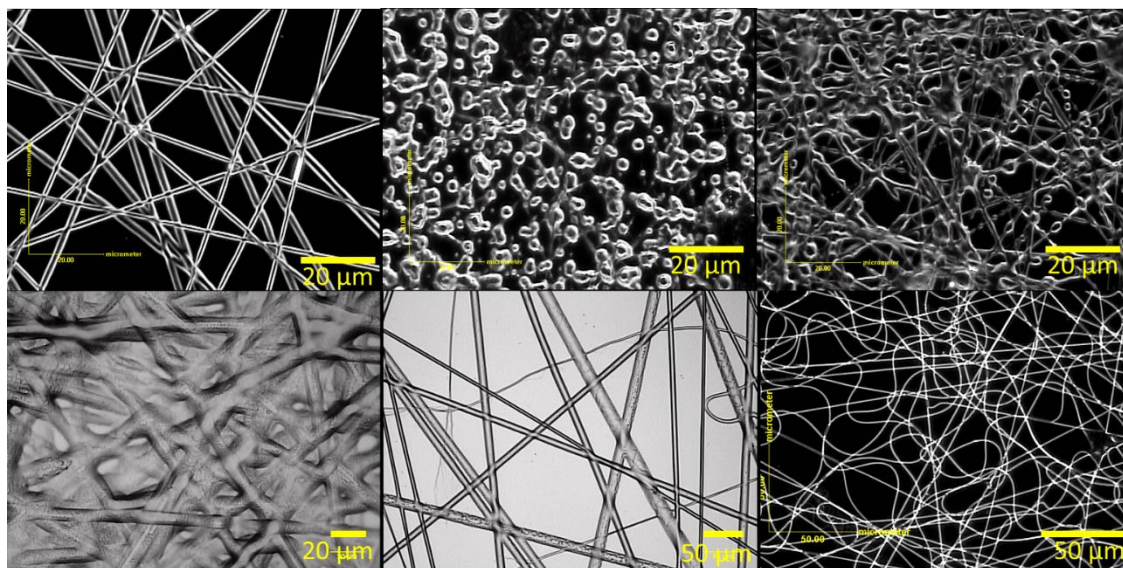
Figure 13: Top row: Regular fibers (left), electrospraying: no fiber formation (center), beaded fibers (right). Bottom row: incomplete solvent evaporation leading to fused fibers (left), large variations in fiber diameter (center), coiled fibers (right)

For concentrations of 15 wt% PEG$_{2000}$-OEOAcr or lower, at least 7 wt% of the PEG additive needed to be added. For concentrations of 20 wt% or higher, 2 wt% of the high molar mass PEG additive was sufficient to obtain a stable process. Although spinning with 1 wt% of PEG additive was possible as well, this was not always reproducible. Therefore, 2 wt% of the high molecular weight additive was selected. Regarding the PEG$_{2000}$-OEOAcr concentration: as the ratio between the precursor and the additive increases, more crosslink points will be present in the fiber, leading to improved crosslinking. Therefore, the maximal PEG$_{2000}$-OEOAcr concentration was selected. At a concentration of 50 wt%; fiber formation was not witnessed. Therefore, a concentration of 45% was used for further experiments.

Table 1: Overview of evaluated electrospinning parameters, with the range that was evaluated and the optimal value. Process parameters in bold are for the sample in Figure 14.

Parameter (unit)	Evaluated range	Optimal value
PEG$_{2000}$-OEOAcr (wt%)	5-50	45
PEG 10^6g mol^{-1} (wt%)	1-9	2
EtOH/H$_2$O ratio	0/100 - 85/15	1/1
Needle distance (cm)	15-20	15 - **20**
Flow rate (mL/h)	0.5 – 2.5	0.5 -**1.5**
Potential difference (kV)	10-20 kV	12.5- **15**

Concerning the solvent selection, the volatility of the solvent is highly important: if the solvent is to volatile, it will start evaporate from the Taylor cone and eventually lead to needle blockage. This was the case when electrospinning in chloroform was attempted. Electrospinning in pure demineralized water was possible, but more regular fibers and reproducible results were obtained when a mixture of ethanol (EtOH) and water was used. Pure ethanol as a solvent was not possible, as the precursor and PEG additive did not dissolve in sufficiently high concentrations for electrospinning. A 1/1 mixture of EtOH and demineralized water was selected as a solvent system. For this composition, high solubility and excellent fiber formation where be observed.

In addition, for the electrospinning experiments a photo-initiator was added (2 mol% relative to the acrylate concentration of Irgacure 2959). As the fibers are quite small (in the range of 10µm), fewer crosslink points will be present in a fiber compared larger samples such as disks or 3D-printed constructs. In addition, the large surface-to-volume ratio of these fibers will increase the effect of oxygen inhibition on the polymerization. To help increase the double bond conversion, a photo-initiator was added. The effects of a photo-initiator on the polymerization process will be explained in more detail in the following chapter. The presence of a photo-initiator will help to increase the stability of the fiber mats: without the photo-initiator, it was noticed that part of the fibers would dissolve or detach when immersed in water, while this was no longer an issue when a photo-initiator was added.

For all electrospinning compositions, three process parameters where varied and their effect on fiber formation and morphology was studied: the distance from the needle to the collector plate, the flow rate of the polymer from the syringe and the applied potential difference. Another parameter that plays a major role in the electrospinning process is the air humidity. As the electrospinning device is not in an air-conditioned room, this parameter could not be controlled. This impacted the reproducibility of the results, especially the effects of the process parameters. Currently, a hygrometer is present to measure the air humidity during the experiment. Unfortunately, this was not available at the time of these experiments, therefore differences in air humidity could not be determined.

A first process parameter is the needle distance. The needle distance will impact the evaporation of the solvent (longer distance gives more time to evaporate) and will have

an influence on the electrical field (longer distance reduces field strength). As the air humidity also impacts the solvent evaporation, this will affect the influence of needle distance. For example, when looking at the effect of needle distance for all evaluated samples, a needle distance of 20 cm gave a slightly improved result compared to 15 cm. However, for the samples in Figure 14, the best result was achieved with a needle distance of 15 cm. The second evaluated parameter was the flow rate, which was varied between 0.5 and 2.5 mL/h. Optimal results were observed for a flow rate between 0.5 and 1.5 mL/h, although this needed to be optimized for each experiment as small air bubbles or minor blockages in the needle and tubing will have an impact. The last parameter was the applied voltage, which was varied between 10 and 20 kV. Again, the voltage needed to be optimized for each experiment, however better results were observed for the lower voltages between 12.5 and 15 kV.

In Figure 14, electrospun precursor fibers, obtained using the improved parameters discussed above (45 wt% PEG_{2000}-OEOAcr, 2 wt% PEG additive, 2 mol% Irgacure 2959, 1:1 EtOH/H2O mixture, needle distance of 15 cm, flow rate of 1,5 mL/h and potential difference of 15 kV) are shown before and after UV exposure and after swelling in water demonstrating the successful curing. Before water swelling, the fiber diameter was 7.70 ± 1.38 µm, which increased to 10.16 ± 1.30 µm after equilibrium swelling. The decrease in fiber smoothness after crosslinking is due to shrinkage phenomena during polymerization. This volume contraction is monomer dependent, and will occur when polymerizing acrylates and methacrylates.[42]
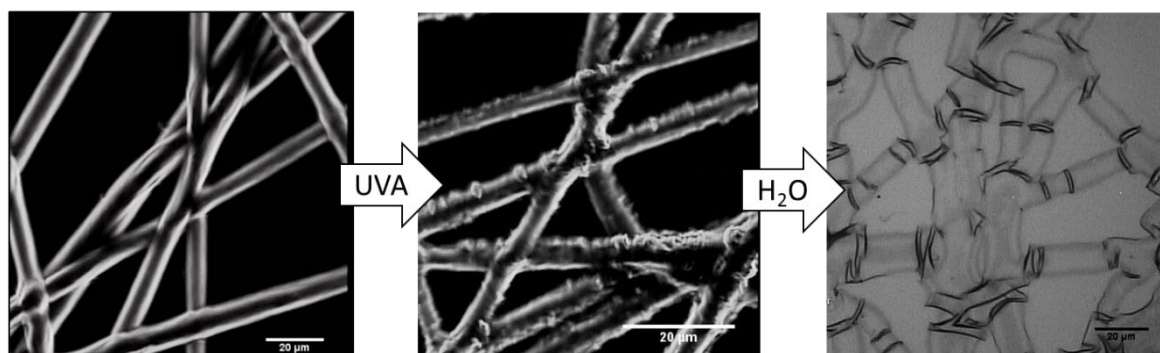
Figure 14: From left to right: fibers after electrospinning, fibers after crosslinking and water swollen crosslinked fibers (room temperature).

2.3.3.2.   Solid freeform fabrication of the solid state reactive polymer

Another frequently used processing technique is solid freeform fabrication. Extrusion-based printing of photo-crosslinkable hydrogel precursors is highly challenging and mainly uses thermo-responsive polymers or shear-thickening additives.[5,43] The novel materials described herein could be printed by fused deposition modeling and again crosslinked in the solid state afterwards. To enhance the printing process, temperature, needle diameter, speed (in XY and in Z planes) and layer thickness where varied as summarized in Table 2.

Table 2: Evaluated and optimal solid freeform fabrication parameters

Parameter (unit)	Evaluated range	Optimal value
Printing temperature (°C)	40-60	57
Needle diameter (µm)	160-210	160
XY-printing speed (mm min^{-1})	180-240	220
Z-printing speed (mm min^{-1})	500-760	700
Layer thickness (mm)	0.12-0.23	0.14

The needle diameter will have a direct influence on the strut size: the precursor melt will more easily flow from a needle with a larger diameter, however the printing resolution will increase as the needle diameter decreases. Initially, a needle diameter of 210 µm was selected as printing with this needle was most straightforward. However, after optimization of the other printing parameters, the needle diameter could be reduced to 160 µm. Another important parameter is the printing temperature, which was varied between 40°C and 60°C. If the temperature is to low, the printing solution will not flow from the needle easily and blockages or interrupted struts will be observed. If the temperature is too high, the structure will not cool down fast enough and keep flowing after printing, as shown in Figure 15 (left). The XY speed will influence the thickness of the struts and was varied between 180 mm min^{-1} and 240 mm min^{-1}. A higher speed will lead to thinner struts, however if the speed becomes too high, the struts will become interrupted. As thinner struts lead to a higher printing resolution, the maximum achievable speed was selected (220 mm min^{-1}).
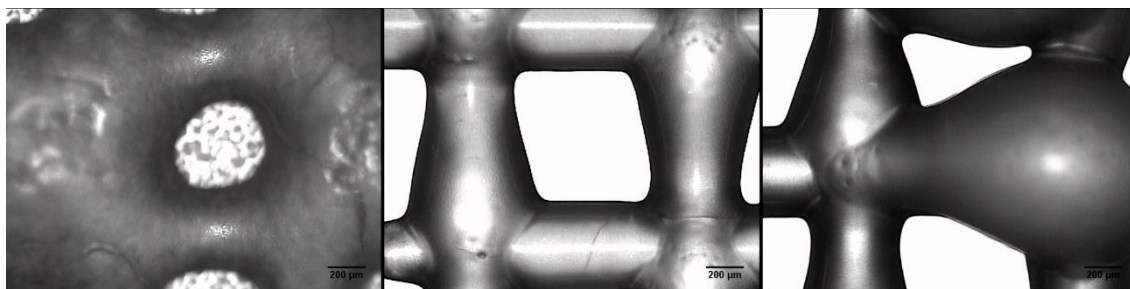
Figure 15: Common defects observed during the optimization of solid freeform fabrication as a result of incorrect printing parameters. Left: printing temperature is too high. Center: layer height is too high. Right: Z printing speed is too low.

The layer height influences the deposition of the struts. If the set value is too low, the printed layer will destroy the layer below as the needle moves through printed struts. If the value is too high, the deposited strut does not touch the strut below, leading to irregular shaped struts as depicted in Figure 15 (center). The Z speed is the speed at which the needle moves up after a layer is printed. If this speed is too high, the last part of the deposited strut will break and cause a defect. If the speed is too low, a droplet of material will be deposited on the edge of the scaffold, as shown in Figure 15 (right).

Using the selected printing parameters, regular scaffolds could be printed as shown in Figure 16A. The use of this technique has never been reported before for photo-reactive hydrogel building blocks as it is mainly applied for thermoplastic polyesters. A pore size of 1 mm was selected, and the actual distance was determined to be 562 ± 36 µm. This difference is due to the fact that the software assumes the needle distance will equal the strut size. For this scaffold, the needle diameter was 160 µm, while the strut size was 535 ± 108 µm. Clearly, the strut size is much larger compared to the needle diameter, explaining the difference in set strut size and printed strut size.

As shown in Figure 16A, the printed structure becomes quite flexible after swelling in water. Clearly, the printed structure no longer dissolves, demonstrating the curing effectiveness. As the surface to volume ratio is much lower for these printed constructs compared to electrospun fibers, no photo-initiator needed to be added. Printing of larger and more complex shapes was also possible as illustrated in Figure 16B, where a printed meniscus is shown as a proof of concept that more complex shapes are attainable as well, based on a design from a magnetic resonance imaging (MRI) scan of a real human specimen.
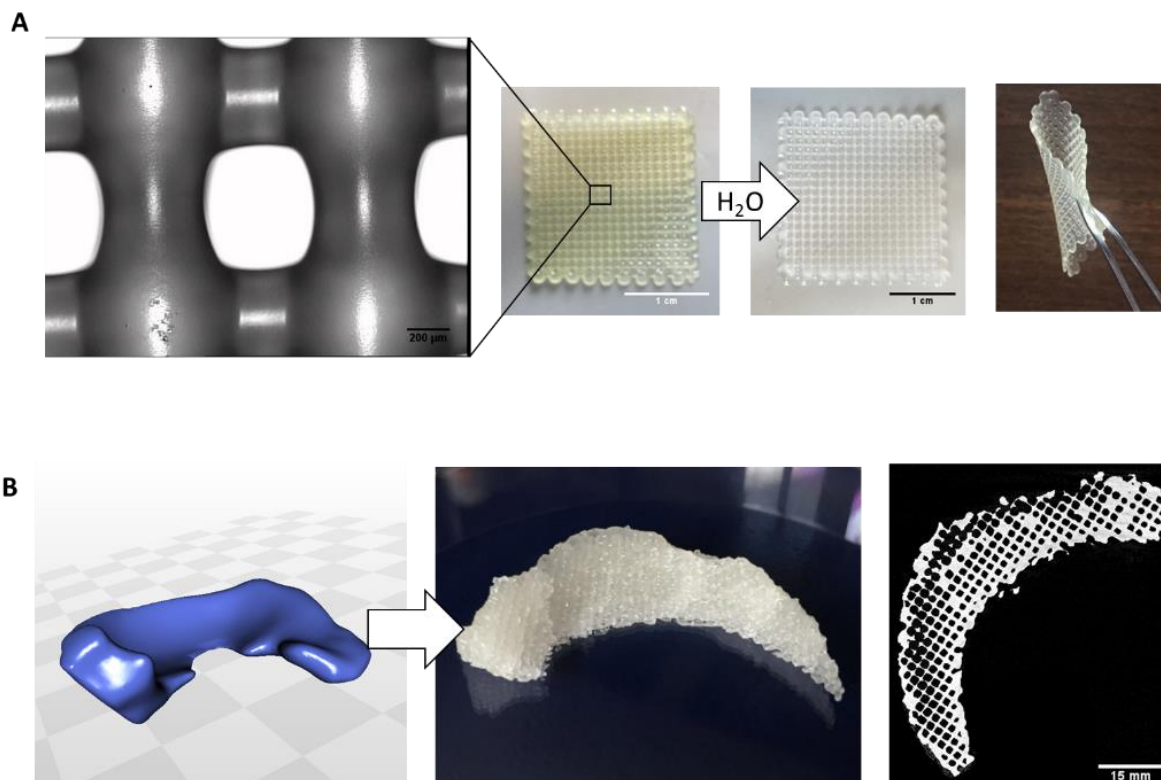
Figure 16: A: Magnified and overview image of the 3D-printed scaffold, and scaffold after incubation in water. B: From left to right: 3D model of a meniscus (32 x 25 x 12 mm³) based on an MRI scan of the patients meniscus, the 3D printed scaffold and a µ-computed tomography cross-section.

2.3.3.3. Two photon polymerization in the solid state

The last processing technique explored in this work is two-photon polymerization (2PP), a technique during which a tightly focused laser beam (voxel) is scanned through a photo-reactive material resulting in localized polymerization. The latter enables the creation of complex 3D-microstructures at sub-micrometer resolution.[44] However, there are some challenges associated with hydrogel optimization for 2PP purposes. Since hydrogel precursors are often processed in dilute conditions (< 20 wt%), a loosely crosslinked network is usually obtained exhibiting structural distortions because of the lack of structural support.[45] Furthermore, structuring in solutions can result in problems related to the support of 'hanging' structures during fabrication. Another limitation is the availability of biocompatible and water-soluble photo-initiator systems suitable for two-photon absorption.[45,46] Obviously, the reported initiator-free solid state crosslinking approach eliminates problems related to photo-initiator toxicity and complex geometrical structures. In addition, the highly crosslinked network (gel fraction of 93.5 ± 1.2 % for circular disks in the solid state) leads to a low swelling degree (1.5 times its original dry weight), which will minimize structural distortions. To demonstrate the 2PP potential of the solid state reactive materials, a 3D Atomium model was printed, as illustrated in Figure 17. As can be observed, high shape fidelity was obtained, and the printed structure did not collapse, illustrating the supporting capacity of the solid state crosslinked hydrogel. [45]
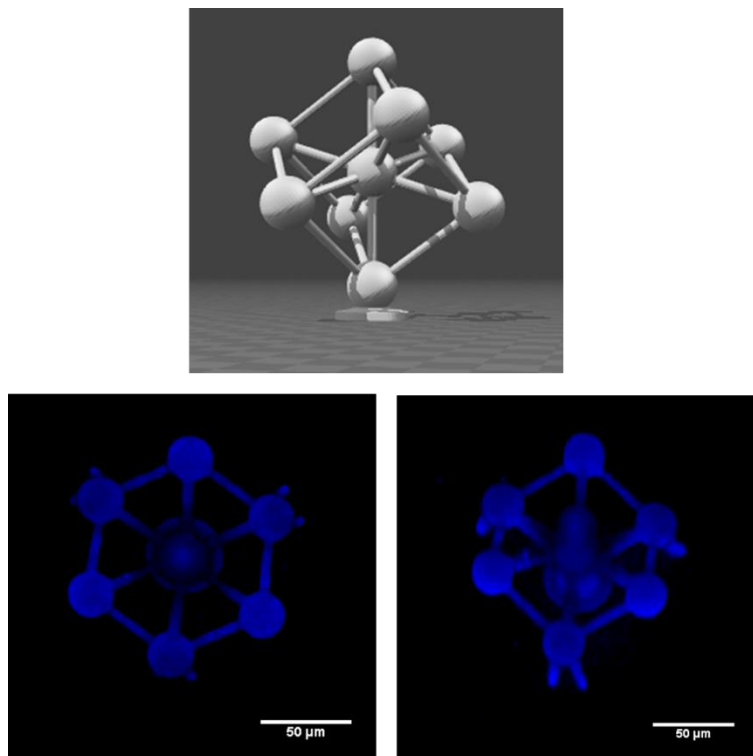
Figure 17: Atomium model (top) used to create the 2-photon polymerization structures (bottom) from PEG$_{2000}$-OEOAcr.

2.3.4. Biological evaluation of fused deposition modelling scaffolds with and without gelatin methacrylamide coating

The tissue engineering potential of PEG$_{2000}$-OEOAcr was evaluated by seeding adipose-tissue derived mesenchymal stem cells (ATMSC) and mouse osteoblast cells (MC3T3) onto 3D-printed scaffolds. The developed precursor is PEG-based (see Figure 1), it can be anticipated that it will not be prone to cell adhesion.[47] However, for applications for which cell adhesion is desired, a gelatin methacrylamide coating can be applied. As depicted in Figure 18, no cell adhesion was observed for the uncoated material over the duration of the experiment (i.e. 23 days). Conversely, the samples coated with modified gelatin showed excellent cell adhesion with cells displaying an elongated morphology as visualized by fluorescence microscopy (Figure 18) and SEM (Figure 19). Consistent with the seeding density, which was selected in relation to the expansion rate of the selected cell type (ATMSC: 250 000 cells/40 µl and MC3T3:150 000 cells/40 µl), the cells formed a confluent monolayer on the scaffolds at early times (d1 for the ATMSC's, d7 for the MC3T3's).[48] Ideally, cell densities should be adjusted to reach confluency at the same timepoint. However, it is difficult to estimate the interactions between the material and the cells, therefore this was different

117

for the 2 cell types. After a confluent layer was reached, the cells started to bridge the pores (visible from d7 at both timepoints. As evidenced from the vital staining images, the excellent viability of the adhering cells was maintained for 23 days, ascertaining the preliminary biocompatibility of these materials. A more quantitative analysis (e.g. metabolic activity assay) could be suitable here to determine the viability and indicate the amount of adhering cells, and proliferation at the different timepoints.[48]
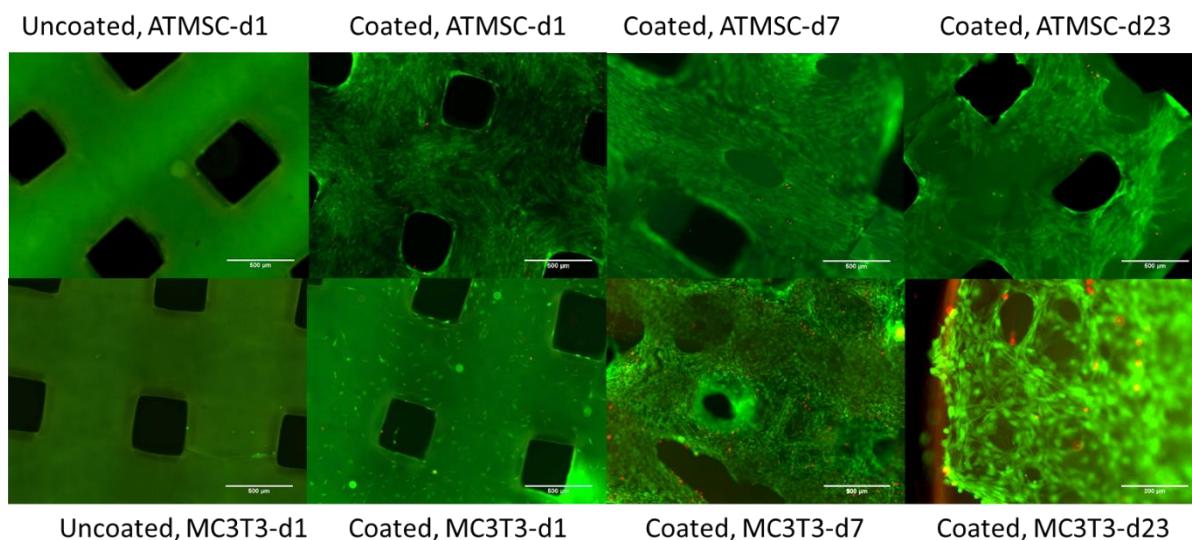
Figure 18: Cell adhesion and proliferation of ATMSC and MC3T3 cells on uncoated and 1 wt% gelatin methacrylamide coated scaffolds, studied by fluorescence microscopy of calcein-AM/propidium iodide stained cells.
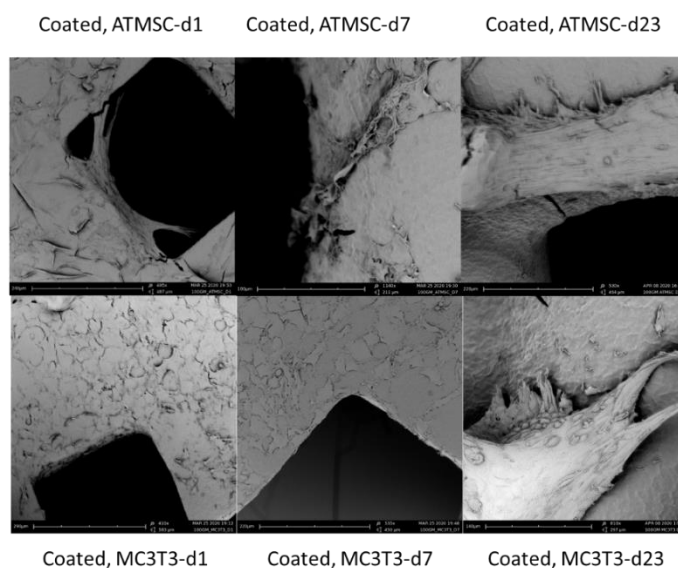
Figure 19: Cell adhesion and proliferation of ATMSC and MC3T3 cells on 1 wt% gelatin methacrylamide coated scaffolds, studied scanning electron microscopy of fixated samples

2.4.   Conclusions

In conclusion, for the first time, a solid-state reactive hydrogel precursor has been developed by linking an acrylate moiety, attached to a short (5 ethylene oxide or 2 ε-caprolactone units) flexible oligomer spacer, to a semi-crystalline polymer backbone. The resulting prepolymers exhibited excellent photo-reactivity at room temperature, below their melting point and in the absence of a photo-initiator. This solid state reactivity can be explained by the structuring of the precursor into acrylate-rich amorphous zones and crystalline zones constituted by the polymer backbones. The introduction of a spacing segment with a low stiffness (Cn ratio of 3.96) has a clear positive effect on the reaction kinetics. A model PEG-based hydrogel precursor could successfully be processed and crosslinked using three techniques that are incompatible with conventional photo-reactive hydrogels; i.e. (i) electrospinning (with PI), (ii) melt-based additive manufacturing (without PI), both followed by a separate curing step, and (iii) 2PP in the solid state without PI, demonstrating the versatile application spectrum of the new precursor. Finally, using 3D-scaffolds, it has been shown that no cell adhesion takes place on uncoated scaffolds whereas excellent cell adhesion could be observed after application of a gelatin methacrylamide coating.

2.5.   References

1.   Houben, A. *et al.* Flexible Oligomer Spacers as the Key to Solid-State Photopolymerization of Hydrogel Precursors. *Mater. Today Chem.* **4,** 84–89 (2017).

2.   Andrzejewska, E. Photopolymerization kinetics of multifunctional monomers. *Prog. Polym. Sci.* **26,** 605–665 (2001).

3.   Williams, C. G., Malik, A. N., Kim, T. K., Manson, P. N. & Elisseeff, J. H. Variable cytocompatibility of six cell lines with photoinitiators used for polymerizing hydrogels and cell encapsulation. *Biomaterials* **26,** 1211–1218 (2005).

4.   Martens, P. & Anseth, K. . Characterization of hydrogels formed from acrylate modified poly(vinyl alcohol) macromers. *Polymer (Guildf).* **41,** 7715–7722 (2000).

5.   Billiet, T., Gevaert, E., De Schryver, T., Cornelissen, M. & Dubruel, P. The 3D printing of gelatin methacrylamide cell-laden tissue-engineered constructs with high cell viability. *Biomaterials* **35,** 49–62 (2014).

6.   Van Nieuwenhove, I. *et al.* Photo-crosslinkable biopolymers targeting stem cell

adhesion and proliferation: the case study of gelatin and starch-based IPNs. *J. Mater. Sci. Mater. Med.* **26,** 104 (2015).

7. Thiele, J., Ma, Y., Bruekers, S. M. C., Ma, S. & Huck, W. T. S. 25th anniversary article: Designer hydrogels for cell cultures: a materials selection guide. *Adv. Mater.* **26,** 125–47 (2014).

8. Hutmacher, D. W. Biomaterials offer cancer research the third dimension. *Nat. Mater.* **9,** 90–93 (2010).

9. Hollister, S. J. Porous scaffold design for tissue engineering. *Nat. Mater.* **4,** 518–24 (2005).

10. Billiet, T. *et al.* A review of trends and limitations in hydrogel-rapid prototyping for tissue engineering. *Biomaterials* **33,** 6020–6041 (2012).

11. Houben, A. *et al.* Indirect Rapid Prototyping: Opening Up Unprecedented Opportunities in Scaffold Design and Applications. *Ann. Biomed. Eng.* **45,** 1–26 (2016).

12. Van Hoorick, J. *et al.* Indirect additive manufacturing as an elegant tool for the production of self-supporting low density gelatin scaffolds. *J. Mater. Sci. Mater. Med.* **26,** 247 (2015).

13. Berchtold, K. A. *et al.* Rapid Solid-State Photopolymerization of Cyclic Acetal-Containing Acrylates. *Macromolecules* **42,** 2433–2437 (2009).

14. Wang, J., Jian, Y., Nie, J. & He, Y. Solid photopolymerization and polymer properties of octadecyl vinyl ether. *J. Photochem. Photobiol. A Chem.* **271,** 105–110 (2013).

15. Jian, Y., He, Y., Wang, J., Yang, W. & Nie, J. Rapid solid-state photopolymerization of octadecyl acrylate: low shrinkage and insensitivity to oxygen. *Polym. Int.* **62,** 1692–1697 (2013).

16. Lee, J. W., Park, Y. J., Lee, S. J., Lee, S. K. & Lee, K. Y. The effect of spacer arm length of an adhesion ligand coupled to an alginate gel on the control of fibroblast phenotype. *Biomaterials* **31,** 5545–51 (2010).

17. DePhillips, P., Lagerlund, I., Färenmark, J. & Lenhoff, A. M. Effect of spacer arm length on protein retention on a strong cation exchange adsorbent. *Anal. Chem.* **76,** 5816–22 (2004).

18. Hern, D. L. & Hubbell, J. A. Incorporation of adhesion peptides into nonadhesive hydrogels useful for tissue resurfacing. *J. Biomed. Mater. Res.* **39,** 266–76 (1998).

19. Liang, H.-C., Chang, W.-H., Liang, H.-F., Lee, M.-H. & Sung, H.-W. Crosslinking structures of gelatin hydrogels crosslinked with genipin or a water-soluble carbodiimide. *J. Appl. Polym. Sci.* **91,** 4017–4026 (2004).

20. Shin, H., Jo, S. & Mikos, A. G. Modulation of marrow stromal osteoblast adhesion on biomimetic oligo[poly(ethylene glycol) fumarate] hydrogels modified with Arg-Gly-Asp peptides and a poly(ethylene glycol) spacer. *J. Biomed. Mater. Res.* **61,** 169–179 (2002).

21.   Schuster, M. *et al.* Evaluation of Biocompatible Photopolymers I: Photoreactivity and Mechanical Properties of Reactive Diluents. *J. Macromol. Sci. Part A* **44,** 547–557 (2007).

22.   Dworak, C., Koch, T., Varga, F. & Liska, R. Photopolymerization of biocompatible phosphorus-containing vinyl esters and vinyl carbamates. *J. Polym. Sci. Part A Polym. Chem.* **48,** 2916–2924 (2010).

23.   Van Den Bulcke, A. I. *et al.* Structural and Rheological Properties of Methacrylamide Modified Gelatin Hydrogels. *Biomacromolecules* **1,** 31–38 (2000).

24.   Van Vlierberghe, S. *et al.* Hydrogel network formation revised: high-resolution magic angle spinning nuclear magnetic resonance as a powerful tool for measuring absolute hydrogel cross-link. *Appl. …* **64,** 1176–1180 (2010).

25.   Ovsianikov, A. *et al.* Laser photofabrication of cell-containing hydrogel constructs. *Langmuir* **30,** 3787–3794 (2014).

26.   Kim, B. K. & Paik, S. H. UV-curable poly (ethylene glycol)-based polyurethane acrylate hydrogel. *J. Polym. Sci. Part A Polym. Chem.* **37,** 2703–2709 (1999).

27.   Nising, C. F. & Bräse, S. Recent developments in the field of oxa-Michael reactions. *Chem. Soc. Rev.* **41,** 988–99 (2012).

28.   Mather, B. D., Viswanathan, K., Miller, K. M. & Long, T. E. Michael addition reactions in macromolecular design for emerging technologies. *Prog. Polym. Sci.* **31,** 487–531 (2006).

29.   Flory, P. *Principles of polymer chemistry.* (1953).

30.   Velankar, S. & Cooper, S. Microphase separation and rheological properties of polyurethane melts. 2. Effect of block incompatibility on the microstructure. *Macromolecules* (2000).

31.   Tanzi, M. C., Mantovani, D., Petrini, P., Guidoin, R. & Laroche, G. Chemical stability of polyether urethanes versus polycarbonate urethanes. *J. Biomed. Mater. Res.* **36,** 550–559 (1997).

32.   Bryant, S. J., Nuttelman, C. R. & Anseth, K. S. Cytocompatibility of UV and visible light photoinitiating systems on cultured NIH/3T3 fibroblasts in vitro. *J. Biomater. Sci. Polym. Ed.* **11,** 439–57 (2000).

33.   Li, Z. *et al.* Initiation efficiency and cytotoxicity of novel water-soluble two-photon photoinitiators for direct 3D microfabrication of hydrogels. *RSC Adv.* **3,** 15939 (2013).

34.   Scherzer, T., Knolle, W., Nanmov, S. & Prager, L. Investigations on the photoinitiator-free photopolymerization of acrylates by vibrational spectroscopic methods. *Macromol. Symp.* **230,** 173–182 (2005).

35.   Knolle, W., Scherzer, T., Naumov, S. & Mehnert, R. Direct (222 nm) photopolymerisation of acrylates. A laser flash photolysis and quantum chemical study. *Radiat. Phys. Chem.* **67,** 341–345 (2003).

36.   Brandrup, J. & Immergut, E. H. *Polymer Handbook 3rd ed.* (John Wiley and

Sons, 1989).

37.   Kokubo, S. & Vana, P. Easy Access to the Characteristic Ratio of Polymers Using Ion-Mobility Mass Spectrometry. *Macromol. Chem. Phys.* **218,** 1600373 (2017).

38.   Lin-Gibson, S. *et al.* Synthesis and characterization of PEG Dimethacrylates and their hydrogels. *Biomacromolecules* **5,** 1280–1287 (2004).

39.   Kim, S. H., Kim, S.-H., Nair, S. & Moore, E. Reactive Electrospinning of Cross-Linked Poly(2-hydroxyethyl methacrylate) Nanofibers and Elastic Properties of Individual Hydrogel Nanofibers in Aqueous Solutions. *Macromolecules* **38,** 3719–3723 (2005).

40.   Ji, Y. *et al.* Dual-syringe reactive electrospinning of cross-linked hyaluronic acid hydrogel nanofibers for tissue engineering applications. *Macromol. Biosci.* **6,** 811–7 (2006).

41.   Shenoy, S. L., Bates, W. D., Frisch, H. L. & Wnek, G. E. Role of chain entanglements on fiber formation during electrospinning of polymer solutions: Good solvent, non-specific polymer-polymer interaction limit. *Polymer (Guildf).* **46,** 3372–3384 (2005).

42.   Watts, D. C. & Cash, A. J. Determination of polymerization shrinkage kinetics in visible-light-cured materials: methods development. *Dent. Mater.* **7,** 281–287 (1991).

43.   Hong, S. *et al.* 3D Printing of Highly Stretchable and Tough Hydrogels into Complex, Cellularized Structures. *Adv. Mater.* **27,** n/a-n/a (2015).

44.   Ovsianikov, A., Mironov, V., Stampf, J. & Liska, R. Engineering 3D cell-culture matrices: multiphoton processing technologies for biological and tissue engineering applications. *Expert Rev. Med. Devices* **9,** 613–33 (2012).

45.   Torgersen, J. *et al.* Hydrogels for two-photon polymerization: A toolbox for mimicking the extracellular matrix. *Adv. Funct. Mater.* **23,** 4542–4554 (2013).

46.   Qin, X.-H., Ovsianikov, A., Stampfl, J. & Liska, R. Additive manufacturing of photosensitive hydrogels for tissue engineering applications. *BioNanoMaterials* **15,** 49–70 (2014).

47.   Kim, P. *et al.* Fabrication of nanostructures of polyethylene glycol for applications to protein adsorption and cell adhesion. *Nanotechnology* **16,** 2420–6 (2005).

48.   Awad, H., Butler, D., Harris, M., Ibrahim, R. & Wu, Y. In vitro characterization of mesenchymal stem cell-seeded collagen scaffolds for tendon repair: effects of initial seeding density on contraction kinetics. *researchgate.net*

Chapter 3:
Kinetic aspects of solid state reactive polymers

Herein, the kinetics of the solid state reactive materials developed in the previous chapter are more thoroughly analyzed based on photo-DSC experiments and by developing a model describing the solid state polymerization. In addition, the versatility of the solid state reactive polymers was explored by synthesizing a range of materials, and the effect of the different chemical structures on the material properties was determined.

3.1. Introduction

Photo-initiated polymerization is a versatile polymerization mechanism that can be performed solvent-free (above the melting point) and at ambient conditions.[1] It offers both spatial and temporal control, and is used in a number of applications such as dental materials, contact lenses[2], coatings[3] and tissue engineering matrices.[4–7] Although the photopolymerization procedure is fairly straightforward, the underlying mechanisms are quite complex. The free radical polymerization involves behaviors such as auto-acceleration and decelaration[8], quenching[9], radical entrapment[10], volume shrinkage[11], microstructural heterogeneity[12] and incomplete functional group conversion.[13]

A distinction can be made between linear and non-linear (crosslinking) systems, and in this specific case, between polymerization in the solid and in the liquid state (polymer melt or solution). The elementary reaction steps (i.e. initiation, propagation and termination) will not differ between the different systems and conditions, yet the kinetic aspects of the reaction will be significantly impacted.[14] The different features of a crosslinkable photopolymerizable mixture and the network formed after completion of the photopolymerization process, are depicted in Figure 1. In this example, a bifunctional, macromonomer, also called prepolymer, is crosslinked in the melt using a photo-initiator to generate radicals. The most important kinetic aspects of a conventional free radical polymerization, valid for mono- and multifunctional monomers polymerized in the liquid and solid state are outlined in the following paragraphs. Differences between linear and crosslinkable systems, as well as polymerizations occurring in solid versus liquid state will be mentioned when relevant.
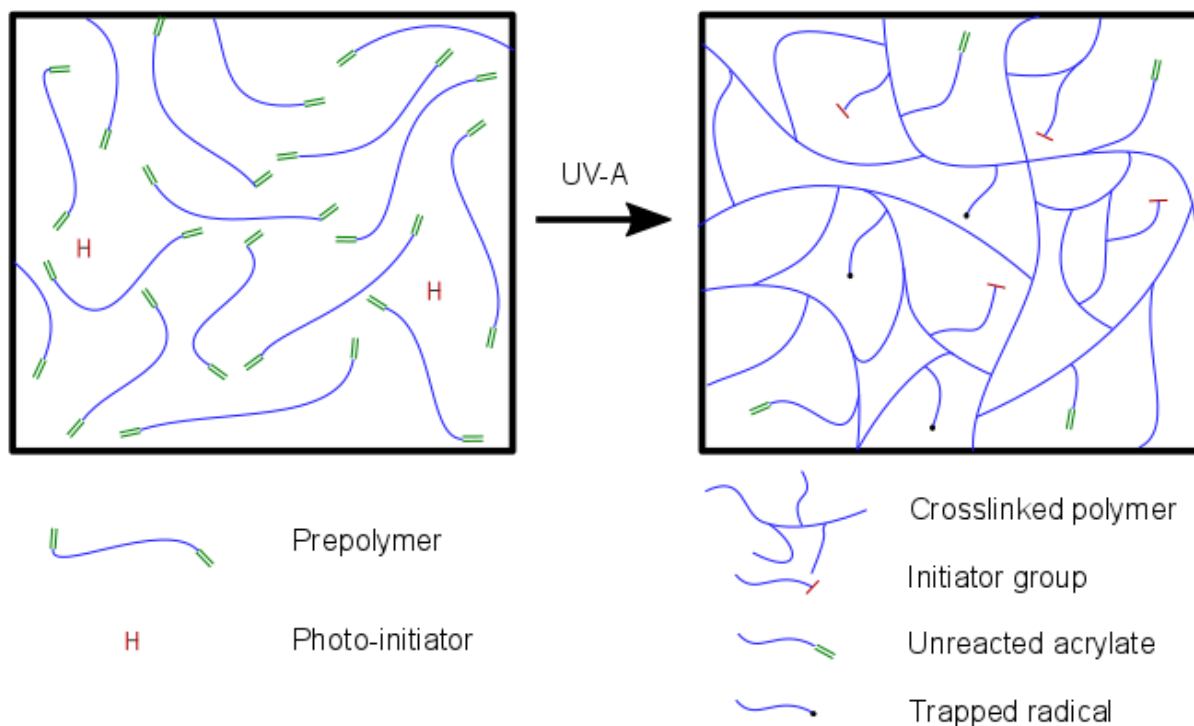
Figure 1: Illustration of the photopolymerization process presenting the system before and after UV irradiation. In this schematic representation, the amount of crosslinking points is reduced compared to the actual situation, for reasons of clarity.

Three main steps can be distinguished for free radical polymerizations including initiation, propagation and termination (see Figure 3).[3,15] The diffusion reactions of the initiator, reactive groups (double bonds) and radicals significantly influence the observed reaction rates of initiation, propagation and termination reactions, and are influenced by viscosity, temperature, monomer structure and solvent.[15] Three diffusion types can be considered in this respect, as shown in Figure 2:[16–19]

- Translational diffusion: center of mass diffusion
- Segmental fluctuation: reorientation of the radical-containing polymer segment
- Reaction diffusion: diffusion of the radical through propagation
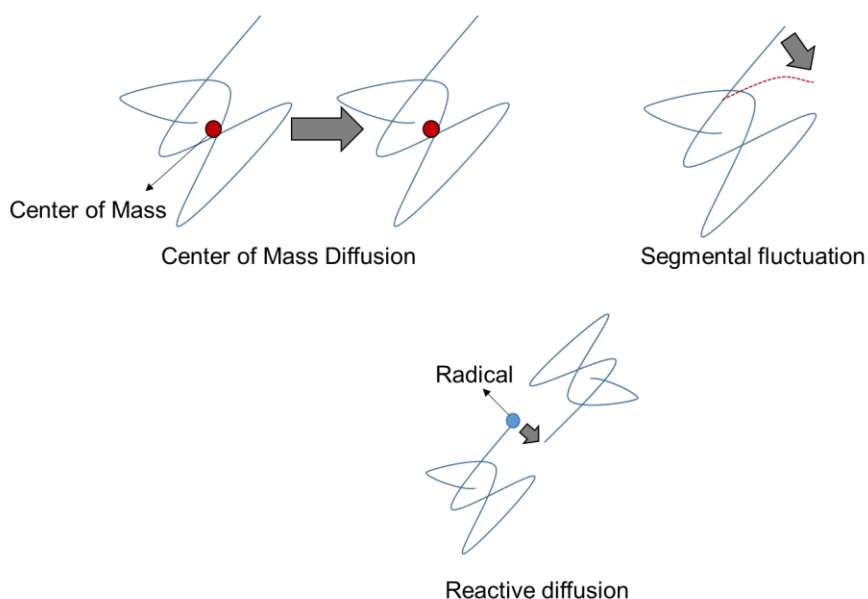
Figure 2: Different diffusion types

Therefore, the observed rate coefficients will vary as the reaction progresses. For polymerizations in the semi-crystalline state, it can be anticipated translational diffusion will be completely suppressed, and propagation and termination reactions can only occur through segmental fluctuation and reaction diffusion.

Initiation
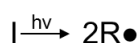
$I \xrightarrow{h\nu} 2R\bullet$ \qquad Initiator decay into primary radicals (I)
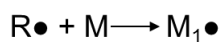
$R\bullet + M \longrightarrow M_1\bullet$ \qquad Reaction of primary radical and monomer (II)

Propagation
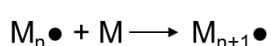
$M_n\bullet + M \longrightarrow M_{n+1}\bullet$ \qquad Monomer addition (III)

Termination

$M_n\bullet + M_m\bullet \longrightarrow M_{n+m}$ \qquad Recombination (IV)
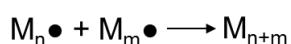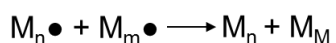
$M_n\bullet + M_m\bullet \longrightarrow M_n + M_M$ \qquad Disproportionation (V)

$M_n\bullet$ \qquad Radical trapping (VI)
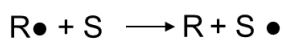
$R\bullet + S \longrightarrow R + S\bullet$ \qquad Scavenged primary radical (VII)
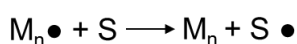
$M_n\bullet + S \longrightarrow M_n + S\bullet$ \qquad Scavenged growing radical (VIII)

Figure 3: Typical reaction steps involved in a free radical polymerization

In free radical polymerizations, different types of initiating systems can be distinguished including photo-, thermal- and redox-initiation. In this work, the focus will lie on photo-initiation, for which initiators can be classified according to two radical producing

mechanisms.[15] The type I photo-initiators generate radicals through a highly efficient α-cleavage process. In this category, benzoin ether derivatives, benzyl ketals, hydroxyalkylphenones, α-amino ketones and acylphosphine oxides can be found.[15] Type II photo-initiators act indirectly by hydrogen abstraction from a radical precursor containing a weak covalent bond. Examples include aromatic ketones, xanthones and thioxanthones, aromatic diketones and 3-keto-coumarins.[15]

In case of a type I photo-initiator, initiation is a one-step process of which the rate R_i depends on the absorbed light intensity of the sample I_a and the efficiency of the photo-initiator to generate radicals, which is expressed as the quantum yield Φ_i. The quantum yield expresses the amount of radicals produced for each absorbed photon.[3] This results in the following equation for step (I) in Figure 3:[3]

$$R_i = \phi_i I_a \tag{1}$$

In the second step of the initiation, the radicals react with the monomer (step II), creating a new radical on the monomer group. When comparing the different reaction steps, the initiation reaction is least influenced by limitations associated with mass and heat transfer.[1] To enable further propagation of the reaction, the radical will continue reaction with other monomers, thereby generating a growing polymer chain as shown in step III in Figure 3. The overall propagation reaction R_p is generally written as:[3,15,20]

$$R_p = k_p [M \cdot][M] \tag{2}$$

where k_p represents the propagation rate coefficient, [M] the double bond concentration and [M·] the radical concentration. The rate of the addition of a primary radical to a monomer (II) is different from the rate when a radical on a monomer reacts with another monomer (III). However, often the generation of the primary radical (I) and the first addition to a monomer (II) are combined into one expression for R_i. In addition, the bimolecular reaction rate is assumed to be chain length independent, although there is evidence that there can be an effect, especially when the monomer results in a more rigid polymer (e.g. methacrylates are more rigid compared to acrylates).[17,21,22] The rate coefficient k_p therefore encompasses a number of different reactions which are combined into one constant. In addition to the reaction of growing polymer chains with different lengths, these include reactions of pendant and monomeric double bonds and chain transfer reactions.[23]

For crosslinking systems specifically, a difference in reactivity arises between free and pendant double bonds. As the reaction propagates, multifunctional monomers are incorporated in the growing polymer chain resulting in pendant double bonds. As a result, the reaction can either propagate by addition of the next monomer, or by reaction with one of these pendant bonds on the same polymer chain (intramolecular) or on a different polymer chain (intermolecular). As the concentration of these pendant bonds on the same chain is higher in the vicinity of the propagating radical, the intramolecular reaction will lead to cyclisation reactions and the formation of compact crosslinked regions called microgels.[15] The occurrence of these cyclization reactions will decrease if the chain length between the double bonds increases (i.e. when polymerizing macromonomers).[15,24–26] Furthermore, unreacted pendant double bonds as well as propagating radicals can become entrapped in the microgel regions and their reactivity decreases due to steric hindrance (see Figure 1). Upon percolation of these microgel regions, a space-filling crosslinked network is formed.[15,23] The resulting structural inhomogeneity leads to internal stress, brittleness and a lower degree of conversion.[1]

In free radical polymerizations, a range of different termination reactions can occur. The importance of each of these termination reactions depends on different factors, including the monomer type, the monomer functionality, the conversion degree, the atmosphere and the viscosity of the reaction mixture.[15] For polymerization reactions in solution, the main termination reaction is assumed to be bimolecular, for which the radicals of two growing polymer chains react either through recombination (IV) or disproportionation (V).[15] As both termination reactions don't have specific effects on the polymerization kinetics, they can be combined in the expression for the bimolecular termination rate. The diffusion mechanisms for this bimolecular mechanism vary depending on the monomer type and reaction conditions.[15] For linear systems in the liquid state, translational diffusion will have an important effect, especially in the first stages of the reaction. For crosslinking systems on the other hand, the larger polymer chains will become entangled or crosslinked in the network, thereby suppressing translational diffusion. Furthermore, in the solid state reactions center-of-mass diffusion is completely inhibited. Under these conditions, bimolecular reactions can still occur either through segmental fluctuation or reactive diffusion.[15] The overall bimolecular termination rate can be expressed as: [3,15,20]

$$R_{tB} = 2k_{tB}\left[M\cdot\right]^2 \tag{3}$$

with R_{tB} being the bimolecular termination rate and k_{tB} the apparent termination rate coefficient. For this ideal behavior, no chain length dependence or radical trapping reactions (VI) are assumed. The latter type of reactions become more important as the reaction progresses and radicals cease to propagate and become "trapped" in the highly crosslinked regions. In addition, for polymers polymerized in the solid state specifically and for crosslinking systems in general, it can be anticipated that this monomolecular termination mechanism will be more important compared to liquid systems. As explained above, under both conditions, translational diffusion is suppressed or completely inhibited. Therefore, even from the onset of the reaction, radical entrapment will play a significant role. For all conditions, the monomolecular termination rate R_{tT} can be expressed as: [3,15,20]

$$R_{tT} = k_{tT}\left[M\cdot\right] \tag{4}$$

with k_{tT} being the rate coefficient.

In addition, radical scavenging by quenching molecules such as O_2 can result in termination, especially when the polymerization is carried out under air atmosphere. These reactions will occur both at the interface of the sample and in bulk, as O_2 molecules can diffuse into the reaction mixture. These can react with a primary radical (VII) or with a radical on the growing polymer chain (VIII).[15] The combined termination rate R_{tS} is expressed using the scavenging rate coefficient k_{tS} and the concentration [S] of the scavenging species: [3,15,20]

$$R_{tS} = k_{tS}\left[M\cdot\right]\left[S\right] \tag{5}$$

Often it is assumed that the radical concentration achieves a steady-state behavior (low and constant global concentration of macro-radicals) early in the polymerization process.[14] Under this assumption, the rate of initiation R_i is equal to the rate of termination R_t. For polymerizations under inert atmosphere for which bimolecular termination and radical entrapment are the predominant termination pathways, this leads to the following expression:[3,15,20]

$$R_i = R_{tB} + R_{tT} \tag{6}$$

or

$$\phi_i I_a = 2k_{tB}[M\cdot]^2 + k_{tT}[M\cdot] \tag{7}$$

The solution of this quadratic equation reads as

$$[M\cdot] = \frac{1}{4k_{tB}}\left(-k_{tT} + \sqrt{k_{tT}^2 + 8\phi_i I_a k_{tB}}\right) \tag{8}$$

Combining equations (8) and (6) results in an expression for the polymerization rate (valid in the liquid and solid state for mono- and multifunctional monomers):

$$R_p = \frac{k_p}{4k_{tB}}[M]\left(-k_{tT} + \sqrt{k_{tT}^2 + 8\phi_i I_a k_{tB}}\right) \tag{9}$$

This can also be expressed as a function of the degree of polymerization (or double bond conversion) p:

$$R_p = \frac{k_p}{4k_{tB}}[M]_0(1-p)\left(-k_{tT} + \sqrt{k_{tT}^2 + 8\phi_i I_a k_{tB}}\right) \tag{10}$$

In liquid polymerizations of both linear and crosslinkable systems, an auto-acceleration or gel effect can be observed at relatively low conversions after which the polymerization rate rapidly increases to several times its original value despite monomer consumption.[15] This will lead to a maximum in the polymerization speed, followed by a deceleration when the reaction proceeds until vitrification sets in. This behavior is mostly governed by the termination reactions. The observed biomolecular termination rate is diffusion- controlled from the start of the reaction. The onset of this auto-acceleration will differ when comparing liquid and crosslinking systems.

For linear polymerizations, translational diffusion will decrease with increasing conversion due to the increased viscosity, the increasing hydrodynamical volume (due to the increasing chain length) and the degree of crosslinking of the system.[21] The segmental fluctuation on the other hand will increase as the polymer chain length increases. Initially, these two will be balanced and the termination rate remains constant. However, early in the reaction (e.g. around 20-25% conversion for methyl methacrylate),[15] the translational diffusion starts to control the termination, while the propagation will stay unaffected. This leads to an increased radical concentration and an auto-accelerating effect on the overall reaction rate (gel-effect). As the conversion

further increases, the translational diffusion decreases and the propagation speed becomes affected as well, resulting in deceleration. Near the maximum of the polymerization rate, the controlling mechanism changes from translational diffusion to reaction diffusion, effectively preventing an even larger decrease of the overall polymerization speed. [15] The reaction continues until the onset of vitrification, at which the reaction stops due to a complete lack of mobility.

A similar rate profile can be observed for crosslinking reactions. However, the mobility of the macroradicals is restricted from the onset of the reaction because of the network formation. The gel point, which is the stage at which the microgel regions join to form a connected network, occurs at very low conversions of typically 1-2%. Therefore, the auto-acceleration step of crosslinking systems will occur at the onset (conversions < 5%) of polymerization.[15,27]

In this chapter, the kinetics of the solid state reactive polymers are investigated both in solution, melt and in the semi-crystalline solid state. In a first part, a qualitative description of the polymerization is provided. The auto-initiation and the effect of the atmosphere, the polymerization temperature and the thermal history are investigated. In addition, the versatility of the system is demonstrated by synthesizing and characterizing a range of polymers with different backbones and different molar masses. In a second part, a model is developed for the polymerization in the solid state of which the main focus will lie on the importance of mono- and bimolecular termination reactions.

3.2. Materials and methods

3.2.1. Polymer synthesis

The polymers were synthesized as described in Chapter 2. Poly(ethylene glycol) with a molar mass of 2000 g mol^{-1}, 4000 g mol^{-1}, 8000 g mol^{-1}, 10000 g mol^{-1} and 20000 g mol^{-1} and poly(ε-caprolactone) with a molar mass of 2200 g mol^{-1} were obtained from Merck. The molecular weight of the backbone is mentioned in the polymer code (e.g. PCL$_{2200}$-OEOAcr was prepared using a PCL backbone of 2200 g mol^{-1}). With increasing molar mass, the viscosity started to increase as well. For the polymer with a backbone of 8000 g mol^{-1}, the viscosity after completion of the reaction became too high to remove the polymer from the reactor. Therefore, double distilled water was added (30 wt% on total mass in the reactor). This was subsequently removed using lyophilization (Christ alpha I-5).

For the polymers with molar masses of 10000 g mol^{-1} and 20000 g mol^{-1}, the viscosity was too high at the onset of the reaction, preventing effective stirring and reaction. Therefore, 2-butanone (Sigma-Aldrich) was added as an inert solvent (10 wt% on the total mass in the reactor). During the initial drying step, part of the 2-butanone evaporated (about 15% of the amount initially added). This was first replaced with fresh 2-butanone, before continuing the reaction.

Once the reaction was completed, double distilled water was added (30 wt% of the total mass in the reactor) and the 2-butanone was stripped until the amount of 2-butanone that was initially added (10 wt% on the total mass in the reactor) was recovered. After synthesis, the polymers were dried in the vacuum oven at 80°C during 24h to remove water and traces of 2-butanone. Although it can be anticipated that a significant part of the inhibitors will be consumed during this drying step, no stability issues were experienced with the polymers during use. Further stability studies can determine if the inhibitor amounts need to be adjusted to guarantee long-term stability.

The theoretical acrylate concentration for each polymer can be calculated by dividing the amount of acrylates (in mole) by the combined mass of the backbone, the diisocyanate and the end group incorporated during synthesis. For example, when preparing 1.161 kg of PEG$_{2000}$-OEOAcr, the double bond concentration can be calculated as follows: 0.745 mole of double bonds, divided by the total mass of 1.161

kg (745 g PEG 2000 + 165.6 g IPDI + 250.3 g OEOAcr). This results in a theoretical acrylate concentration of 0.642 mmole g^{-1}.

3.2.2. UV absorption spectroscopy

UV-VIS spectra were recorded on a Varian Cary 100 Bio UV-VIS spectrophotometer equipped with a Cary temperature and stir control. Samples were measured in quartz cuvettes with a path length of 1.0 cm in the wavelength range of 200 to 400 nm. The concentration of each sample was 0.5 wt% in acetonitrile. A baseline correction was performed and the absorbance of each spectrum was normalized to 1.

3.2.3. Photo-DSC measurements

The photo-DSC measurements were performed as described previously in Chapter 2 (section 2.1.5). The effect of thermal history was investigated for two temperatures, i.e. isothermal crystallization at 20°C and dynamic crystallization with an end temperature of -20°C. After crystallization, photoolymerization was conducted at temperatures ranging from -20 to 90°C, as indicated for each measurement. The photopolymerization rate and double bond conversion were calculated as mentioned earlier (section 2.1.5).

For qualitative purposes, the measured heat flow profiles are shown and compared. However, for heat-flux DSC instruments as used in this work, the recorded signal does not reflect the true heat flow consumed or evolved from the sample but is actually smeared by the experimental system function, which is influenced by many factors such as instrument design, crucibles, atmosphere, etc.[28,29] The smearing is mathematically expressed by a convolution integral and a deconvolution procedure is required to return to the true sample heat flow. The characteristic response time of the system is usually within the order of a few seconds and has a minor effect on thermal events which are slow enough (higher than the characteristic response time).However, the timescale of the initial acceleration step for the photopolymerizations studied herein is within the range of seconds and the instrumental response needs to be eliminated in order to recover the correct polymerization exotherm for subsequent kinetic modeling. The system function can be determined from the heat flow output resulting from a rectangular input signal generated by the simultaneous illumination of the sample and reference positions using a UV-light source controlled with a shutter. The deconvolution theorem was applied to solve the inversion problem for the system

function which finally could be approximated using $h(t) = At^{\beta}e^{-t/\tau}$ with β=2.7 and τ=0.71s.

The latter function was then used to extract the corrected heat flow signal from the measured polymerization exotherm.

The reproducibility of the photo-DSC measurements was high, evidenced by random repeat measurements which showed minor deviations of a few percentages. A slightly stronger effect was determined when measuring polymers from different batches, e.g. in chapter 2 and 3 two different batches were used, leading to a different double bond conversion in figure 7 (chapter 2) (around 50% without PI) and figure 7 (chapter 3) (around 65% without PI). As this technique is quite exact, the double bond conversion or polymerization kinetics were not checked using other techniques (e.g. ATR-FTIR).

3.2.4. Swelling experiments

Swelling experiments were performed as described in Chapter 2 (section 2.1.7).

3.2.5. Mechanical tests

The influence of the polymer backbone length on the mechanical properties of the crosslinked samples was evaluated by tensile tests using the Universal tester 10-KM (Hounsfield) with a load cell of 100 N. Dog-bone shaped samples with a length of 30 mm were prepared from cross-linked hydrogel films (thickness 1 mm). The tensile properties of the hydrogel samples were determined immediately after UV-curing with their initial water content or after equilibrium swelling in double distilled water (swollen samples). All measurements were performed at room temperature. A preload force of 0.3 N was applied and the specimens were deformed with a crosshead velocity of 10 mm/min. The Young's modulus was calculated from the slope of the initial, linear part of the stress/strain curves using the QMat software.

3.3. Qualitative aspects of solid-state photopolymerization

3.3.1. Investigation of the auto-initiation

In a typical photo-initiation process, the initiator molecule absorbs one quantum of radiation to become energetically excited.[30] It is important that the energy of the absorbed photon corresponds to the energy difference between the ground state and the excited state. Following intersystem crossing, a triplet state can arise from the

excited singlet state. In case of type I photo-initiators, from this triplet state, radicals are formed by α-cleavage of the C-C bond or by hydrogen abstraction from a donor molecule for type II photo-initiators.[30]

In Chapter 2, the auto-initiation capabilities of the materials developed in this work were demonstrated using photo-DSC. Auto-initiation of acrylates has been reported in literature, although this has been mainly observed at high energy UV light (λ < 230 nm).[31,32] Knolle *et al* proposed three initiation mechanisms based on quantum chemical calculations and absorption spectra, depicted in Figure 4. [31,32] The first structure (a) is the short-lived primary triplet state at which the double bond generates two radicals after irradiation. This state can further react by hydrogen abstraction, most likely intermolecular from the CH_2 group next to the oxygen leading to structure (b). In addition, the triplet state acrylate can react with another acrylate in the ground state, leading to structure (c).
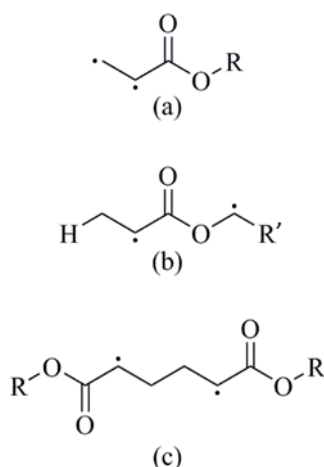
Figure 4: Possible radical species formed by irradiation of acrylates

At 222 nm, tripropylene glycol diacrylate could be efficiently photopolymerized in the absence of a photo-initiator. At this wavelength, thin films (less than 1.5 µm) of tripropylene glycol diacrylate and other acrylate monomers and oligomers were cured. However, at 313 nm (one of the most prominent emission lines of a medium-pressure mercury lamp), no reaction was detected for tripropylene glycol diacrylate.[31] In contrast, Huang *et al* reported that hyperbranched acrylates could be cured at higher wavelengths using medium-pressure mercury lamps.[33] They propose that the structure of their hyperbranched acrylates causes a red shift of the π-π* absorption, possibly due to overlap of π-π orbitals from neighboring acrylate groups. This red shift causes the absorption to shift towards the UV-A wavelength range, enabling the auto-initiation.
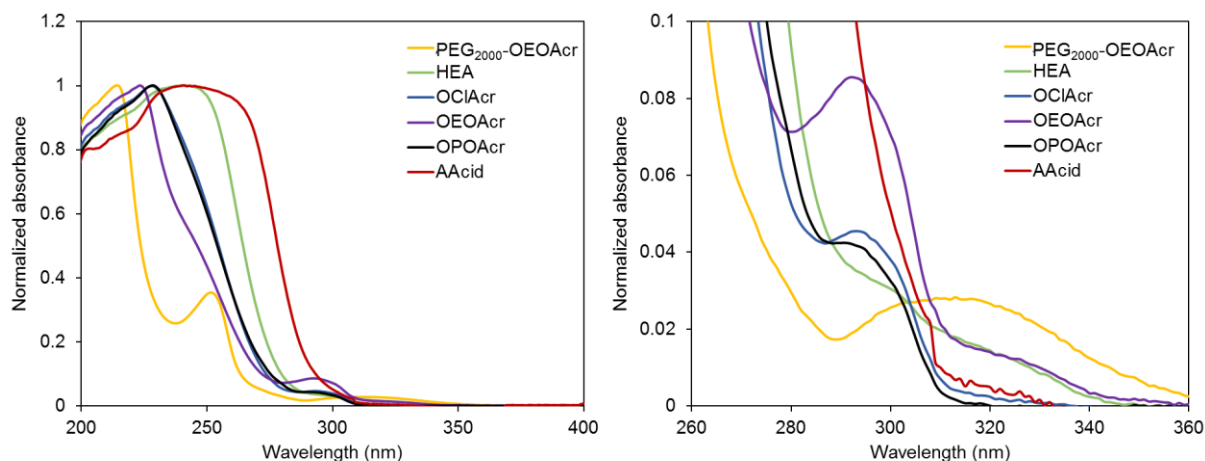
Figure 5: Scaled UV absorption spectra for the model prepolymer (PEG$_{2000}$-OEOAcr)), hydroxy ethyl acrylate (HEA), oligo(caprolactone) acrylate (OClAcr), oligo(ethylene oxide) acrylate (OEOAcr), oligo(propylene oxide) acrylate (OPOAcr) and acrylic acid (AAcid). The left image is the full spectrum, while the right image represents a magnification of a region of interest in the spectrum.

In Figure 5, the UV absorption spectrum determined in acetonitrile for the model polymer PEG$_{2000}$-OEOAcr is shown. In addition, absorption spectra were determined for the different end groups applied and described in Chapter 2 (hydroxy ethyl acrylate (HEA), oligo(caprolactone) acrylate (OClAcr), oligo(ethylene oxide) acrylate (OEOAcr), oligo(propylene oxide) acrylate (OPOAcr)) as well as for acrylic acid (AAcid). From these spectra, it is clear that the investigated (macro)monomers show a significant absorption above 300 nm. Although the absorption is dependent on experimental conditions such as concentration and solvent, these measurements clearly show that the π-π* absorption band is strongly influenced by the chemical environment of the acrylate. For the polymer (yellow plot) the absorption peak broadens and shifts towards higher wavelengths, which explains its auto-initiating capability. This can also be observed for the (macro)monomers, especially OEOAcr and HEA. The photo-DSC measurements of these compounds shown in Chapter 2 indeed show that they can be photopolymerized quite efficiently. Although no exact explanation was found for the absorption differences of these monomers, oligomers and prepolymers, it can be hypothesized that there will be an effect of hydrogen bonding.

It can be anticipated that in the solid state, the auto-initiation of the acrylates will be influenced as a result of the structural changes. The phase separation into amorphous acrylate-rich zones and crystalline PEO-rich zones will result in areas with an increased concentration of acrylates. This will benefit the reaction of the short-lived primary radical state (a) in Figure 4 with a nearby acrylate to create structure (c) as their π-π

orbitals can more easily overlap. This overlap will also shift the absorption maximum of the π-π* transition, resulting in more efficient initiation at lower energy irradiation. Therefore, it can be expected that the auto-initiation will be more efficient in the solid state compared to the molten state.

3.3.1.1. Comparing the polymerization with and without a photo-initiator.

In this work, 1-hydroxycyclohexyl phenyl ketone (HCPK) was selected as a photo-initiator. For many years, α-hydroxyketones have been used as photo-initiators as they can efficiently produce benzoyl-ketyl radical pairs through type I cleavage upon UV irradiation (see Figure 6). Both radicals have a different reactivity. More specifically, for the reaction with acrylates, the rate coefficient of the ketyl radical was determined to be 1.3×10^7 M^{-1} s^{-1}, while the benzoyl radical has a significantly lower rate coefficient of 2.7×10^5 M^{-1} s^{-1}.[34,35]
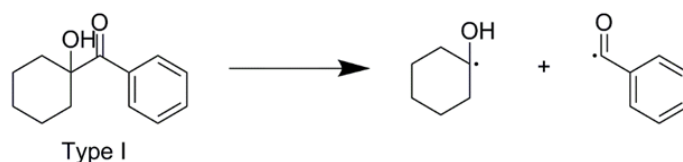
Figure 6: Photocleavage upon UV-irradiation of 1-Hydroxycyclohexyl phenyl ketone (HCPK)

In Figure 7, the heat flow and double bond conversion of the model precursor PEG$_{2000}$-OEOAcr is shown with and without 2 wt% HCPK during the first 40 seconds of UV illumination. A first observation is that the reactivity and double bond conversion both increase upon addition of a photo-initiator. Indeed, the maximum heat flow increases from 3.4 W g^{-1} to 7.2 W g^{-1} in the solid state and from 2.1 W g^{-1} to 7.1 W g^{-1} in the molten state when a photo-initiator is added. The final double bond conversion (after max 260 s of irradiation) increases from 65 % to 76% in the solid state, and from 84% to 87% in the molten state. Based on equations (9) and (10), the polymerization speed is proportional to the square root of the initiation rate. As it is anticipated that the photo-initiator will be more efficient in generating radicals than any self-initiation mechanism, adding a photo-initiator will result in a higher polymerization rate and double bond conversion. Similar results were obtained by Scherzer and Decker as an increase in photo-initiator concentration resulted in an increased polymerization rate and double bond conversion.[36,37]
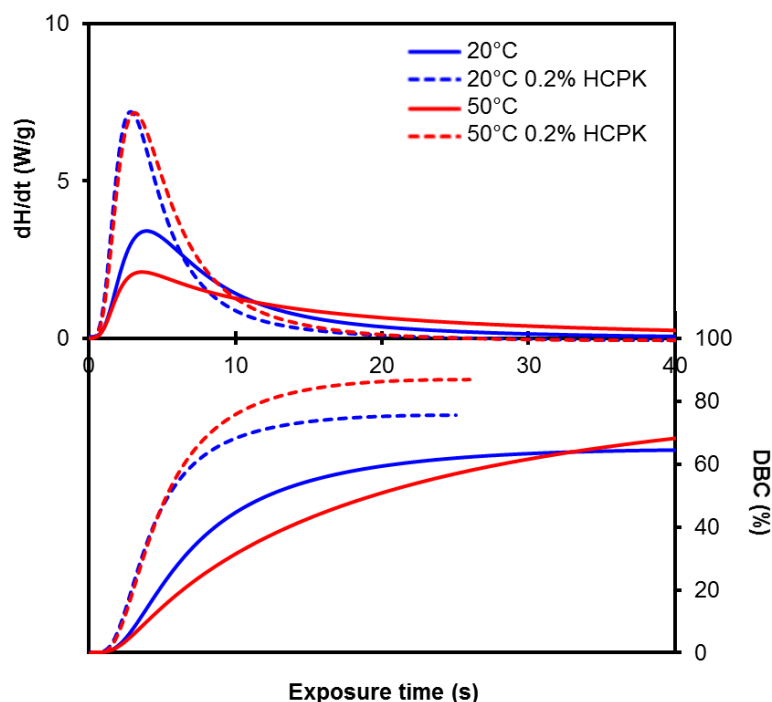
Figure 7: Photo-reactivity of the model precursor PEG2000-OEOAcr in the solid (20° C) and molten (50°C) state with and without a photo-initiator (0.2 wt% HCPK).

Another interesting observation is that the maximum polymerization speed is almost equal (7.2 and 7.1 W g^{-1} respectively) in the solid and the molten state in the presence of the photo-initiator. If one assumes the radical generation of the photo-initiator is not significantly affected by the crystallization, the initiation rate will be similar in the solid or the molten state. Therefore, the reduced mobility for propagation in the solid state is compensated by the local packing of double bonds and suppresses termination through translational diffusion, leading to equal maximal polymerization speeds. The difference in double bond conversion (76% in the solid state and 87% in the molten state) can be explained by the increased mobility in the molten state, allowing the reaction to continue longer and reducing the amount of trapped radicals and double bonds. Without a photo-initiator, there is a difference in maximal polymerization speed at the two temperatures. More specifically, the increased solid state polymerization speed is likely due to more efficient initiation. As the double bonds are closer together, the π-π orbitals can more easily overlap as described above. As a result, more radicals will be formed in the solid state compared to the molten state.
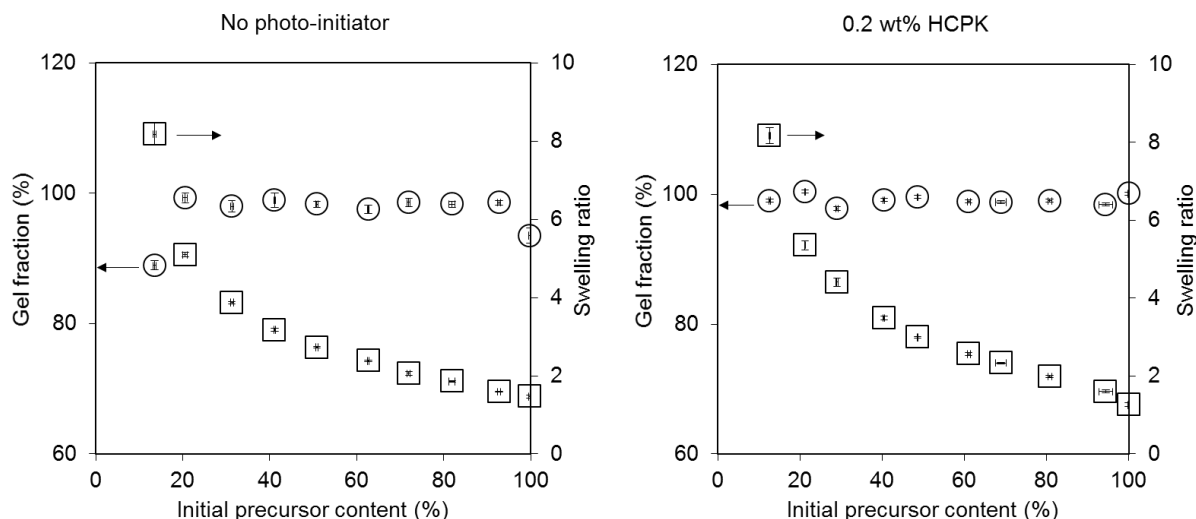
Figure 8: Gel fraction (circles) and swelling ratio (squares) as a function of precursor content for polymerizations with (right) and without (left) 0.2 wt% HCPK as photo-initiator

Next, the auto-initiating efficiency was investigated using swelling experiments for aqueous solutions of AUP. More efficient crosslinking will lead to a higher network density. This results in an increased gel fraction and a decreased swelling ratio. Due to the unique solubility of the precursors, as described in the previous chapter, this could be determined over the whole concentration range. In Figure 8, the gel fraction and the swelling ratio are shown for concentrations ranging from 10 to 100 wt%, in the presence and absence of 0.2 wt% HCPK. Samples at a 100 wt% concentration were crosslinked in the solid state. The results show that there is no significant effect of the presence of a photo-initiator on the swelling ratio (See Figure 8). Regarding the gel fraction, values between 98 and 99% where obtained over the concentration range, with exceptions for the lowest concentration (10 wt%, gel fraction of 89%) and the highest concentration (100 wt%, i.e. in solid state). For the lowest concentration the auto-initiating capacity is decreased due to the dilute conditions which results in a reduced gel fraction . The results in solid state are in line with the observations made during the photo-DSC measurements. Indeed, when adding a photo-initiator, higher conversions were reached which results in a higher gel fraction. The gel fraction reached 93.5 ± 1.2 % in the solid state and increased to 100.1 ± 2.5 % upon addition of a photo-initiator.

3.3.2. Effect of atmosphere on the photopolymerization

It is well established that the presence of atmospheric oxygen has a detrimental effect on radical vinyl polymerizations.[38] Indeed, the onset of the reaction is delayed and is accompanied by a reduction of both the final double bond conversion as well as the polymerization rate. Oxygen molecules can interfere in different steps of the photo-polymerization.[15,20,30] They can quench the excited triplet state of the initiator or react with propagating radicals resulting in the formation of oxygenated radicals. The latter are more stable and therefore less reactive towards double bonds and can further react to form hydroxyperoxides and carbonyl groups.[30] Initially, the oxygen will quench the initiation, resulting in a delay of the polymerization. As a result, the onset of polymerization is delayed until most of the dissolved oxygen is consumed. However, as the small oxygen molecules can easily diffuse into the reaction mixture, they can cause further inhibition of the reaction in the vicinity of the surface. Oxygen inhibition is less pronounced in highly viscous compositions or near the end of the polymerization as the diffusion becomes more restricted.[15] An increase in temperature will also reduce oxygen inhibition as it will decrease oxygen solubility.[39]
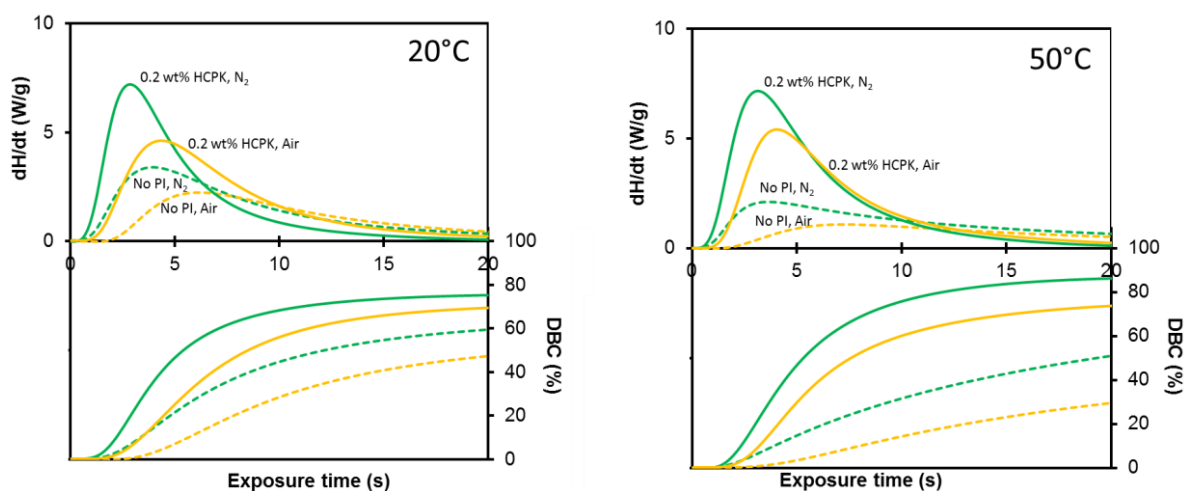
Figure 9: Effect of the atmosphere on the photo-polymerization heat flow (upper panel) and the double bond conversion (lower panel) for the model precursor PEG$_{2000}$-OEOAcr in the solid state (20°C) and the molten state (50°C). The green curves represent the polymerization occurring under inert nitrogen atmosphere, while the yellow curves show the polymerization in air. Full lines are photo-polymerizations in the presence of a photo-initiator (0.2 wt% HCPK), while the dotted lines represent the polymerization occurring without a photo-initiator. Only the first 20 seconds of the polymerization are shown.

Figure 9 shows the effect of oxygen inhibition on the photopolymerization reaction in the solid state (20°C) and in the molten state (50°C) both with and without a photo-initiator for the model precursor with a backbone of 2000 g mol^{-1}. From these curves, it is clear that the typical effects of oxygen inhibition (delay in onset of polymerization, the reduced polymerization speed and reduced double bond conversion) were

observed in this system. The presence of oxygen will cause a delay in the onset of polymerization and this effect is most pronounced for systems without a photo-initiator. As the radical concentration in these systems is lower, the inhibition effect will be higher. This is especially visible in the molten state, where the auto-initiation efficiency decreases and the time to reach the maximum polymerization speed increases from 3.6 to 7.2 s in air atmosphere. In addition to the polymerization delay, the maximum polymerization speed and double bond conversion decrease as well. As a result of oxygen inhibition, for samples without a photo-initiator the maximum heat flow decreases from 3.39 to 2.7 W g^{-1} in the solid state and from 2.1 to 1.1 W g^{-1}, while the final conversion decreases from 59 to 47% at 20°C and from 51 to 29%. Furthermore, the addition of a photo-initiator cannot sufficiently prevent the effects of oxygen inhibition, although it clearly improves the polymerization kinetics as explained earlier.

3.3.3. Influence of the crystallization conditions and the polymerization temperature

Temperature changes will significantly impact the kinetics of photopolymerization reactions, as propagation and termination processes typically follow an Arrhenius-type temperature behavior. In addition, there will be a severe influence on the different diffusion mechanisms. With an increase in temperature, viscosity decreases and diffusion mechanisms such as translational and segmental fluctuations will be enhanced. The overall effect of temperature on photo-initiated polymerizations is quite complex and not fully understood to date.[15,40] For semi-crystalline precursors, another interesting aspect is the effect of the thermal history on the photo-reactivity. As discussed in Chapter 2 (section 2.2.2), the solid state reactivity is related to the crystalline morphology developed upon crystallization. In Figure 10, the melting profiles for polymers that were cooled isothermally (20°C) and dynamically (-20°C) are shown. It is clear that the latter results in a large melting peak indicating a ~~single~~ predominant crystal shape (around 37°C) with a minor shoulder peak (around 29,5 °C). The former results in two distinct peaks (around 31°C and 37°C), indicating a significant presence of two different crystal shapes. This will undoubtedly affect the polymerization kinetics. The total melting enthalpy was 9.04 J g^{-1} for the isothermal crystallization, and 9.72 J g^{-1} for the dynamic crystallization. The exact degree of crystallinity cannot be determined from these values, as no reference material with a known crystallinity

exists. However, based on the heat of fusion of 100% crystalline PEG 2000, which is 188 J g^{-1}, it can be estimated that the degree of crystallinity will be quite low.[41]
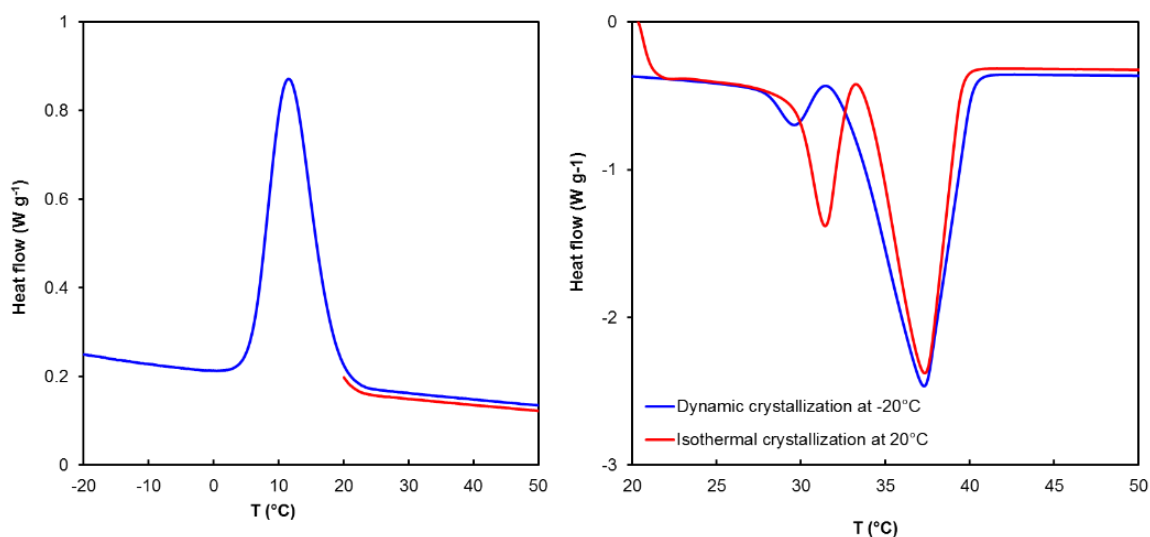
Figure 10: Left: cooling peaks for dynamic (blue) and isothermal (red) crystallization. Right: Melting peaks after dynamic (blue) and isothermal (red) crystallization at 20°C.

To investigate the effect of the crystallization conditions and polymerization temperature, a series of photo-DSC measurements were performed. For the crystallization of the polymer prior to polymerization, an isothermal crystallization was performed at 293 K (20°C) and compared to a dynamic crystallization for which the temperature is reduced to 353 K (-20°C). Secondly, the polymerization was performed with and without 0.2 wt% HCPK as photo-initiator. For these four conditions, the heat of polymerization was measured at 18 different temperatures ranging from 253 K (-20°C) to 363 K (90°C). From the measured heat flow, the polymerization speed was calculated and plotted as a function of time and temperature as shown in Figure 11.
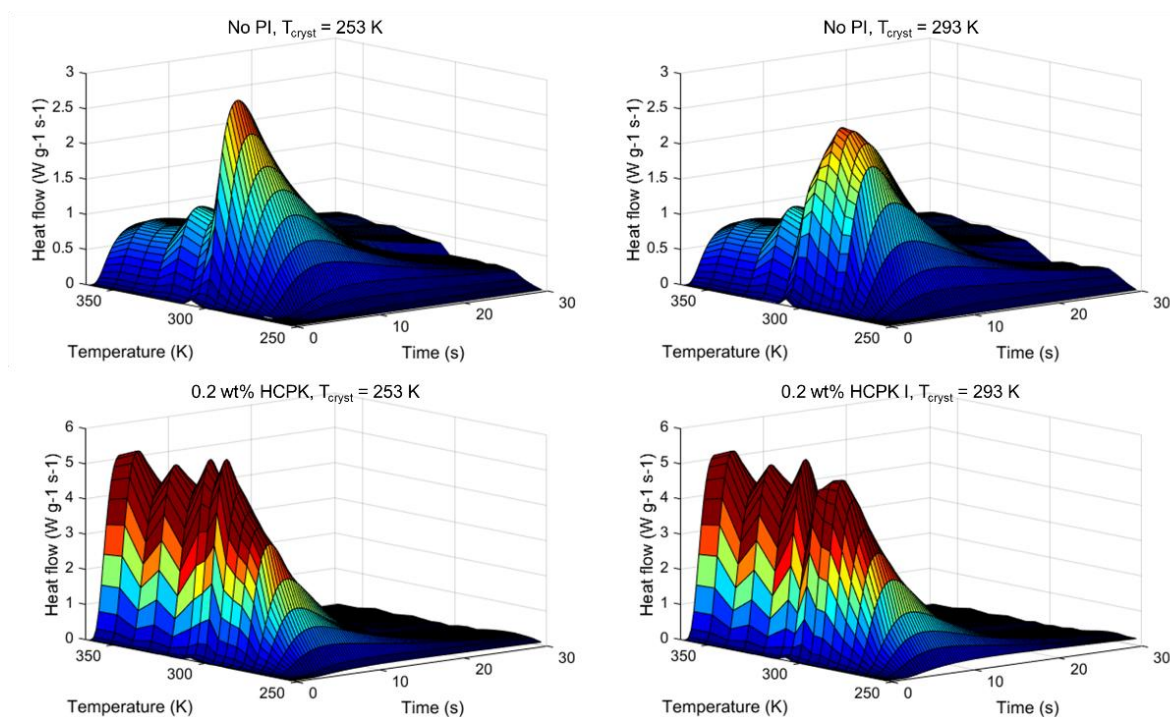
Figure 11: Heat flow as a function of time and temperature for two different crystallization conditions (253 K and 293 K) and with and without 0.2 wt% photo-initiator.

A first observation is that there is a distinct difference between the polymerizations with (bottom panel in Figure 11) and without (upper panel in Figure 11) a photo-initiator. Without a photo-initiator, the polymerization efficiency steadily increases to a maximum close to the melting point of the polymer, followed by a large drop in efficiency in the molten state after which it levels off. When a photo-initiator is present, the behavior in the solid state is quite similar to the behavior in the absence of a photo-initiator, as it increases to a maximum around the melting point. However, after this maximum is reached, the polymerization efficiency seems to remain at this maximum value as the temperature increases and the polymerization continues in the molten state.

The effect of the crystallization conditions is more subtle. Evidently, this effect is only present in the solid state, as the thermal history will be erased when the polymer is in the molten state. When the crystallization is performed dynamically at 253 K (-20°C), the polymerization efficiency will display a sharper increase with temperature and a clear drop after the maximum is reached, in correspondence with the prominent melting peak observed in Figure 10. In contrast, for the polymer that was crystallized isothermally at a temperature of 293 K (20°C), the polymerization speed reaches a maximum, after which it starts to decrease until the polymer is completely molten. The effect of the crystallization conditions is quite similar in the presence and in the absence

142

of a photo-initiator, although the overall polymerization rate is increased at all temperatures when 0.2 wt% HCPK is added. To further understand the interesting behavior of these polymers, the maximum polymerization rate and the final double bond conversion are plotted in Figure 12.
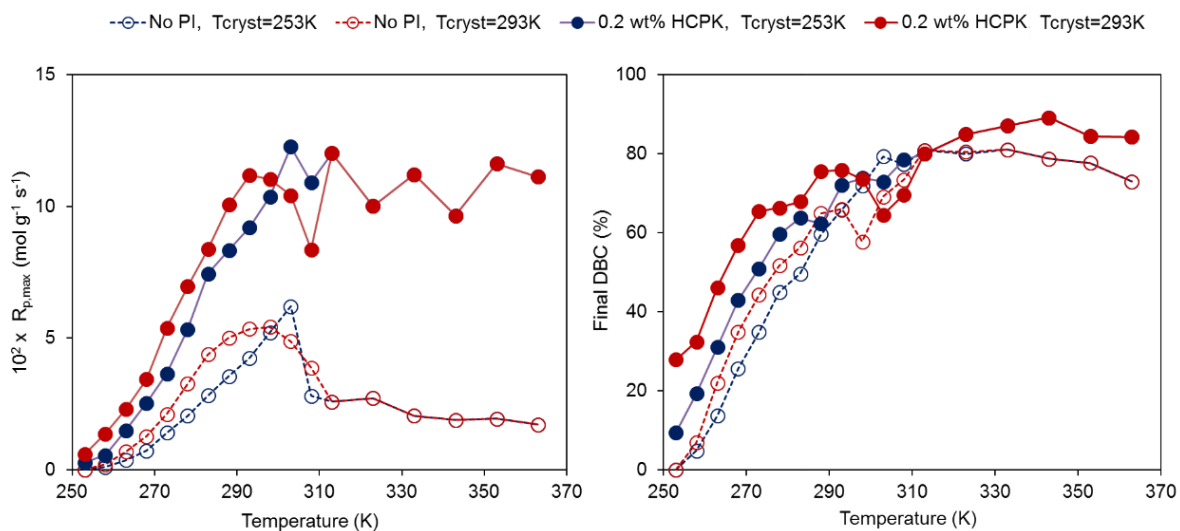
Figure 12: Maximum polymerization speed and final double bond conversion as a function of temperature.

The trends in Figure 11 can be clearly observed in the evolution of the maximum polymerization speed as a function of temperature (Figure 12). Without a photo-initiator, the polymerization speed sharply decreases (from 6.2 mol g^{-1} s^{-1} to 2.8 mol g^{-1} s^{-1} for dynamic crystallization and from 3.8 mol g^{-1} s^{-1} to 2.6 mol g^{-1} s^{-1} for isothermal crystallization) when the polymer is molten (from 303 K for dynamic crystallization and from 308 K for isothermal crystallization). This can be explained by a more efficient initiation in the solid state as the π-π orbitals show superior overlap due to the phase separation which will locally increase the acrylate concentration. Furthermore, translational diffusion is suppressed in the solid state, resulting in a decrease in termination rate. This will also lead to an increased polymerization rate for lower radical concentrations compared to the molten state. However, with a higher radical concentration (in the presence of a photo-initiator), termination through reactive diffusion and segmental fluctuations will increase and the decrease in termination rate will no longer compensate the mobility gain in the solid state. This will result in a lower rate compared to the molten state when a photo-initiator is present, as explained above.

For the dynamic crystallization (blue curves, 253 K or -20°C), a large melting peak can be observed around 37°C, with a minor shoulder peak at 29.5 °C. For the isothermal crystallization (red curves, 293 K or 20°C), the maxima of two melting peaks are around 31°C and 37°C. In the solid state, an exponential-like increase of polymerization rate for the dynamic crystallization (253 K) can be observed both with and without a photo-initiator being present. The maximum value is reached just before the polymer is completely in the molten state, after which the rate drops in the absence of a photo-initiator. This can imply that the reactivity is mostly influenced by the melting of the large peak, and that there is no observable effect of the smaller peak. Isothermal crystallization at 293 K will lead to a different behavior, as the polymerization speed reaches a maximum value and slowly starts to decrease before it reaches the molten state. This is likely a direct result of the presence of the two prominent melting peaks. Indeed, just before the first melting peak (around 304 K), the maximum polymerization speed (5.4×10^2 mol g^{-1} s^{-1}) is reached. The polymerization starts to decrease to 3.8×10^2 mol g-1 s-1 when the second melting peak is reached (around 310 K), after which the polymerization rate further decreases in the molten state (2.6×10^2 mol g^{-1} s^{-1}).

As this behavior is observed both with and without a photo-initiator, it cannot be attributed to differences in initiation rate. The structural differences that occur when the crystallization is carried out under different conditions will affect termination and propagation, resulting in a different behavior as the polymerization temperature increases. For temperatures far from the melting point, the maximum polymerization speed will be higher (maximum difference of 1.2×10^2 mol g^{-1} s^{-1}) when the crystallization occurs at higher temperature. However, close to the melting point, the maximum polymerization speed is higher for the system crystallized at lower temperature (6.2×10^2 mol g^{-1} s^{-1} at 303 K) compared to the system crystallized at higher temperature (5.4×10^2 mol g^{-1} s^{-1} at 298 K).

In the molten state, the maximum polymerization speed seems to fluctuate around a constant value in the presence of a photo-initiator and even shows a slightly decreasing trend in the absence of a photo-initiator. An influence of the different initiators on the temperature-dependent behavior of the photopolymerization was discovered by Scherzer and Decker.[40] At lower temperatures, the propagation dominates while the mobility of free radical chain ends increases with temperature which will affect the

termination rate.[40] For bimolecular termination, the reaction speed is proportional to the square of the radical concentration (see equation 3). At high radical concentrations, the extent of termination reactions will increase leading to a deviation from Arrhenius behavior upon temperature increase, where the rate of termination reactions remains constant or even decreases with increasing temperature.[40]

An overall increase in double bond conversion can be observed with increasing temperature. With a rising temperature, the segmental mobility of the double bonds in the growing network increases, which makes them more accessible for polymerization.[36] This can occur both in the solid state, for which the mobility of the spacer group increases, or in the molten state for which the mobility of both the spacer group and the larger molecular segments increases. Addition of a photo-initiator will increase the final conversion both above and below the melting point. Again, the effect of the crystallization conditions is visible both with and without a photo-initiator in the solid state (see Figure 11 and Figure 12). The dynamic crystallization will lead to a continuous increase with temperature, while the higher temperature creates a maximum, after which the conversion decreases with temperature until the melting point is reached. Above the melting point, a photo-initiator will result in an initial increase in conversion up to 343 K for which a maximum of 89% is reached. After this maximum, the polymerization drops to 84% after which it remains constant. Without a photo-initiator, a slightly decreasing trend in conversion can be observed going from an initial value of 80.1 % to 73.0 %.

The dependence of the polymerization rate R_p can be expressed using an Arrhenius-rate equation:[20]

$$\ln R_p = c - \frac{E_{a,app}}{RT} \tag{11}$$

With c being a constant and $E_{a,app}$ the apparent activation energy for the polymerization. The latter is a highly complex function combining initiation, propagation and termination reactions. This equation is only valid when R_p is measured at a given conversion. Therefore, R_p was plotted as a function of 1/T at a set of given conversions (5-80%) in Figure 13.
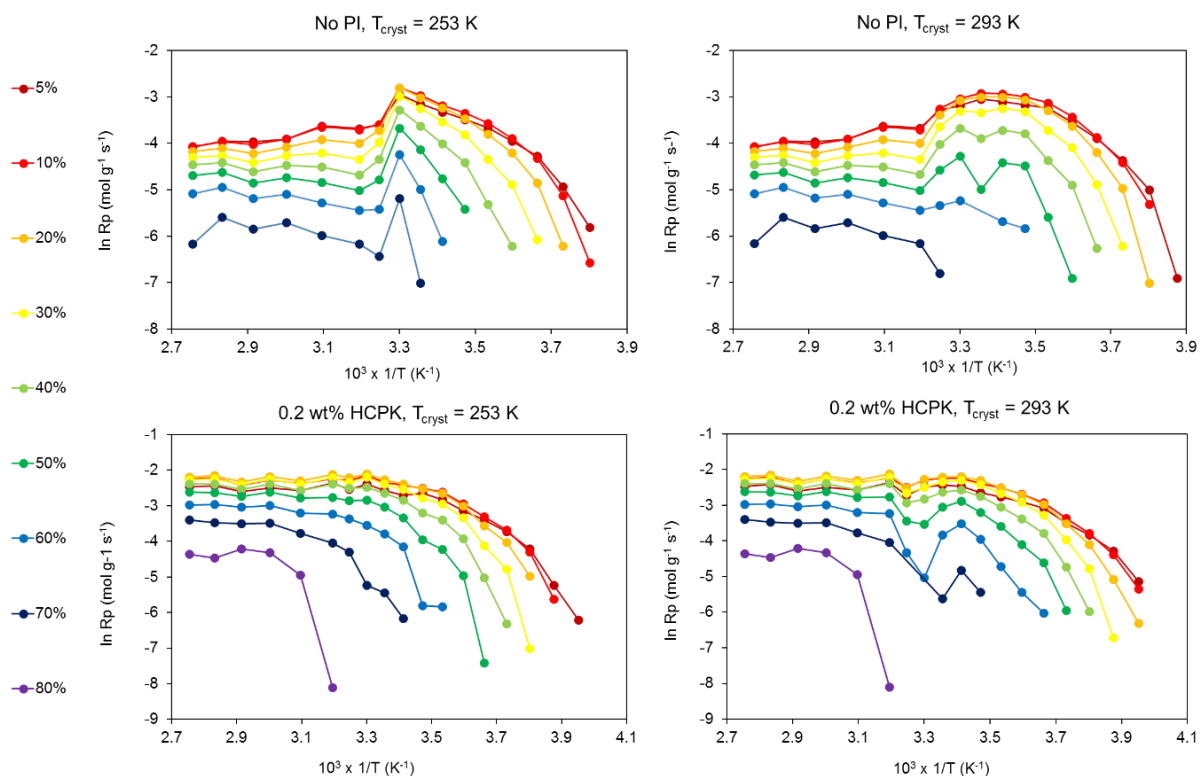
Figure 13: Ln R_p is plotted as a function of the inverse of temperature at a set of given conversions (5-80 %) (Arrhenius plot). The upper panels indicate the photopolymerization without photo-initiator, while the bottom panels represent the photopolymerizationin the presence of 0.2 wt% HCPK. Left panels show samples crystalized at 253 K prior to polymerization while the right panels show samples crystalized at 295K.

Below the melting point, similar observations as those discussed in the previous paragraphs can be made. The crystallization conditions affect the polymerization speed and the effects are more obvious in the absence of a photo-initiator. Interestingly, polymerization in the solid state shows a non-linear behavior as a function of temperature. Again, for the dynamic crystallization, the speed sharply increases to a maximum just before the melting point, while for the isothermal crystallization, a maximum is reached earlier after which the speed slightly decreases until the melting point is reached.

3.3.4. Effect of the polymer structure on the solid state reactivity
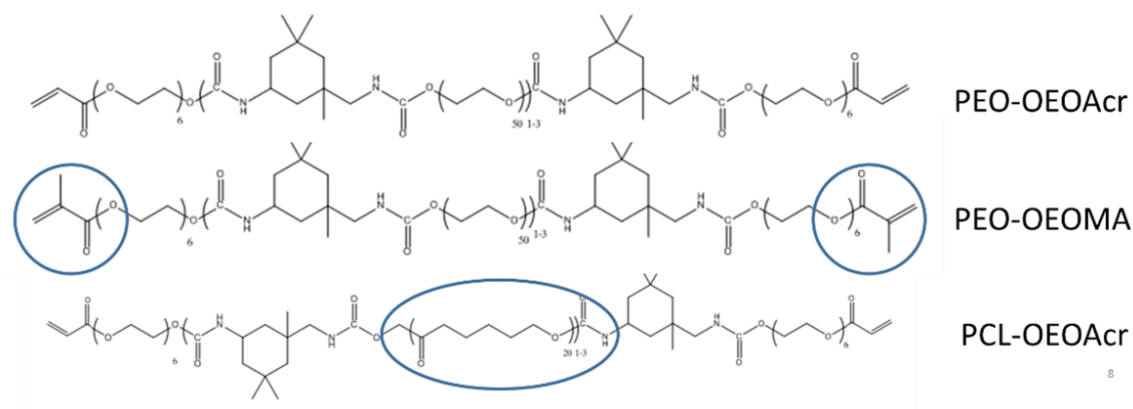
Figure 14: Overview of prepolymer structures applied: model prepolymer (PEO backbone, OEO spacer and acrylate end group, top); acrylate end group in the model polymer has been substituted with a methacrylate group (center); backbone in the model prepolymer has been substituted with a poly(ε-caprolactone) backbone (MW 2200 g mol^{-1}) (bottom)

In Chapter 2, the effect of using different spacer groups on the solid and molten state reactivity was evaluated. To further investigate the versatility of the spacer-based approach enabling solid state polymerizations, two more variations with respect to the polymer structure were implemented. In a first adaptation, the acrylate group was replaced with a methacrylate group (PEG$_{2000}$-OEOMA). It can be anticipated that this will lead to a reduced polymerization speed, as methacrylates are known to be less reactive compared to acrylates.[11,15,27] Furthermore, it is likely that the change from acrylate to methacrylate will affect the auto-initiation, as this takes place within the acrylate group.

Secondly, the backbone polymer was changed from poly(ethylene oxide) to poly(ε-caprolactone) (PCL$_{2200}$-OEOAcr). This is quite a drastic change for the system, as the phase separation that occurs during crystallization plays a major role in the solid state reactivity. By changing the polymer type, the crystal structure will change as well which could influence the solid state reactivity. In addition, the viscosity will change which will affect the kinetics in the molten state.
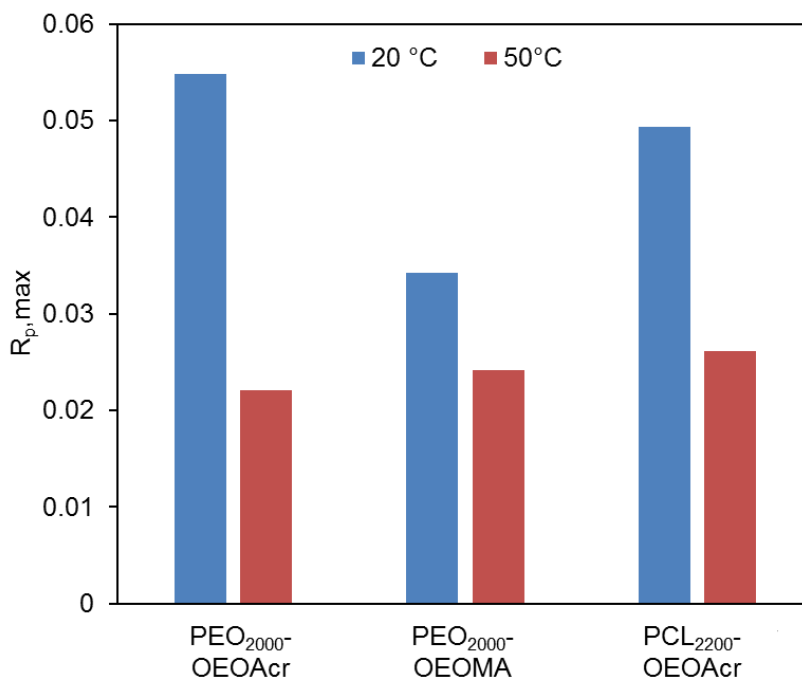
Figure 15: Comparison of the maximum polymerisation rate in the solid (blue) and molten (red) state for the different polymers (PEG$_{2000}$-OEOMAcr, PEG$_{2000}$-OEOAcr, PCL$_{2200}$-OEOAcr)

Figure 15 shows the maximum polymerization speed of PEG$_{2000}$-OEOAcr, PEG$_{2000}$-OEOMA and PCL$_{2200}$-OEOAcr in the solid and the molten state in absence of a photo-initiator determined using photo-DSC. The methacrylate polymer maintains an good reactivity in the solid state (r$_{p,max}$ of 3.2 x 10^2 mol g^{-1} s^{-1}) although the maximum polymerization speed is lower compared to the acrylate polymer (5.4 x 10^2 mol g^{-1} s^{-1}). This can be explained by the lower reactivity of methacrylates compared to acrylates, and possibly by a difference in auto-initiation capacity. Surprisingly, the molten state reactivity remains almost unaffected by the change in end group from acrylate to methacrylate (2.2 x 10^2 mol g^{-1} s^{-1} for PEG$_{2000}$-OEOAcr versus and 2.4 x 10^2 mol g^{-1} s^{-1} for the PEG$_{2000}$-OEOMA). As the change from acrylate to methacrylate will affect initiation, termination and propagation reactions occurring in solution and in the molten state, it is not possible to determine the exact cause of this behavior. The prepolymer with a PCL backbone (PCL$_{2200}$-OEOAcr) shows quite similar reactivity to the model prepolymer (4.9 x 10^2 mol g^{-1} s^{-1} at 20°C and 2.8 x 10^2 mol g^{-1} s^{-1} at 50°C) with a solid state reactivity that is just slightly lower. Possibly, this effect can be attributed to the different crystal structure. Surprisingly, whereas the backbone chemical structure has a profound effect on the final material properties, it does not significantly affect the solid state reactivity.

3.3.5. Effect of the polymer backbone molar mass on the reactivity and physical properties
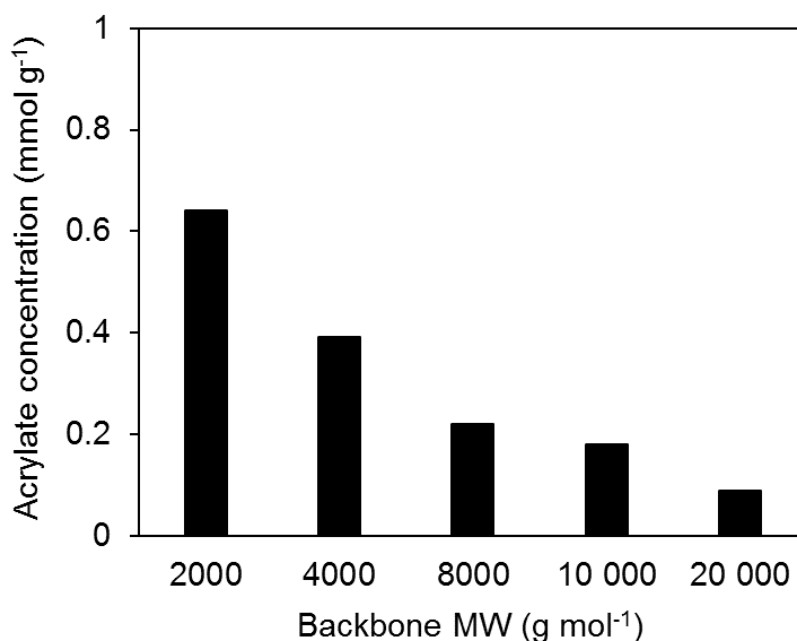
Figure 16: Theoretical acrylate concentration as a function of backbone molar mass

As the backbone molar mass increases, the concentration of acrylates in the system decreases, as shown in Figure 16. Based on the results described in the paragraphs above and in the previous chapter for solutions with a decreasing polymer concentration, it can be anticipated that a decreased initiation capacity is likely to result from an increase in backbone molecular weight. Therefore, it can be anticipated that from a critical molar mass, the polymerization will no longer be successful. In addition, the decreasing acrylate concentration will lead to a decreased network density, which will affect the swelling and mechanical properties of the polymers, as shown in the upcoming paragraphs.

3.3.5.1. Effect of the backbone molar mass on photopolymerization
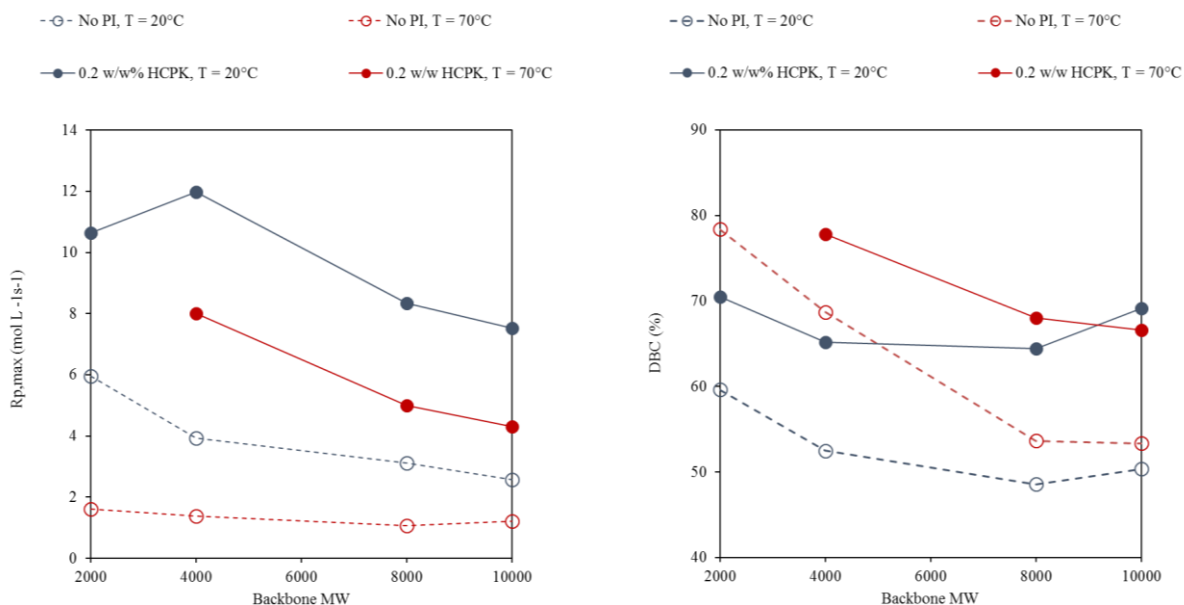
Figure 17: Maximum polymerization rate (left) and double bond conversion (right) as a function of backbone molar mass. The red curves represent the results for polymerizations in the molten state (70°C) while the blue curves show the maximum polymerization rate and double bond conversion for polymerizations in the solid state (20°C). Open circles and dotted lines represent polymerization reactions without PI, Filled circles and full lines are polymerizations with 0.2 wt% HCPK.

Since the melting point increases with increasing molar mass, the temperature was increased from 50°C to 70°C to compare the photo-reactivity of the polymers with increasing backbone molar mass in the melt by photo-DSC. In Figure 17, the maximal polymerization speed and double bond conversion are shown for the different polymers in the presence and in the absence of a photo-initiator. Even for backbone polymers with a molar mass of 10000 g mol^{-1}, efficient crosslinking in the solid state remained possible. Moreover, swelling studies showed that even at 20000 g mol^{-1}, the polymers could still be crosslinked in the solid state(samples swell and do not dissolve, proving the presence of crosslinks). However, the heat flow evolved from the polymerization of these precursors was too low to enable measurement using photo-DSC. The maximum polymerization speed without a photo-initiator decreased from 6.0 x 10^2 mol g^{-1} s^{-1} (PEG$_{2000}$-OEOAcr) to 2.8 x 10^2 mol g^{-1} s^{-1} (PEG$_{10000}$-OEOAcr) in the solid state and from 1.6 x 10^2 mol g^{-1} s^{-1} (PEG$_{2000}$-OEOAcr without PI) to 1.2 x 10^2 mol g^{-1} s^{-1} (PEG$_{10000}$-OEOAcr without PI) in the molten state. Similar trends can be observed for the polymerizations with a photo-initiator, although in the molten state there was an initial increase of the maximum polymerization speed going from 10.6 x 10^2 mol g^{-1} s^{-1} (PEG$_{2000}$-OEOAcr) to 12 x 10^2 mol g^{-1} s^{-1} (PEG$_{4000}$-OEOAcr).

3.3.5.2. Effect of the polymer backbone molar mass on the physical and mechanical properties of the crosslinked hydrogels

3.3.5.2.1. Swelling behavior and gel fraction as a function of backbone molar mass

In Figure 18 and Table 1, the swelling ratio and gel fraction are shown for the different polymers at various concentrations (from 10 wt% to 100 wt%(solid state)) and crosslinked in the absence of a photo-initiator. As the molar mass of the backbone increased from 2000 to 20 000 g mol^{-1}, the solubility of the polymers decreased (data not shown), especially for the polymers with a backbone characterized by a molecular weight of 20 000 g mol^{-1} (PEG$_{20\,000}$-OEOAcr). Indeed, for the latter, a 10 wt% polymer concentration could not be dissolved. Therefore, the swelling degree and the gel fraction were only determined in the solid state for the latter sample. As anticipated, the swelling ratio decreased with increasing precursor concentration, and increased with increasing backbone molar mass. (e.g. for solid state crosslinking (100 wt% concentration), the swelling ratio increased from 1.3 for PEG$_{2000}$-OEOAcr to 16.3 for PEG$_{20000}$-OEOAcr) Similar results were obtained by Padmavathi and Chatterji who observed an increase of about four times for the swelling ratio at a 40 wt% concentration when the molar mass of PEG-diacrylate increased from 200 g mol^{-1} to 3400 g mol^{-1}.[42] In addition, they observed that the swelling ratio for PEG-diacrylate (molar mass 1000 g mol-1) at 40 wt% was about two thirds of the swelling ratio at 20 wt%.
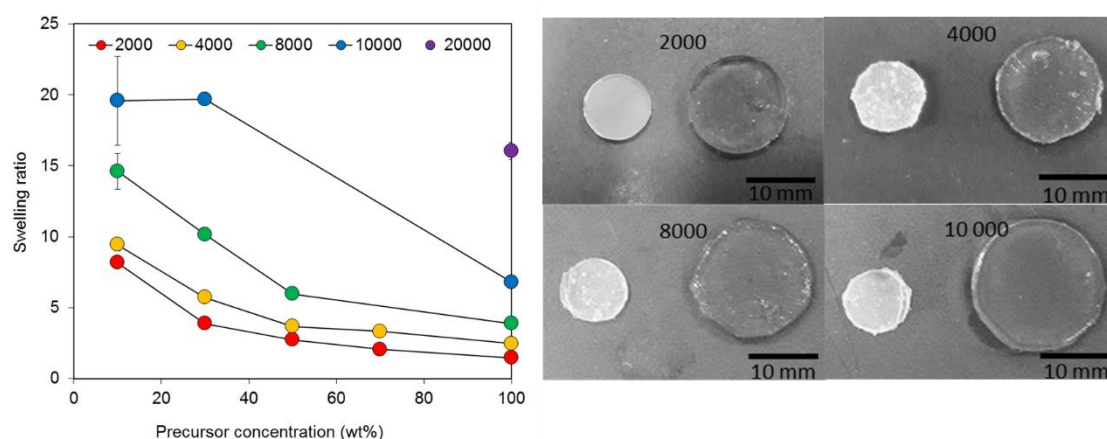
Figure 18: Left: Degree of swelling as a function of precursor concentration for the polymers with different molar mass (2 – 10 kg mol^{-1}), as indicated by the different colors. Samples at a 100wt% concentration where crosslinked in the solid state. Right: Polymers with different backbone molar mass crosslinked in the solid state before and after equilibrium swelling in double-distilled water.

In the solid state, the gel fraction remained above 80% for all polymers, demonstrating the excellent crosslinking efficiency even in the absence of a photo-initiator. For aqueous solutions, the gel fraction remained above 80% as well, except for the lowest polymer concentration evaluated being 10 wt%. Dilute conditions along with an increasing backbone length result in a decreasing gel fraction, ultimately dropping to 56% for the polymers with a backbone molecular weight of 10000 g mol^{-1}. In literature, similar trends where observed for PEG-diacrylates with molar mass between 600 and 3400 g mol^{-1}.[42]

Table 1: Gel fraction (G.F) at different concentrations in water for polymers with a backbone molar mass ranging from 2 to 20 kg mol^{-1}.

		2000 (g mol^{-1})	4000 (g mol^{-1})	8000 (g mol^{-1})	10000 (g mol^{-1})	20000 (g mol^{-1})
10 wt%	*G.F.. (%)*	88.93 ± 0.69	78.71 ± 2.73	75.97 ± 2.66	56.14 ± 14.28	n.a.
30 wt%	*G.F.. (%)*	97.99 ± 0.88	88.83 ± 0.42	95.26 ± 2.83	89.65 ± 1.11	n.a.
50 wt%	*G.F.. (%)*	98.36 ± 0.47	83.93 ± 0.38	85.54 ± 1.21	n.a.	n.a.
70 wt%	*G.F.. (%)*	98.6 ± 0.63	101.59 ± 1.08	n.a.	n.a.	n.a.
100 wt%	*G.F.. (%)*	93.51 ± 1.18	85.33 ± 1.07	89.94 ± 1.73	81.6 ± 1.7	80.12 ± 1.63

3.3.5.2.2. Tensile properties of the polymers with increasing backbone molar mass
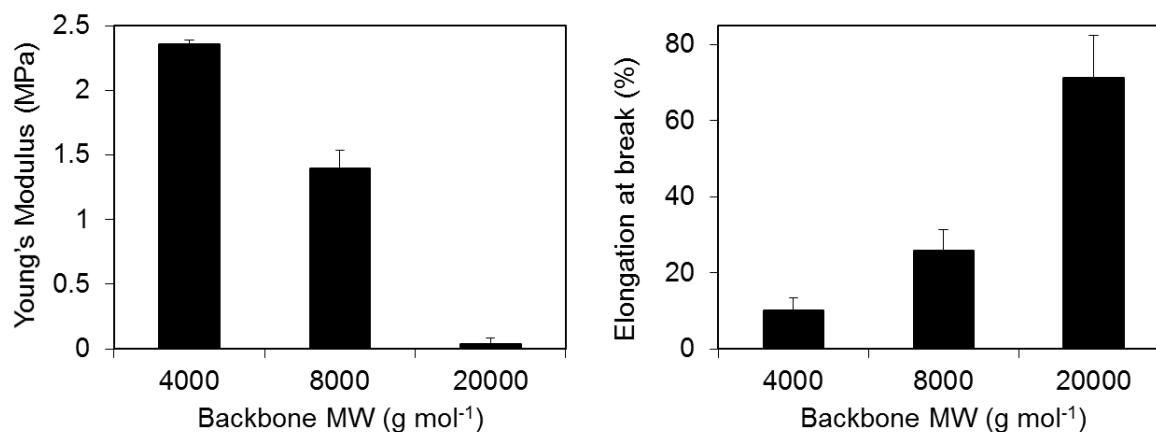
Figure 19: Young's modulus and elongation at break for samples with different molecular masses, crosslinked in the solid state and equilibrium swollen in double distilled water (room temperature).

In Figure 19, the Young's modulus and elongation at break are shown for a selection of polymers with different molar masses, crosslinked in the solid state in the absence of a photo-initiator after equilibrium swelling. The increasing backbone molar mass results in a decreasing network density, which leads to a decreasing Young's modulus,

and an increasing elongation at break. For example, the Young's modulus decreased from 2.4 MPa for PEG$_{4000}$-OEOAcr to 0.04 MPa for PEG$_{20\ 000}$-OEOAcr. The elongation at break on the other hand increased from 10% for PEG$_{4000}$-OEOAcr to 71% for PEG$_{20000}$-OEOAcr. This clearly demonstrates that the backbone molar mass can be used to tune the mechanical properties of the polymers developed.
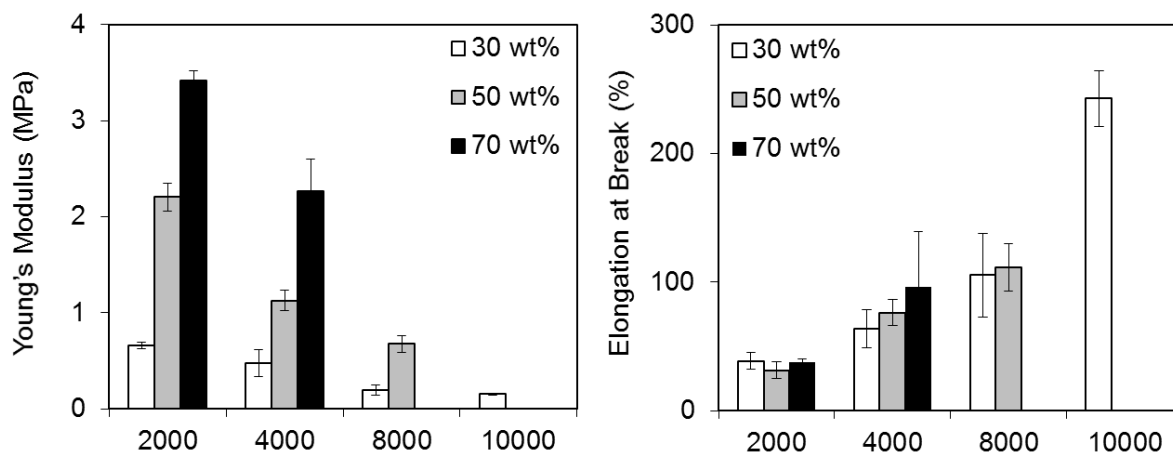
Figure 20 Young's modulus and elongation at break for samples with different molar masses, crosslinked at concentrations ranging from 30 to 70 wt%.

In addition to the backbone molar mass, the water content prior to crosslinking also influences the final mechanical properties. In Figure 20, the results are shown for samples with concentrations ranging from 30 to 70 wt% and molar masses varying between 2000 and 10000 g mol^{-1}. Again, due to solubility issues with the higher molar masses, the samples with high molar mass and high precursor content could not be measured. Similar to the results in the solid state, upon increasing the molar mass, the Young's modulus will decrease while the elongation increases. For example, at a 30 wt% polymer concentration, the Young's modulus decreases from 0.66 MP[43]a for PEG$_{2000}$-OEOAcr to 0.15 for PEG$_{10000}$-OEOAcr. The water content prior to crosslinking will have a strong influence on the elasticity modulus (for PEG$_{2000}$-OEOAcr, the Young's modulus increases from 0.66 MPa for a 30 wt% concentration up to 3.4 MPa upon increasing the concentration to 70 wt%). These values within the same range of those obtained in literature for PEG-diacrylate (e.g. 0.09 MPa for a 10 wt% hydrogel of PEG with a molar mass of 3400 g mol^{-1})[44,45]. However, the water content prior to crosslinking does not significantly affect the elongation at break. A similar observation was made in literature for a low molar mass PEG-dacrylate (508 g mol^{-1}), where there was a 2% difference in elongation for a concentration increase from 65 wt% to 80 wt%. [45,46]For the samples with a high water content and a high molar mass, the sample

becomes quite stretchable(around 37% for PEG_{2000}-OEOAcr, up to 243% for PEG_{10000}-OEOAcr) with an ultimate elongation close to 250%.

3.4. Kinetics of the solid-state polymerization: a scaling model

3.4.1. Model development

In this part of the work, a model is developed based on scaling laws to capture the structural dynamics behind the reaction kinetics of solid state photo-polymerization. Structural aspects associated with polymer properties are often expressed using scaling laws (e.g. network formation and gelation).[47] As the solid state photo-polymerization of macromonomers has never been described earlier in literature, kinetic models are not yet available. The various initiation, propagation and termination reactions occurring in the solid state will be different from those witnessed in solution or melt. However, the overall reaction profile is still quite similar, with the polymerization speed displaying an initial acceleration step, followed by a decrease until the reaction stops. In the molten state, this reaction profile is governed by bimolecular termination through translational diffusion (except in the later stages of polymerization when network formation reduces the mobility within the system). However, in the solid state, the translational diffusion mechanism is inhibited as the crystallinity restricts any translational movement. In the proposed model, three different mechanisms determine the reaction profile:

- a zero-order initiation mechanism which is assumed to be independent of the macromonomer concentration
- a first order monomolecular termination mechanism being for instance radical trapping
- second order bimolecular mechanisms for propagation and termination, which are still possible in the solid state through reactive diffusion modulated by segmental fluctuations of the flexible spacers

The dependence of the first and second order mechanisms on the structural changes occurring during polymerization is captured by scaling laws expressed in terms of the functional conversion p. Herein, a power law expression is applied for the structurally-controlled dynamic rate constants. After determining the coefficients, information can be derived on the structural dependence of the different reaction mechanisms.

The present modeling approach is based on a quasi-steady-state assumption for the polymerization leading to an expression for the polymerization rate as derived in equation (10) in the introduction of this chapter. In this equation, the first and second order termination mechanisms are included. Second order termination reactions are combined in a single bimolecular rate coefficient k_{tb}, while k_{tT} expresses first order termination.

$$R_p = \frac{k_p}{4k_{tB}}[M]_0(1-p)\left(-k_{tT} + \sqrt{k_{tT}^2 + 8\phi_i I_a k_{tB}}\right) \tag{10}$$

which can rewritten in the simple parametrized form

$$R_p = (1-p)\left(-K_{Tbp} + \sqrt{K_{Tpb}^2 + K_{ipb}}\right) \tag{12}$$

where

$$K_{Tpb} = [M]_0 \frac{k_{tT}k_p}{4k_{tb}} \tag{13}$$

$$K_{ipb} = [M]_0 \frac{\phi_i I_a k_p^2}{2k_{tb}} \tag{14}$$

If the second factor in Eq. (12) is constant, R_p should decrease linearly with conversion from an initial value $R_{p0} = K_{Tbp} + \sqrt{K_{Tpb}^2 + K_{ipb}}$ down to zero. Obviously, other conversion-dependent factors control the overall polymerization rate to account for the experimentally measured acceleration-deceleration polymerization profiles.

Using Eyring's theory, the apparent (effective) rate coefficients for bimolecular propagation and termination ($i = p, tb$) can be expressed as a function of the chemical rate constant $k_{c,i}$ and a dynamic rate constant $k_{d,i}$ reflecting structurally-dependent dynamic changes (e.g. the different diffusion/fluctuation mechanisms occurring throughout the reaction).

$$k_{e,i} = \frac{k_{c,i}}{1 + k_{c,i}/k_{d,i}} \tag{15}$$

Assuming that the structural mechanisms effectively control the apparent reaction rate ($k_{d,i} \ll k_{c,i}$), equation (15) can be reduced to:

$$k_{e,i} \approx k_{d,i} \tag{16}$$

Structural aspects affecting polymer properties are often expressed using scaling laws (e.g. network formation and gelation). Hence, a power law expression is introduced for the structurally controlled dynamic rate constants including a cut-off conversion $p_{m;i}$.

$$k_{e,i} = k_{d,i} = k_{d,i}^0 (1 - p / p_{m,i})^{m_i} \qquad (17)$$

As the first order termination equation is assumed to be monomolecular, it has no chemical contribution and is only structurally controlled, i.e.

$$k_{tT} = k_{tT}^0 \ (1 - p / p_{m,tT})^{m_{tT}} \qquad (18)$$

The cut-off value for the propagation, bimolecular termination and trapping can be approximated by the maximum conversion p_{max}

$$p_{m,p} \approx p_{m,tb} \approx p_{m,tT} \approx p_{\max} \qquad (19)$$

Introducing this cut-off value in equations (13) and (14), results in:

$$K_{ipb} = [M]_0 \frac{\phi_i I_a k_p^2}{2 k_{tb}} = A(1 - p / p_{\max})^\alpha \qquad (20)$$

$$K_{Tpb} = [M]_0 \frac{k_{tT} k_p}{4 k_{tb}} = B(1 - p / p_{\max})^\beta \qquad (21)$$

where

$$A = [M]_0 \phi_i I_a \frac{(k_{d,p}^0)^2}{2 k_{d,tb}^0} \qquad (22)$$

$$\alpha = 2 m_p - m_{tb} \qquad (23)$$

$$B = [M]_0 \frac{k_{tT}^0 k_{d,p}^0}{4 k_{d,tb}^0} \qquad (24)$$

$$\beta = m_{tT} + m_p - m_{tb} \qquad (25)$$

A priori, translational diffusion can be neglected in the solid state and both propagation and termination occur through similar mechanisms (reactive diffusion, segmental fluctuation). Therefore, it is reasonable to assume that both m_p and m_{tb} are of the same

order of magnitude. As a result, the orders α and β (equations 23 and 24) can be approximated as

$$\alpha = 2m_p - m_{tb} \approx m_p \approx m_{tb} \tag{26}$$

$$\beta = m_{tT} + m_p - m_{tb} \approx m_{tT} \tag{27}$$

Therefore, the exponent α expresses the rate dependence for bimolecular mechanisms, while β expresses the dependence for monomolecular mechanisms. The polymerization rate as a function of conversion (equation 12) can now be expressed as a general equation with the four adjustable parameters:

$$R_p = (1-p)\left(-B(1-p/p_{max})^\beta + \sqrt{B^2(1-p/p_{max})^{2\beta} + A(1-p/p_{max})^\alpha}\right) \tag{28}$$

When applying this model, the polymerization speed is modelled as a function of the conversion p and the maximal conversion p_{max} (the specific p_{max} value for each set of experimental conditions (polymerization and crystallization temperature) was used). The photo-DSC data are fitted using 4 parameters α, β, A and B. The initial values for these parameters were estimated based on literature and experience to estimate their order of magnitude, and the Levenberg–Marquardt algorithm was used to obtain fitted values. The main strength of this model is that it gives an indication of the contribution of mono- and bimolecular termination reactions on the polymerization speed, through parameters α and β. However, A and B are a complex function of rate constants, initial monomer concentration and initiation efficiency. Therefore, these two parameters lose their physical relevance. As this model is specifically developed for solid state photopolymerization, it is not generally applicable to radical polymerization as there are a number of assumptions only valid under these specific conditions. Therefore, only photo-DSC data obtained in the solid state will be fitted using this model in the following paragraphs.

3.4.2. Applying this model to the photo-DSC results

Applying this model to the series of measurements described in section 3.3.3, resulted in an excellent fit of the experimental data ($r^2 \geq 0.996$). In Figure 21, the experimentally determined polymerization speed as a function of conversion is shown, with the resulting model for polymerizations occurring at 293 K (20°C) with and without a photo-initiator and for the two different crystallization conditions. In addition, the experimental

data and the fitting curves are shown for a range of different polymerization temperatures in Figure 22, for a polymerization in the solid state without a photo-initiator after crystallization occurring at 293 K.
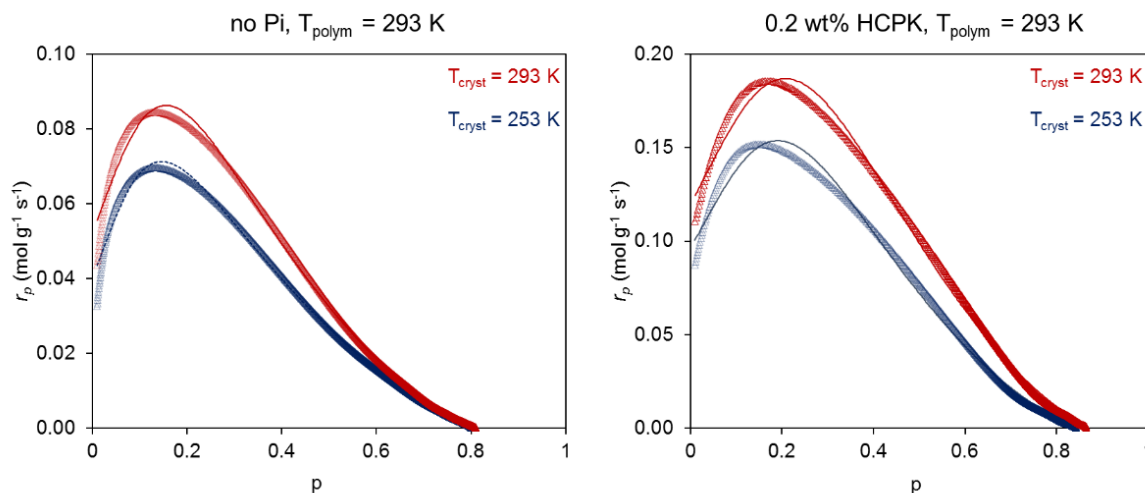
Figure 21: Experimental polymerization speed (symbols) and fitting curves (lines) for precursors crystallized dynamically at 253 K (blue) and isothermally at 293 K (red) and polymerized at 293 K. The left graph represents polymerizations without a photo-initiator while the right graph is in the presence of 0.2 wt% HCPK (corrected DSC thermograms, as described in materials and methods).
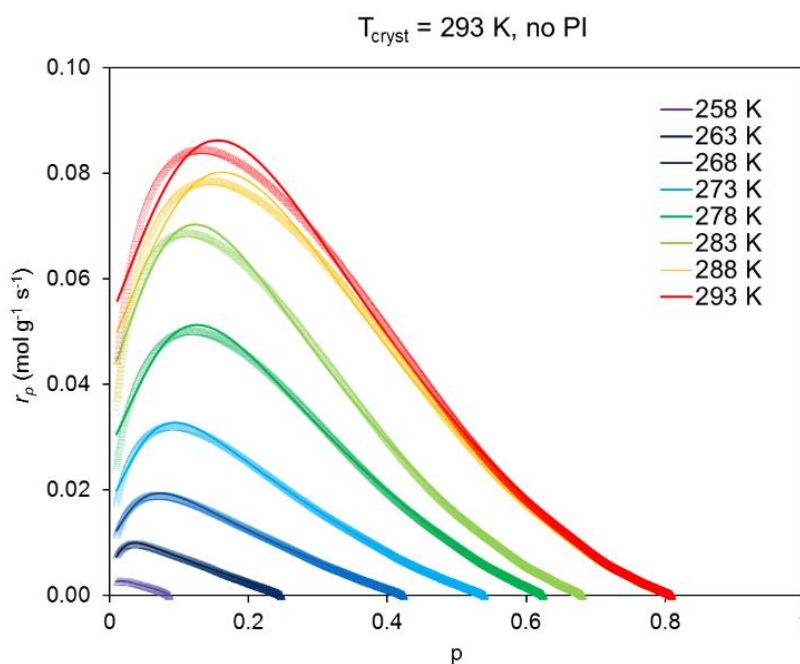
Figure 22: Experimental polymerization speed (symbols) and fitting curves (lines) for precursors crystallized at 293 K without a photo-initiator. The colors represent the different polymerization temperatures going from 258 K to 293 K.

Equation (28) describes the dependence of the polymerization rate on the monomer concentration (1-p), which is modulated using power law dependencies. The initial part of the polymerization curve showing the acceleration, is described by exponent β, and is governed by the monomolecular mechanisms. The last part of the curve before reaching the final conversion, is determined by bimolecular mechanisms expressed using the exponent α. In Figure 23, the variation of the fit exponents α and β is shown as a function of temperature. It is anticipated that there will not be a strong dependence of the exponents on the polymerization temperature, as the temperature dependence is already comprised in pre-factors A and B, which are a complex combination of the different rate coefficients. This is the case for exponent α, which remains between 1 and 2 over the whole temperature range. This means that there is no strong dependence on structural changes for the bimolecular mechanisms. Furthermore, there is no effect of a photo-initiator nor of the crystallization temperature on α.
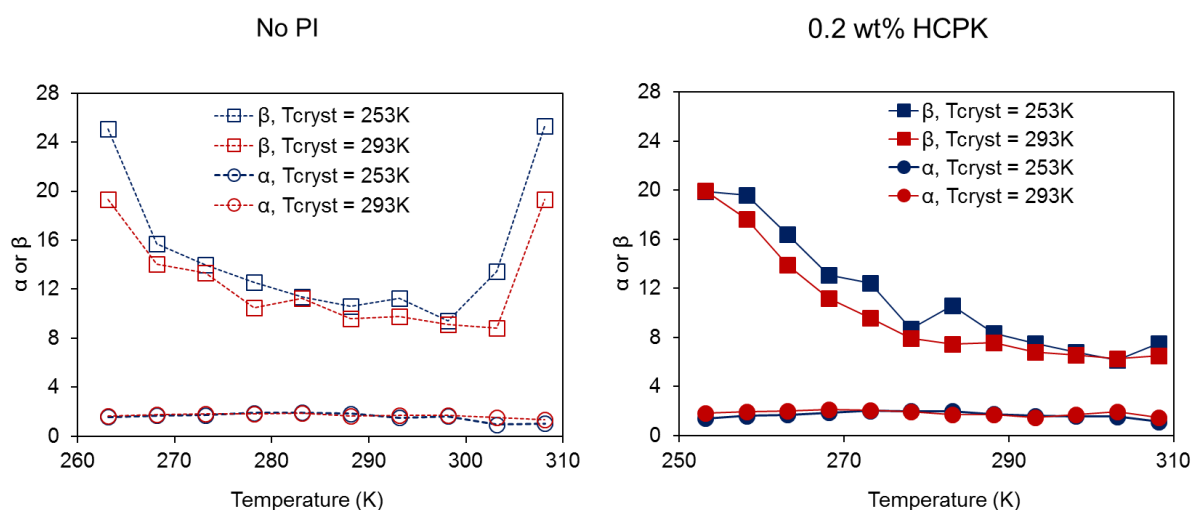
Figure 23: Evolution of fit coefficients α (circles) and β (squares) as a function of temperature for the crystallization at 253 K (blue curves) and at 293 K (red curves) without (left) and with (right) 0.2 wt% HCPK.

The exponent β on the other hand is significantly higher, indicating the monomolecular mechanisms are much more sensitive to structural changes during photo-polymerization. Both with and without a photo-initiator, the coefficient is slightly higher for the prepolymers crystallized dynamically at 253 K (e.g. for polymerizations at 20°C (293 K), β is 9.7 for isothermal crystallization and 11.3 for dynamic crystallization). In the presence of a photo-initiator, the coefficient continuously decreases with polymerization temperature (from 19.9 at 253 K to 6.5 at 308 K for polymerization after

isothermal crystallization). Without a photo-initiator, the same trend can be observed (from 193 at 253 K to 8.8 at 303 K for isothermal crystallization). However, around the melting point, it starts to increase again (to 19.3 at 308 K for isothermal crystallization). The area close to the melting point can be considered a kinetic grey zone, because the system is neither completely molten, nor completely solid. For auto-initiated polymerizations, the polymerization rate will drastically drop after the melting point. In the presence of a PI, the rate maintains a more constant value, close to the maximum value in the solid state. This behavior which can be observed in Figure 12, is reflected in the variation coefficient β as a function of the temperature, close to the melting point with and without a photo-initiator.

3.5.   Conclusions

In the current chapter, an in-depth analysis of the solid state reactive polymers, introduced in the previous chapter, was conducted. In a first part, the polymerization reaction was characterized based on a qualitative approach using photo-DSC. The results showed that the auto-initiation of the polymers can be attributed to radical generation by the acrylate groups. The absorption wavelength is strongly dependent on the chemical environment of the acrylates. Depending on the structure, it can shift to values within the UV-A range, as observed for the polymers developed in this work. In addition, the auto-initiation in the solid state is more efficient, as the π- π^* orbitals of the acrylates can more efficiently overlap due to phase separation.

Without a photo-initiator, the maximum polymerization speed will significantly drop when transitioning from the solid to the molten state (the maximum heat flow decreases from 3.4 W g^{-1} to 2.1 W g^{-1}). In addition, it was shown that polymerization is less efficient under air atmosphere, both with and without a photo-initiator. As a result of oxygen inhibition, for samples without a photo-initiator the maximum heat flow decreased from 3.39 to 2.7 W g^{-1} in the solid state and from 2.1 to 1.1 W g^{-1}. Furthermore, it was determined that an increase in temperature resulted in an increase in maximum polymerization speed until close to the melting point. Above the melting point, the polymerization speed remained constant. In addition, the crystallization conditions affected the solid state polymerization. The maximum polymerization speed and double bond conversion were slightly higher (maximum difference of 1.2 x 10^2 mol g^{-1} s^{-1}) at the different polymerization temperatures when the crystallization occured at a higher temperature, except when approaching the melting temperature.

The versatility of the polymers was demonstrated by synthesizing a series of polymers with a different backbone polymer (PCL versus PEO), a different end group (methacrylate versus acrylate) and an increasing backbone length (ranging from 2000 to 20000 g mol^{-1}). All polymers could be efficiently polymerized in the solid state. An increase in backbone length resulted in a reduction of the maximum polymerization speed and double bond conversion, as the acrylate concentration was reduced. The maximum polymerization speed without a photo-initiator decreased from 6.0 x 10^2 mol g^{-1} s^{-1} (PEG$_{2000}$-OEOAcr) to 2.8 x 10^2 mol g^{-1} s^{-1} (PEG$_{10000}$-OEOAcr) in the solid state and from 1.6 x 10^2 mol g^{-1} s^{-1} (PEG$_{2000}$-OEOAcr without PI) to 1.2 x 10^2 mol g^{-1} s^{-1} (PEG$_{10000}$-OEOAcr without PI) in the molten state.

The demonstrated versatility of this system offers the possibility to tune the mechanical properties of the polymers towards specific future applications. Another way to tune the properties was by varying the water content prior to polymerization. An increase in water content decreased the moduli and resulted in an increase of the swelling capacity of the hydrogels after crosslinking. For example, for solid state crosslinking (100 wt% concentration), the swelling ratio increased from 1.3 for PEG$_{2000}$-OEOAcr to 16.3 for PEG$_{20000}$-OEOAcr.

In a final part of this chapter, a model was suggested to describe the solid state reactivity starting from a steady-state assumption. The model was based on the different monomolecular and bimolecular reactions occurring throughout the polymerization and uses scaling laws to describe the effect of the structural changes on the occurrence of these reactions. An excellent fit was obtained for the different reaction conditions. It was shown that the bimolecular mechanisms do not have a strong dependence on the structural changes and are independent of temperature. The monomolecular reactions showed a stronger dependence and were responsible for the auto-acceleration of the reaction. In addition, the monomolecular exponent decreased with increasing temperature.

3.6. References

1.   Bowman, C. N. & Kloxin, C. J. Toward an enhanced understanding and implementation of photopolymerization reactions. *AIChE J.* **54,** 2775–2795 (2008).

2.   Zwiers, R. J. M. & Dortant, G. C. M. Aspherical lenses produced by a fast high-precision replication process using UV-curable coatings. *Appl. Opt.* **24,** 4483

(1985).

3.   Ibrahim, A. *et al.* Investigation of termination reactions in free radical photopolymerization of UV powder formulations. *Eur. Polym. J.* **48,** 1475–1484 (2012).

4.   Van Hoorick, J. *et al.* Indirect additive manufacturing as an elegant tool for the production of self-supporting low density gelatin scaffolds. *J. Mater. Sci. Mater. Med.* **26,** 247 (2015).

5.   Micic, M. & Suljovrujic, E. Network parameters and biocompatibility of p(2-hydroxyethyl methacrylate/itaconic acid/oligo(ethylene glycol) acrylate) dual-responsive hydrogels. *Eur. Polym. J.* **49,** 3223–3233 (2013).

6.   Jansen, J. F. G. a., Dias, A. a., Dorschu, M. & Coussens, B. Fast Monomers: Factors Affecting the Inherent Reactivity of Acrylate Monomers in Photoinitiated Acrylate Polymerization. *Macromolecules* **36,** 3861–3873 (2003).

7.   Billiet, T., Gevaert, E., De Schryver, T., Cornelissen, M. & Dubruel, P. The 3D printing of gelatin methacrylamide cell-laden tissue-engineered constructs with high cell viability. *Biomaterials* **35,** 49–62 (2014).

8.   Anseth, K. S., Wang, C. M. & Bowman, C. N. Kinetic evidence of reaction diffusion during the polymerization of multi(meth)acrylate monomers. *Macromolecules* **27,** 650–655 (1994).

9.   Gleeson, M. R. & Sheridan, J. T. Nonlocal photopolymerization kinetics including multiple termination mechanisms and dark reactions Part I Modeling. *J. Opt. Soc. Am. B* **26,** 1736 (2009).

10.   Yuemei Zhang, †, David E. Kranbuehl, *,†, Henry Sautereau, ‡, Gerard Seytre, ‡ and & Dupuy‡, J. Study of UV Cure Kinetics Resulting from a Changing Concentration of Mobile and Trapped Radicals. (2007). doi:10.1021/MA702117E

11.   Bowman, C. N. & Peppas, N. a. Coupling of Kinetics and Volume Relaxation During Polymerizations of Multiacrylates and Multimethacrylates. *Macromolecules* **24,** 1914–1920 (1991).

12.   Mitchell, G. E. *et al.* Quantitative Characterization of Microscopic Variations in the Cross-Link Density of Gels. *Macromolecules* **35,** 1336–1341 (2002).

13.   Simon, G. P., Allen, P. E. M., Bennett, D. J., Williams, D. R. G. & Williams, E. H. Nature of residual unsaturation during cure of dimethacrylates examined by CPPEMAS carbon-13 NMR and simulation using a kinetic gelation model. *Macromolecules* **22,** 3555–3561 (1989).

14.   Awad, H., Butler, D., Harris, M., Ibrahim, R. & Wu, Y. In vitro characterization of mesenchymal stem cell-seeded collagen scaffolds for tendon repair: effects of initial seeding density on contraction kinetics. *researchgate.net*

15.   Andrzejewska, E. Photopolymerization kinetics of multifunctional monomers. *Prog. Polym. Sci.* **26,** 605–665 (2001).

16.   Soh, S. K. & Sundberg, D. C. Diffusion-controlled vinyl polymerization. II. Limitations on the gel effect. *J. Polym. Sci. Polym. Chem. Ed.* **20,** 1315–1329

(1982).

17. Buback, M. *et al.* Consistent values of rate parameters in free radical polymerization systems. II. Outstanding dilemmas and recommendations. *J. Polym. Sci. Part A Polym. Chem.* **30,** 851–863 (1992).

18. Buback, M., Huckestein, B. & Russell, G. T. Modeling of termination in intermediate and high conversion free radical polymerizations. *Macromol. Chem. Phys.* **195,** 539–554 (1994).

19. Panke, D. Modelling the free-radical polymerization of methyl methacrylate over the complete range of conversion. *Macromol. Theory Simulations* **4,** 759–772 (1995).

20. Brandrup, J. & Immergut, E. H. *Polymer Handbook 3rd ed.* (John Wiley and Sons, 1989).

21. Russel, G., Gilbert, R. & Napper, D. Chain-Length-Dependent Termination Rate Processes in Free Radical Polymerizations. 1. Theory. *Macromolecules* **25,** 2459–2469 (1992).

22. and, G. A. O. & John M. Torkelson*, †,‡. Modeling Insight into the Diffusion-Limited Cause of the Gel Effect in Free Radical Polymerization. (1999). doi:10.1021/MA9811324

23. Kloosterboer, J. G. in *Electronic Applications* 1–61 (Springer-Verlag, 1988). doi:10.1007/BFb0025902

24. Jagur-Grodzinski, J. Polymeric gels and hydrogels for biomedical and pharmaceutical applications. *Polym. Adv. Technol.* **21,** 27–47

25. Martens, P. & Anseth, K. . Characterization of hydrogels formed from acrylate modified poly(vinyl alcohol) macromers. *Polymer (Guildf).* **41,** 7715–7722 (2000).

26. Gundogan, N., Okay, O. & Oppermann, W. Swelling, Elasticity and Spatial Inhomogeneity of Poly(N,N-dimethylacrylamide) Hydrogels Formed at Various Polymer Concentrations. *Macromol. Chem. Phys.* **205,** 814–823 (2004).

27. Andrzejewska, E., Lindén, L.-Å. & Rabek, J. F. Modelling the Kinetics of Photoinitiated Polymerization of Di(meth)acrylates. *Polym. Int.* **42,** 179–187 (1997).

28. Flammersheima, H. J., Eckardta, N., Kunzeb, W. & Gmbh, B. P. lbe deconvolutlon of DSCeunm In the expetlmenhl time domain h (O) / f (O). **187,** 269–274 (1991).

29. Moukhina, E. & Kaisersberger, E. Temperature dependence of the time constants for deconvolution of heat flow curves. *Thermochim. Acta* **492,** 101–109 (2009).

30. Fouassier, J. in *Radiation curing in polymer science and technology* 50–113 (1993).

31. Scherzer, T., Knolle, W., Nanmov, S. & Prager, L. Investigations on the photoinitiator-free photopolymerization of acrylates by vibrational spectroscopic methods. *Macromol. Symp.* **230,** 173–182 (2005).

32. Knolle, W., Scherzer, T., Naumov, S. & Mehnert, R. Direct (222 nm) photopolymerisation of acrylates. A laser flash photolysis and quantum chemical study. *Radiat. Phys. Chem.* **67,** 341–345 (2003).

33. Huang, L., Li, Y., Yang, J., Zeng, Z. & Chen, Y. Self-initiated photopolymerization of hyperbranched acrylates. *Polymer (Guildf).* **50,** 4325–4333 (2009).

34. Colley, C. S. *et al.* Probing the Reactivity of Photoinitiators for Free Radical Polymerization: Time-Resolved Infrared Spectroscopic Study of Benzoyl Radicals. *J. Am. Chem. Soc.* **124,** 14952–14958 (2002).

35. Jockusch, S. & Turro, N. J. Radical Addition Rate Constants to Acrylates and Oxygen: α-Hydroxy and α-Amino Radicals Produced by Photolysis of Photoinitiators. *J. Am. Chem. Soc.* **121,** 3921–3925 (1999).

36. Scherzer, T. & Decker, U. Kinetic investigations on the UV-induced photopolymerization of a diacrylate by time-resolved FTIR spectroscopy: the influence of photoinitiator concentration, light intensity and temperature. *Radiat. Phys. Chem.* **55,** 615–619 (1999).

37. Scherzer, T. & Decker, U. Real-time FTIR–ATR spectroscopy to study the kinetics of ultrafast photopolymerization reactions induced by monochromatic UV light. *Vib. Spectrosc.* **19,** 385–398 (1999).

38. Lee, T. Y., Guymon, C. a., Jönsson, E. S. & Hoyle, C. E. The effect of monomer structure on oxygen inhibition of (meth)acrylates photopolymerization. *Polymer (Guildf).* **45,** 6155–6162 (2004).

39. Davidson, S. *Exploring the science, technology and applications of U.V. and E.B. curing. SITA Series In Surface Coatings Technology* (SITA Technology LImited, 1999).

40. Scherzer, T. & Decker, U. The effect of temperature on the kinetics of diacrylate photopolymerizations studied by Real-time FTIR spectroscopy. *Polymer (Guildf).* **41,** 7681–7690 (2000).

41. Martuscelli, E., Silvestre, C. & Gismondi, C. Morphology, crystallization and thermal behaviour of poly(ethylene oxide)/poly(vinyl acetate) blends. *Die Makromol. Chemie* **186,** 2161–2176 (1985).

42. Padmavathi, N. C. & Chatterji, P. R. Structural Characteristics and Swelling Behavior of Poly(ethylene glycol) Diacrylate Hydrogels [†]. *Macromolecules* **29,** 1976–1979 (1996).

43. Nguyen, Q. T., Hwang, Y., Chen, A. C., Varghese, S. & Sah, R. L. Cartilage-like mechanical properties of poly (ethylene glycol)-diacrylate hydrogels. *Biomaterials* **33,** 6682–6690 (2012).

44. Hou, Y. *et al.* Photo-cross-linked PDMSstar-PEG hydrogels: Synthesis, characterization, and potential application for tissue engineering scaffolds. *Biomacromolecules* **11,** 648–656 (2010).

45. Nguyen, Q. T., Hwang, Y., Chen, A. C., Varghese, S. & Sah, R. L. Cartilage-like mechanical properties of poly (ethylene glycol)-diacrylate hydrogels. *Biomaterials* **33,** 6682–6690 (2012).

46. LaNasa, S. M., Hoffecker, I. T. & Bryant, S. J. Presence of pores and hydrogel composition influence tensile properties of scaffolds fabricated from well-defined sphere templates. *J. Biomed. Mater. Res. Part B Appl. Biomater.* **96B,** 294–302 (2011).

47. Rubinstein, M. & Colby, R. H. *Polymer Physics. Book* (Oxford University Press, 2003). doi:10.1017/CBO9780511975691

Chapter 4:

Indirect Solid Freeform Fabrication of an Initiator-Free Photo-Crosslinkable Hydrogel Precursor for the Creation of Porous Scaffolds

This chapter describes an indirect approach to create three-dimensional scaffolds for tissue engineering purposes. Parts of this chapter were published as a research article entitled "Indirect Solid Freeform Fabrication of an Initiator-free Photocrosslinkable Hydrogel Precursor for the Creation of Porous Scaffolds."[1] (*Houben, A. et al. Indirect Solid Freeform Fabrication of an Initiator-free Photocrosslinkable Hydrogel Precursor for the Creation of Porous Scaffolds. Maromolecular Biosci. (16, 1883–1894 (2016)).*

4.1. Introduction

As described in chapter 1, it is of crucial importance to generate a 3D environment that mimics the natural extracellular matrix (ECM) to achieve optimal support for cell adhesion and growth. [2–6] Ideally, a scaffold which provides mechanical support, is seeded with cells which then gradually substitute the scaffold material with ECM. [7,8] In this respect, hydrogels are ideal scaffold materials as they can closely mimic the water uptake potential and network structure of the native ECM.[9–11] In this respect, synthetic hydrogels have the advantage that they can be produced in a controlled and reproducible way, resulting in tailored properties including elasticity and swelling behavior.

Synthetic, urethane-based polymers are widely used due to their outstanding mechanical and chemical characteristics. Furthermore, their properties can be tailored by selecting the appropriate building blocks. Due to hydrogen bonding occurring between the nitrogen proton donor and carboxylic proton acceptor in the urethane bonds, elastic materials are obtained. The latter have already been extensively used in various biomedical applications of which an overview has been provided in the introduction (section 1.2.3.1.1). By incorporating hydrophilic segments (e.g. poly(ethylene oxide)), urethane-based hydrogels could be developed as described in chapters 2 and 3.[12–16] The latter combine the favorable polyurethane characteristics with the ECM-similarity of hydrogels. However, because their hydrophilic surface has a low interfacial free energy in contact with body fluids, PEG-based materials are used for applications where cell and protein adhesion are not desired. (e.g. in PCL/PEG-based materials or PLA/PEG based hydrogels)[17–19] In contrast, natural hydrogels often show high cell adhesion, but show a large batch to batch variability in mechanical, biological and chemical properties as explained in the first chapter (section 1.2.3.2).[10,20–23]

Scaffold porosity is another important parameter to be considered during scaffold design, as it enables the diffusion of oxygen and nutrients towards the cells and drainage of waste products away from the cells. In addition, the porous network aids in achieving efficient and homogeneous cell seeding as well as cell distribution throughout the entire scaffold.[24–26] In this respect, solid freeform fabrication (SFF) techniques have proven to be highly suitable as they offer superior control over both

macro- as well as microstructure compared to conventional scaffold production technologies.[6,27] Processing of non-thermo-responsive hydrogels using SFF can be quite challenging. Therefore, the iSFF method, described in chapter 1 (section 1.3.2) is an ideal approach to process these challenging materials. In literature, a range of natural hydrogel materials such as collagen, gelatin, alginate have already been successfully processed into three-dimensional structures using iSFF. [8,23,28–31] Fewer papers report on the processing of synthetic hydrogels using iSFF. In this respect, the work of Bertassoni *et al* and Miller *et al* focusses on the use of PEG-based hydrogels for the creation of vascular networks.[26,32]

Herein, a FDM-based iSFF approach has been optimized to generate tissue engineering scaffolds starting from the acrylate end-capped, urethane-based poly(ethylene glycol) precursor (PEG$_{2000}$-OEOAcrP) developed in chapter 2. The solid state reactivity enables SFF of the pure polymer precursor (100 wt%), while iSFF is a broadly applicable methodology enabling processing of the precursor at various concentrations, thereby influencing the mechanical properties. In addition, it offers a method to create 3D scaffolds for other hydrogel materials that cannot be crosslinked in the solid state. Similar to the approach described in chapter 1, a gelatin-methacrylamide (GM) coating was applied onto the PEG$_{2000}$-OEOAcr scaffolds developed for tissue engineering applications.[33]
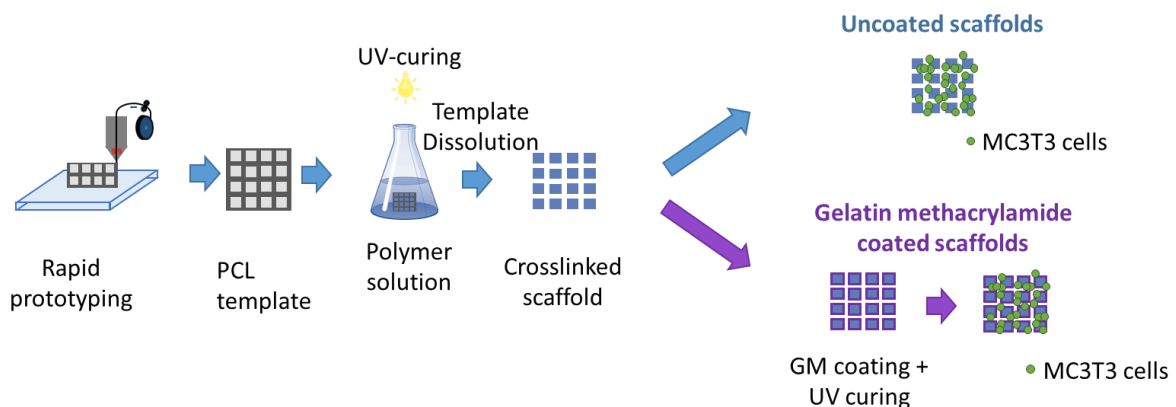
Figure 1: Overview of the preparation steps required for scaffold production

A scheme of the followed route towards scaffold development is depicted in Figure 1. Mouse calvaria preosteoblast cells (MC3T3-E1) were used to evaluate cell viability, adhesion and morphology on the different scaffolds developed.

4.2. Materials and Methods

4.2.1. Synthesis of PEG$_{2000}$-OEOAcr

The synthesis of the hydrogel precursor PEG$_{2000}$-OEOAcr was performed as described in chapter 2 (section 2.1.1.). Polyethylene Glycol (MW 2000 g/mol) was coupled to monoacrylate oligo(ethylene oxide) (MW 336 g/mol) using isophorone diisocyanate as a linker.

4.2.2. Rheological Analysis

Rheological analysis was performed according to the method described in chapter 2 (section 2.1.6.)

4.2.3. Determination of the Swelling Degree

The swelling degree was determined gravimetrically, as described in chapter 2 (section 2.1.7.)

4.2.4. Tensile Testing

For tensile experiments, hydrogel sheets were prepared with a thickness of +/- 1 mm, similar to those for the swelling tests, and cut into dogbone-shaped samples with a length of 50 mm and a central width of 4 mm. All tests were performed on a Universal tester 10-KM (Hounsfield) at an extension rate of 10 mm/min using a 100 N load cell. The Young's modulus was derived from the stress-strain curves. Experiments were conducted both on samples containing their initial water content as well as samples after equilibrium swelling.

4.2.5. Printing of the PCL Templates

The templates were produced in a similar fashion as previously reported.[23][34] More specifically, G-codes were obtained using in-house developed software written in visual basic for applications. Next, the G-codes were transferred to an Ultimaker 1 with a standard nozzle diameter of 400 μm via Cura 13.06.4 (Ultimaker, Geldermalsen, The Netherlands). PCL templates were produced in meander at 11 mm/s with a lay-down pattern of 0/90° and a layer height of 250 μm. The temperature ranged from 130 to 160 °C while standard extrusion was set to 0.017 mm filament/mm deposited strut which

corresponds to a volume of 0.1009 mm³ PCL/mm deposited strut. To optimize the extrusion, a multiplication factor (extrusion rate) was applied varying between 1 and 1.75 and the inter-strut center distance was set between 600 and 900 μm. The filament was a PCL filament obtained from Luxilon (Antwerp, Belgium) with a diameter of 2.75 mm and a molecular weight of 130,000 g/mol with a polydispersity of 1.41 as determined by size exclusion chromatography. After optimization of the printing parameters, a standard extrusion rate of 1.2, a temperature of 120 °C and an inter-strut center distance of 700 μm were selected to produce the samples for the biological evaluation.

4.2.6. Preparation of the Hydrogel Scaffolds

The hydrogel scaffolds were prepared by immersing the PCL templates in a solution of 60 wt% PEG_{2000}-OEOAcr. The container containing the immersed templates was subjected to a vacuum treatment for at least 1 hour to ensure complete filling of the pores. Afterwards, the samples were removed from the solution and crosslinked for 1h using UVA light (300-400 nm, 2 x 8 mW cm^{-2} from top and bottom). After crosslinking, excessive material surrounding the PCL template was removed using a scalpel. Next, the PCL templates were dissolved in 10 ml of chloroform for 1 week, changing the chloroform solution daily. Finally, the obtained hydrogel scaffolds were dried using a vacuum oven at 30°C under reduced pressure (10 mbar).

4.2.7. Micro-computed Tomography

The 3D morphology of the scaffolds was determined using high resolution X-ray computed tomography (μCT). To visualize the sample containing both the hydrogel scaffold and the PCL template, 0.25 g/mL β-tricalcium phosphate (Sigma) was added to the hydrogel precursor solution to enhance contrast. The samples were scanned using the custom-designed system HECTOR at the Ghent University Centre for X-ray Tomography (UGCT)[35]. During the scan, 2000 radiographic images were acquired at an exposure time of 1 s each, resulting in a total scan time of 36 minutes. The projection data were reconstructed to a 3D volume using an in-house developed software package: Octopus Reconstruction[36] (Inside Matters, Belgium) and rendered using VGStudioMax2.2 (Volume Graphics, Germany). Using geometrical magnification, a reconstructed voxel size of 7³ μm³ was achieved on a 2000 * 2000 *

500 voxel grid. Edge enhancement effects from X-ray phase contrast were observed but left unprocessed as they do not hinder proper visualization and interpretation.

4.2.8. Surface Texture Analysis

Texturometry tests were performed in both dry and equilibrium swollen state using a Lloyd TA500 Texture Analyser, equipped with a 10 N load cell. When analyzing the equilibrium swollen hydrogel scaffolds, the samples were first removed from double distilled water, gently dipped with tissue paper to remove residual water and positioned on a flat bottom plate. On top of this bottom plate, a plate was placed with a round opening (Ø 5 mm) to prevent the sample from slipping away upon exposure to the applied force. A texture profile analysis (TPA) test was performed using a cylindrical probe (Ø 3 mm). During the measurement, the samples were compressed twice over a distance of 0.5 mm at a rate of 5 mm/min. The maximum force applied on the scaffolds is measured during the first and the second run. All samples were compressed in the longitudinal (Z) direction.

4.2.9. Gelatin Methacrylamide Modification and subsequent Hydrogel Coating

The modification of Gelatin was performed as described in chapter 2. The scaffolds where coated using the modified gelatin as described in chapter 2 (section 2.1.10)

4.2.10. In Vitro Biological Evaluation

Both GM coated and non-coated samples, prepared from a 60 wt% PEG_{2000}-$OEOAcr$ solution, were evaluated. The samples were sterilized using ethylene oxide treatment (cold cycle, 35°C for 3 days). Mouse calvaria preosteoblast cells (MC3T3-E1) (ATCC) were cultured in alpha-minimal essential medium (Thermo-Fisher) supplemented with 10% fetal bovine serum and 1% penicillin/streptomycin (both from Thermo Fisher) at 37°C and 5% CO_2. For each scaffold, 10,000 cells were seeded in 0.075 ml medium. After 1 hour, 0.5 ml medium was added. The medium was refreshed every other day.

At different time points, an Alamar blue assay (Invitrogen) was performed by first washing the samples with PBS and subsequently adding 1% Alamar blue solution (diluted in PBS). After 1 hour, the absorbance was measured on a plate reader (Infinite M200, Tecan). Blank samples without cells were examined as a reference, to exclude any interference of the scaffold. The relative absorbance was calculated by dividing

the absorbance of the sample by the background absorbance of the blank reference. For visual evaluation, Carboxyfluorescein diacetate succinimidyl ester (CFDA) staining (Invitrogen) was used. After washing the sample with PBS buffer (T=37°C), 10 µM solution was added and the samples were incubated for 15 min. Next, medium was added (T=37°C) and the samples were incubated for another 30 min prior to analysis using fluorescence microscopy (Nikon Eclipse TE2000).

Calcein-AM/propidium iodine staining (Sigma) was performed by washing the samples with PBS buffer (T=37°C) followed by the addition of 1 µM of calcein-AM solution and 1 µM of propidium iodide solution. Prior to analysis by fluorescence microscopy, the samples were incubated for 30 min. Fluorescence microscopy was applied at 485 nm excitation and emission at 530 nm. For the picogreen assay (Invitrogen), lysis buffer (500 µl) was added to the samples and three freeze-thaw cycles were applied. The picogreen dye was diluted in PBS (5 uL/mL) and for each sample, 50 µl of reagent and 50 µl of lysis buffer from the incubated sample were mixed and immediately analyzed on the plate reader.

Statistical analysis was performed using PSPP (GNU Free Software Foundation). For comparison between multiple groups, ANOVA was performed with a Tukey Post-hoc test.

4.3. Results and Discussion

4.3.1. Influence of the Hydrogel Precursor Concentration on the Material Properties

One of the unique properties of the herein developed PEG_{2000}-OEOAcr is that it is water compatible over almost the entire concentration range, from 10 – 90 wt%, with all concentrations resulting in the formation of a homogeneous network after UV curing. By varying the concentration, the final material properties can be tailored depending on the envisaged application. In addition, the material can be crosslinked efficiently in the absence of a photo-initiator, avoiding pre-processing mixing steps and potential toxic effects of the photo-initiator.[37] To select the most appropriate hydrogel concentration for the scaffold fabrication, rheology, tensile and swelling tests were conducted. Samples of varying concentrations between 10 and 100 wt% were irradiated during 10 min with UV light and the final storage moduli obtained are plotted in Figure 2 (filled circles), giving an indication of the properties of the network formed after photopolymerization. An increasing trend in storage modulus, ranging from 6 kPa for the lowest concentration to 1410 kPa for the highest concentration, can be observed with increasing polymer concentration.
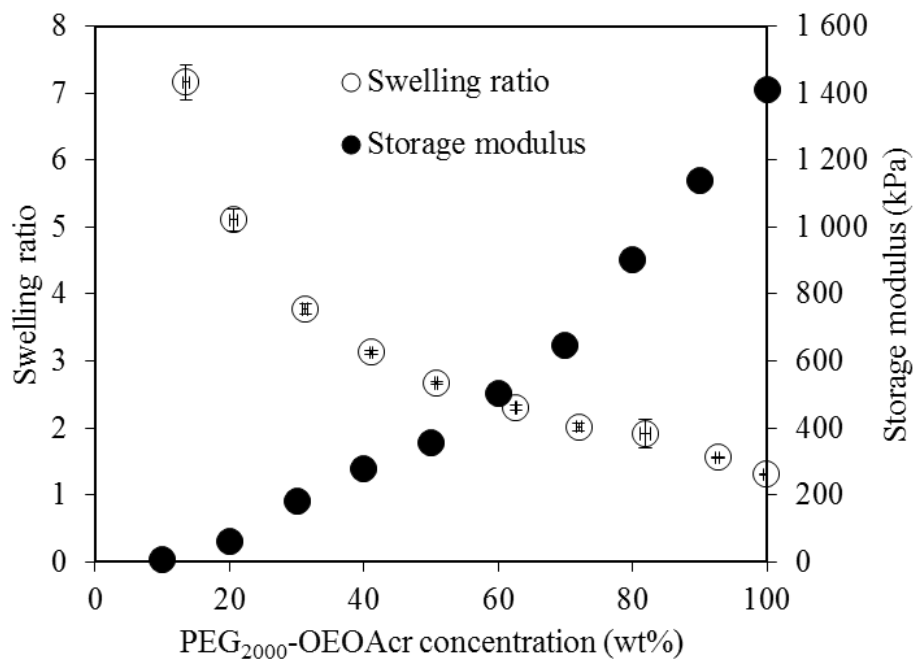
Figure 2: Swelling ratio (open circles) and final value of the storage modulus after 10 10 min UVA illumination (filled circles) for different PEG_{2000}-OEOAcr *concentrations.*

An inverse trend is observed for the swelling ratio (open circles) which ranges from 7.16 to 1.3 times the initial dry weight. During the propagation of the polymerization reaction, molecules can either react inter- or intramolecular, the latter leading to cyclization reactions. This will result in the formation of so-called microgel structures, formed at the early stages of polymerization. Unreacted double bonds can become entrapped in the microgel regions, where sterical hindrance will reduce their reactivity. In further stages of the polymerization, these microgel regions will connect with each other, resulting in network formation on a macroscopic scale.[38,39] With increasing water concentration, the probability of bridging between these microgel regions will decrease, and the number of intramolecular cyclization reactions will increase. This will lead to a more diluted and inhomogeneous network, with a higher concentration of unreacted acrylates. Therefore, by diluting the hydrogel precursor solution, the swelling of the crosslinked network increases, while the mechanical properties decrease, as is observed in these experiments.
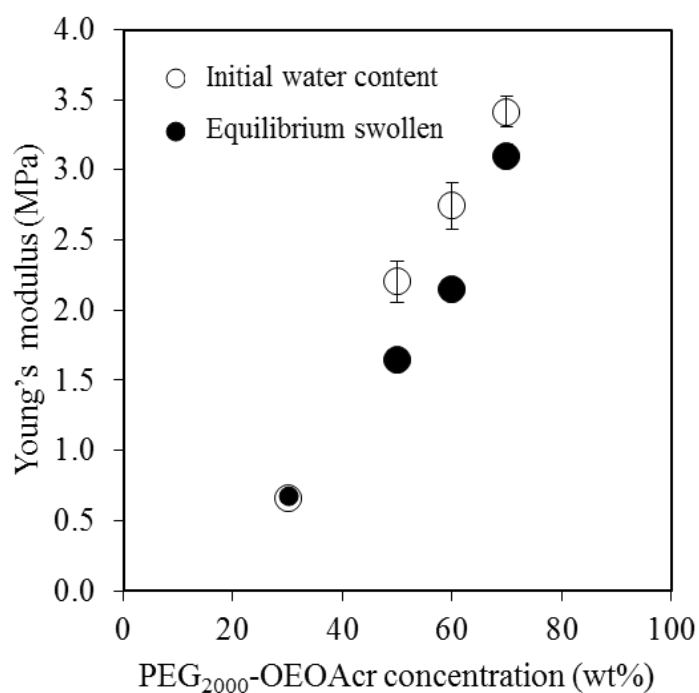
Figure 3: Young's modulus for different PEG$_{2000}$-OEOAcr concentrations for their initial water content and after equilibrium swelling.

Furthermore, these differences in network properties are also reflected by the tensile properties of the samples with various concentrations as shown in Figure 3. The samples were evaluated both in the presence of their initial water content as well as in the equilibrium swollen state. Water swelling loosens the network, resulting in fewer

polymer chains per volume element thereby reducing the mechanical properties of the material. When evaluating the effect of the polymer concentration, similar trends can be observed before and after equilibrium swelling. With increasing polymer concentration, the Young's modulus of the dry samples increased from 0.66 MPa for a 30 wt% sample to 3.41 MPa for a 70 wt% sample. This can again be attributed to network dilution effects occurring with increasing water concentration. This reduces the concentration of elastically active chains, the polymer segments in between two crosslinks. After equilibrium swelling, a similar trend was observed with a Young's modulus of 0.68 MPa and 3.10 MPa for the 30 and 70 wt% concentrations respectively.

These values are quite high compared to alternative hydrogels composed of one single component.[40] For example for crosslinked poly(ethylene glycol) diacrylate hydrogels in a similar molecular weight range (1-5 kg/mol), the tensile modulus remains below 1 MPa over their whole solubility range (up to 40 wt%).[41] Elongation at break was not significantly affected by the polymer concentration and was characterized by an average value of 25% for samples in the presence of their initial water content for the evaluated concentrations. After equilibrium swelling, this value increased to 37%.

To select a suitable concentration, several factors have to be taken into account. Indeed, as the native ECM contains large amounts of water, a high water content and a high swelling degree are desirable. In addition, an increased diffusion of nutrients and metabolites is generally realized in high water content conditions. [42] In this respect, low polymer concentrations are preferential as they lead to a more loosely crosslinked network and a higher swelling degree. On the other hand, the scaffolds need to possess sufficient mechanical integrity to enable implantation and withstand the *in vivo* environment. [43] In a preliminary test, samples containing 30wt%, 60 wt% and 90 wt% were synthesized and their handling, swelling behavior and mechanical integrity was assessed. Samples with the lowest hydrogel concentration were fragile and difficult to handle. Samples with the highest concentration on the other hand were more difficult to prepare as the solution became quite viscous and efficient scaffold infiltration was difficult. Furthermore, due to the high crosslinking density, the scaffolds could become slightly brittle when equilibrium swollen. Based on the arguments mentioned above, and the practical evaluation of samples at different concentrations, 60 wt% was selected as the a good compromise for hydrogel concentration for scaffold fabrication.

4.3.2. Optimization of the Fused Deposition Modelling Parameters

To obtain 3D hydrogel scaffolds, an iSFF approach was applied as indicated in Figure 1. In a first step of the approach, PCL templates were generated via FDM. The influence of different processing parameters on the obtained template was assessed in terms of pore and strut size of the obtained template in Figure 4. A first parameter which was evaluated was the extrusion rate, which corresponds to the speed at which the filament is extruded relative to the movement of the extrusion head. The extrusion rate was increased stepwise from 1 to 1.8, which implies that more filament is extruded to print the same strut length, resulting in the deposition of thicker struts. Lower extrusion rates result in the formation of thinner struts. The difference between the lowest and highest extrusion rate resulted in a difference in average strut diameter of about 200 µm (from 326 ± 37 µm to 523 ± 57 µm). The spacing between the centers of the struts remained constant, therefore a higher extrusion rate leads to a smaller pore size. A maximum difference in pore size of 200 µm (from 509 ±42 µm to 309 ± 62 µm) was observed when comparing scaffolds produced at the lowest extrusion rate to those produced at the highest extrusion rate. This trend can clearly be observed in Figure 4 (left).
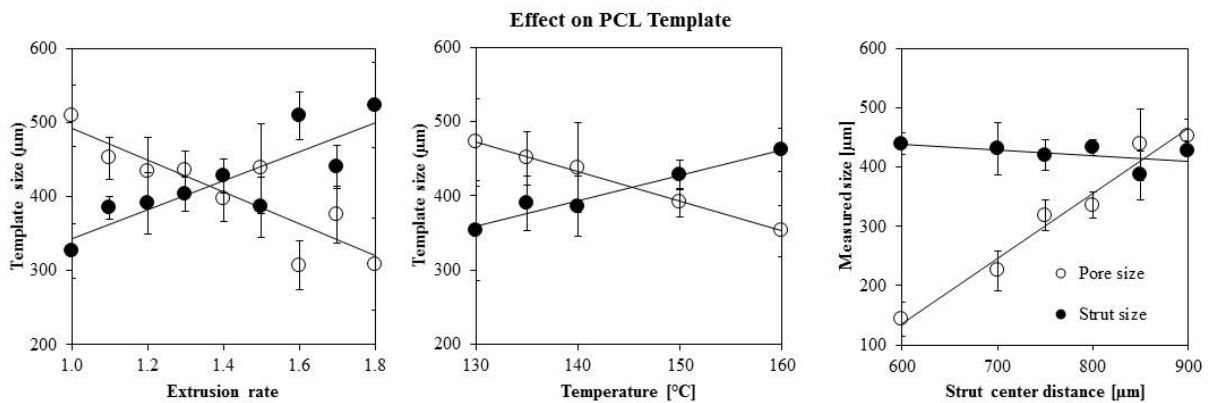
Figure 4: Effect of the plotting parameters (poly(ε-caprolactone) (PCL) filament extrusion factor, printing temperature and set channel size) on the struts (filled circles) and channels (open circles) of the PCL templates.

A second evaluated parameter was the extrusion temperature, which was varied from 130°C to 160°C. Higher temperatures reduce the viscosity of the melt, which results in an increased polymer flow. A higher flow will again lead to thicker struts and smaller pores. An overall difference in strut size of about 110 µm (from 353 ±67 µm to 462 ±

29 µm), and an overall difference in pore size of 120 µm (from 472 ± 59 µm to 352 ± 35 µm) were observed.

A final parameter which was assessed was the inter-strut center distance, the distance from the center of one strut to the center of the adjacent strut, which will determine the pore size. Inter-strut center distance was varied from 600 µm to 900 µm, resulting in a measured pore size ranging from 143 ± 29 µm to 452 ± 29 µm. A subtle decreasing trend in strut size, from 439 ± 18µm to 428 ± 17 µm can be observed with increasing pore size. This effect can be attributed to the distance the material needs to bridge between two struts. When the pores become larger, the struts bridging these gaps will start to deform, resulting in strut thinning.

Based on these results, the optimal parameters were selected to create scaffolds for further experiments. In addition to the measured pore and strut size, the ease of printing and a visual inspection of the samples were also taken into account. An extrusion factor of 1.2 was selected (corresponding to the deposition of 0.121 mm³ of PCL/mm deposited strut) in combination with an extrusion temperature of 140°C. Higher and lower temperatures resulted in a higher frequency of printing problems associated with nozzle blockage and the production of flawed scaffolds. If the temperature is too high, the material will not cool down and crystallize fast enough, resulting in poor bridging of the gaps and finally, scaffold collapse. Conversely, low temperatures result in an increased viscosity of the material, often leading to nozzle blockage. Finally, an inter- strut center distance of 700 µm was selected, resulting in an average strut size of 385 µm and an average pore size of 294 µm.

4.3.3. Fabrication and characterization of PEG$_{2000}$-OEOAcr scaffolds

In a next step, the templates were used to fabricate the PEG$_{2000}$-OEOAcr hydrogel scaffolds. These templates were submerged in the hydrogel precursor solution and subjected to a vacuum treatment to ensure complete filling of the template. The PEG$_{2000}$-OEOAcr solution was crosslinked using UVA illumination and the scaffolds were subsequently dissolved in chloroform. Using this procedure, a strut of the scaffold will become a channel in the final scaffold and vice versa. The vertical pores are formed in areas where two struts of the template overlap, which prevents infiltration of the

precursor solution in this area, which will result in the formation of longitudinal pores after template dissolution.
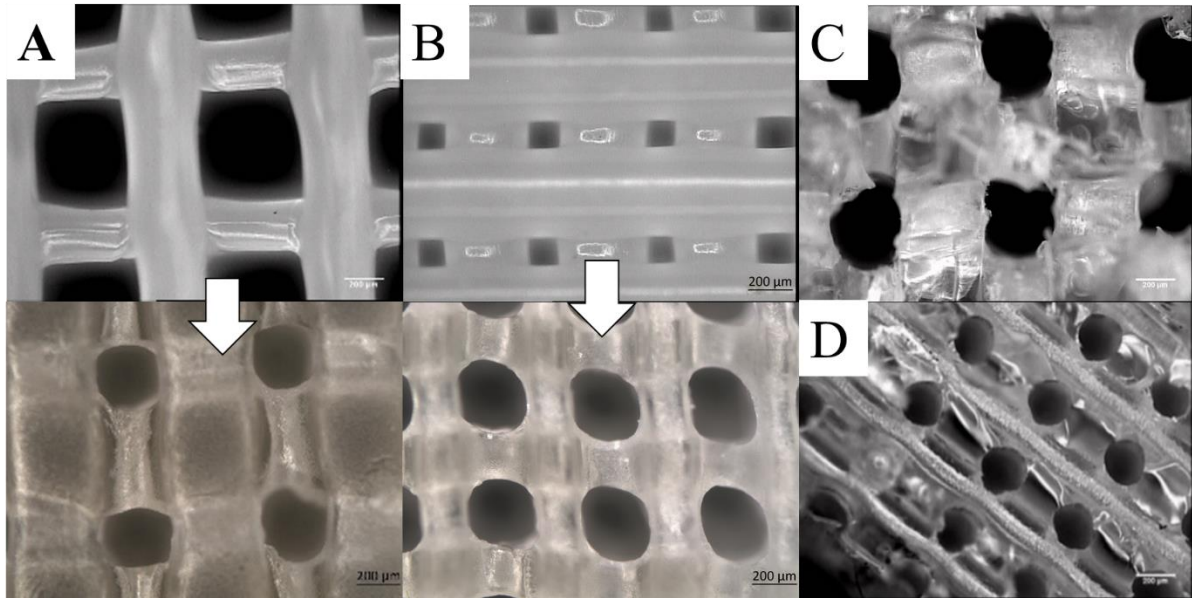
Figure 5: Optical microscopy images of A) PCL template with large pores (top) and the resulting scaffold (bottom). The struts of the template will form channels in the scaffold, while the scaffold vertical pores are formed an area where two template struts overlapped. B) Template with small pores (top) and the resulting scaffold (bottom). C) Horizontal cross-section of the scaffold. D) Vertical cross-section of the scaffold.

As shown in Figure 5, the struts of the PCL template become the channels in the PEG$_{2000}$-OEOAcr scaffold, while the pores exist in areas where the original PCL struts overlapped. The result of the PCL processing parameters on the channel and strut size of the PEG$_{2000}$-OEOAcr scaffolds is depicted in Figure 6. The trends in pore and strut size of the PCL template are transferred to the PEG$_{2000}$-OEOAcr scaffolds strut and pore size, respectively. As the channel and strut size were measured on dry samples, sample shrinkage was observed resulting in an average size reduction for the scaffold channels of 25 % relative to the template struts, and 10 % for the scaffold struts relative to the template pores. Equilibrium swelling of the scaffolds will affect these dimensions, however quantitative measurements on swollen samples were not possible due to the low contrast of the obtained images.
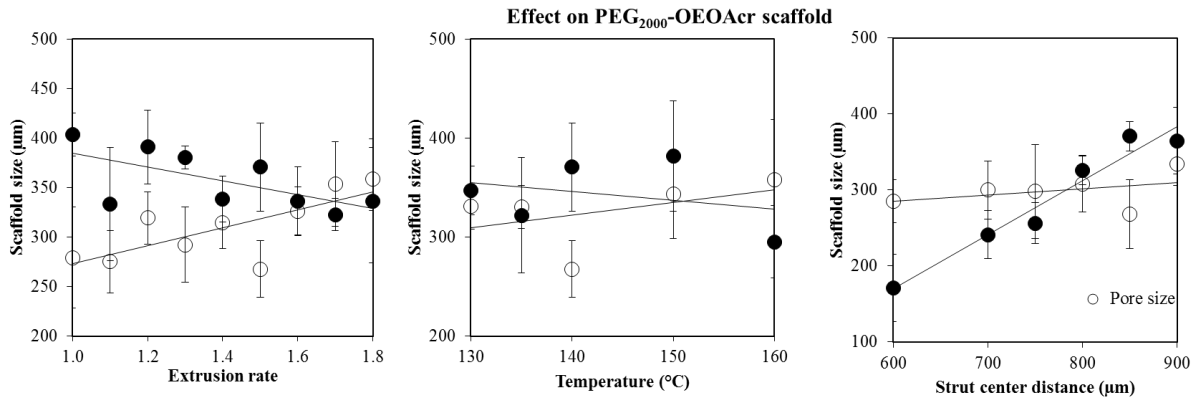
Figure 6: Effect of the plotting parameters (poly(ε-caprolactone) (PCL) filament extrusion factor, printing temperature and set channel size) on the struts (filled circles) and channels (open circles) of the PEG$_{2000}$-OEOAcr *hydrogel scaffolds based on the PCL templates. Note that a pore of the template will become a strut in the scaffold and a strut of the template will become a channel in the scaffolds.*

To further investigate the scaffolds, μCT images were recorded from a template with a scaffold and the final scaffold in the absence of the template Figure 7a shows the PCL template surrounded by a solution of 60 wt% PEG$_{2000}$-OEOAcr. As the difference in contrast between PEG$_{2000}$-OEOAcr and PCL is quite low on the μCT images, 2.5 mg/mL CaP was added to the PEG$_{2000}$-OEOAcr solution to increase contrast. After template removal, a porous scaffold was obtained from the PEG$_{2000}$-OEOAcr solutions (Figure 7b). The cross-sections clearly show that the sample is effectively cured as uncross-linked polymer was extracted during the PCL dissolution step. Furthermore, the sample shows excellent porosity in both the vertical as well as the lateral planes, which is beneficial towards cell infiltration and - viability.
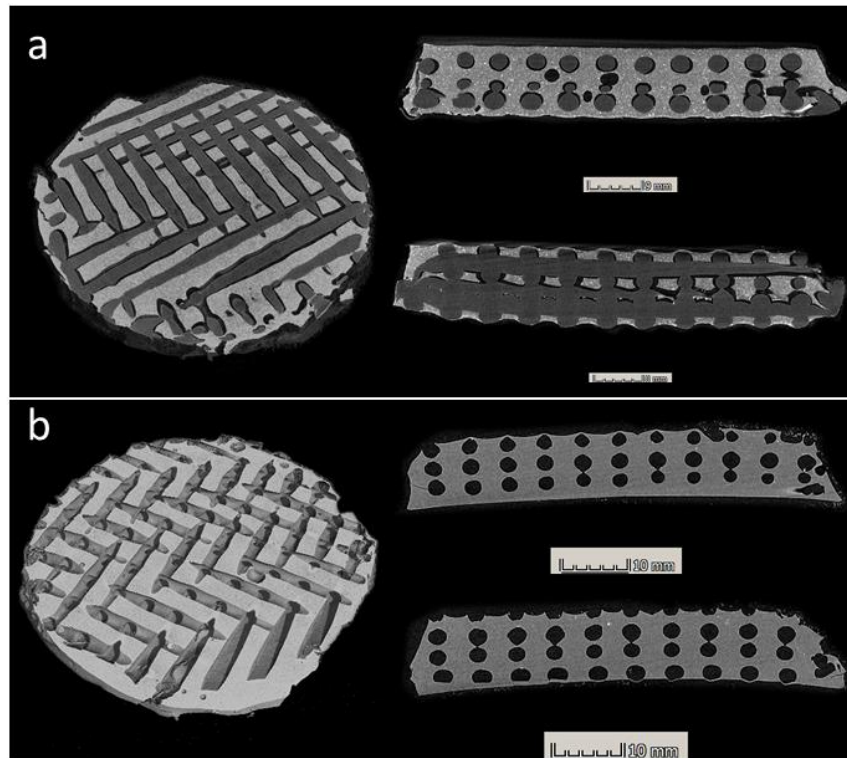
Figure 7: μ-CT images showing 3D cut-through, ZX and ZY cross-section of a) PEG$_{2000}$-OEOAcr scaffold with added β-tricalcium phosphate to enhance contrast between the hydrogel and the PCL template, which is still present, b) PEG$_{2000}$-OEOAcr scaffold.

The different scaffolds were characterized both in the dry and the equilibrium swollen state using texturometry. As shown in Figure 8, a 1 mm indentation was applied to the sample, and the required force was measured to determine the sample hardness. Again, there was a clear effect of the processing parameters, both in the dry and the equilibrium swollen state. The hardness showed a decreasing trend from 43 N to 15.5 N with increasing extrusion rate. Indeed, as the struts of the PCL template become thicker with increasing extrusion rate, larger channels are formed in the final PEG$_{2000}$-OEOAcr scaffold. Larger channels result in a higher compressibility of the scaffold and therefore, in a reduced hardness. A similar decreasing trend, from 9 N to 29 N, was observed upon increasing the extrusion temperature. Larger template struts result in larger empty channels for the final scaffold. Evidently, with increasing template pore size, the scaffold strut size increases, resulting in a higher hardness. When comparing the samples in the dry and swollen state, an average ten-fold reduction in hardness can be observed for the swollen samples. Similar trends with varying processing parameters can be observed in both the dry and in the equilibrium swollen state.
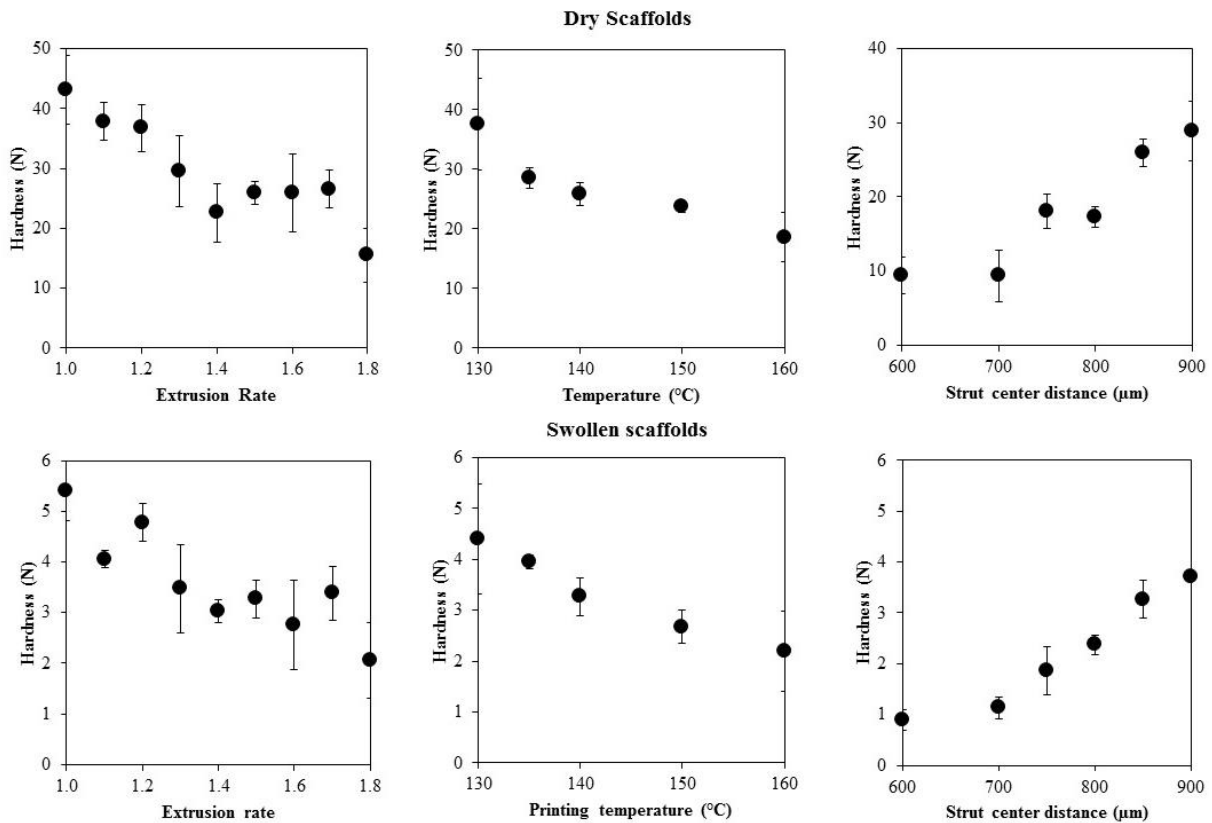
*Figure 8: Effect of template plotting parameters, as determined by a texturometrical indentation test on
the* PEG$_{2000}$-OEOAcr *scaffolds in the dry (upper panel) and equilibrium swollen state (lower panel).*

4.3.4. *In Vitro* Evaluation of Selected Scaffolds

For the biological evaluation, 3D hydrogel scaffolds with and without a gelatin
methacrylamide coating were compared. A visual evaluation of the MC3T3 cells
seeded onto these scaffolds at 10 or 12 days is depicted in Figure 9. A relatively low
number of cells, 10,000 cells per scaffold, was selected as this is representative for
cases with limited autologous cell availability.[44–47] An example are osteoprogenitor
cells for bone regeneration, where only a limited number of cells can be isolated from
the periosteum using currently available techniques. Furthermore, by using a low
seeding density, the interaction between the cells and the scaffold becomes more
pronounced. Both CFDA-SE and Calcein-AM/PI staining were used. CFDA-SE was
used as it is a non-toxic staining that allows fluorescent visualization of the cells over
a time period of several days, while the latter was used only at the end point of the
experiment (d12). For the PEG$_{2000}$-OEOAcr scaffolds, infiltration of the cells into the
different channels of the scaffold can be observed both with and without the GM
coating. Quantitative analysis of the fluorescence microscopy and SEM images

showed a low amount of cells on the uncoated samples, while on the coated samples, a larger number of cells could be observed. Furthermore, the SEM images show a pronounced effect of the GM coating on the cell morphology. Indeed, without the coating, the cells show a more rounded morphology on the PEG_{2000}-OEOAcr scaffold. Conversely, in the presence of the GM coating, cells show a flattened and more elongated morphology
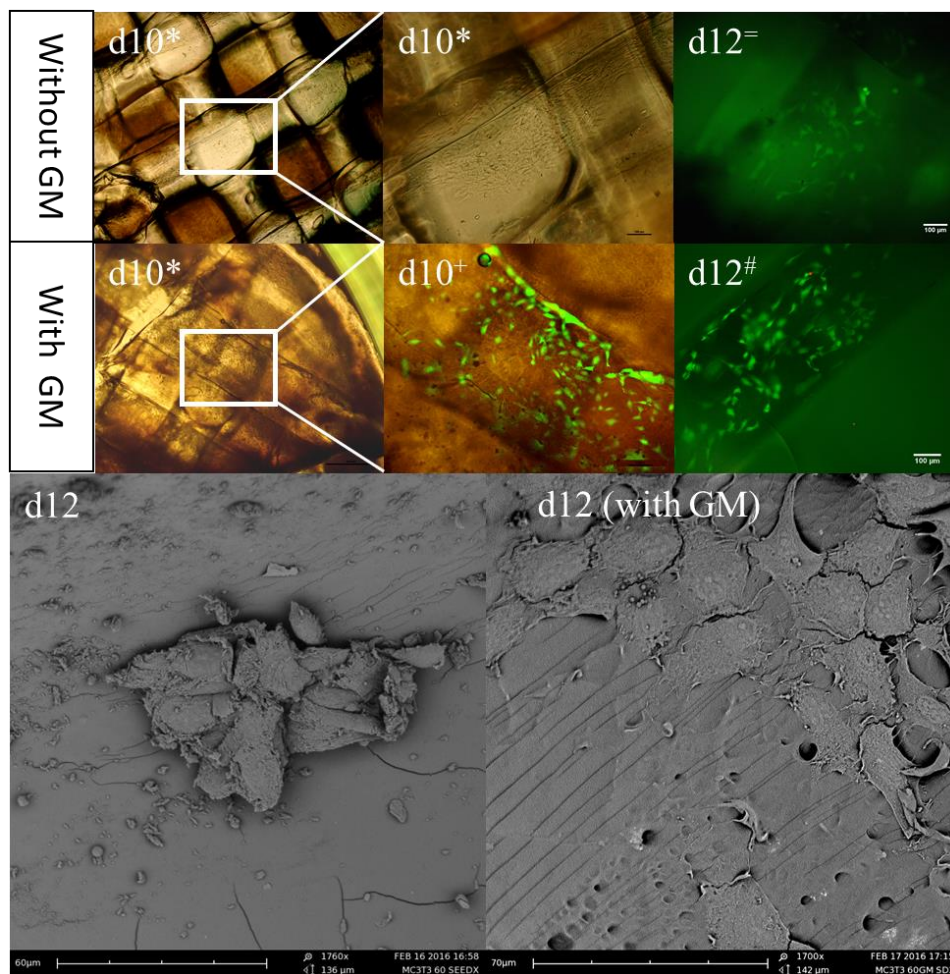
*Figure 9: Analysis of the scaffolds after seeding with MC3T3 cells at 10 or 12 days (indicated on each image). Greyscale images have been obtained using SEM, images marked with * are brightfield optical microscopy images, + represent overlays of brightfield images with CFDA-SE stained fluorescence images, = depicts CFDA-SE stained fluorescence images and # shows live/dead stained fluorescence images.*

The qualitative observations were confirmed by quantitative analysis. At different time points, the metabolic activity of the samples was analyzed using an Alamar Blue assay. The absorbance is expressed relative to a blank sample, also prepared with or without GM coating, to exclude any interference of the scaffold material. At the last time point,

the DNA content was determined using a picogreen assay, as depicted in Figure 10. A clear beneficial effect of the GM coating can be observed in both assays, confirming the optical microscopy and SEM results. Indeed, the metabolic activity shows a steady increase over the different time points for the coated hydrogel samples, which have a higher DNA content in comparison to the uncoated samples. While the differences in the metabolic assay were not statistically different, a similar significantly different ($p < 0.05$) effect was observed for the DNA content.
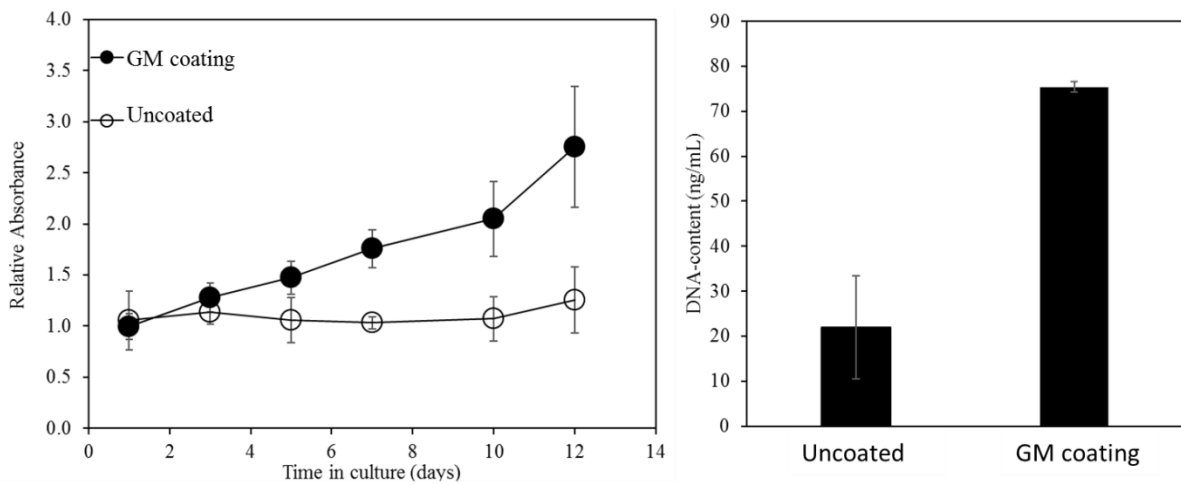
Figure 10: Left: Alamar Blue assay showing the absorbance of samples seeded with MC3T3 relative to the absorbance of a blank scaffold at different time points, indicating metabolic activity of the cells (uncoated scaffold in white, scaffold with gelatin methacrylamide (GM) coating in black).. Right: Picogreen assay showing the DNA content of the samples with and without Gelatin methacrylamide coating (GM) at d12 of the experiment. (results were significantly different at P < 0.05).

4.4. Conclusion

The hydrogel precursor PEG$_{2000}$-OEOAcr developed in chapter 2 was successfully applied to create porous 3D scaffolds. The high reactivity of the material and its unique water compatibility were exploited to create a tunable network structure. The latter altered the rheological properties (from 10.6 kPa to 1410 kPa), swelling degree (from 7.16 to 1.3 times the initial dry weight) and tensile properties (from 0.67 MPa up to 3.1 MPa). Indirect solid freeform fabrication has proven to be an elegant solution to circumvent processing limitations associated with the use of hydrogel materials and via this approach, 3D scaffolds could be generated starting from the hydrogel precursor. By varying the processing parameters of the PCL template such as the extrusion rate, the temperature and the inter-strut center distance, the properties of the final hydrogel scaffolds could be altered, both from a morphological as well as a mechanical perspective with the latter determined by texturometry. The presence of a completely interconnected porous network within these scaffolds was demonstrated using µ-CT. Biological evaluation of the samples using mouse osteoblasts showed that the cell adhesion and - proliferation were greatly improved by applying a gelatin methacrylamide coating.

4.5. References

1.   Houben, A. *et al.* Indirect Solid Freeform Fabrication of an Initiator-free Photocrosslinkable Hydrogel Precursor for the Creation of Porous Scaffolds. *Maromolecular Biosci.* **16,** 1883–1894 (2016).

2.   Langer, R. & Vacanti, J. P. Tissue Engineering. *Science (80-.).* **260,** (1993).

3.   Landers, R. *et al.* Fabrication of soft tissue engineering scaffolds by means of rapid prototyping techniques. *journals Mater. Sci.* **37,** 3107–3116 (2002).

4.   Graulus, G.-J. J. *et al.* Cross-linkable alginate-graft-gelatin copolymers for tissue engineering applications. *Eur. Polym. J.* **72,** 494–506 (2015).

5.   Woodfield, T. B. F. *et al.* Design of porous scaffolds for cartilage tissue engineering using a three-dimensional fiber-deposition technique. *Biomaterials* **25,** 4149–61 (2004).

6.   Chia, H. N. & Wu, B. M. Recent advances in 3D printing of biomaterials. *J. Biol. Eng.* **9,** 4 (2015).

7.   Maria, C. De, Acutis, A. De & Vozzi, G. *Indirect Rapid Prototyping for Tissue Engineering. Essentials of 3D Biofabrication and Translation* (Elsevier Inc., 2015). doi:10.1016/B978-0-12-800972-7/00008-6

8.   Liu, C. Z., Sachlos, E., Wahl, D. A., Han, Z. W. & Czernuszka, J. T. On the manufacturability of scaffold mould using a 3D printing technology. *Rapid Prototyp. J.* **13,** 163–174 (2007).

9.   Tibbitt, M. W. & Anseth, K. S. Hydrogels as extracellular matrix mimics for 3D cell culture. *Biotechnol. Bioeng.* **103,** 655–663 (2009).

10.   Van Vlierberghe, S., Dubruel, P. & Schacht, E. Biopolymer-based hydrogels as scaffolds for tissue engineering applications: a review. *Biomacromolecules* **12,** 1387–408 (2011).

11.   Peppas, N. A. *et al.* Hydrogels in biology and medicine: from molecular principles to bionanotechnology. *Adv. Mater.* **18,** 1345–1360 (2006).

12.   Petrini, P., Fare, S., Piva, A. & Tanzi, M. C. Design, synthesis and properties of polyurethane hydrogels for tissue engineering. *J. Mater. Sci. Mater. Med.* **14,** 683–686 (2003).

13.   Kim, B. K. & Paik, S. H. UV-curable poly (ethylene glycol)-based polyurethane acrylate hydrogel. *J. Polym. Sci. Part A Polym. Chem.* **37,** 2703–2709 (1999).

14.   Mequanint, K., Patel, A. & Bezuidenhout, D. Synthesis, Swelling Behavior, and Biocompatibility of Novel Physically Cross-Linked Polyurethane-b lock-Poly (glycerol methacrylate) Hydrogels. *Biomacromolecules* **7,** 883–891 (2006).

15.   Petrini, P., Tanzi, M. C., Moran, C. R. & Graham, N. B. Linear poly (ethylene oxide)-based polyurethane hydrogels: polyurethane-ureas and polyurethane-amides. *J. Mater. Sci. Mater. Med.* **10,** 635–639 (1999).

16.   Loh, X. J., Colin Sng, K. B. & Li, J. Synthesis and water-swelling of thermo-

responsive poly (ester urethane) s containing poly (Îμ-caprolactone), poly (ethylene glycol) and poly (propylene glycol). *Biomaterials* **29,** 3185–3194 (2008).

17. Thiele, J., Ma, Y., Bruekers, S. M. C., Ma, S. & Huck, W. T. S. 25th anniversary article: Designer hydrogels for cell cultures: a materials selection guide. *Adv. Mater.* **26,** 125–47 (2014).

18. Shah, N. M., Pool, M. D. & Metters, A. T. Influence of network structure on the degradation of photo-cross-linked PLA-b-PEG-b-PLA hydrogels. *Biomacromolecules* **7,** 3171–7 (2006).

19. Zhang, C., Zhang, N. & Wen, X. Synthesis and characterization of biocompatible, degradable, light-curable, polyurethane-based elastic hydrogels. *J. Biomed. Mater. Res. A* **82,** 637–50 (2007).

20. Van Vlierberghe, S. *et al.* Hydrogel network formation revised: high-resolution magic angle spinning nuclear magnetic resonance as a powerful tool for measuring absolute hydrogel cross-link. *Appl. …* **64,** 1176–1180 (2010).

21. VanRie, J. *et al.* Cryogel-PCL combination scaffolds for bone tissue repair. *J. Mater. Sci. Mater. Med.* **26,** 5465 (2015).

22. Vlierberghe, S. Van, Schacht, E. & Dubruel, P. Reversible gelatin-based hydrogels: Finetuning of material properties. *Eur. Polym. J.* **47,** 1039–1047 (2011).

23. Van Hoorick, J. *et al.* Indirect additive manufacturing as an elegant tool for the production of self-supporting low density gelatin scaffolds. *J. Mater. Sci. Mater. Med.* **26,** 247 (2015).

24. Park, S., Kim, G., Jeon, Y. C., Koh, Y. & Kim, W. 3D polycaprolactone scaffolds with controlled pore structure using a rapid prototyping system. *J. Mater. Sci. Mater. Med.* **20,** 229–234 (2009).

25. Billiet, T., Gevaert, E., De Schryver, T., Cornelissen, M. & Dubruel, P. The 3D printing of gelatin methacrylamide cell-laden tissue-engineered constructs with high cell viability. *Biomaterials* **35,** 49–62 (2014).

26. Bertassoni, L. E. *et al.* Hydrogel bioprinted microchannel networks for vascularization of tissue engineering constructs. *Lab Chip* **14,** 2202–2211 (2014).

27. Manjubala, I. *et al.* Biomimetic mineral-organic composite scaffolds with controlled internal architecture. *J. Mater. Sci. Mater. Med.* **16,** 1111–9 (2005).

28. Yeong, W., Chua, C., Leong, K., Chandrasekaran, M. & Lee, M. Comparison of Drying Methods in the Fabrication of Collagen Scaffold Via Indirect Rapid Prototyping. 260–266 (2006). doi:10.1002/jbmb

29. Sachlos, E., Reis, N., Ainsley, C., Derby, B. & Czernuszka, J. T. Novel collagen scaffolds with predefined internal morphology made by solid freeform fabrication. *Biomaterials* **24,** 1487–1497 (2003).

30. Tan, J. Y., Chua, C. K. & Leong, K. F. Fabrication of channeled scaffolds with

ordered array of micro-pores through microsphere leaching and indirect Rapid Prototyping technique. 83–96 (2013). doi:10.1007/s10544-012-9690-3

31. Kang, H.-W. & Cho, D.-W. Development of an indirect stereolithography technology for scaffold fabrication with a wide range of biomaterial selectivity. *Tissue Eng. Part C. Methods* **18,** 719–29 (2012).

32. Miller, J. S. *et al.* Rapid casting of patterned vascular networks for perfusable engineered three-dimensional tissues. *Nat. Mater.* **11,** 768–774 (2012).

33. VanDenBulcke, A. I. *et al.* Structural and Rheological Properties of Methacrylamide Modified Gelatin Hydrogels. *Biomacromolecules* **1,** 31–38 (2000).

34. Markovic, M. *et al.* Hybrid Tissue Engineering Scaffolds by Combination of Three-Dimensional Printing and Cell Photoencapsulation. *J. Nanotechnol. Eng. Med.* **6,** 21004 (2015).

35. Masschaele, B. *et al.* HECTOR: A 240kV micro-CT setup optimized for research. *J. Phys. Conf. Ser.* **463,** 12012 (2013).

36. Vlassenbroeck, J. *et al.* Software tools for quantification of X-ray microtomography at the UGCT. *Nucl. Instruments Methods Phys. Res. Sect. A Accel. Spectrometers, Detect. Assoc. Equip.* **580,** 442–445 (2007).

37. Houben, A. *et al.* Flexible Oligomer Spacers as the Key to Solid-State Photopolymerization of Hydrogel Precursors. *Mater. Today Chem.* **4,** 84–89 (2017).

38. Andrzejewska, E. Photopolymerization kinetics of multifunctional monomers. *Prog. Polym. Sci.* **26,** 605–665 (2001).

39. Kloosterboer, J. G. in *Electronic Applications* 1–61 (Springer-Verlag, 1988). doi:10.1007/BFb0025902

40. Calvert, P. Hydrogels for Soft Machines. *Adv. Mater.* **21,** 743–756 (2009).

41. Nguyen, Q. T., Hwang, Y., Chen, A. C., Varghese, S. & Sah, R. L. Cartilage-like mechanical properties of poly (ethylene glycol)-diacrylate hydrogels. *Biomaterials* **33,** 6682–6690 (2012).

42. Hoffman, A. S. Hydrogels for biomedical applications. *Adv. Drug Deliv. Rev.* **64,** 18–23 (2012).

43. Drury Mooney, D.J., J. L., Drury, J. L. & Mooney, D. J. Hydrogels for tissue engineering: scaffold design variables and applications. *Biomaterials* **24,** 4337–4351 (2003).

44. Makris, E. A., Hadidi, P. & Athanasiou, K. A. The knee meniscus: Structure–function, pathophysiology, current repair techniques, and prospects for regeneration. *Biomaterials* **32,** 7411–7431 (2011).

45. Stock, U. a & Vacanti, J. P. TISSUE E NGINEERING : Current State and Prospects. *Annu Rev Med* **52,** 443–451 (2001).

46. Angele, P., Kujat, R., Koch, M. & Zellner, J. Role of mesenchymal stem cells in

meniscal repair. *J. Exp. Orthop.* **1,** 12 (2014).

47.   Fox, A. J. S., Bedi, A. & Rodeo, S. a. The basic science of human knee
       menisci: structure, composition, and function. *Sports Health* **4,** 340–51 (2012).

Chapter 5:

Development of a Synthetic Composite Hydrogel Ink for Solid Freeform Fabrication

This chapter describes the formulation of a 3D ink for solid freeform fabrication using a silicate nanoclay additive. Parts of this chapter will be published as a research article entitled "Development of a Synthetic Composite Hydrogel Ink for Solid Freeform Fabrication." (*Houben, A. et al. In preparation).*

5.1. Introduction

When targeting the regeneration of lost or damaged tissue, a conventionally applied approach is to develop a porous, three-dimensional (3D) scaffold that can be combined with cells. Upon combination, tissue can be regenerated by guiding the cells to produce their own extracellular matrix (ECM) and by providing a physical support for the growing tissue as introduced in the first chapter.[1–4] Solid freeform fabrication (SFF) techniques, also known as 3D-printing or rapid prototyping, offer the possibility to produce scaffolds with high control over the geometry and morphology.[5,6] A crucial aspect in this process is the selection of a suitable printing ink. The selected material has to lead to a final construct which is self-supporting, compatible with the available SFF technique and biocompatible.[7,8]

Hydrogels are of great interest for the design of scaffolds, particularly when targeting soft tissue engineering, due to their good biocompatibility, their ability to absorb large quantities of water and their similarity to the ECM.[7,9–11] However, only a limited number of cell-interactive hydrogel printing inks are commercially available.[8] These rely on the use of photo-crosslinkable gelatin (Gel4Cell® from Bioink solutions Inc and BioGel from Biobot) or combine a synthetic polymer with gelatin (Bioink® from RegenHU). However, despite their lack of cell adhesion sites, the use of synthetic hydrogels is advantageous as they have a straightforward, scalable and reproducible synthesis, which is associated with tunable physical properties of the final material.[7,12,13]

In the previous chapters, a synthetic UV-curable acrylate-terminated urethane based poly(ethylene glycol) (PEG$_{2000}$-OEOAcr) hydrogel precursor was developed and characterized.[14,15] This PEG$_{2000}$-OEOAcr hydrogel precursor is an attractive SFF ink candidate due to a range of interesting properties. It can be synthetized on an industrial scale using low-cost reagents.[14] In addition, the material can be used over its entire concentration range (10-100 wt%), resulting in efficient hydrogel formation with excellent mechanical properties.[14,16] Furthermore, the material can be UV-cured in the absence of a photo-initiator, which circumvents any possible toxic effects of photo-initiators.[17]

To increase cell interactive properties of synthetic materials, bulk modification or coating with biological molecules such as ECM proteins, peptide sequences and/or growth factors is a commonly used approach, as was applied in chapter 2 (gelatin methacrylamide coating).[18–20] Alternatively, bioactive properties have been enhanced via the fabrication of

composite hydrogels by the integration of inorganic compounds such as calcium phosphate or silicate-based materials into the hydrogel.[13,21–25] The latter approach can be considered more advantageous due to the ease of fabrication resulting in composites with enhanced mechanical and biological properties, and the more cost-efficient character of the method.[24]

In this approach, Laponite, a silicate nano-clay, was used as an additive as it conveniently improves both cellular response and the mechanical and rheological properties of the printing solutions and the printed constructs.[26–28] It is composed of layered aggregates (nano-clay platelets) of magnesium silicate with the empirical formula $Si_8[Mg_{5.5}Li_{0.4}H_{4.0}O_{24}]^{-0.7}$ $Na^{+0.7}$. The material shows a thixotropic rheological behavior which is ideal towards extrusion-based SFF methods, as the printing material should easily flow from the needle, while the printed structure needs to be retained. [29,30] Furthermore, when the nano-clay platelets are combined with polymers, they act as multifunctional physical crosslinks between polymer chains leading to enhanced mechanical properties of the network, of which the crosslinks are reversible upon deformation due to adsorption/desorption phenomena of the polymer chains to/from the nano-clay platelets.[31,32]

Besides favorable Laponite effects on the physical properties of polymers, its ability to promote cell response has also been reported using mouse osteoblasts, human mesenchymal stem cells and humane bone marrow stromal cells.[11,26,33–35] Similar to bioactive glass, Laponite has dissolution products such as Mg^{2+} and $Si(OH)_4$ which interact with cell integrins and stimulate collagen-I formation.[33,36] On the other hand, protein adhesion is promoted in presence of the nano-clay materials on the surface, which subsequently results in improved cell adhesion.[37] Chang et al. fabricated polyethylene glycol diacrylate (PEGDA)/Laponite composites and reported that the addition of Laponite improved cellular interactions with mouse osteoblasts.[26]

In the present chapter, the aim was to develop a novel, low-cost, cell-interactive and fully synthetic (not protein based) 3D-printing ink. To this end, a recently developed PEG-based hydrogel material was combined with the nano-clay additive. The beneficial properties of Laponite have been described in literature (as mentioned above), however the development of a fully synthetic 3D printing ink for tissue engineering applications, evidenced by direct cell seeding on a printed scaffold has not been described. Calvert et al created cross-linked polyacrylamide and polyacrylic acid freeformed constructs by

combining a monomer, a crosslinking agent and a catalyst with fumed silica and printing on a hot plate to induce polymerization.[29] However, they do not describe cell seeding experiments on these scaffolds. Hong *et al* use laponite for 3D printing experiments, in combination with calcium-crosslinked alginate and PEG in a partly synthetic, partly biopolymer based ink.[38]. However, for the biological evaluation, they do not seed cells onto the printed scaffolds, but rather encapsulated them in a collagen solution which was injected into the pores of the printed scaffold. In this work, the properties of the ink solution before and after crosslinking were assessed using rheology, swelling tests, gel fraction experiments, tensile test and contact angle measurements. Next, the ink composition was optimized for SFF after which the resulting 3D-printed constructs where evaluated for their cellular response by seeding mouse osteoblast cells (MC3T3) directly onto the printed scaffolds.

5.2. Materials and Methods

5.2.1. Polymer synthesis

An acrylate-endcapped urethane-based poly(ethylene glycol) hydrogel precursor (PEG_{2000}-OEOAcr)[14–16] was synthesized by first reacting poly(ethylene glycol) (Mn 2000 g/mol) (PEG 2000, Sigma) with isophorone diisocyanate (IPDI, BASF) at 75°C in a 1:2 stoichiometric ratio using 300 ppm bismuth neodecanoate (Shepherd) as a catalyst. In a second step, a monoacrylated PEG (Bisomer PEA 6, GEO Specialty Chemicals UK Ltd) was added together with 300 ppm bismuth neodecanoate and a temperature of 80°C was maintained until a residual NCO value below 0.02 meq g^{-1}, determined by potentiometric titration, was considered for the reaction to be complete (after 3 hours).

5.2.2. Preparation of composite ink solutions

Three different types of nanosilicates, available under the commercial name Laponite (provided by BYK) were used herein. For initial characterization tests, Laponite RD and RDS were used (general purpose grade). The first purely consists of silicate nano-clay particles, while the latter also contained pyrophosphate groups to postpone gelation of the solution, enabling a more efficient mixing. For cell tests, Laponite XLS was used which has the same composition as Laponite RDS but of a higher purity (personal care grade: high purity, certified low heavy metal and low microbiological content). To prepare the precursor-nano-clay composite formulations, Laponite was dissolved in double distilled water at room temperature under heavy stirring. When Laponite was completely dissolved, the PEG_{2000}-OEOAcr hydrogel precursor powder was added and the mixture was heated up to 50° C overnight under mechanical stirring until a homogeneous solution was obtained. The same protocol was followed for all compositions prepared and characterized in this study.

5.2.3. Preparation of crosslinked hydrogel samples

Thin hydrogel films, to be applied for swelling tests, mechanical characterization and static contact angle measurements, were prepared by film-casting the ink solutions containing the synthetic hydrogel building block (30-50 wt%) and Laponite RD or RDS (0-3 wt%) in between two glass plates, as described in chapter 2. The samples were

exposed from both sides to UV-A light for 20 minutes (LEDENGIN LZ1-00U600 LED, Ultra Violet, SMD, 4.1 V, 365 nm, 2×8 mW cm^{-2}).

For printed hydrogels, samples were placed onto a glass plate and crosslinked using the same setup during 30 minutes to ensure complete curing of the sample.

5.2.4. Rheological analysis of ink compositions

The influence of shear on the viscosity of the polymer solutions with and without additives was studied by oscillatory rheology using an Anton Paar Physica MCR 300 rheometer. A parallel plate setup was used with a top plate diameter of 25 mm. All measurements were performed at room temperature (21°C), after introducing approximately 500 µl precursor solution between the plates and setting a gap size of 0.5 mm. The complex viscosity was measured as a function of the frequency (0.01 - 100 s^{-1}) and plotted on a logarithmic scale.

Polymerization/cross-linking kinetics of the different ink compositions were studied by linear rheology using an Anton Paar Physica MCR 300 rheometer equipped with an EXFO novacure 2000 UVA light for sample irradiation from the bottom through a quartz plate (140 mW cm^{-2}). A parallel plate setup was used with a top plate diameter of 25 mm. In order to study the network formation, the elastic shear modulus (G') was recorded over time upon UV exposure. Frequency and strain sweeps were recorded to establish the linear visco-elastic(LVE) range of the materials. A shear frequency of 1 Hz and an amplitude of 1 % were selected as they were well within this LVE range. The gap was set at 0.35 mm. The UV-A light was switched on after 60 s and the samples were irradiated for 10 min followed by a 60 s interval without UV exposure to determine the final G' value.

5.2.5. Assessment of the swelling degree and the gel fraction of the crosslinked inks

The effect of the Laponite content in the ink solutions on the crosslinking degree and the swelling capacity was evaluated gravimetrically, as explained in Chapter 2.

Statistical analysis was performed using the Analysis ToolPack for Excel. A single factor analysis of variance was performed. For significantly different means, a F-test was executed. All variances were found to be unequal. Therefore two sample T-tests

were performed assuming unequal or equal variances depending on the outcome of the F test.

5.2.6. Mechanical characterization of the crosslinked inks

The influence of the clay concentration on the mechanical properties of crosslinked inks was evaluated by tensile tests using a Universal tester 10-KM (Hounsfield) with a load cell of 100 N. Dog-bone shaped samples with a length of 30 mm were obtained from cross-linked hydrogel films (thickness 1 mm). The tensile properties of the hydrogel samples were determined immediately after UV-curing (samples with initial water content) and after equilibrium swelling in double distilled water (swollen samples). All measurements were performed at room temperature. A preload force of 0.3 N was applied and the specimens were pulled with a crosshead velocity of 10 mm/min. The mechanical tensile modulus was calculated from the slope of the first linear portion of the stress/strain curves.

5.2.7. Bioplotting of Laponite-containing inks

Three-dimensional porous scaffolds were fabricated via the Bioplotter technology starting from the different ink compositions, with an PEG_{2000}-OEOAcr precursor concentration from 30 to 50 wt% in the presence of Laponite RDS (3 wt %). Printing with a lower or higher Laponite concentration did not result in reproducible scaffolds. Ink solutions were transferred into a syringe and inserted in the printing head of the Bioplotter. The optimization and selected printing parameters are described below. During the printing process, the 3D structure self-supporting character was further enhanced through scaffold cross-linking using 2 UV-A LED's (365 nm) mounted on the printer head. For complete crosslinking, samples were also irradiated with UV light after the printing process (as described in section 2.3). The morphology of the samples was observed using a Axiotech 100 – Carl Zeiss with an Axiocam 105 Color from Zeiss and analysed using ImageJ software.

5.2.8. Static contact angle measurements of cross-linked inks

Static contact angle values of the samples were obtained by the sessile drop method using an OCA 20 (DataPhysics Instrument GmbH, Filderstadt, Germany) device, and analysed with SCA 20 (DataPhysics Instrument GmbH, Filderstadt, Germany) software. After placing 1 µl deionized water onto hydrogel discs, the drop was imaged

via a micro camera and the contact angle was calculated via the circle fitting method. SCA values were recorded immediately and after 1 minute contact.

5.2.9. Biological evaluation

Mouse calvaria preosteoblast cells (MC3T3-E1, P14, ATCC) were cultured in alfa-minimal essential medium supplemented with 10% fetal bovine serum, 2 mM L-glutamine and 0.5 v % penicillin-streptomycin (104 U mL^{-1}- 104 µg mL^{-1}). The scaffolds were sterilized using ethylene oxide (cold cycle, AZ Sint-Jan hospital, Brugge). Prior to cell seeding, the scaffolds were incubated in serum-free culture medium for 1 hour to reach equilibrium swelling. After removal of the serum-free culture medium, MC3T3 cells (300 000 cells/80 µl/scaffold) were seeded by drop-seeding. After 4 hours, additional culture medium was added and the cell/scaffold constructs were incubated (37°C, 5% CO$_2$) for 21 days. Calcein AM/propidium iodide staining was performed to evaluate cell viability by fluorescence microscopy (Type U-RFL-T, Olympus).

Statistical analysis was performed according to the methods described in section 2.5.

5.3. Results and Discussion

5.3.1. Combination of the shear thinning properties of Laponite and the UV photocrosslinking behavior of the PEG$_{2000}$-OEOAcr hydrogel precursor: a rheology study

One of the Laponite key features is the shear thinning behavior. When dispersed in aqueous medium, platelet-like nanoparticles are formed.[39,40] The dissolved nanoparticles crosslink trough ionic interactions, leading to a solution viscosity increase. When stress is applied, the gel structure is distorted resulting in a significant viscosity reduction. When the stress is removed, the re-orienting platelets result in gelation. This behavior was investigated using birefringence experiments, which have shown that upon applying shear stress, the clay platelets orient themselves along the direction of the applied shear.[41] Furthermore, when a PEO-based polymer is present in the solution, the polymer chains adsorb to the clay particles through electrostatic interactions. This reversible binding results in shear thinning behavior, which is beneficial for extrusion-based solid freeform fabrication. In this first characterization section, the shear thinning effect of Laponite was characterized using a 30 wt% concentration of PEG$_{2000}$-OEOAcr. As the aim was to understand the properties of Laponite, this was performed prior to the solid freeform fabrication experiments. Therefore, these concentrations are not optimized for solid freeform fabrication.

Figure 1 (top left panel) represents the Laponite RD concentration dependent shear thinning properties of aqueous solutions. For the lowest concentration of 2 wt%, only minor shear thinning can be observed as the viscosity of the solution ranged from 0.72 Pa·s to 0.04 Pa·s. The concentration of silicate nanodiscs is too low to enable significant ionic crosslinks. For a 3 wt% concentration however, a significantly higher viscosity increase of the solution to a value of 188 Pa·s was observed at the lowest shear rate of 0.01 s^{-1}.The observed viscosity linearly decreases with an increasing shear rate to a value of 0.18 Pa·s. When the Laponite concentration is further enhanced, higher viscosities were obtained while maintaining the shear-thinning properties.

In a next step, we were interested to study whether or not the Laponite shear thinning behavior is preserved in combination with the herein developed PEG$_{2000}$-OEOAcr hydrogel precursor. From figure 1 (top right panel), it is obvious that 30 wt% PEG$_{2000}$-

OEOAcr solutions reveal Newtonian behavior, characterized by a frequency independent constant viscosity. The figure further indicates that upon addition of 2-5 wt% Laponite RD, a significant viscosity increase is observed at low frequency, with a decreasing trend at higher frequencies, confirming the prevalence of the Laponite shear thinning behavior when combined with PEG$_{2000}$-OEOAcr.
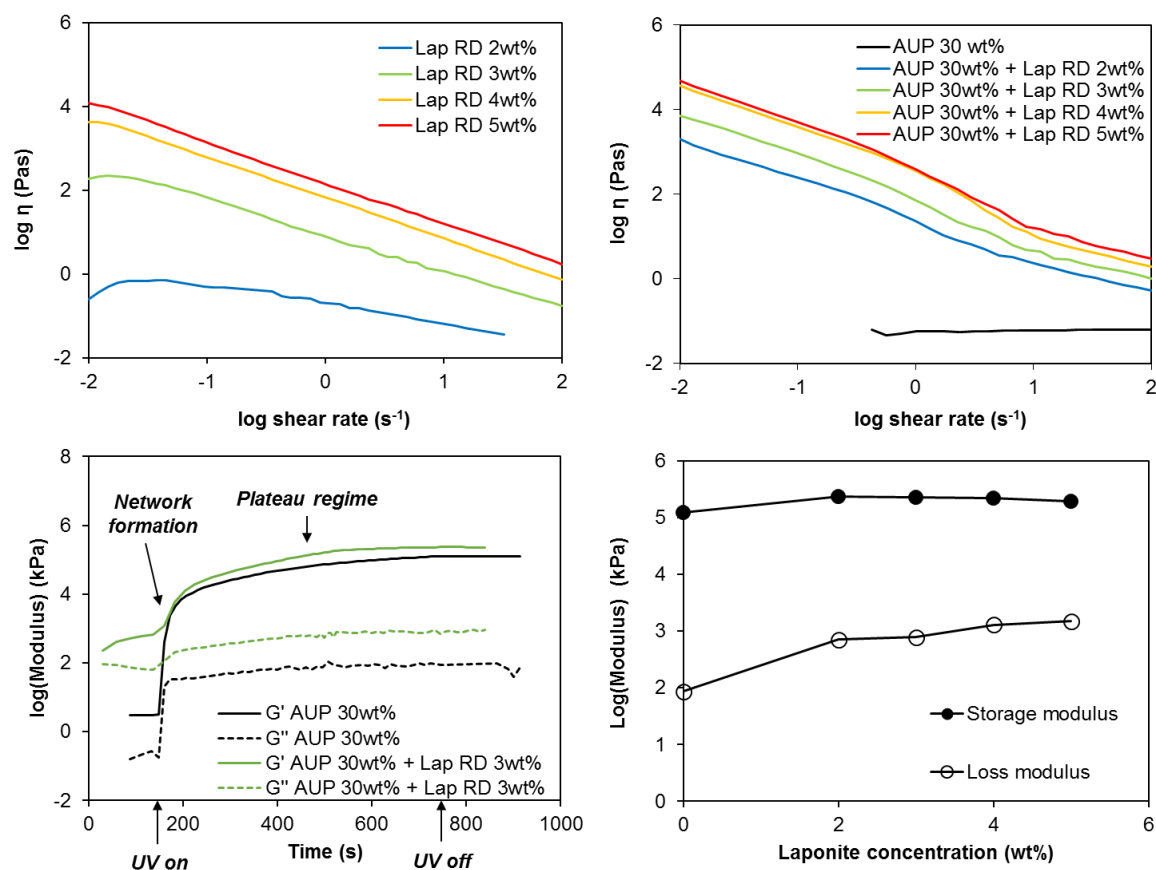
Figure 1: Top: Complex viscosity as a function of the frequency for (left panel) varying concentrations of Laponite RD and (right panel) 30 wt% PEG$_{2000}$-OEOAcr (indicated as prec.) with a Laponite RD concentration ranging between 0 and 5 wt% as determined using rotational rheology. Bottom (left panel) Effect of Laponite (3 wt%) on the crosslinking behavior of 30 wt% PEG$_{2000}$-OEOAcr solutions(prec.) and (right panel) effect of Laponite RD concentration (0-5 wt%) on the storage and loss moduli of 30 wt% PEG$_{2000}$-OEOAcr solutions as determined using oscillatory photo-rheology.

Next, we assessed a possible influence of Laponite RD (3 wt %) on the UV-curing of 30 wt% PEG$_{2000}$-OEOAcr solutions.. Prior to UV crosslinking the storage and the loss moduli were about respectively 200 and 1500 times higher for the Laponite containing PEG$_{2000}$-OEOAcr solution. The latter is the result of the crosslinking effect of the Laponite particles. Upon UV-illumination, both moduli rapidly increase, indicating the onset of effective curing and the excellent auto-initiation of the synthetic PEG$_{2000}$-

OEOAcr hydrogel precursor (i.e. in the absence of a photo-initiator). The slight increase once the plateau regime is reached corresponds to post-crosslinking reactions occurring in the gel.[28] The original difference in storage modulus between solutions with and without Laponite decreases upon UV-curing. This is due to the elastic behavior of the hydrogel which is dominated by the chemical crosslinks formed.. As the viscous behavior of the sample is influenced by the Laponite-mediated reversible crosslinking of the PEG backbone of PEG$_{2000}$-OEOAcr, the loss modulus of the crosslinked sample was influenced to a greater extend by Laponite addition. As evidenced from Figure 1 (bottom right panel), a similar effect was observed upon increasing the Laponite concentration. Indeed, the storage modulus shows a slight increase upon Laponite addition, but remains unaffected at increasing Laponite concentrations. On the other hand, an increasing trend in the loss modulus was observed with increasing Laponite concentration. This confirms the elastic behavior is mostly governed by the chemical crosslinks, while the viscous behavior is affected by the reversible Laponite induced crosslinking.

5.3.2. Optimization of the ink formulation: towards 3D printing of porous scaffolds

After understanding the effect of Laponite on the shear thinning properties and UV-curing of the PEG2000-OEOAcr - Laponite dispersions, the formulation was optimized for solid freeform fabrication prior to further characterization. During the optimization process, it was observed that especially for high Laponite concentrations or large sample volumes (over 10 g), it became increasingly difficult to obtain a homogeneous mixture. Therefore, the silicate particles were combined with tetrasodium pyrophosphate (commercially available as Laponite RDS). When dissolved, the pyrophosphate anions $(P_2O_7)^{4-}$ will associate with the positively charged edges of the Laponite crystal. As a result, both the surface as well as the edges of the Laponite particles have the same charge and the electrostatic repulsion will prevent the formation of a gel structure, as shown in Figure 2. Using Laponite RDS, a low viscosity dispersion is created that is more easily mixable with the polymer. When the polymer is added to this dispersion, this effect is rapidly overcome as the pyrophosphate anions are adsorbed in the polymer matrix due to the partial charges present (e.g. urethane bonds, ester and ether functions, …). As a result, the Laponite crystals will again interact and associate with themselves and the polymer, resulting in a viscosity increase. This allows for a more straightforward mixing procedure, resulting in

homogeneous dispersions with identical printing properties to those prepared with Laponite RD. To enable full activation of the Laponite particles (i.e. viscosity build-up as a result of dissociation of the pyrophosphate anions with the Laponite particles and association of the Laponite particles with themselves and the polymer), the dispersions were stirred overnight prior to performing the 3D-printing experiments and the characterization assays.
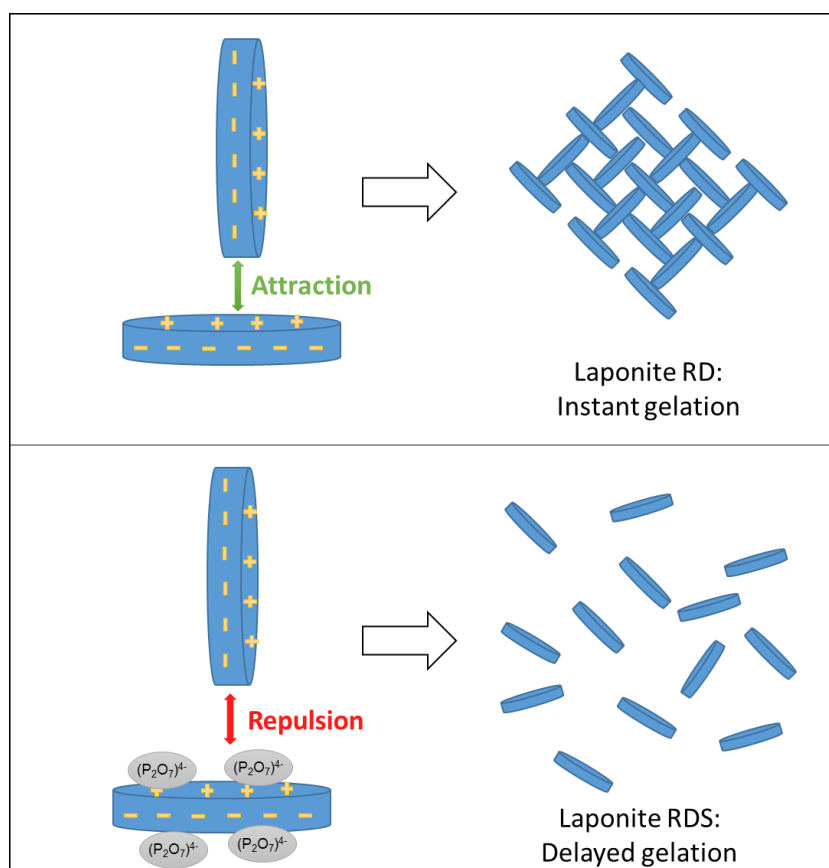
Figure 2: Schematic representation of the association and gelation of Laponite RD (top) and the effect of the pyrophosphate anions in Laponite RDS on these processes (bottom). .

In Figure 4 the viscosity as a function of shear rate is compared for a 30 wt% dispersion and a 50 wt% dispersion of PEG$_{2000}$-OEOAcr, both containing 3 wt% Laponite RDS. It can be observed that at all shear rates, the viscosity of the 50 wt% dispersion is higher compared to the 30 wt% dispersion. Both dispersions show the typical shear-thinning behavior due to the presence of Laponite. Because the exact shear rate during and after solid freeform fabrication cannot be determined as the device uses an air controlled dispense system, the effect of viscosity can be understood from a qualitative point of view. When designing a bio ink, it is important to have a low viscosity at higher shear rate, as this ensures that the polymer will easily flow from the plotting needle.

However, if the viscosity after printing is too low this will drastically reduce the printing resolution as printed struts will fuse together. At low shear rates, both dispersions have a high viscosity, which will result in excellent structure retention of printed scaffolds. To have this ideal balance of the viscosities at different shear rates, the composition was optimized by increasing the PEG_{2000}-OEOAcr concentration from 30 up to 60 wt%. When the PEG_{2000}-OEOAcr concentration was lower than 50 wt%, solid freeform fabrication was not possible as the flow of the material after deposition is too high, resulting in very broad and flat struts. When printing multiple layers, they fused together. This is evidenced by the viscosity at low frequency (0.1 s^{-1}): the complex viscosity of the 30 wt% dispersion with 3 wt% Laponite RDS increases to 316 Pa s, while the 50 wt% dispersion with the same Laponite RDS concentration has a complex viscosity that is more than twice as high, 794 Pa s (see Figure 4). Furthermore, the slope of these curves is below -1, which indicates that some sedimentation occurs in the mixture. This implies imperfect dispersion of the laponite particles, so to have a more in-depth analysis of the solutions the mixing procedure should be optimized further. Over this PEG_{2000}-OEOAcr concentration range, the Laponite concentration was varied from 1-7 wt%, but only solutions with 3 wt % had the ideal shear thinning behavior to flow easily from the needle, while retaining the structure after printing. In conclusion, a dispersion of 50 wt% PEG_{2000}-OEOAcr combined with 3 wt% was determined to be ideal for solid freeform fabrication.
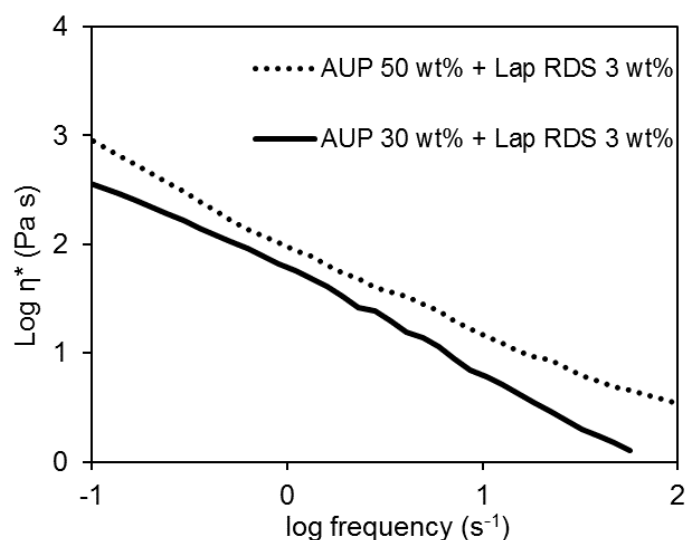
Figure 4: Complex viscosity as a function of the frequency for a 30 wt% and a 50 wt% PEG_{2000}-OEOAcr dispersion with 3 wt% Laponite RDS.

To maximize the printing resolution, the samples were illuminated with 2 UVA-LED's during printing, resulting in a partial crosslinking of the acrylate groups, further increasing the structure retention of the printed samples. Complete crosslinking of the samples was achieved post processing by irradiating (t = 30 min) the samples using UVA lamps. The solid freeform fabrication process was optimized by selecting an appropriate layer thickness, speed in the XY plane, speed in the Z direction, pressure and strand distance. An overview of these parameters, with the evaluated range and the selected value is described in Table 1.

Table 1: Optimized parameters during solid freeform fabrication

Parameter (unit)	Evaluated range	Optimal value
Pressure (bar)	0.5-5	1-1.2
Temperature (°C)	10-25	10
XY-printing speed (mm min^{-1})	400-1200	600
Z-printing speed (mm min^{-1})	500-1200	500
Layer thickness (mm)	0.2-0.25	0.2
Strand distance (mm)	1-1.4	1.2

A first optimized parameter is the pressure, which was varied between 0.5 and 5 bar. The pressure will determine the speed at which the printing ink flows from the syringe. If the pressure is too low, the ink will not be extruded due to the shear thinning behavior of the dispersions. The pressure, XY and Z speed and temperature all need to be optimized together: when the pressure increases, the flow will increase. Therefore the XY and Z speed need to be increased to maintain thin struts. A decreased temperature will increase the viscosity of the solutions, and the pressure will need to be adjusted together with the XY and Z speed. The optimal value for the printing pressure was determined to be 1-1.2 bar. Imperfect sealing of the plotting syringe led to small variations in the applied pressure and the actual pressure (typically between 0.1-0.7 bar), therefore the pressure needed to be optimized each time the printing syringe was changed. It was observed that high viscosities aided the printing process and led to

better structure retention. Therefore, the temperature was set to the lowest possible value of 10°C.

As mentioned, the optimization of the printing pressure and temperature are closely related to the optimization of XY and Z speed. After the pressure was set to obtain a continuous and regular flow of the ink from the needle, the XY speed was optimized. When the speed becomes too low, the struts will become thicker, eventually leading to pore blockage. If the speed is too high, the struts will no longer be continuous, leading to incomplete layers. The ideal XY speed was determined to be 600 mm min^{-1}. As illustrated in the previous chapter, the Z speed is the speed at which the needle moves up after a layer is printed. If this speed is too high, the last part of the deposited strut will break and cause a defect. If the speed is too low, a droplet of material will be deposited on the edge of the scaffold (see chapter 2, section 2.2.3.2). For the selected ink composition, the ideal Z speed was 500 mm min^{-1}. After optimization of the plotting parameters, the structural parameters (layer height and strut distance) could be optimized. By printing multiple layers, measuring the height of the construct and dividing this by the number of printed layers, the actual value of the layer height could be determined, which was 0.2 mm on average. Finally, the strand distance was set to 1.2 mm, to obtain a regular porosity throughout the scaffold.

With these optimized plotting parameters, regular scaffolds were printed starting from these dispersions, as depicted in Figure 5. An average strut size of 575 ±111 µm and pore size of 684 ±99 µm were obtained. The sum of the measured strut size and measured pore size is in close accordance to the set strand distance (1.2 mm), indicating a good match between CAD and CAM. In addition, a 3D meniscus shape (width 31.52 mm, length 1.39 mm and height 2.79 mm) was printed as a proof of concept demonstrating the ability of the ink to be used for the printing of larger constructs.
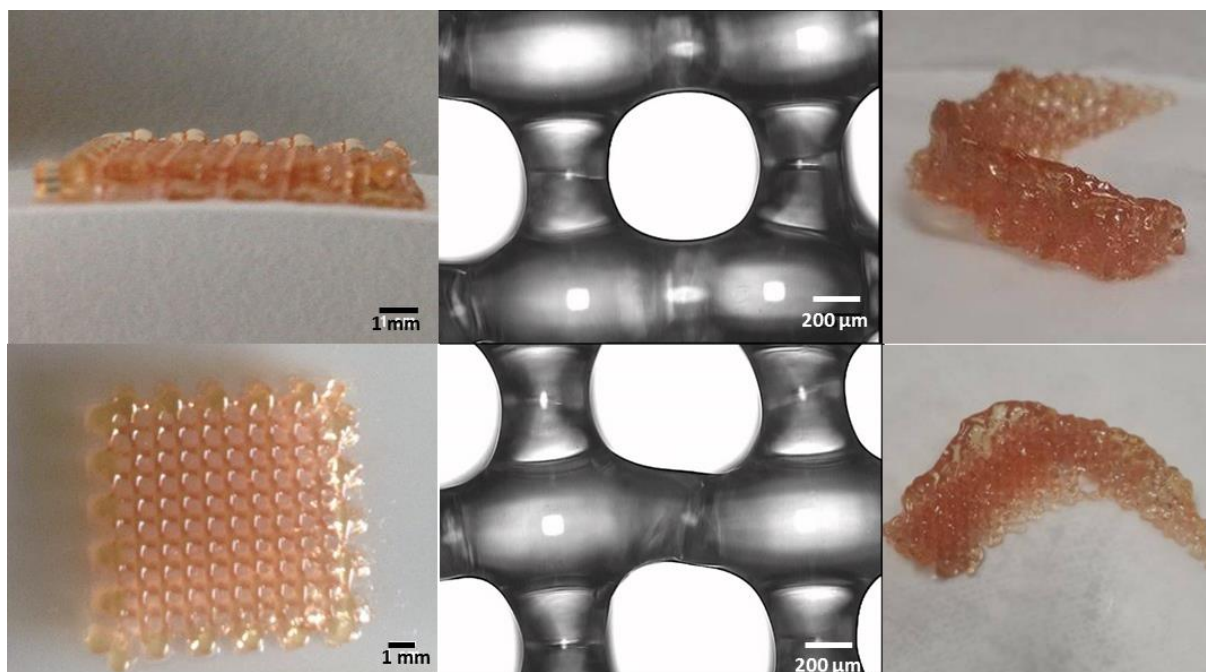
Figure 5: Photographs (left) and optical microscopy images (middle) of 3D scaffold starting from a 50 wt% PEG$_{2000}$-OEOAcr dispersion containing 3 wt% Laponite RDS. Right: Human meniscus scaffold (31.52 mm x 1.39 mm x 2.79 mm) printed as a proof of concept.

5.3.3. Further characterization of the selected ink composition

Further optimization of the solid freeform fabrication ink was performed based on the optimized concentration of 50 wt% PEG$_{2000}$-OEOAcr and 0-3 wt% Laponite RDS. Samples were prepared by photo-initiator free UV initiated polymerization and the gel fractions and swelling degrees of the obtained gels were determined (depicted in Figure 3). The gel fraction remained unaffected in the investigated Laponite concentration range and was above 99% for all concentrations. This indicates that even without the addition of a photo-initiator, a strongly crosslinked network was formed. Furthermore, there is no significant impact of Laponite on the crosslinking efficiency. For the swelling ratio, a statistically significant decrease was observed with increasing Laponite concentration. The additional crosslinking thus decreases the water uptake of the samples. Similar results were obtained by Chang *et al.* for PEGDA crosslinked with various concentrations of Laponite.[26]
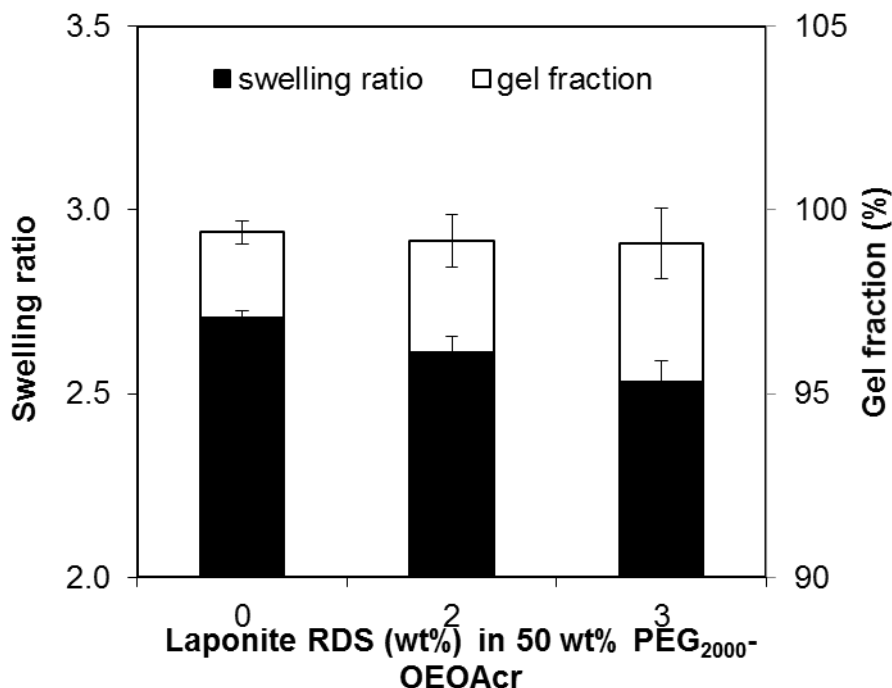
Figure 3: Swelling degree and gel fraction of a 50 wt% PEG$_{2000}$-OEOAcr hydrogel in the presence of 0-3 wt% Laponite RDS. All gel fractions did not reveal statistical differences, whereas all swelling ratios where significantly different (p < 0.5)

The mechanical characterization of crosslinked hydrogel sheets was performed both in the presence of the initial water content and after equilibrium swelling for scaffolds starting from 50 wt% polymer concentration containing 0-3 wt% Laponite RDS (see *Figure 6*). Although a decreasing trend could be observed, there was no statistically significant difference in elongation upon applying different Laponite concentrations (p < 5). An average value of 29% was obtained for the samples with their initial water content, which decreased to an average value of 23 % after equilibrium swelling in water. Initially, an increase of both the Young's modulus (from 2.2 MPa to 2.6 MPa) and the tensile strength (from 0.60 to 0.68 MPa) could be observed which can be attributed to the additional crosslinking of the samples due to the presence of Laponite, similar to what was observed in literature.[26,30,33]
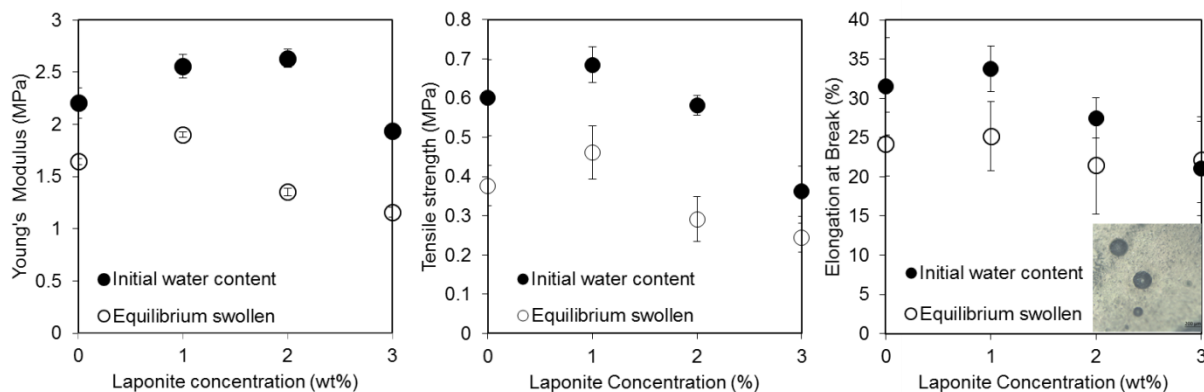
Figure 6: Young's modulus, tensile strength and elongation at break for a 50 wt% dispersion of crosslinked PEG$_{2000}$-OEOAcr hydrogels containing a Laponite RDS concentration ranging between 0 and 3 wt%. Inset image: air bubbles present in the sample containing 3 wt% of Laponite

However, for Laponite RDS concentrations exceeding 2 wt%, a decreasing trend in tensile properties was observed due to the presence of air bubbles trapped in the samples, weakening the mechanical properties. These air bubbles (ranging in size from 10 to 300 µm), as shown in a crosslinked sample (see inset image in *Figure 6*) could not be removed because of the viscous nature of the mixture. Different mixing methods, including vacuum treatment and heating were explored with no effect. For the dispersions containing 3 wt% Laponite RDS, the Young's modulus for samples with their initial water content was reduced from 2.2 MPa for the Laponite free sample to 1.9 MPa. After equilibrium swelling, the Young's modulus was reduced from 1.6 MPa to 1.2 MPa.

5.3.4. *In vitro* biological evaluation of 3D-printed scaffolds

The increased cell interactivity in the presence of Laponite has already been reported previously in literature: in addition to the release of dissolution products that stimulate collagen production, an increased protein adsorption on the surface of the nanocomposites further enhances cell adhesion. [23,33,37] In addition to the change in chemical composition of the surface, the presence of Laponite will also affect the hydrophilicity of the surface, which can be beneficial for cell adhesion.[42] This effect was characterized by measuring the contact angle of crosslinked hydrogel sheets starting from ink dispersions with 50 wt% PEG$_{2000}$-OEOAcrand 0-3 wt% Laponite RDS (see Figure 7). A decreasing trend in SCA, both immediately after droplet deposition and 1 minute later, can be observed. This indicates the effect of Laponite on the

surface properties of the material: the SCA decreases, indicating an increased surface wettability by water. The change is SCA will contribute to the cell adhesion properties of the material. Research performed by Tamada *et al* has already shown that a moderately hydrophilic material, with a contact angle between 60° and 80°, results in maximal cell adhesion.[42] Upon addition of Laponite, the static contact angle of the material reaches this region, as the SCA after contact is reduced from 101° for the sample without Laponite, to 80° for the sample containing 3 wt% Laponite RDS. In literature, a similar decrease in SCA was observed for agar-based films with increasing nanoclay content.[43]
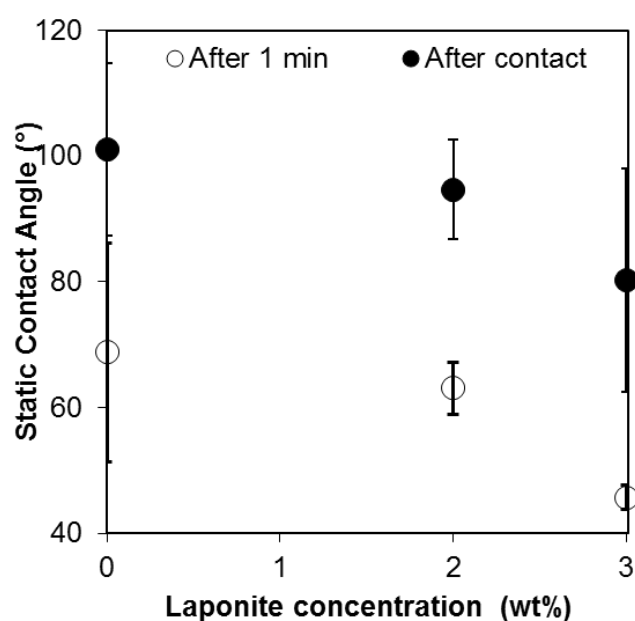
Figure 7: Static contact angle measurements of crosslinked samples of 50 wt% PEG$_{2000}$-OEOAcr with 0-3 wt% Laponite RDS. The SCA is measured immediately and 2 minute after deposition of the droplet.

Qualitative analysis using live/dead staining (see 8 and 9) revealed the effect of Laponite on MC3T3 adhesion and viability. Since SFF was not possible in the absence of Laponite, hydrogel discs with and without Laponite were used to evaluate the effect on the cell adhesion and viability. As this experiment was performed prior to the solid freeform fabrication experiments, the initially selected PEG$_{2000}$-OEOAcr concentration of 30 wt% was used to assess the effect of Laponite on cell adhesion. For the experiments with 3D scaffolds, the optimized concentration of 50 wt% was used, as printing with the 30 wt% dispersion was not possible. Although cell adhesion still occurs on the samples without Laponite, most likely due to protein adsorption, a clearly

beneficial effect of Laponite can be observed. Especially at d1, a significant difference in cell viability of about 46% can be observed. After three days, the cell viability on the scaffolds without Laponite has recovered from 54% to 94%, while the viability on the scaffolds with Laponite has further increased from 90% to 98%. Furthermore, as can be observed on the fluorescence microscopy images (figure 8 right part) cells seeded on the Laponite disks have formed a confluent monolayer after three days, while this is not the case for the hydrogel only scaffolds.
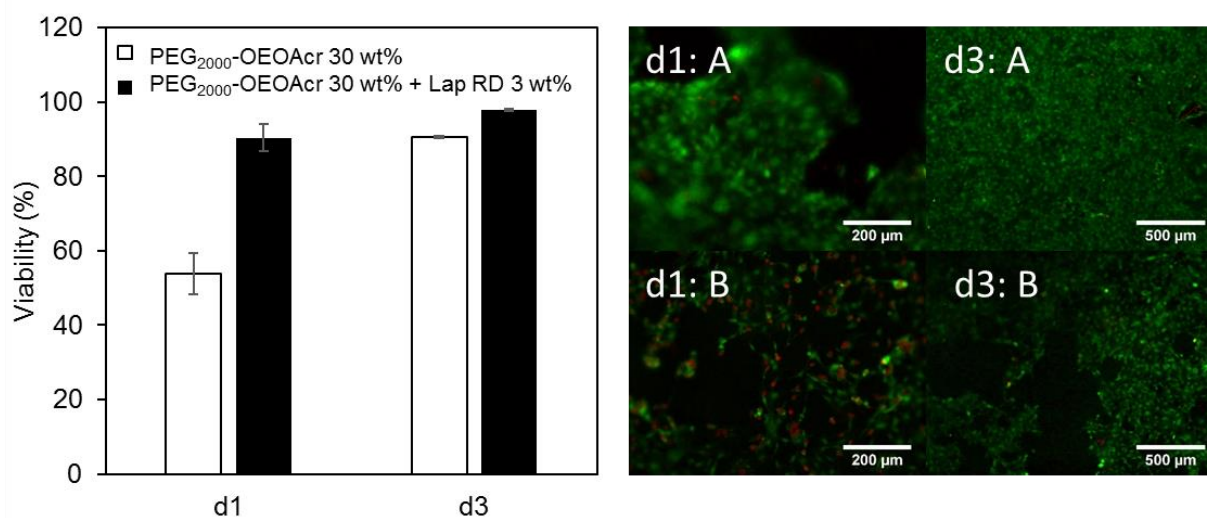
Figure 8: Left: Mouse calvaria preosteoblast cell (MC3T3-E1) viability for scaffolds with and without Laponite XLS after one and three days of culture. Results at both time points were significantly different at a P < 0.05. Right: vital staining images of MC3T3 cells seeded on 30 wt% PEG$_{2000}$-OEOAcr disks with (A) and without (B) 3wt% Laponite XLS after one day (d1) and three days (d3) of incubation.

Similar results were obtained on the Laponite-containing 3D printed scaffolds depicted in Figure 9. After 24h of contact, the cells on the 3D printed scaffolds show excellent viability and an elongated morphology, indicating a good adhesion between the cells and the scaffold. Furthermore, after 7 days the cells formed a confluent monolayer on the 3D scaffold, which was maintained throughout the duration of the experiment (23

days). At this timepoint, in some areas a typical bridging behavior can be observed, where adjacent cells act as support to allow growth into the pores of the scaffold. [44]
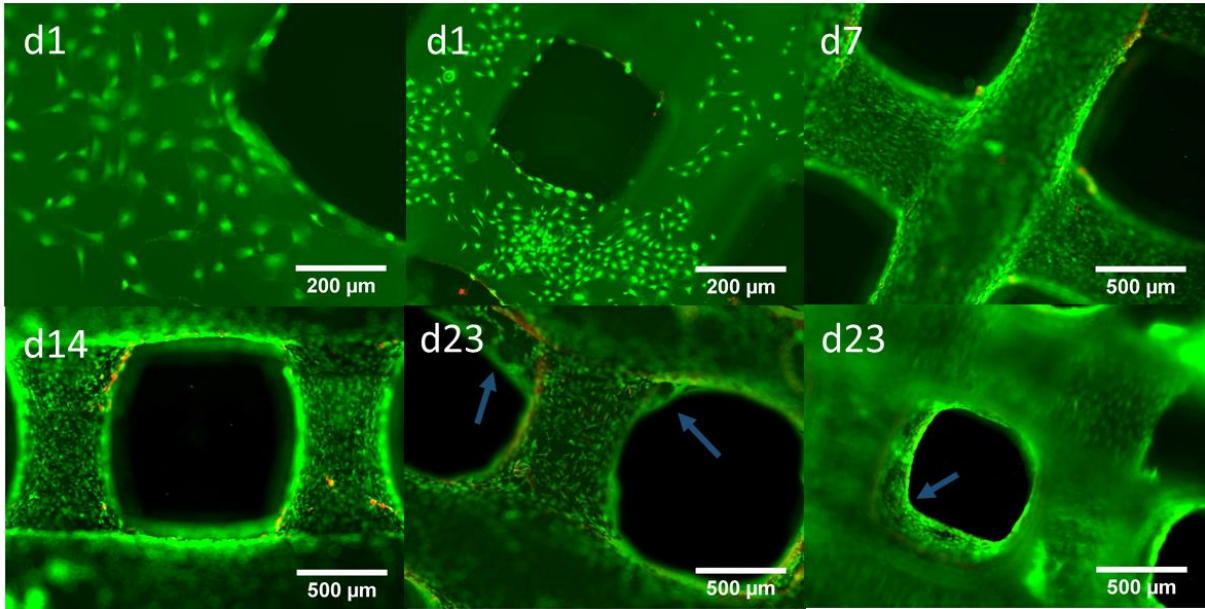
Figure 9: Vital staining of mouse calvaria preosteoblast cells (MC3T3-E1 as a function of time on 3D scaffolds containing 50 wt% PEG$_{2000}$-OEOAcr and 3 wt% Laponite RDS. Arrows indicate areas where cells are starting to bridge the pores of the scaffold.

5.4. Conclusion and future perspectives

In conclusion, the proposed composite synthetic ink is an ideal addition to the biopolymer based solid freeform fabrication inks currently available. By combining the synthetic PEG$_{2000}$-OEOAcr hydrogel precursor with the Laponite silicate nanoclays, ideal ink properties were obtained, including technical capability and cell interactive properties. For the final composition, a concentration of 50 wt% for the synthetic hydrogel building block, and 3 wt% for the nanosilicate clay were selected. The desired shear thinning behavior was observed as the viscosity decreased from 24.0 Pa·s at a shear of 0.3 s^{-1} to 0.2 Pa·s at a shear rate of 100 s^{-1} for this dispersion. Excellent mechanical properties of the crosslinked ink hydrogels were obtained, with a Young's modulus of 1.9 MPa for the selected ink composition. Furthermore, the addition of nanosilicate promotes cell adhesion and enhances cell viability, as evidenced by cell seeding experiments on 2D discs and 3D-printed scaffolds. Future perspectives include the evaluation of these materials for cell encapsulation, with the aim to develop the material into a cell-containing bio-ink. This can lead to scaffolds containing encapsulated cells rather than seeding the cells after printing, to maximize the (autologous) cell content into (patient-specific) scaffolds.

5.5. References

1. Kim Mooney, D.J., B.-S. Development of biocompatible synthetic extracellular matrices for tissue engineering. *Trends Biotechnol.* **16,** 224–230 (1998).

2. Griffith, L. G. Polymeric biomaterials. *Acta Mater.* **48,** 263–277 (2000).

3. Chen Takashi, U., Tateishi, T., G. Scaffold design for tissue engineering. *Macromol. Biosci.* **2,** 67–77 (2002).

4. Yeong, W.-Y. Y. *et al.* Rapid prototyping in tissue engineering: challenges and potential. *Trends Biotechnol.* **22,** 643–652 (2004).

5. Billiet, T. *et al.* A review of trends and limitations in hydrogel-rapid prototyping for tissue engineering. *Biomaterials* **33,** 6020–6041 (2012).

6. Houben, A. *et al.* Indirect Rapid Prototyping: Opening Up Unprecedented Opportunities in Scaffold Design and Applications. *Ann. Biomed. Eng.* **45,** 1–26 (2016).

7. Drury Mooney, D.J., J. L., Drury, J. L. & Mooney, D. J. Hydrogels for tissue engineering: scaffold design variables and applications. *Biomaterials* **24,** 4337–4351 (2003).

8. Hölzl, K. *et al.* Bioink properties before, during and after 3D bioprinting. *Biofabrication* **8,** 32002 (2016).

9. Lee, K. Y., Mooney, D. J. & Lee Mooney, D.J., K. Y. Hydrogels for tissue engineering. *Chem. Rev.* **101,** 1869–1880 (2001).

10. Nguyen, K. T., West, J. L. & Nguyen West, J.L., K. T. Photopolymerizable hydrogels for tissue engineering applications. *Biomaterials* **23,** 4307–4314 (2002).

11. Wu Gaharwar, A.K., Schexnailder, P.J., Schmidt, G., C.-J. Development of biomedical polymer-silicate nanocomposites: a materials science perspective. *Materials (Basel).* **3,** 2986–3005 (2010).

12. Hoffman, A. S. Hydrogels for biomedical applications. *Adv. Drug Deliv. Rev.* **64,** 18–23 (2012).

13. Jia Kiick, K.L., X. Hybrid multicomponent hydrogels for tissue engineering. *Macromol. Biosci.* **9,** 140–156 (2009).

14. Houben, A. *et al.* Flexible Oligomer Spacers as the Key to Solid-State Photopolymerization of Hydrogel Precursors. *Mater. Today Chem.* **4,** 84–89 (2017).

15. Houben, A. *et al.* Novel urethane based materials, derivatives, methods of their preparation and uses. (2015).

16. Houben, A. *et al.* Indirect Solid Freeform Fabrication of an Initiator-free Photocrosslinkable Hydrogel Precursor for the Creation of Porous Scaffolds. *Maromolecular Biosci.* **16,** (2016).

17. Bryant, S. J., Nuttelman, C. R. & Anseth, K. S. Cytocompatibility of UV and visible light photoinitiating systems on cultured NIH/3T3 fibroblasts in vitro. *J.*

Biomater. Sci. Polym. Ed. **11,** 439–57 (2000).

18. Bryant, S. J., Nicodemus, G. D. & Villanueva, I. Designing 3D Photopolymer Hydrogels to Regulate Biomechanical Cues and Tissue Growth for Cartilage Tissue Engineering. *Pharm. Res.* **25,** 2379–2386 (2008).

19. Rutz, A. L., Hyland, K. E., Jakus, A. E., Burghardt, W. R. & Shah, R. N. A Multimaterial Bioink Method for 3D Printing Tunable, Cell-Compatible Hydrogels. *Adv. Mater.* **27,** 1607–1614 (2015).

20. Whitaker, M. J., Quirk, R. A., Howdle, S. M. & Shakesheff, K. M. Growth factor release from tissue engineering scaffolds. *J. Pharm. Pharmacol.* **53,** 1427–1437 (2001).

21. Meenach Anderson, K.W., Hilt, J.Z., S. A. in *Safety of nanoparticles* 131–157 (Springer New York, 2009).

22. Seliktar, D. Extracellular stimulation in tissue engineering. *Ann. New York Acad. Sci.* **1047(1),** 386–394 (2005).

23. Gaharwar Peppas, N.A., Khademhosseini, A., A. K. Nanocomposite hydrogels for biomedical applications. *Biotechnol. Bioeng.* **111,** 441–453 (2014).

24. Schexnailder Gaharwar, A.K., Bartlett II, R.L., Seal, B.L., Schmidt, G., P. J. Tuning cell adhesion by incorporation of charged silicate nanoparticles as cross-linkers to polyethylene oxide. *Macromol. Biosci.* **10,** 1416–1423 (2010).

25. Zhu Marchant, R.E., J. Design properties of hydrogel tissue-engineering scaffolds. *Expert Rev. Med. Devices* **8,** 607–626 (2011).

26. Chang van Spreeuwel, A., Zhang, C., Varghese, S., C.-W. PEG/clay nanocomposite hydrogel: a mechanically robust tissue enginereing scaffold. *Soft Matter* **6,** 5157–5164 (2010).

27. Memic, A. *et al.* Hydrogels 2.0: improved properties with nanomaterial composites for biomedical applications. *Biomed. Mater.* **11,** 14104 (2015).

28. Okay, O. & Oppermann, W. Polyacrylamide−Clay Nanocomposite Hydrogels: Rheological and Light Scattering Characterization. *Macromolecules* **40,** 3378–3387 (2007).

29. Calvert Liu, Z., P. Freeform fabrication of hydrogels. *Acta Mater.* **46,** 2565–2571 (1998).

30. Hong, S. *et al.* 3D Printing of Highly Stretchable and Tough Hydrogels into Complex, Cellularized Structures. *Adv. Mater.* **27,** n/a-n/a (2015).

31. Schexnailder Schmidt, G., P. Nanocomposite polymer hydrogels. *Colloid Polym. Sci.* **287,** 1–11 (2009).

32. Haraguchi Takehisa, T., K. Nanocomposite hydrogels: a unique organic-inorganic network structure with extraordinary mechanical, optical, and swelling/de-swelling properties. *Adv. Mater.* **14,** 1120–1124 (2002).

33. Gaharwar, A. K., Rivera, C. P., Wu, C. J., Schmidt, G. & Gaharwar Rivera ,C.P., Wu, C.-J., Schmidt, G., A. K. Transparent, elastomeric and tough hydrogels from poly(ethylene glycol) and silicate nanoparticles. *Acta Biomater.*

7, 4139–4148 (2011).

34. Gaharwar Schexnailder, P.J., Kline, B.P., Schmidt, G., A. K. Assessment of using Laponite® cross-linked poly(ethylene oxide) for controlled cell adhesion and mineralization. *Acta Biomater.* **7,** 568–577 (2011).

35. Dawson Kanczler, J.M., Yang, X.B., Attard, G.S., Oreffo, R.O.C., J. I. Clay gels for the delivery of regenerative microenvironments. *Adv. Mater.* **23,** 3304–3308 (2011).

36. Hoppe Güldal, N.S., Bocaccini, A.R., A. A review of the biological response to ionic dissolution products from bioactive glasses and glass-ceramics. *Biomaterials* **32,** 2757–2774 (2011).

37. Haraguchi Takehisa, T., Ebato, M., K. Control of cell cultivation and cell sheet detachment on the surface of polymer/clay nanocomposite hydrogels. *Biomacromolecules* **7,** 3267–3275 (2006).

38. Hong, S. *et al.* 3D Printing of Highly Stretchable and Tough Hydrogels into Complex, Cellularized Structures. *Adv. Mater.* **27,** 4035–4040 (2015).

39. Willenbacher, N. Unusal thixothropic properties of aqueous dispersions of laponite RD. *J. Colloid Interface Sci.* **182,** 501–510 (1996).

40. Au Leong, Y.-K., P.-I. Surface chemistry and rheology of Laponite dispersions — Zeta potential, yield stress, ageing, fractal dimension and pyrophosphate. *Appl. Clay Sci.* **107,** 36–45 (2015).

41. Schmidt, G., Nakatani, A. I., Butler, P. D., Karim, A. & Han, C. C. Shear orientation of viscoelastic polymer-clay solutions probed by flow birefringence and SANS. *Macromolecules* **33,** 7219–7222 (2000).

42. Tamada, Y. & Ikada, Y. Effect of Preadsorbed Proteins on Cell Adhesion to Polymer Surfaces. *J. Colloid Interface Sci.* **155,** 334–339 (1993).

43. Rhim, J.-W. Effect of clay contents on mechanical and water vapor barrier properties of agar-based nanocomposite films. *Carbohydr. Polym.* **86,** 691–699 (2011).

44. O'Brien, F. J., Harley, B. A., Yannas, I. V. & Gibson, L. J. The effect of pore size on cell adhesion in collagen-GAG scaffolds. *Biomaterials* **26,** 433–441 (2005).

Chapter 6: Conclusions and future perspectives

6.1. Conclusions

In a first part, a novel, solid state reactive hydrogel building block was developed by introducing a short, flexible spacer separating the reactive acrylate end groups from the semi-crystalline backbone, based on poly(ethylene glycol) with a molecular weight of 2000 g/mol. This prepolymer could be synthesized on a large scale (up to 5 kg) and solvent-free. During crystallization of the prepolymer, phase separation occurs between the acrylate groups and the backbone polymer. The flexible spacer provides the acrylates with sufficient mobility to crosslink with excellent reactivity in the solid state, even in the absence of a photo-initiator. This auto-initiation, which is more efficient in the solid state, can be explained by a shift in absorption maximum of the acrylates from the UV-B and UV-C range towards the UV-A range. Due to the phase separation, in the solid state, the π-π orbitals of the acrylates can overlap better, leading to an increased efficiency of the auto-initiation (maximum photo-DSC heat flow increased from 2.1 W g-1 (melt) to 3.4 W g^{-1} (solid state)). Furthermore, the prepolymers could be dissolved over almost the entire concentration range (up to 90 wt%) in water. The latter enables to tune hydrogel properties such as swelling behavior (going from 1.5 to 8.2 times the original dry weight) and mechanical properties (from 0.66 MPa at a 30 wt% concentration to 3.41 MPa at 70 wt%).

In addition, the properties of the polymers could be tuned by varying the different building blocks. A first example is by changing the molecular weight of the backbone polymer. This was varied from 2000 g mol^{-1} up to 20,000 g mol^{-1}, without losing the solid state reactivity. The swelling ratio of the samples crosslinked in the solid state increased from 1.47 up to 16.03 times for the lowest and highest molecular weight respectively, while the Young's modulus decreased respectively from 0.66 MPa to 0.15 MPa for 30 wt% samples. Another approach was to change the backbone chemical structure from poly(ethylene glycol) to poly(ε-caprolactone), which resulted in a polymer that is still solid state reactive, being biodegradable and no longer water-soluble. Furthermore, end group variations from acrylate to methacrylate were realized as a decrease in the toxicity of uncrosslinked polymers can be anticipated. Finally, different spacer groups were used (e.g. oligo(ε-caprolactone) and oligo(ethylene glycol)) to tune the degradation of the crosslinked hydrogels, as it can be anticipated that an ε-caprolactone spacer will be more susceptible towards hydrolysis.

Based on a series of photo-DSC experiments, the reaction kinetics of the polymers were thoroughly characterized. Adding a photo-initiator results in a accelerating effect on the reaction kinetics, increasing the maximum polymerization speed and double bond conversion in the solid and in the molten state. Indeed, the maximum heat flow increases from 3.4 W g^{-1} to 7.2 W g^{-1} in the solid state and from 2.1 W g^{-1} to 7.1 W g^{-1} in the molten state when a photo-initiator is added. The final double bond conversion (after max 260 s of irradiation) increases from 65 % to 76% in the solid state, and from 84% to 87% in the molten state. The presence of oxygen on the other hand has a detrimental effect reducing the polymerization speed and conversion in both the solid as well as the molten state. For samples without a photo-initiator the maximum heat flow decreases from 3.39 to 2.7 W g^{-1} in the solid state and from 2.1 to 1.1 W g^{-1}, while the final conversion decreases from 59 to 47% at 20°C and from 51 to 29%. Furthermore, it was observed that an increase in temperature increases the polymerization speed from 0.3 mol g^{-1} s^{-1} at 253 K up to 5.4 mol g^{-1} s^{-1} at 298 K in the solid state (except at temperatures close to the melting point), while there was no significant temperature effect in the molten state. Similar effects were observed when adding a photo-initiator. The temperature at which the polymers are crystallized also played a profound role. Crystallizing the polymer at a lower temperature (from 293 K to 253 K) reduces the maximum polymerization speed and double bond conversion (maximum difference of 1.2 x 10^2 mol g^{-1} s^{-1}) except at temperatures close to the melting point. To further understand the solid state reactivity, a model was developed using scaling laws to describe the effect of structural changes on the mono- and bimolecular reactions occurring during photopolymerization. The results showed that the auto-acceleration was mainly caused by monomolecular termination reactions and that the latter are much more sensitive to the structural changes and to temperature compared to the bimolecular propagation and termination reactions.

Using a range of different strategies, processing difficulties associated with hydrogel building bocks have been successfully surpassed. The solid state reactive polymers developed in this work could be successfully processed by melt-based solid freeform fabrication, a method never used before for hydrogels. When printing was complete, the structures were cross-linked by UV-A irradiation in absence of a photo-initiator. The printed constructs were quite flexible after crosslinking and subsequent swelling. No cell adhesion occurred on the printed constructs, while excellent cell adhesion and

proliferation were observed after applying a gelatin methacrylamide coating. Furthermore, the prepolymers could be used to create electrospun fibers, followed by a separate UV-crosslinking step. For the electrospinning experiments a photo-initiator was added, as the fibers are quite small (10μm range), fewer crosslink points will be present in a fiber compared larger samples such as disks or 3D-printed constructs. In addition, the large surface-to-volume ratio of these fibers will increase the effect of oxygen inhibition on the polymerization. To help increase the double bond conversion, a photo-initiator was added. Finally, an alternative processing technique, being two-photo-polymerization, was used to create microstructures in the solid state, in the absence of a photo-initiator.

In a last part of the polymer processing work, two additional universally applicable processing methods were applied starting from the prepolymers developed in this work. The first method was indirect solid freeform fabrication, which is used to create three-dimensional constructs from materials that are generally difficult to process. This method was successfully applied to create scaffolds with an interconnective porous network, as revealed using μCT. Using this approach, scaffolds with tunable mechanical (compression force for 1mm indentation between 9 N and 43 N) and swelling properties (between 1.30 and 7.16 times the initial dry weight) could be developed by changing the template printing parameters (extrusion rate from 1.0 to 1.8, temperature from 130 °C to 160 °C, strut distance from 600 μm to 900 μm) and/or the hydrogel concentration (from 10-100 wt%). Again, the cell adhesion and proliferation on these scaffolds was improved by applying a gelatin- methacrylamide coating.

Although the materials developed herein are very promising for a range of applications, they are not cell-interactive. Therefore, the second method included the development of a solid freeform fabrication composite ink based on the silicate nanoclay Laponite in aqueous solutions of the hydrogel precursor. In addition to its cell-interactive properties, the nanoclay results in shear-thinning behavior ideal for solid freeform fabrication purposes. The formulation was optimized towards a concentration of 50 wt% polymer and 3 wt% Laponite, which resulted in excellent mechanical properties and straightforward printing procedures. Excellent cell-adhesive properties were obtained on two- and three-dimensional discs and scaffolds respectively.

6.2. Future perspectives

The unique solid state reactivity and its advantages towards hydrogel processing hold great potential. To gain more insight in the phase separation into amorphous, acrylate rich zones and crystalline, backbone rich zones other techniques could be explored such as solid state NMR and XRD. Furthermore, the effect of crosslinking density and crystallinity on the mechanical properties could be further investigated. However, as the crystallinity will also affect the network formation during photopolymerization (as shown in Chapter 3), it is difficult to separate these effects from each other. A first step towards this would be to evaluate the mechanical properties of polymers with different conversion degrees and crystallinities. On a material development level, it can be interesting to further explore the limits of the solid state reactivity, on the one hand by selecting different building blocks such as semi-crystalline poly(esters) and poly(ethers), or by using temperature- or pH-responsive backbone polymers. Examples include poly(lactides), poly(glycolides) and poly(lactide-co-glycolide) to tune the degradability of the materials and the mechanical properties, or Pluronics® (ABA-block copolymers of poly(propylene oxide) and poly(ethylene oxide)) to achieve temperature responsive behavior. On the other hand, it will be interesting to explore the limits of the elaborated system. Currently, the PEO backbone molecular weight can be increased up to 20,000 g mol^{-1} without losing the solid state reactivity. However, with increasing molecular weight, the double bond concentration will further decrease. So, it can be anticipated that from a certain molecular weight threshold, the polymers will no longer be solid-state reactive.

Furthermore, the ease of processing opens up unprecedented opportunities towards applications in the biomedical and non-biomedical field. Due to their processing capabilities, they are ideal solid freeform fabrication resins, compatible with different techniques such as solid freeform fabrication from the melt, 2-photon polymerization or even as a bio-ink by combining the PEG-based materials with Laponite. When used as a bio-ink, cells will be encapsulated in the material prior to printing. Therefore, it is relevant to evaluate the capability of the materials to encapsulate cells. These experiments are currently ongoing in a collaboration with the University of New South Wales (Sydney, Australia) .

Regarding the indirect solid freeform fabrication approach, another advantage of the technique is that constructs which combine zones of different materials can be used.

For example, a scaffold could be created which is partially cell-interactive by combining the polymer with Laponite and partially non-cell-interactive by using the material as such. Alternatively, different prepolymers can be selected to create zones with different mechanical properties. Another relevant aspect would be the assessment of the technique to be used to create scaffolds with a more complex shape, although the dimensions of the construct might be limited by the limited penetration depth of UV-light.

In the field of tissue engineering, a fascinating application can be meniscus engineering, as the mechanical properties of meniscus scaffolds are highly important. In addition, to replace a meniscus, the scaffold needs to mimic the two zones of the meniscus, the outer red zone (vascular) and the inner white zone (avascular). With the solid state reactive materials, one of the main advantages is that they are highly tunable by either varying the different prepolymer building blocks, or by changing the water content prior to cross-linking. Furthermore, due to their ease of processing, the implants can be tailor made for each patient, by printing a scaffold from a CAD-model based on scans of the initial defect. In addition, by changing the building blocks of the polymers, the properties of the vascular and avascular zone can be represented in the scaffold. Therefore, these materials are ideal candidates for meniscal tissue engineering.

Another potential application involves coatings. The molten polymer can be applied as a coating using spraycoating, spincoating or dipcoating. As the coating can be crosslinked after solidification, the coating and crosslinking can be performed in two different steps, after solidification of the coated layer. For some coating-related applications, cell and protein adhesion is not desired, e.g. stents (blood contact area). It was demonstrated that no cell adhesion occurs on the PEG-based materials after crosslinking in the solid state. Therefore, these materials are ideal candidates for this type of applications. Furthermore, after the coating has been applied, selected zones can be crosslinked by applying masks prior to UV crosslinking. As a result, a patterned coating of the surface can be achieved, which can be interesting for applications that require regions where cell or protein adhesion is required, in combination with areas where this is unwanted.

Nederlandstalige Samenvatting
Summary in Dutch

Om het tekort aan donoren te bestrijden voor gevallen waar orgaantransplantatie nodig is, en om gangbare problemen met protheses en getransplanteerde organen te voorkomen (bvb. verschil in mechanische eigenschappen of afmetingen, infecties, afstoting, …)[1–3] is gedurende de laatste decennia weefselregeneratie een steeds populairdere tak geworden in het biomedische onderzoeksdomein. [4] Weefselregeneratie heeft als doel om biologische substituanten te ontwikkelen die weefselfunctie herstellen, onderhouden of verbeteren.[2] In dit verband zijn hydrogels een belangrijke materiaalcategorie, omdat hun eigenschappen (zacht, elastisch gedrag, netwerkstructuur en een hoog watergehalte) sterk lijken op die van de extracellulaire matrix. [5–8]

Hydrogels kunnen worden gedefinieerd als gezwollen, drie dimensionele netwerken. Afhankelijk van hun samenstelling kunnen ze tot duizenden keren hun oorspronkelijk droog gewicht aan water opnemen. De aard van het netwerk kan zowel fysisch als chemisch zijn. Fysische vernetting is reversibel en kan tot stand komen door middel van microkristallijne zones, ionische bindingen, waterstofbruggen, van der Waals interacties of combinaties van deze interacties. Chemische vernetting anderzijds wordt gecreëerd door het vormen van covalente bindingen. Hydrogels kunnen zowel van natuurlijke oorsprong zijn (bvb gelatine methacrylamide)[9] of van synthetische oorsprong (bvb poly(ethyleen glycol) diacrylaat)[10].

Voor weefselregeneratie is het belangrijk dat er een 3D cultuuromgeving wordt ontwikkeld die de cellen ondersteunt op vlak van biomechanica en biologische eigenschappen om zo implantaten te ontwikkelen met behulp van cellen van het beschadigde weefsel.[11–17] Om dit te bereiken worden de cellen gecombineerd met zogenaamde "scaffolds" of draagstructuren. Bij het ontwikkelen van deze scaffolds is het belangrijk dat deze gebaseerd zijn op niet toxische materialen en voldoende poreus zijn. Zo krijgt het gevormde weefsel voldoende ruimte om te groeien, en is een continue aan- en afvoer van voedingsstoffen, zuurstof en metabolische producten mogelijk.[18]

Een populaire techniek om deze scaffolds te ontwikkelen is 3D printen. Met deze techniek worden structuren gecreëerd door de sequentiële toevoer van energie en/of materiaal volgens een computer gestuurd ontwerp ('computer-aided design', CAD).[7] Met deze techniek kan op een reproduceerbare en homogene manier een scaffold ontwikkeld worden met een hoge mate van controle over de macro- en microstructuur. [19–22] Het belangrijkste nadeel van deze techniek is dat slechts een beperkte selectie aan materialen compatibel is met een gekozen 3D-print techniek. Vooral wat betreft hydrogels zijn deze vaak moeilijk te verwerken met 3D-print technieken.[7]

Een gangbare techniek om covalent gebonden hydrogels te creëren is fotopolymerizatie.[23] Hierbij wordt een foto-initiator gebruikt, die radicalen genereert bij blootstelling aan UV-licht. Deze radicalen reageren dan met functionele groepen die aanwezig zijn op het polymeer (bvb acrylaten) om zo een netwerk te vormen. Het belangrijkste nadeel van deze techniek is de functionele groepen voldoende mobiel moeten zijn, daarom wordt de reactie steeds uitgevoerd in vloeibare toestand. Daarom is deze methode incompatibel met een groot deel van de verwerkingstechnieken (bvb 3D printen of electrospinnen), aangezien de gecreëerde structuren na verwerking in de vaste toestand zijn.[7,24–27]

In dit werk werd daarom een nieuw materiaal ontwikkeld dat nog steeds kan vernet worden met UV-licht in de vaste, semi-kristallijne toestand. Dit materiaal werd ontwikkeld door een semi-kristallijn, hydrofiel polymeer te linken met acrylaat eindgroepen, waartussen een kort, flexibel oligomeer werd geplaatst. Wanneer dit materiaal kristalliseert, zal er een fasescheiding optreden tussen de eindgroep en het semi-kristallijne polymeer. Hierdoor komen de acrylaten in een gescheiden zone terecht, en het oligomeer tussenstuk geeft de acrylaten nog net voldoende mobiliteit om te reageren met elkaar. Dit tussenstuk speelt dus een belangrijke rol, die werd onderzocht door een serie polymeren te synthetiseren met verschillende tussenstukken: 6 ethyleen oxide eenheden (PEG$_{2000}$-OEOAcr), 6 propyleen oxide eenheden (PEG$_{2000}$-OPOAcr), 2 ε-caprolacton eenheden (PEG$_{2000}$-OClAcr) en tenslotte ook een polymeer met een zeer kort tussenstuk van slechts 1 ethyleen oxide eenheid (PEG$_{2000}$-HEAcr).

De verschillende polymeren werden gekarakteriseerd met behulp van foto-differentiële scanning calorimetrie (DSC) metingen. Daaruit bleek dat de polymerisatie ook efficiënt kon worden uitgevoerd wanneer geen foto-initiator werd toegevoegd. Zo kunnen dus

eventuele toxische effecten van de foto-initiator worden vermeden, dienen er geen extra mengstappen uitgevoerd te worden, en moet er geen foto-initiator gezocht worden die compatibel is met de geselecteerde verwerkingstechniek. [28–30] Uit de foto-DSC metingen bleek dat het referentiepolymeer PEG_{2000}-OEOAcr zelfs 2.5 keer sneller reageerde in de vaste toestand (20°C) dan in de gesmolten toestand (50°C). Verder bleek uit de metingen ook dat een flexibel tussenstuk een positief effect heeft op de reactiviteit in vaste toestand. Dit was het geval voor PEG_{2000}-OEOAcr en PEG_{2000}-OClAcr, die beiden erg flexibel zijn (met een karakteristieke ratio van ongeveer 4). Een kort of niet flexibel tussenstuk, zoals bij PEG_{2000}-HEAcr en PEG_{2000}-OPOAcr leidt tot een verlaagde reactiviteit in vaste toestand.

Door zijn hoge reactiviteit in vaste toestand, kon PEG_{2000}-OEOAcr verwerkt worden met verschillende technieken. Een eerste techniek was extrusie-gebaseerd 3D printen, wat tot op heden enkel werd gebruikt voor thermo responsieve polymeren of waarbij additieven werden toegevoegd om dilatatie te creëren.[5,31] Voor deze techniek werd het polymeer eerst verwarmd tot boven zijn smeltpunt, en door afkoeling onmiddellijk na het printen werden vaste structuren gecreëerd. Deze konden vervolgens na het printen met UV licht vernet worden. Deze scaffolds werden ook gebruikt voor de cultuur van cellen (osteoblasten van een muis, en menselijke stamcellen afgeleid van vetweefsel). Aangezien het materiaal zelf niet cel-interactief is, werd een coating van gelatine gemodificeerd met methacrylamide zijgroepen aangebracht op de scaffolds. Uit de celtesten bleek dat voor de materialen met coating de cellen uitstekend vasthechten aan het materiaal, en een hoge viabiliteit behielden gedurende het experiment (23 dagen). Zonder de coating echter werd geen cel adhesie geobserveerd.

Een tweede verwerkingstechniek die werd toegepast was electrospinnen. Met deze techniek worden micro- en nanovezels gecreëerd door een hoog potentiaalverschil aan te leggen tussen een naald waardoor een polymeeroplossing wordt gepompt, en een collecteerplaat. Hierdoor wordt de druppel polymeeroplossing geladen, en ontsnapt een vloeistofstraal aan de druppel. Deze vloeistofstraal zal vervolgens naar de collectorplaat worden getrokken, waarbij het solvent verdampt. Op deze manier wordt een mat van vaste vezels gevormd op de collecteerplaat. Door de reactiviteit in vaste toestand, konden de vezels na het electrospinnen nog steeds vernet worden. Om een zo hoog mogelijke vernettingsgraad van de dunne vezels (7.70 ± 1.38 μm

voor zwellen in water, en 10.16 ± 1.30 µm na zwellen in water) te verkrijgen, was het noodzakelijk een foto-initiator toe te voegen (2 mol% Irgacure 2959).

Een laatste techniek die werd toegepast is 2-foton-polymerizatie (2FP). Hierbij wordt een laserstraal doorheen een foto-reactief materiaal gescand waarbij lokaal de foto-polymerisatie wordt geïnitieerd. Zo kunnen structuren worden gecreëerd met een sub-micrometer resolutie.[32] Deze techniek werd voor hydrogels nog nooit toegepast in vaste toestand. Verder is het ook moeilijk om een foto-initiator te vinden die absorbeert bij de exacte golflengte van de laser, maar toch nog steeds biocompatibel is.[33,34] Dit is geen probleem meer voor de materialen ontwikkeld in dit werk, die konden verwerkt worden met 2FP in de vaste toestand en zonder foto-initiator. Dit werd geïllustreerd door een 3D model van het atomium te printen, met een afmeting van slechts 100 µm.

Vervolgens werden de kinetische aspecten van de ontwikkelde polymeren verder gekarakteriseerd met behulp van foto-DSC experimenten. Hieruit bleek dat de auto-initiatie mogelijk is door het ontstaan van radicalen op de acrylaat groepen tijdens UV belichting. Door de acrylaten met de verschillende eindgroepen (die eerder beschreven werden) te analyseren met UV-spectrofotometrie, bleek dat de geabsorbeerde .golflengte sterk afhankelijk is van de chemische omgeving van de acrylaten. Afhankelijk van de structuur, kan deze verschuiven naar de UVA-golflengtes, waardoor de auto initiatie mogelijk wordt. Dit proces wordt efficiënter wanneer het polymeer zich in vaste toestand bevindt, en de π- π* orbitalen van de acrylaten beter kunnen overlappen. Zonder foto-initiator, daalt de maximale vrijgekomen warmte bij fotopolymerisatie van 7.2 W g^{-1} naar 3.4 W g^{-1} bij overgang van vaste naar gesmolten toestand. Verder werd ook aangetoond dat de polymerisatiesnelheid in vaste toestand zal toenemen met toenemende temperatuur, maar constant blijft boven het smeltpunt.

De veelzijdigheid van de in dit doctoraatswerk ontwikkelde materialen werd aangetoond door polymeren te synthetiseren met een verschillend type centraal polymeer (poly(ε-caprolacton of PCL)) of een verschillend moleculair gewicht van het centrale polymeer (PEG2000 – 20 000 g mol^{-1}). Al deze polymeren konden efficiënt gepolymeriseerd worden in de vaste toestand. Verder werd ook aangetoond dat de mechanische eigenschappen en zwellingsgraad van de polymeren konden beïnvloed worden door het moleculaire gewicht van het centrale polymeer te wijzigen. De zwellingsgraad bijvoorbeeld nam toe van 1.3 tot 16.3 voor een toename van moleculair

gewicht van 2000 naar 20 000 g mol^{-1}. Dit kon ook worden bereikt door de hoeveelheid water toegevoegd voor fotopolymerisatie te variëren. Als deze hoeveelheid verhoogt, zal ook de zwellingsgraad verhogen. Voor de polymeren met moleculair gewicht van het centrale polymeer van 2000 g mol^{-1} was de zwellingsgraad 8.18 voor een 10% concentratie, en 1.47 voor een 100% concentratie.

In een volgend hoofdstuk werd een scafffold productiemethode ontwikkeld die toepasbaar is op materialen die moeilijk rechtstreeks te verwerken zijn met behulp van 3D-printen. Alhoewel dit mogelijk is voor het polymeer vanuit de smelt, lukt dit niet voor waterige oplossingen van het polymeer. De ontwikkelde methode maakt gebruik van indirect 3D-printen: een materiaal dat gemakkelijk kan geprint worden (e.g. PCL) wordt gebruikt om een initiële templaat te maken. Deze templaat wordt dan gevuld met de polymeeroplossing die vervolgens vernet wordt. Ten slotte wordt de PCL templaat opgelost in chloroform, waardoor de scaffold in het uiteindelijke materiaal overblijft. Door de concentratie van het polymeer te variëren, konden de reologische eigenschappen gewijzigd worden: de opslagmodulus stijgt van 10.6 kPa tot 1410 kPa voor een concentratietoename van 10 – 90 m%. De zwellingsgraad zal dalen als de concentratie verhoogt, van 7.16 naar 1.3 keer het oorspronkelijke droge gewicht. De Young's modulus zal dan weer toenemen als de concentratie stijgt, van 0.67 naar 3.1 MPa.

Met de indirecte aanpak konden op een efficiënte manier 3D scaffolds gecreëerd worden vertrekkende van precursoroplossingen met verschillende concentraties. Door de printinstellingen voor het printen van de PCL templaat te variëren (extrusiesnelheid, temperatuur, poriegrootte), konden ook de eigenschappen van de finale scaffold beïnvloed worden. Zowel de morfologie als de mechanische eigenschappen werden hierdoor beïnvloed, wat gekarakteriseerd werd door middel van optische microscopie en texturometrie. Vervolgens kon met behulp van μ-CT metingen aangetoond worden dat ook binnenin de scaffold een geconnecteerd poreus netwerk aanwezig was. Ten slotte toonde de biologische evaluatie aan dat de cel adhesie en proliferatie op de scaffold sterk kon verbeterd worden door een gelatine methacrylamide coating aan te brengen.

In het laatste hoofdstuk ten slotte werd een inkt ontwikkeld voor 3D printen door het ontwikkelde polymeer te combineren met een additief bestaande uit een silicaat nanokristal (Laponiet). Het voordeel van dit additief is dat het thixotroop gedrag van de

dispersie veroorzaakt, waarbij de viscositeit hoog is bij lage afschuifsnelheid, en laag bij hoge afschuifsnelheid. Dit is ideaal voor 3D-printen: het materiaal kan gemakkelijk uit de naald vloeien, maar zal zijn vorm behouden eens geprint. Daarnaast zorgt het additief er ook voor dat cellen goed adheren, waardoor een gelatine methacrylamide coating niet langer noodzakelijk is.

Na optimalisatie werd een polymeerconcentratie van 50 m% gecombineerd met een Laponiet concentratie van 3 m%. Voor deze oplossing werd met behulp van reologiemetingen een thixotroop gedrag waargenomen waarbij de viscositeit daalde van 24.0 Pa s bij een afschuifsnelheid van 0.3 s^{-1} tot 0.2 Pa s voor een afschuifsnelheid van 100 s^{-1}. Ook de mechanische eigenschappen van deze inkt waren goed: na fotopolymerizatie werd een Young's modulus van 1.9 MPa bekomen. Verder werd met behulp van celcultuur op 2D en 3D scaffolds aangetoond dat het Laponiet inderdaad de celviabiliteit ten goede komt. Een volgende stap is het printen van deze inkt waarbij cellen reeds tijdens het printen worden toegevoegd, en zo dus ingekapseld kunnen worden in de scaffold. Zo kan uiteindelijk de (autologe) celinhoud gemaximaliseerd worden om patient-speciefieke scaffolds te creëren voor weefselregeneratie.

Overige toekomstperspectieven voor dit werk zijn onder meer de effectiviteit van de reactiviteit in vaste toestand verder opzoeken, door de bouwstenen verder te variëren, bvb door poly(lactides) of pluronics te gebruiken als centraal polymeer, of door het moleculair gewicht van het centraal polymeer verder te laten toenemen. Zo kan de limiet gevonden worden tot waar het materiaal nog steeds reactief is in de vaste toestand. Ook naar verwerking toe zijn er verschillende mogelijkheden voor de materialen. Allereerst zijn het natuurlijk ideale grondstoffen voor 3D-printers: zowel voor extrusie-gebaseerde printers (in de vaste toestand), als in oplossing (met Laponiet) of voor 2-foton polymerisatie. Deze 3D-print technieken kunnen worden gebruikt voor het creëren van scaffolds voor weefselregeneratie, bijvoorbeeld voor het creëren van een meniscus implantaat dat specifiek op maat van de patiënt wordt gemaakt. Met behulp van de indirecte methode kunnen ook scaffolds gemaakt worden die bestaan uit verschillende zones met verschillende materialen, om zo het autologe weefsel zo goed mogelijk na te bootsen. Ook kan het creëren van meer complexe vormen met deze techniek worden geëvalueerd.

Referenties

1. Rayes, N. *et al.* Causes of death after liver transplantation: an analysis of 41 cases in 382 patients. *Zentralbl. Chir.* **120,** 435–438 (1995).

2. Langer, R. & Vacanti, J. P. Tissue Engineering. *Science (80-.).* **260,** (1993).

3. Lanza, R., Langer, R. & Vacanti, J. P. *Principles of Tissue Engineering.* (Academic Press, 2013).

4. Vacanti, J. P. & Langer, R. Tissue engineering: the design and fabrication of living replacement devices for surgical reconstruction and transplantation. *Lancet* **354,** SI32-I34 (1999).

5. Hong, S. *et al.* 3D Printing of Highly Stretchable and Tough Hydrogels into Complex, Cellularized Structures. *Adv. Mater.* **27,** n/a-n/a (2015).

6. Bigi, A., Panzavolta, S. & Rubini, K. Relationship between triple-helix content and mechanical properties of gelatin films. *Biomaterials* **25,** 5675–5680 (2004).

7. Billiet, T. *et al.* A review of trends and limitations in hydrogel-rapid prototyping for tissue engineering. *Biomaterials* **33,** 6020–6041 (2012).

8. Zohuriaan-mehr, M. J. & Kabiri, K. Superabsorbent Polymer Materials: A review. *Iran. Polym. J.* **17,** 451–477 (2008).

9. Van Den Bulcke, A. I. *et al.* Structural and Rheological Properties of Methacrylamide Modified Gelatin Hydrogels. *Biomacromolecules* **1,** 31–38 (2000).

10. Cruise, G. M., Scharp, D. S. & Hubbell, J. A. Characterization of permeability and network structure of interfacially photopolymerized poly(ethylene glycol) diacrylate hydrogels. *Biomaterials* **19,** 1287–94 (1998).

11. Landers, R. *et al.* Fabrication of soft tissue engineering scaffolds by means of rapid prototyping techniques. *journals Mater. Sci.* **37,** 3107–3116 (2002).

12. Graulus, G.-J. J. *et al.* Cross-linkable alginate-graft-gelatin copolymers for tissue engineering applications. *Eur. Polym. J.* **72,** 494–506 (2015).

13. Ovsianikov, A., Ostendorf, A. & Chichkov, B. N. Three-dimensional photofabrication with femtosecond lasers for applications in photonics and biomedicine. *Appl. Surf. Sci.* **253,** 6599–6602 (2007).

14. Melchels, F. P. W., Feijen, J. & Grijpma, D. W. A review on stereolithography and its applications in biomedical engineering. *Biomaterials* **31,** 6121–6130 (2010).

15. Ovsianikov, A. *et al.* Laser Fabrication of Three-Dimensional CAD Scaffolds from Photosensitive Gelatin for Applications in Tissue Engineering. *Biomacromolecules* **12,** 851–858 (2011).

16. Ovsianikov, A. *et al.* Laser Fabrication of 3D Gelatin Scaffolds for the Generation of Bioartificial Tissues. *Materials (Basel).* **4,** 288–299 (2011).

17. Woodfield, T. B. F. *et al.* Design of porous scaffolds for cartilage tissue engineering using a three-dimensional fiber-deposition technique. *Biomaterials* **25,** 4149–61 (2004).

18. Liu, C. Z., Sachlos, E., Wahl, D. A., Han, Z. W. & Czernuszka, J. T. On the manufacturability of scaffold mould using a 3D printing technology. *Rapid Prototyp. J.* **13,** 163–174 (2007).

19. Chu, T.-M. G. M. G., Halloran, J. W., Hollister, S. J. & Feinberg, S. E. Hydroxyapatite implants with designed internal architecture. *J. Mater. Sci. Mater. Med.* **12,** 471–478 (2001).

20. Tan, J. Y., Chua, C. K. & Leong, K. F. Fabrication of channeled scaffolds with ordered array of micro-pores through microsphere leaching and indirect Rapid Prototyping technique. 83–96 (2013). doi:10.1007/s10544-012-9690-3

21. Chia, H. N. & Wu, B. M. Recent advances in 3D printing of biomaterials. *J. Biol. Eng.* **9,** 4 (2015).

22. Manjubala, I. *et al.* Biomimetic mineral-organic composite scaffolds with controlled internal architecture. *J. Mater. Sci. Mater. Med.* **16,** 1111–9 (2005).

23. Fisher, J. P., Dean, D., Engel, P. S. & Mikos, A. G. Photoinitiated Polymerization of Biomaterials. *Annu. Rev. Mater. Res.* **31,** 171–181 (2001).

24. Hutmacher, D. W. Biomaterials offer cancer research the third dimension. *Nat. Mater.* **9,** 90–93 (2010).

25. Hollister, S. J. Porous scaffold design for tissue engineering. *Nat. Mater.* **4,**

518–24 (2005).

26. Houben, A. *et al.* Indirect Rapid Prototyping: Opening Up Unprecedented Opportunities in Scaffold Design and Applications. *Ann. Biomed. Eng.* **45,** 1–26 (2016).

27. Van Hoorick, J. *et al.* Indirect additive manufacturing as an elegant tool for the production of self-supporting low density gelatin scaffolds. *J. Mater. Sci. Mater. Med.* **26,** 247 (2015).

28. Bryant, S. J., Nuttelman, C. R. & Anseth, K. S. Cytocompatibility of UV and visible light photoinitiating systems on cultured NIH/3T3 fibroblasts in vitro. *J. Biomater. Sci. Polym. Ed.* **11,** 439–57 (2000).

29. Li, Z. *et al.* Initiation efficiency and cytotoxicity of novel water-soluble two-photon photoinitiators for direct 3D microfabrication of hydrogels. *RSC Adv.* **3,** 15939 (2013).

30. Ovsianikov, A. *et al.* Laser photofabrication of cell-containing hydrogel constructs. *Langmuir* **30,** 3787–3794 (2014).

31. Billiet, T., Gevaert, E., De Schryver, T., Cornelissen, M. & Dubruel, P. The 3D printing of gelatin methacrylamide cell-laden tissue-engineered constructs with high cell viability. *Biomaterials* **35,** 49–62 (2014).

32. Ovsianikov, A., Mironov, V., Stampf, J. & Liska, R. Engineering 3D cell-culture matrices: multiphoton processing technologies for biological and tissue engineering applications. *Expert Rev. Med. Devices* **9,** 613–33 (2012).

33. Qin, X.-H., Ovsianikov, A., Stampfl, J. & Liska, R. Additive manufacturing of photosensitive hydrogels for tissue engineering applications. *BioNanoMaterials* **15,** 49–70 (2014).

34. Torgersen, J. *et al.* Hydrogels for two-photon polymerization: A toolbox for mimicking the extracellular matrix. *Adv. Funct. Mater.* **23,** 4542–4554 (2013).

List of Abbreviations

ECM	extra-cellular matrix
SFF	solid freeform Fabrication
2D	two dimensional
2PP	two photon polymerization
3D	three dimensional
3DP	three dimensional printing
µm	micrometer
AJS	air jet solidification
AM	additive manufacturing
BMP	bone-morphogenic proteins
CAD	computer aided design
CAM	computer aided manufacturing
DDP	drop on demand printing
DLP	digital light projection
CPD	critical point drying
CT	computed tomography
DMD	digital micromirror device
ECM	extra cellular matrix
eiRP	external indirect rapid prototyping
FDM	fused deposition modelling
HA	hydroxyapatite
h-MSC	humane mesenchymal stem cells
HFF	human foreskin fibroblasts
IJP	ink-jet printing
iiRP	internal indirect rapid prototyping
iRP	indirect rapid prototyping
LoC	lab on a chip
MC3T3	Mouse osteoblasts

MEW	melt electrospinning writing
mPa	millipascal
MPa	megapascal
MRI	magnetic resonance imaging
MSTL	micro stereolithography
PCL	poly-(ε-caprolactone)
PDL	periodontal ligament
PDMS	poly(dimethylsiloxane)
PEG	poly-(ethylene glycol)
PGA	poly-(glycolic acid)
PLA	poly-(lactic acid)
PLGA	poly-(lactic-co-glycolic acid)
PPF	poly-(propylene fumarate)
RP	rapid prototyping
SFF	solid freeform fabrication
SLA	stereolithography
SLS	selective laser sintering
SMD	selective mould dissolution
TCP	tricalcium phosphate
UV	ultra violet
HUVECs	human umbilical vein endothelial cells
LCST	lower critical solution temperature
UCST	upper critical solution temperature

List of Materials

Below, an overview of the materials developed in this work is provided. The first material is the reference material, used in the majority of characterization and processing experiments. Adaptations made to this material are indicated in bold in the table below.

Name	Backbone (g mol^{-1})	Diisocyanate	Spacer	End group
PEG$_{2000}$-OEOAcr	PEG 2000	IPDI	Oligo(ethylene oxide)	Acrylate
PEG$_{4000}$-OEOAcr	PEG **4000**	IPDI	Oligo(ethylene oxide)	Acrylate
PEG$_{8000}$-OEOAcr	PEG **8000**	IPDI	Oligo(ethylene oxide)	Acrylate
PEG$_{10000}$-OEOAcr	PEG **10000**	IPDI	Oligo(ethylene oxide)	Acrylate
PEG$_{20000}$-OEOAcr	PEG **20000**	IPDI	Oligo(ethylene oxide)	Acrylate
PEG$_{2000}$-OPOAcr	PEG 2000	IPDI	**Oligo(propylene oxide)**	Acrylate
PEG$_{2000}$-OClAcr	PEG 2000	IPDI	**Oligo(ε-caprolactone)**	Acrylate
PEG$_{2000}$-HEAcr	PEG 2000	IPDI	**Hydroxyethyl**	Acrylate
PEG$_{2000}$-OEOMAcr	PEG 2000	IPDI	Oligo(ethylene oxide)	**Methacrylate**
PCL$_{2200}$-OEOAcr	**PCL 2200**	IPDI	Oligo(ethylene oxide)	Acrylate

Annemie Houben

PROFILE

- Master in Chemistry
- Date of birth: 04/04/1989
- Belgian nationality
- Languages: Dutch (Native language), English, French

EDUCATION

Ghent University   Gent, Belgium

Master of Science in Chemistry (Great distinction)   2013

Major: Molecular and Macromolecular design

Minor: Industry and Management

Ghent University   Gent, Belgium

Bachelor of Science in Chemistry   2011

Major: Research

EXPERIENCE

Phd with Industrial Partner   Gent, Belgium

Polymer chemistry and biomaterials (Gent University)   2013 – 2017

Allnex R&D (Drogenbos)

- International mobility: Uppsala University (Sweden) in 2016, UNSW (Australia) in 2016
- ConcepTT project (2016): funding for support and valorization of the patent
  (in collaboration with UGent Business Developer)
- Supervision of 2 master students, 2 erasmus students and a scientific co-worker.

Intern at Inspectorate   Antwerp, Belgium

Project: Introducing Lean in the lab   2012

PUBLICATIONS

Houben, A., H. Van Den Bergen, P. Roose, D. Bontinck, S. Van Vlierberghe, P. Dubruel, "Novel urethane based materials, derivatives, methods of their preparation and uses." Patent 2015 (EP15175956, Pending, 1st search report received)

Houben, A., J. Van Hoorick, J. Van Erps, H. Thienpont, S. Van Vlierberghe, and P. Dubruel. Indirect Rapid Prototyping: Opening Up Unprecedented Opportunities in Scaffold Design and Applications. Ann. Biomed. Eng. 1–26, 2016

Houben, A., N. Pien, X. Lu, F. Bisi, M. N. Boone, Van Hoorick, J., P. Roose, D. Van den Bergen, Hugues Bontinck, T. Bowden, P. Dubruel, and S. Van Vlierberghe. Indirect Solid Freeform Fabrication of an Initiator-free Photocrosslinkable Hydrogel Precursor for the Creation of Porous Scaffolds. Maromolecular Biosci. (16, 1883–1894 (2016)

Houben, A., P. Roose, H. Van den Bergen, H. Declercq, J. Van Hoorick, P. Gruber, A. Ovsianikov, D. Bontinck, S. Van Vlierberghe, P. Dubruel. Flexible Oligomer Spacers as the Key to Solid-State Photopolymerization of Hydrogel Precursors. Mater. Today Chem. 4, 84–89 (2017)

Houben, A., P. Roose, H. Van den Bergen, D. Bontinck, H. Declercq, S. Van Vlierberghe, P. Dubruel. Development of a Synthetic Composite Hydrogel Ink for Solid Freeform Fabrication.. (in preparation)

Van Hoorick, J., H. Declercq, A. De Muynck, A. Houben, L. Van Hoorebeke, R. Cornelissen, J. Van Erps, H. Thienpont, P. Dubruel, and S. Van Vlierberghe. Indirect additive manufacturing as an elegant tool for the production of self-supporting low density gelatin scaffolds. J. Mater. Sci. Mater. Med. 26:247, 2015.

Cama, G., D. Mogusanu, A. Houben, P. Dubruel. Synthetic biodegradable medical polyesters: Polycaprolactone. Science and principles of biodegradable and bioresorbable medical polymers: Materials and properties, Elsevier (2016)

GEO®
SPECIALTY CHEMICALS

SAFETY DATA SHEET

Revision date 2017-01-04   **Revision number** 1.05

1. IDENTIFICATION OF THE SUBSTANCE/MIXTURE AND OF THE COMPANY/UNDERTAKING

1.1 Product identifier

Product name	BISOMER® PPA 6
Product code	745786
Synonyms	Polypropylene glycol monoacrylate

1.2 Relevant identified uses of the substance or mixture and uses advised against

Recommended use [RU]	Monomer for special polymers Cross-linking agent
Uses advised against	None known

1.3 Details of the supplier of the safety data sheet

Supplier
GEO Specialty Chemicals UK Ltd
Charleston Road, Hardley, Hythe
Southampton, Hampshire SO45 3ZG
United Kingdom
Phone: +44 (0)23 80894666
Fax No: +44 (0)23 80243113

Responsibility Statement   For further information, please contact **safety-data-sheet-fp@geosc.com**

1.4 Emergency telephone number

Emergency telephone   24 Hour Emergency Phone Number
GEO Specialty Chemicals UK Ltd
+44 (0)23 80891806

2. HAZARDS IDENTIFICATION

2.1 Classification of the substance or mixture

Classification according to Regulation (EC) No. 1272/2008 [CLP]

Skin sensitization	Category 1
Acute aquatic toxicity	Category 2
Chronic aquatic toxicity	Category 2

2.2 Label elements

Labeling according to Regulation (EC) No. 1272/2008 [CLP]

_____

Signal word WARNING

Hazard statements
H317 - May cause an allergic skin reaction
H411 - Toxic to aquatic life with long lasting effects

Precautionary statements
P262 - Do not get in eyes, on skin, or on clothing
P280 - Wear protective gloves
P302 + P352 - IF ON SKIN: Wash with plenty of soap and water
P273 - Avoid release to the environment

Hazard components for labeling Polypropylene glycol monoacrylate.

2.3 Other Information

None known

3. COMPOSITION/INFORMATION ON INGREDIENTS

3.1 Substances

Component	EU EINECS	weight-%	Classification according to Regulation (EC) No. 1272/2008 [CLP]	(REACh) Regulation (EC 1907/2006)
Polypropylene glycol monoacrylate 50858-51-0	Not applicable	>= 70%	Skin Sens. 1 (H317) Aquatic Chronic 2 (H411)	In compliance
2-Hydroxypropyl acrylate 25584-83-2	247-118-0	< 5%	Acute Tox. 3 (H301) Acute Tox. 3 (H311) Acute Tox. 3 (H331) Skin Corr. 1B (H314) Skin Sens. 1 (H317)	In compliance

For the full text of the H-Statements mentioned in this Section, see Section 16.

3.2 Mixtures

Not applicable

4. FIRST AID MEASURES

4.1 Description of first aid measures

General advice
In case of adverse health effects seek medical advice.

Eye contact
Remove contact lenses, if worn. Immediately flush with plenty of water for at least 10 minutes, holding eyelids apart to ensure flushing of the entire surface. Seek medical advice immediately.

Skin contact
Immediately wash thoroughly with soap and water, remove contaminated clothing and footwear. Wash clothing before reuse. Get medical attention if irritation should develop.

_____

_____

Ingestion
If swallowed, give 1-2 glasses of water, but do not induce vomiting. Do not give anything by mouth to an unconscious or convulsing person. Get medical attention. If vomiting should occur spontaneously, keep airway clear.

Inhalation
Remove to fresh air. If not breathing, give artificial respiration. If breathing is difficult, give oxygen. Get medical attention.

4.2 Most important symptoms and effects, both acute and delayed

Most important symptoms and effects
No information available.

Chronic effects
Repeated or prolonged exposure may result in liver or kidney damage.

4.3 Indication of any immediate medical attention and special treatment needed

Note to physicians
Treat symptomatically.

5. FIRE-FIGHTING MEASURES

5.1 Extinguishing media

Suitable extinguishing media
Water spray jet, Alcohol-resistant foam, Extinguishing powder, Carbon dioxide.

Extinguishing media which must not be used for safety reasons
High pressure waterjet.

5.2 Special hazards arising from the substance or mixture

Special Hazard
Formation of toxic gases is possible during heating or in fires. The product may undergo spontaneous polymerization at high temperatures. Polymerization is exothermic and may cause damage to the container and/or release of thermal decomposition products.

5.3 Advice for firefighters

Special protective equipment for firefighters
Firefighters should wear self-contained breathing apparatus and full firefighting turnout gear.

Firefighting measures
Cool exposed containers with water spray after extinguishing fire.

6. ACCIDENTAL RELEASE MEASURES

6.1 Personal precautions, protective equipment and emergency procedures

Personal precautions
Wear suitable protective clothing and gloves.

6.2 Environmental precautions

Environmental precautions
Do not empty into drains/surface water/ground water. Inform authorities in the event of product spillage to water courses or sewage systems.

6.3 Methods and material for containment and cleaning up

_____

_____

Methods for cleaning up
Remove with liquid-absorbing material (sand, peat, sawdust). Dispose of contaminated material as waste according to Section 13.

6.4 Reference to other sections

See Section 12 for additional Ecological Information

7. HANDLING AND STORAGE

7.1 Precautions for safe handling

Advice on safe handling
Avoid contact with eyes, skin and clothing
Avoid breathing vapor or mist
Use only in well-ventilated areas
Personal protective equipment comprising: suitable protective gloves, safety goggles and protective clothing.
Wash thoroughly after handling
Ensure that eyewash stations and safety showers are close to the workstation location

7.2 Conditions for safe storage, including any incompatibilities

Technical measures and storage conditions
The product is stabilized against spontaneous polymerization before delivery. However, if the permissible storage time or storage temperature are greatly exceeded the product may polymerize.
Keep only in the original container in a cool, well-ventilated place
Store at temperatures not exceeding 25 °C/ 77 °F
Store in a dry place
Store away from direct heat or sunlight.
Tanks should preferably contain no dead spaces where the product can be trapped and polymerize. Internal structural members should therefore be kept to a minimum and tanks should be welded.
Storage tank vents, especially those fitted with flame arrestors, should be inspected regularly for polymer fouling which can arise from vapor phase polymerization.
Do not store together with reductants.
Do not store together with oxidants.

7.3 Specific end use(s)

Specific use(s)
 Not applicable

8. EXPOSURE CONTROLS/PERSONAL PROTECTION

8.1 Control parameters

Occupational exposure limit value

Component	European Union	United Kingdom	Spain	Germany	Turkey
2-Hydroxypropyl acrylate 25584-83-2	NAV	NAV	NAV	NAV	NAV

Component	Austria	Belgium	Switzerland	Poland
2-Hydroxypropyl acrylate 25584-83-2	NAV	NAV	NAV	TWA: 2.8 mg/m^3 Skin STEL: 6 mg/m^3

Biological limit values

Component	European Union	United Kingdom	Spain	Germany	Turkey
2-Hydroxypropyl acrylate 25584-83-2	NAV	NAV	NAV	NAV	NAV

_____

_____

<u>**Legend**</u>
NAV - Not available

8.2 Exposure controls

Personal Protective Equipment

Eye/face Protection
If splashes are likely to occur: Chemical Goggles.

Hand Protection
Polychloroprene gloves. Coating thickness 1.1 mm. Level 5 > 240 min breakthrough time.

Skin and body protection
Wear suitable protective clothing.

Respiratory protection
Filter A2 is recommended in cases of prolonged exposure.

Other personal protection data
Eyewash fountains and safety showers must be easily accessible.

Hygiene measures
Handle in accordance with good industrial hygiene and safety practice.

Environmental exposure controls
No information available.

9. PHYSICAL AND CHEMICAL PROPERTIES

9.1 Information on basic physical and chemical properties

Physical state	liquid
Color	colorless
Appearance	clear
Odor	characteristic
Odor threshold	No information available

Property	Values	Remarks
pH	No information available	No information available
Melting / freezing point	No information available	No information available
Boiling point / boiling range	No information available	No information available
Flash point	128 °C / 262.4 °F	PMC D93A
Evaporation rate	No information available	No information available
Flammability (solid, gas)	No information available	No information available
Flammability Limit in Air		
Upper flammability limit	No information available	No information available
Lower flammability limit	No information available	No information available
Vapor pressure	No information available	No information available
Vapor density	No information available	No information available
Specific gravity	No information available	No information available
Solubility (water)	emulsifiable	No information available

_____

_____

Solubility in other solvents	No information available	No information available
Partition coefficient: n-octanol/water	No information available	No information available
Autoignition temperature	No information available	No information available
Decomposition temperature	No information available	No information available
Kinematic viscosity	46.00 mm2/s @ 25 °C	ASTM D 445-97
Dynamic viscosity	No information available	No information available
Density	1.0220 g/cm^3	ASTM D 1298-99

9.2 Other information

Bulk Density	No information available
Explosive properties	Can polymerize violently.
Oxidizing properties	The substance or mixture is not classified as oxidizing.
Softening point	No information available
Molecular weight	420 g/mol
Volatile Organic Compound (VOC) content, wt.%	No information available
Percent Volatile, wt.%	< 0.5 %

10. STABILITY AND REACTIVITY

10.1 Reactivity

Reactivity
Polymerizes readily unless inhibited. Polymerization is highly exothermic and, if not controlled, may be violent.

10.2 Chemical stability

Chemical stability
Stable under normal conditions of handling, use and transportation. Periodic air sparging in storage will assist long term stability.

10.3 Possibility of hazardous reactions

Hazardous polymerization
May occur if inhibitor is depleted or if exposed to high temperature.

10.4 Conditions to avoid

Conditions to avoid
This product contains a peroxidation inhibitor. To maintain inhibitor activity, oxygen must not be eliminated from the atmosphere above the product. Avoid radical forming substances (metal-ions, peroxides). Avoid heating. If prolonged excursions above the recommended storage temperature occur, then the rate of inhibitor depletion could accelerate, leading to an increased risk of polymerization. In these circumstances it is recommended that the inhibitor level be checked periodically using ASTM procedure D 3125, and more inhibitor added if depletion is observed.

10.5 Incompatible materials

Materials to avoid
Reaction with reducing agents. Reaction with oxidants. Acids or alkalies. Free radical producing initiators. Primary and Secondary Amines.

10.6 Hazardous decomposition products

Hazardous decomposition products
Carbon monoxide. Carbon dioxide. Irritating vapors.
_____

_____

11. TOXICOLOGICAL INFORMATION

11.1 Information on toxicological effects

The product is a tested preparation with following data:

Acute health hazard

Eye contact
May cause slight irritation.

Skin contact
May cause slight irritation.

Ingestion
May be harmful if swallowed.

Inhalation
Inhalation of mist or vapor may cause respiratory tract irritation.

Acute toxicity

Oral LD50	> 2,000 mg/kg Method: OECD Test No. 401: Acute Oral Toxicity
Dermal LD50	No information available
Inhalation LC50	No information available

Skin corrosion/irritation
Slightly irritating, does not require labelling
Method: OECD Test No. 404: Acute Dermal Irritation/Corrosion

Serious eye damage/eye irritation
Slightly irritating, does not require labelling
Method: OECD Test No. 405: Acute Eye Irritation/Corrosion

Sensitization
Dermal sensitization: sensitizing
Method: OECD Test No. 406: Skin Sensitization

Germ cell mutagenicity
No information available

Carcinogenicity
No information available

Reproductive toxicity
No information available

Specific target organ toxicity - Single exposure
No information available

Specific target organ toxicity - Repeated exposure
No information available

Aspiration hazard
No information available

_____

_____

12. ECOLOGICAL INFORMATION

12.1 Toxicity

• The ecological evaluation of the product is based on data from the raw material and/or comparable substances.

Acute aquatic toxicity

Fish	LC50 > 1 - <= 10 mg product/l.
Crustacea	No information available
Bacteria toxicity	EC0 > 1- <= 10 mg product/L.
Algae/aquatic plants	No information available

12.2 Persistence and degradability

Persistence and degradability
No information available

Ultimate biodegradation
The total of the organic components contained in the product achieve values below 60% BOD/COD or CO2 liberation, or below 70% DOC reduction in tests for ease of degradability. Threshold values for ' readily degradable' (e.g. to OECD method 301) are not reached.

12.3 Bioaccumulative potential

Bioaccumulative potential
No information available

12.4 Mobility in soil

Mobility
No information available.

12.5 Results of PBT and vPvB assessment

PBT and vPvB assessment
No information available

12.6 Other adverse effects

Other information
No other ecological studies have been carried out on this product.

13. DISPOSAL CONSIDERATIONS

13.1 Waste treatment methods

Disposal of wastes
Waste incineration with the approval of the responsible local authority.

Contaminated packaging
Packaging that cannot be cleaned are to be disposed of in the same manner as the product. Disposal must be made according to official regulations.

_____

_____

14. TRANSPORT INFORMATION

US DOT
14.1. UN number UN3082
14.2. UN proper shipping name ENVIRONMENTALLY HAZARDOUS SUBSTANCE, LIQUID, N.O.S. (Polypropylene glycol monoacrylate)
14.3. Transport hazard class(es) 9
14.4. Packing group III
14.5. Environmental hazards
14.6. Special precautions for user
    ERG Number 171

Land transport (ADR/RID)
14.1. UN number UN3082
14.2. UN proper shipping name ENVIRONMENTALLY HAZARDOUS SUBSTANCE, LIQUID, N.O.S. (Polypropylene glycol monoacrylate)
14.3. Transport hazard class(es) 9
14.4. Packing group III
14.5. Environmental hazards
14.6. Special precautions for user
    ADR/RID-Labels 9
    Classification code M6
    Hazard identification number (Kemler No.) 90
    Tunnel restriction code (E)

Inland waterway transport (ADN)
14.1. UN number UN3082
14.2. UN proper shipping name ENVIRONMENTALLY HAZARDOUS SUBSTANCE, LIQUID, N.O.S. (Polypropylene glycol monoacrylate)
14.3. Transport hazard class(es) 9
14.4. Packing group III
14.5. Environmental hazards
14.6. Special precautions for user
    Classification code M6

Air transport (ICAO-TI / IATA-DGR)
14.1. UN number UN3082
14.2. UN proper shipping name ENVIRONMENTALLY HAZARDOUS SUBSTANCE, LIQUID, N.O.S. (Polypropylene glycol monoacrylate)
14.3. Transport hazard class(es) 9
14.4. Packing group III
14.5. Environmental hazards
14.6. Special precautions for user
    ERG Code 9L

Sea transport (IMDG)
14.1. UN number UN3082
14.2. UN proper shipping name ENVIRONMENTALLY HAZARDOUS SUBSTANCE, LIQUID, N.O.S. (Polypropylene glycol monoacrylate)
14.3. Transport hazard class(es) 9
14.4. Packing group III
14.5. Environmental hazards
14.6. Special precautions for user
    EmS F-A;S-F

14.7 Transport in bulk according to Annex II of MARPOL 73/78 and the IBC Code
    Not applicable

_____

_____

15. REGULATORY INFORMATION

15.1 Safety, health and environmental regulations/legislation specific for the substance or mixture

International Inventories

Australia (AICS)
All ingredients are on the inventory or exempt from listing

Canada (DSL)
Some ingredients are not on the inventory.

Canada (NDSL)
Some ingredients are on the inventory.

China (IECSC)
All ingredients are on the inventory or exempt from listing

EINECS (European Inventory of Existing Chemical Substances)
All ingredients are on the inventory or exempt from listing

ELINCS (European List of Notified Chemical Substances)
None of the ingredients are on the inventory.

ENCS (Japan)
All ingredients are on the inventory or exempt from listing

South Korea (KECL)
All ingredients are on the inventory or exempt from listing

Philippines (PICCS)
Some ingredients are not on the inventory.

TSCA (United States)
All ingredients are on the inventory or exempt from listing

Legend
 AICS - Australian Inventory of Chemical Substances
 DSL/NDSL - Canadian Domestic Substances List/Non-Domestic Substances List
 IECSC - China Inventory of Existing Chemical Substances
 EINECS/ELINCS - European Inventory of Existing Commercial Chemical Substances/EU List of Notified Chemical Substances
 ENCS - Japan Existing and New Chemical Substances
 KECL - Korean Existing and Evaluated Chemical Substances
 PICCS - Philippines Inventory of Chemicals and Chemical Substances
 TSCA - United States Toxic Substances Control Act Section 8(b) Inventory

15.2 Chemical Safety Report

No information available.

16. OTHER INFORMATION

Product code   745786

Revision date   2017-01-04

Full text of H-Statements referred to under sections 2 and 3
H317 - May cause an allergic skin reaction
H411 - Toxic to aquatic life with long lasting effects
H301 - Toxic if swallowed
H311 - Toxic in contact with skin

_____

_____

H314 - Causes severe skin burns and eye damage
H331 - Toxic if inhaled

Key or legend to abbreviations and acronyms used in the safety data sheet
NAV - Not available

This safety data sheet complies with the requirements of: Regulation (EC) No. 1907/2006.

Additional information
BISOMER® is a registered trademark of GEO Specialty Chemicals UK Ltd.

Disclaimer
The information provided in this Safety Data Sheet is correct to the best of our knowledge, information and belief at the date of its publication. The information given is designed only as a guidance for safe handling, use, processing, storage, transportation, disposal and release and is not to be considered a warranty or quality specification. The information relates only to the specific material designated and may not be valid for such material used in combination with any other materials or in any process, unless specified in the text.

_____

SIGMA-ALDRICH

SAFETY DATA SHEET

SECTION 1: Identification of the substance/mixture and of the company/undertaking

1.1   Product identifiers

Product name   :   **2-Hydroxyethyl acrylate**

Product Number	:	292818
Brand	:	Aldrich
Index-No.	:	607-072-00-8
REACH No.	:	A registration number is not available for this substance as the substance or its uses are exempted from registration, the annual tonnage does not require a registration or the registration is envisaged for a later registration deadline.
CAS-No.	:	818-61-1

1.2   Relevant identified uses of the substance or mixture and uses advised against

Identified uses   :   Laboratory chemicals, Manufacture of substances

1.3   Details of the supplier of the safety data sheet

Company	:	Sigma-Aldrich BVBA Brusselsesteenweg 288 B-3090 OVERIJSE
Telephone	:	+32 3 899 1301
Fax	:	+32 3 899 1311
E-mail address	:	eurtechserv@sial.com

1.4   Emergency telephone number

Emergency Phone #   +(32) 28 083237 (CHEMTREC)
                                               070 245245 (Anti-poison centre)

SECTION 2: Hazards identification

2.1   Classification of the substance or mixture

Classification according to Regulation (EC) No 1272/2008
Acute toxicity, Oral (Category 4), H302
Acute toxicity, Dermal (Category 3), H311
Skin corrosion (Category 1B), H314
Skin sensitisation (Category 1), H317
Acute aquatic toxicity (Category 1), H400

For the full text of the H-Statements mentioned in this Section, see Section 16.

2.2   Label elements

Labelling according Regulation (EC) No 1272/2008
Pictogram

Signal word   Danger

Hazard statement(s)

H302	Harmful if swallowed.
H311	Toxic in contact with skin.
H314	Causes severe skin burns and eye damage.
H317	May cause an allergic skin reaction.
H400	Very toxic to aquatic life.

Precautionary statement(s)

P273	Avoid release to the environment.
P280	Wear protective gloves/ protective clothing/ eye protection/ face protection.
P303 + P361 + P353	IF ON SKIN (or hair): Take off immediately all contaminated clothing. Rinse skin with water/shower.
P304 + P340 + P310	IF INHALED: Remove person to fresh air and keep comfortable for breathing. Immediately call a POISON CENTER or doctor/ physician.
P305 + P351 + P338	IF IN EYES: Rinse cautiously with water for several minutes. Remove contact lenses, if present and easy to do. Continue rinsing.
P333 + P313	If skin irritation or rash occurs: Get medical advice/ attention.
Supplemental Hazard Statements	none

2.3 Other hazards

This substance/mixture contains no components considered to be either persistent, bioaccumulative and toxic (PBT), or very persistent and very bioaccumulative (vPvB) at levels of 0.1% or higher.

SECTION 3: Composition/information on ingredients

3.1 Substances

Formula	:	$C_5H_8O_3$
Molecular weight	:	116,12 g/mol
CAS-No.	:	818-61-1
EC-No.	:	212-454-9
Index-No.	:	607-072-00-8

Hazardous ingredients according to Regulation (EC) No 1272/2008

Component		Classification	Concentration
2-Hydroxyethyl acrylate			
CAS-No. EC-No. Index-No.	818-61-1 212-454-9 607-072-00-8	Acute Tox. 4; Acute Tox. 3; Skin Corr. 1B; Skin Sens. 1; Aquatic Acute 1; H302, H311, H314, H317, H400 Concentration limits: >= 0,2 %: Skin Sens. 1, H317; M-Factor - Aquatic Acute: 1	<= 100 %

For the full text of the H-Statements mentioned in this Section, see Section 16.

SECTION 4: First aid measures

4.1 Description of first aid measures

General advice

Consult a physician. Show this safety data sheet to the doctor in attendance.

If inhaled

If breathed in, move person into fresh air. If not breathing, give artificial respiration. Consult a physician.

In case of skin contact
Take off contaminated clothing and shoes immediately. Wash off with soap and plenty of water. Take victim immediately to hospital. Consult a physician.

In case of eye contact
Rinse thoroughly with plenty of water for at least 15 minutes and consult a physician.

If swallowed
Do NOT induce vomiting. Never give anything by mouth to an unconscious person. Rinse mouth with water. Consult a physician.

4.2 Most important symptoms and effects, both acute and delayed
The most important known symptoms and effects are described in the labelling (see section 2.2) and/or in section 11

4.3 Indication of any immediate medical attention and special treatment needed
No data available

SECTION 5: Firefighting measures

5.1 Extinguishing media

Suitable extinguishing media
Use water spray, alcohol-resistant foam, dry chemical or carbon dioxide.

5.2 Special hazards arising from the substance or mixture
Carbon oxides

5.3 Advice for firefighters
Wear self-contained breathing apparatus for firefighting if necessary.

5.4 Further information
No data available

SECTION 6: Accidental release measures

6.1 Personal precautions, protective equipment and emergency procedures
Wear respiratory protection. Avoid breathing vapours, mist or gas. Ensure adequate ventilation.
Evacuate personnel to safe areas.
For personal protection see section 8.

6.2 Environmental precautions
Prevent further leakage or spillage if safe to do so. Do not let product enter drains. Discharge into the environment must be avoided.

6.3 Methods and materials for containment and cleaning up
Soak up with inert absorbent material and dispose of as hazardous waste. Keep in suitable, closed containers for disposal.

6.4 Reference to other sections
For disposal see section 13.

SECTION 7: Handling and storage

7.1 Precautions for safe handling
Avoid contact with skin and eyes. Avoid inhalation of vapour or mist.
For precautions see section 2.2.

7.2 Conditions for safe storage, including any incompatibilities
Store in cool place. Keep container tightly closed in a dry and well-ventilated place. Containers which are opened must be carefully resealed and kept upright to prevent leakage.

Recommended storage temperature 2 - 8 °C
Storage class (TRGS 510): Non-combustible, acute toxic Cat.3 / toxic hazardous materials or hazardous materials causing chronic effects

7.3 Specific end use(s)
Apart from the uses mentioned in section 1.2 no other specific uses are stipulated

SECTION 8: Exposure controls/personal protection

8.1   Control parameters

Components with workplace control parameters

8.2   Exposure controls

Appropriate engineering controls
Avoid contact with skin, eyes and clothing. Wash hands before breaks and immediately after handling the product.

Personal protective equipment

Eye/face protection
Tightly fitting safety goggles. Faceshield (8-inch minimum). Use equipment for eye protection tested and approved under appropriate government standards such as NIOSH (US) or EN 166(EU).

Skin protection
Handle with gloves. Gloves must be inspected prior to use. Use proper glove removal technique (without touching glove's outer surface) to avoid skin contact with this product. Dispose of contaminated gloves after use in accordance with applicable laws and good laboratory practices. Wash and dry hands.

The selected protective gloves have to satisfy the specifications of EU Directive 89/686/EEC and the standard EN 374 derived from it.

Full contact
Material: Chloroprene
Minimum layer thickness: 0,6 mm
Break through time: 480 min
Material tested:Camapren® (KCL 722 / Aldrich Z677493, Size M)

Splash contact
Material: Nitrile rubber
Minimum layer thickness: 0,4 mm
Break through time: 30 min
Material tested:Camatril® (KCL 730 / Aldrich Z677442, Size M)

data source: KCL GmbH, D-36124 Eichenzell, phone +49 (0)6659 87300, e-mail sales@kcl.de, test method: EN374
If used in solution, or mixed with other substances, and under conditions which differ from EN 374, contact the supplier of the CE approved gloves. This recommendation is advisory only and must be evaluated by an industrial hygienist and safety officer familiar with the specific situation of anticipated use by our customers. It should not be construed as offering an approval for any specific use scenario.

Body Protection
Complete suit protecting against chemicals, The type of protective equipment must be selected according to the concentration and amount of the dangerous substance at the specific workplace.

Respiratory protection
Where risk assessment shows air-purifying respirators are appropriate use a full-face respirator with multi-purpose combination (US) or type ABEK (EN 14387) respirator cartridges as a backup to engineering controls. If the respirator is the sole means of protection, use a full-face supplied air respirator. Use respirators and components tested and approved under appropriate government standards such as NIOSH (US) or CEN (EU).

Control of environmental exposure
Prevent further leakage or spillage if safe to do so. Do not let product enter drains. Discharge into the environment must be avoided.

SECTION 9: Physical and chemical properties

9.1   Information on basic physical and chemical properties

a)	Appearance	Form: liquid Colour: colourless
b)	Odour	No data available
c)	Odour Threshold	No data available
d)	pH	No data available
e)	Melting point/freezing point	Melting point/freezing point: < -60 °C
f)	Initial boiling point and boiling range	90 - 92 °C
g)	Flash point	101 °C - closed cup
h)	Evaporation rate	No data available
i)	Flammability (solid, gas)	No data available
j)	Upper/lower flammability or explosive limits	Lower explosion limit: 1,8 %(V)
k)	Vapour pressure	0,1 hPa at 20 °C
l)	Vapour density	No data available
m)	Relative density	1,106 g/cm3
n)	Water solubility	1.000 g/l at 20 °C - soluble
o)	Partition coefficient: n-octanol/water	log Pow: -0,17 at 25 °C
p)	Auto-ignition temperature	370 °C at 1.013,25 hPa
q)	Decomposition temperature	No data available
r)	Viscosity	No data available
s)	Explosive properties	No data available
t)	Oxidizing properties	No data available

9.2   Other safety information
No data available

SECTION 10: Stability and reactivity

10.1   Reactivity
No data available

10.2   Chemical stability
Stable under recommended storage conditions.
Contains the following stabiliser(s):
Mequinol (>=200 - <=650 ppm)

10.3   Possibility of hazardous reactions
No data available

10.4   Conditions to avoid
No data available

10.5   Incompatible materials
No data available

10.6   Hazardous decomposition products
Other decomposition products - No data available
In the event of fire: see section 5

SECTION 11: Toxicological information

11.1   Information on toxicological effects

Acute toxicity
LD50 Oral - Rat - male and female - 960,5 mg/kg
(OECD Test Guideline 401)

Skin corrosion/irritation
Skin - Rabbit
Result: Causes burns.

Serious eye damage/eye irritation
Eyes - Rabbit
Result: Corrosive

Respiratory or skin sensitisation
Maximisation Test (GPMT) - Guinea pig
Result: May cause sensitisation by skin contact.

Germ cell mutagenicity
Salmonella typhimurium
Result: negative

Rat - male and female
Result: negative

Carcinogenicity

IARC: No component of this product present at levels greater than or equal to 0.1% is identified as
            probable, possible or confirmed human carcinogen by IARC.

Reproductive toxicity

No data available

Specific target organ toxicity - single exposure
No data available

Specific target organ toxicity - repeated exposure
No data available

Aspiration hazard
No data available

Additional Information

Repeated dose   Rat - male and female - Oral - NOAEL : 196 - 305 mg/kg
toxicity
RTECS: Not available

SECTION 12: Ecological information

12.1   Toxicity

Toxicity to fish   flow-through test LC50 - Pimephales promelas (fathead minnow) - 4,8 mg/l -
                             96,0 h

Toxicity to daphnia and   EC50 - Daphnia magna (Water flea) - 0,78 mg/l - 48 h
other aquatic
invertebrates

| Toxicity to algae | Growth inhibition EC50 - Pseudokirchneriella subcapitata (green algae) - 6 mg/l - 72 h |
| | (OECD Test Guideline 201) |

12.2 Persistence and degradability

Biodegradability	Biotic/Aerobic - Exposure time 28 d
	Result: 79 % - Readily biodegradable
	(OECD Test Guideline 301B)

12.3 Bioaccumulative potential
No data available

12.4 Mobility in soil
No data available

12.5 Results of PBT and vPvB assessment
This substance/mixture contains no components considered to be either persistent, bioaccumulative and toxic (PBT), or very persistent and very bioaccumulative (vPvB) at levels of 0.1% or higher.

12.6 Other adverse effects
Very toxic to aquatic life.

SECTION 13: Disposal considerations

13.1 Waste treatment methods

Product
Offer surplus and non-recyclable solutions to a licensed disposal company.

Contaminated packaging
Dispose of as unused product.

SECTION 14: Transport information

14.1 UN number
ADR/RID: 2922   IMDG: 2922   IATA: 2922

14.2 UN proper shipping name
ADR/RID: CORROSIVE LIQUID, TOXIC, N.O.S. (2-Hydroxyethyl acrylate)
IMDG: CORROSIVE LIQUID, TOXIC, N.O.S. (2-Hydroxyethyl acrylate)
IATA: Corrosive liquid, toxic, n.o.s. (2-Hydroxyethyl acrylate)

14.3 Transport hazard class(es)
ADR/RID: 8 (6.1)   IMDG: 8 (6.1)   IATA: 8 (6.1)

14.4 Packaging group
ADR/RID: II   IMDG: II   IATA: II

14.5 Environmental hazards
ADR/RID: yes   IMDG Marine pollutant: yes   IATA: no

14.6 Special precautions for user
No data available

SECTION 15: Regulatory information

This safety datasheet complies with the requirements of Regulation (EC) No. 453/2010.

15.1 Safety, health and environmental regulations/legislation specific for the substance or mixture

15.2 Chemical Safety Assessment
For this product a chemical safety assessment was not carried out

SECTION 16: Other information

Full text of H-Statements referred to under sections 2 and 3.

H302	Harmful if swallowed.
H311	Toxic in contact with skin.
H314	Causes severe skin burns and eye damage.
H317	May cause an allergic skin reaction.
H400	Very toxic to aquatic life.

Further information

The above information is believed to be correct but does not purport to be all inclusive and shall be used only as a guide. The information in this document is based on the present state of our knowledge and is applicable to the product with regard to appropriate safety precautions. It does not represent any guarantee of the properties of the product. Sigma-Aldrich Corporation and its Affiliates shall not be held liable for any damage resulting from handling or from contact with the above product. See www.sigma-aldrich.com and/or the reverse side of invoice or packing slip for additional terms and conditions of sale.

SIGMA-ALDRICH

sigma-aldrich.com

SAFETY DATA SHEET

according to Regulation (EC) No. 453/2010
Version 6.1 Revision Date 17.11.2015
Print Date 15.08.2017
GENERIC EU MSDS - NO COUNTRY SPECIFIC DATA - NO OEL DATA

SECTION 1: Identification of the substance/mixture and of the company/undertaking

1.1 Product identifiers

Product name : **Isophorone diisocyanate**

Product Number	:	317624
Brand	:	Aldrich
Index-No.	:	615-008-00-5
REACH No.	:	01-2119490408-31-XXXX
CAS-No.	:	4098-71-9

1.2 Relevant identified uses of the substance or mixture and uses advised against

Identified uses : Laboratory chemicals, Manufacture of substances

1.3 Details of the supplier of the safety data sheet

Company	:	Sigma-Aldrich BVBA
		Brusselsesteenweg 288
		B-3090 OVERIJSE
Telephone	:	+32 3 899 1301
Fax	:	+32 3 899 1311
E-mail address	:	eurtechserv@sial.com

1.4 Emergency telephone number

Emergency Phone # +(32) 28 083237 (CHEMTREC)
070 245245 (Anti-poison centre)

SECTION 2: Hazards identification

2.1 Classification of the substance or mixture

Classification according to Regulation (EC) No 1272/2008
Acute toxicity, Inhalation (Category 1), H330
Skin irritation (Category 2), H315
Eye irritation (Category 2), H319
Respiratory sensitisation (Category 1), H334
Skin sensitisation (Category 1), H317
Specific target organ toxicity - single exposure (Category 3), Respiratory system, H335
Chronic aquatic toxicity (Category 2), H411

For the full text of the H-Statements mentioned in this Section, see Section 16.

2.2 Label elements

Labelling according Regulation (EC) No 1272/2008
Pictogram

Signal word   Danger

Hazard statement(s)
H315   Causes skin irritation.

H317	May cause an allergic skin reaction.
H319	Causes serious eye irritation.
H330	Fatal if inhaled.
H334	May cause allergy or asthma symptoms or breathing difficulties if inhaled.
H335	May cause respiratory irritation.
H411	Toxic to aquatic life with long lasting effects.

Precautionary statement(s)

P260	Do not breathe dust/ fume/ gas/ mist/ vapours/ spray.
P280	Wear protective gloves/ protective clothing/ eye protection/ face protection.
P284	Wear respiratory protection.
P304 + P340 + P310	IF INHALED: Remove person to fresh air and keep comfortable for breathing. Immediately call a POISON CENTER or doctor/ physician.
P342 + P311	If experiencing respiratory symptoms: Call a POISON CENTER or doctor/ physician.
P403 + P233	Store in a well-ventilated place. Keep container tightly closed.
Supplemental Hazard Statements	none

2.3 Other hazards

This substance/mixture contains no components considered to be either persistent, bioaccumulative and toxic (PBT), or very persistent and very bioaccumulative (vPvB) at levels of 0.1% or higher.
Lachrymator.

SECTION 3: Composition/information on ingredients

3.1 Substances

Synonyms	:	5-Isocyanato-1-(isocyanatomethyl)-1,3,3-trimethylcyclohexane
Formula	:	$C_{12}H_{18}N_2O_2$
Molecular weight	:	222,28 g/mol
CAS-No.	:	4098-71-9
EC-No.	:	223-861-6
Index-No.	:	615-008-00-5
Registration number	:	01-2119490408-31-XXXX

Hazardous ingredients according to Regulation (EC) No 1272/2008

Component		Classification	Concentration
3-isocyanatomethyl-3,5,5-trimethylcyclohexyl isocyanate			
CAS-No. EC-No. Index-No.	4098-71-9 223-861-6 615-008-00-5	Acute Tox. 1; Skin Irrit. 2; Eye Irrit. 2; Resp. Sens. 1; Skin Sens. 1; STOT SE 3; Aquatic Chronic 2; H330, H315, H319, H334, H317, H335, H411 Concentration limits: >= 0,5 %: Resp. Sens. 1, H334; >= 0,5 %: Skin Sens. 1, H317;	<= 100 %

For the full text of the H-Statements mentioned in this Section, see Section 16.

SECTION 4: First aid measures

4.1 Description of first aid measures

General advice

Consult a physician. Show this safety data sheet to the doctor in attendance.

If inhaled
If breathed in, move person into fresh air. If not breathing, give artificial respiration. Consult a physician.

In case of skin contact
Wash off with soap and plenty of water. Take victim immediately to hospital. Consult a physician.

In case of eye contact
Rinse thoroughly with plenty of water for at least 15 minutes and consult a physician.

If swallowed
Never give anything by mouth to an unconscious person. Rinse mouth with water. Consult a physician.

4.2 Most important symptoms and effects, both acute and delayed
The most important known symptoms and effects are described in the labelling (see section 2.2) and/or in section 11

4.3 Indication of any immediate medical attention and special treatment needed
No data available

SECTION 5: Firefighting measures

5.1 Extinguishing media

Suitable extinguishing media
Use water spray, alcohol-resistant foam, dry chemical or carbon dioxide.

5.2 Special hazards arising from the substance or mixture
Carbon oxides, Nitrogen oxides (NOx)

5.3 Advice for firefighters
Wear self-contained breathing apparatus for firefighting if necessary.

5.4 Further information
No data available

SECTION 6: Accidental release measures

6.1 Personal precautions, protective equipment and emergency procedures
Wear respiratory protection. Avoid breathing vapours, mist or gas. Ensure adequate ventilation. Evacuate personnel to safe areas.
For personal protection see section 8.

6.2 Environmental precautions
Prevent further leakage or spillage if safe to do so. Do not let product enter drains. Discharge into the environment must be avoided.

6.3 Methods and materials for containment and cleaning up
Soak up with inert absorbent material and dispose of as hazardous waste. Keep in suitable, closed containers for disposal.

6.4 Reference to other sections
For disposal see section 13.

SECTION 7: Handling and storage

7.1 Precautions for safe handling
Avoid contact with skin and eyes. Avoid inhalation of vapour or mist.
For precautions see section 2.2.

7.2 Conditions for safe storage, including any incompatibilities
Store in cool place. Keep container tightly closed in a dry and well-ventilated place. Containers which are opened must be carefully resealed and kept upright to prevent leakage.

Moisture sensitive.
Storage class (TRGS 510): Non-combustible, acute toxic Cat. 1 and 2 / very toxic hazardous materials

7.3 Specific end use(s)
Apart from the uses mentioned in section 1.2 no other specific uses are stipulated

SECTION 8: Exposure controls/personal protection

8.1   Control parameters

Components with workplace control parameters

8.2   Exposure controls

Appropriate engineering controls
Avoid contact with skin, eyes and clothing. Wash hands before breaks and immediately after handling the product.

Personal protective equipment

Eye/face protection
Face shield and safety glasses Use equipment for eye protection tested and approved under appropriate government standards such as NIOSH (US) or EN 166(EU).

Skin protection
Handle with gloves. Gloves must be inspected prior to use. Use proper glove removal technique (without touching glove's outer surface) to avoid skin contact with this product. Dispose of contaminated gloves after use in accordance with applicable laws and good laboratory practices. Wash and dry hands.

The selected protective gloves have to satisfy the specifications of EU Directive 89/686/EEC and the standard EN 374 derived from it.

Splash contact
Material: Nitrile rubber
Minimum layer thickness: 0,4 mm
Break through time: 110 min
Material tested:Camatril® (KCL 730 / Aldrich Z677442, Size M)

data source: KCL GmbH, D-36124 Eichenzell, phone +49 (0)6659 87300, e-mail sales@kcl.de, test method: EN374
If used in solution, or mixed with other substances, and under conditions which differ from EN 374, contact the supplier of the CE approved gloves. This recommendation is advisory only and must be evaluated by an industrial hygienist and safety officer familiar with the specific situation of anticipated use by our customers. It should not be construed as offering an approval for any specific use scenario.

Body Protection
Complete suit protecting against chemicals, The type of protective equipment must be selected according to the concentration and amount of the dangerous substance at the specific workplace.

Respiratory protection
Where risk assessment shows air-purifying respirators are appropriate use a full-face respirator with multi-purpose combination (US) or type ABEK (EN 14387) respirator cartridges as a backup to engineering controls. If the respirator is the sole means of protection, use a full-face supplied air respirator. Use respirators and components tested and approved under appropriate government standards such as NIOSH (US) or CEN (EU).

Control of environmental exposure
Prevent further leakage or spillage if safe to do so. Do not let product enter drains. Discharge into the environment must be avoided.

SECTION 9: Physical and chemical properties

9.1   Information on basic physical and chemical properties

a)	Appearance	Form: liquid Colour: colourless, yellow
b)	Odour	No data available
c)	Odour Threshold	No data available

d)	pH	No data available
e)	Melting point/freezing point	No data available
f)	Initial boiling point and boiling range	158 - 159 °C at 20 hPa - lit.
g)	Flash point	163 °C - closed cup
h)	Evaporation rate	No data available
i)	Flammability (solid, gas)	No data available
j)	Upper/lower flammability or explosive limits	No data available
k)	Vapour pressure	0,000635 hPa at 20 °C - OECD Test Guideline 104
l)	Vapour density	No data available
m)	Relative density	1,049 g/cm3 at 25 °C - lit.
n)	Water solubility	ca.0,015 g/l at 23 °C - OECD Test Guideline 105
o)	Partition coefficient: n-octanol/water	No data available
p)	Auto-ignition temperature	430 °C at 1.013 hPa
q)	Decomposition temperature	No data available
r)	Viscosity	No data available
s)	Explosive properties	Not explosive
t)	Oxidizing properties	No data available

9.2 Other safety information
No data available

SECTION 10: Stability and reactivity

10.1 Reactivity
No data available

10.2 Chemical stability
Stable under recommended storage conditions.

10.3 Possibility of hazardous reactions
No data available

10.4 Conditions to avoid
Avoid moisture.

10.5 Incompatible materials
Strong oxidizing agents, Strong acids, Alcohols

10.6 Hazardous decomposition products
Other decomposition products - No data available
In the event of fire: see section 5

SECTION 11: Toxicological information

11.1 Information on toxicological effects

Acute toxicity
LD50 Oral - Rat - male and female - 4.814 mg/kg
(OECD Test Guideline 401)

LC50 Inhalation - Rat - male and female - 4 h - 31 mg/m3
(OECD Test Guideline 403)

LD50 Dermal - Rat - male and female - > 7.000 mg/kg
(OECD Test Guideline 402)

Skin corrosion/irritation
Skin - Rabbit
Result: Irritating to skin. - 4 h
(OECD Test Guideline 404)

Serious eye damage/eye irritation
Eyes - Rabbit
Result: Irritating to eyes.
(OECD Test Guideline 405)

Respiratory or skin sensitisation
in vivo assay - Guinea pig
May cause sensitisation by skin contact.
(OECD Test Guideline 406)

in vivo assay - Guinea pig
May cause sensitisation by inhalation.

Germ cell mutagenicity
In vitro mammalian cell gene mutation test
Chinese hamster ovary cells
Result: negative

OECD Test Guideline 474
Mouse - male
Result: negative

Carcinogenicity

IARC: No component of this product present at levels greater than or equal to 0.1% is identified as
           probable, possible or confirmed human carcinogen by IARC.

Reproductive toxicity

Developmental Toxicity - Rat - Inhalation
No significant adverse effects were reported

Specific target organ toxicity - single exposure
No data available

Specific target organ toxicity - repeated exposure
No data available

Aspiration hazard
No data available

Additional Information
RTECS: NQ9370000

Material is extremely destructive to tissue of the mucous membranes and upper respiratory tract, eyes, and
skin., Cough, Shortness of breath, Headache, Nausea

SECTION 12: Ecological information

12.1 Toxicity

Toxicity to fish	static test LC50 - Danio rerio (zebra fish) - >= 72 mg/l - 96 h (Tested according to Directive 92/69/EEC.)
Toxicity to daphnia and other aquatic invertebrates	static test EC50 - Daphnia magna (Water flea) - 27 mg/l - 48 h (Directive 67/548/EEC, Annex V, C.2.)
Toxicity to algae	static test EC50 - Desmodesmus subspicatus (green algae) - > 70 mg/l - 72 h (Tested according to Directive 92/69/EEC.)
Toxicity to bacteria	Respiration inhibition EC50 - activated sludge - 263 mg/l - 3 h (OECD Test Guideline 209)

12.2 Persistence and degradability
Biodegradability   aerobic - Exposure time 28 d
Result: 0 % - Not readily biodegradable.

12.3 Bioaccumulative potential
No data available

12.4 Mobility in soil
No data available

12.5 Results of PBT and vPvB assessment
This substance/mixture contains no components considered to be either persistent, bioaccumulative and toxic (PBT), or very persistent and very bioaccumulative (vPvB) at levels of 0.1% or higher.

12.6 Other adverse effects
Toxic to aquatic life with long lasting effects.

SECTION 13: Disposal considerations

13.1 Waste treatment methods

Product
Offer surplus and non-recyclable solutions to a licensed disposal company.

Contaminated packaging
Dispose of as unused product.

SECTION 14: Transport information

14.1 UN number
ADR/RID: 2290   IMDG: 2290   IATA: 2290

14.2 UN proper shipping name
ADR/RID: ISOPHORONE DIISOCYANATE
IMDG: ISOPHORONE DIISOCYANATE
IATA: Isophorone diisocyanate

14.3 Transport hazard class(es)
ADR/RID: 6.1   IMDG: 6.1   IATA: 6.1

14.4 Packaging group
ADR/RID: III   IMDG: III   IATA: III

14.5 Environmental hazards
ADR/RID: yes   IMDG Marine pollutant: yes   IATA: no

14.6 Special precautions for user
No data available

SECTION 15: Regulatory information

This safety datasheet complies with the requirements of Regulation (EC) No. 453/2010.

15.1 Safety, health and environmental regulations/legislation specific for the substance or mixture

15.2 Chemical Safety Assessment
For this product a chemical safety assessment was not carried out

---

SECTION 16: Other information

Full text of H-Statements referred to under sections 2 and 3.

H315	Causes skin irritation.
H317	May cause an allergic skin reaction.
H319	Causes serious eye irritation.
H330	Fatal if inhaled.
H334	May cause allergy or asthma symptoms or breathing difficulties if inhaled.
H335	May cause respiratory irritation.
H411	Toxic to aquatic life with long lasting effects.

Further information

SIGMA-ALDRICH

SAFETY DATA SHEET

according to Regulation (EC) No. 1907/2006
Version 5.0 Revision Date 08.06.2012
Print Date 15.08.2017
GENERIC EU MSDS - NO COUNTRY SPECIFIC DATA - NO OEL DATA

1.   IDENTIFICATION OF THE SUBSTANCE/MIXTURE AND OF THE COMPANY/UNDERTAKING

1.1   Product identifiers

Product name   :   Poly(ethylene glycol)

Product Number   :   81221
Brand   :   Sigma-Aldrich
CAS-No.   :   25322-68-3

1.2   Relevant identified uses of the substance or mixture and uses advised against

Identified uses   :   Laboratory chemicals, Manufacture of substances

1.3   Details of the supplier of the safety data sheet

Company   :   Sigma-Aldrich BVBA
                             Brusselsesteenweg 288
                             B-3090 OVERIJSE

Telephone   :   +32 3 899 1301
Fax   :   +32 3 899 1311
E-mail address   :   eurtechserv@sial.com

1.4   Emergency telephone number

Emergency Phone #   :   +(32) 28 083237 (CHEMTREC)
                             070 245245 (Anti-poison centre)

2.   HAZARDS IDENTIFICATION

2.1   Classification of the substance or mixture

Not a hazardous substance or mixture according to Regulation (EC) No. 1272/2008.
This substance is not classified as dangerous according to Directive 67/548/EEC.

2.2   Label elements

The product does not need to be labelled in accordance with EC directives or respective national laws.

2.3   Other hazards - none

3.   COMPOSITION/INFORMATION ON INGREDIENTS

3.1   Substances

Synonyms   :   PEG

Formula   : $(C_2H_4O)_nH_2O$

4.   FIRST AID MEASURES

4.1   Description of first aid measures

If inhaled
If breathed in, move person into fresh air. If not breathing, give artificial respiration.

In case of skin contact
Wash off with soap and plenty of water.

In case of eye contact
Flush eyes with water as a precaution.

If swallowed
Never give anything by mouth to an unconscious person. Rinse mouth with water.

4.2 Most important symptoms and effects, both acute and delayed

4.3 Indication of any immediate medical attention and special treatment needed
no data available

5. FIREFIGHTING MEASURES

5.1 Extinguishing media

Suitable extinguishing media
Use water spray, alcohol-resistant foam, dry chemical or carbon dioxide.

5.2 Special hazards arising from the substance or mixture
Carbon oxides
Nature of decomposition products not known.

5.3 Advice for firefighters
Wear self contained breathing apparatus for fire fighting if necessary.

5.4 Further information
no data available

6. ACCIDENTAL RELEASE MEASURES

6.1 Personal precautions, protective equipment and emergency procedures
Avoid dust formation. Avoid breathing vapors, mist or gas.

6.2 Environmental precautions
Do not let product enter drains.

6.3 Methods and materials for containment and cleaning up
Sweep up and shovel. Keep in suitable, closed containers for disposal.

6.4 Reference to other sections
For disposal see section 13.

7. HANDLING AND STORAGE

7.1 Precautions for safe handling
Provide appropriate exhaust ventilation at places where dust is formed.

7.2 Conditions for safe storage, including any incompatibilities
Store in cool place. Keep container tightly closed in a dry and well-ventilated place.

7.3 Specific end uses
no data available

8. EXPOSURE CONTROLS/PERSONAL PROTECTION

8.1 Control parameters

Components with workplace control parameters

8.2 Exposure controls

Appropriate engineering controls
General industrial hygiene practice.

Personal protective equipment

Eye/face protection
Use equipment for eye protection tested and approved under appropriate government standards such as NIOSH (US) or EN 166(EU).

Skin protection
Handle with gloves. Gloves must be inspected prior to use. Use proper glove removal technique (without touching glove's outer surface) to avoid skin contact with this product. Dispose of

contaminated gloves after use in accordance with applicable laws and good laboratory practices. Wash and dry hands.

The selected protective gloves have to satisfy the specifications of EU Directive 89/686/EEC and the standard EN 374 derived from it.

Immersion protection
Material: Nitrile rubber
Minimum layer thickness: 0,11 mm
Break through time: > 480 min
Material tested:Dermatril® (Aldrich Z677272, Size M)

Splash protection
Material: Nitrile rubber
Minimum layer thickness: 0,11 mm
Break through time: > 30 min
Material tested:Dermatril® (Aldrich Z677272, Size M)

data source: KCL GmbH, D-36124 Eichenzell, phone +49 (0)6659 873000, e-mail sales@kcl.de, test method: EN374
If used in solution, or mixed with other substances, and under conditions which differ from EN 374, contact the supplier of the CE approved gloves. This recommendation is advisory only and must be evaluated by an Industrial Hygienist familiar with the specific situation of anticipated use by our customers. It should not be construed as offering an approval for any specific use scenario.

Body Protection
Choose body protection in relation to its type, to the concentration and amount of dangerous substances, and to the specific work-place., The type of protective equipment must be selected according to the concentration and amount of the dangerous substance at the specific workplace.

Respiratory protection
Respiratory protection is not required. Where protection from nuisance levels of dusts are desired, use type N95 (US) or type P1 (EN 143) dust masks. Use respirators and components tested and approved under appropriate government standards such as NIOSH (US) or CEN (EU).

---

9.   PHYSICAL AND CHEMICAL PROPERTIES

9.1   Information on basic physical and chemical properties

a)	Appearance	Form: solid
b)	Odour	no data available
c)	Odour Threshold	no data available
d)	pH	no data available
e)	Melting point/freezing point	Melting point/range: 50 - 53 °C
f)	Initial boiling point and boiling range	no data available
g)	Flash point	no data available
h)	Evaporation rate	no data available
i)	Flammability (solid, gas)	no data available
j)	Upper/lower flammability or explosive limits	no data available
k)	Vapour pressure	< 0,01 hPa at 20 °C
l)	Vapour density	no data available
m)	Relative density	no data available
n)	Water solubility	no data available
o)	Partition coefficient: n-	no data available

octanol/water

p)	Autoignition temperature	305 °C
q)	Decomposition temperature	no data available
r)	Viscosity	no data available
s)	Explosive properties	no data available
t)	Oxidizing properties	no data available

9.2 Other safety information
no data available

---

10. STABILITY AND REACTIVITY

10.1 Reactivity
no data available

10.2 Chemical stability
no data available

10.3 Possibility of hazardous reactions
no data available

10.4 Conditions to avoid
no data available

10.5 Incompatible materials
Strong oxidizing agents

10.6 Hazardous decomposition products
Other decomposition products - no data available

---

11. TOXICOLOGICAL INFORMATION

11.1 Information on toxicological effects

Acute toxicity
LD50 Oral - rat - 45.000 mg/kg

Skin corrosion/irritation
no data available

Serious eye damage/eye irritation
no data available

Respiratory or skin sensitization
no data available

Germ cell mutagenicity
no data available

Carcinogenicity

IARC: No component of this product present at levels greater than or equal to 0.1% is identified as probable, possible or confirmed human carcinogen by IARC.

Reproductive toxicity
no data available

Specific target organ toxicity - single exposure
no data available

Specific target organ toxicity - repeated exposure
no data available

Aspiration hazard
no data available

Potential health effects

Inhalation	May be harmful if inhaled. May cause respiratory tract irritation.
Ingestion	May be harmful if swallowed.
Skin	May be harmful if absorbed through skin. May cause skin irritation.
Eyes	May cause eye irritation.

Additional Information
RTECS: Not available

---

12. ECOLOGICAL INFORMATION

12.1 Toxicity
no data available

12.2 Persistence and degradability
no data available

12.3 Bioaccumulative potential
no data available

12.4 Mobility in soil
no data available

12.5 Results of PBT and vPvB assessment
no data available

12.6 Other adverse effects
no data available

---

13. DISPOSAL CONSIDERATIONS

13.1 Waste treatment methods

Product
Offer surplus and non-recyclable solutions to a licensed disposal company.

Contaminated packaging
Dispose of as unused product.

---

14. TRANSPORT INFORMATION

14.1 UN number
ADR/RID: -   IMDG: -   IATA: -

14.2 UN proper shipping name
ADR/RID: Not dangerous goods
IMDG: Not dangerous goods
IATA: Not dangerous goods

14.3 Transport hazard class(es)
ADR/RID: -   IMDG: -   IATA: -

14.4 Packaging group
ADR/RID: -   IMDG: -   IATA: -

14.5 Environmental hazards
ADR/RID: no   IMDG Marine pollutant: no   IATA: no

14.6 Special precautions for user
no data available

---

15. REGULATORY INFORMATION

This safety datasheet complies with the requirements of Regulation (EC) No. 1907/2006.

15.1 Safety, health and environmental regulations/legislation specific for the substance or mixture
no data available

15.2 Chemical Safety Assessment
no data available

---

16. OTHER INFORMATION

Further information

Copyright 2012 Sigma-Aldrich Co. LLC. License granted to make unlimited paper copies for internal use only.

The above information is believed to be correct but does not purport to be all inclusive and shall be used only as a guide. The information in this document is based on the present state of our knowledge and is applicable to the product with regard to appropriate safety precautions. It does not represent any guarantee of the properties of the product. Sigma-Aldrich Corporation and its Affiliates shall not be held liable for any damage resulting from handling or from contact with the above product. See www.sigma-aldrich.com and/or the reverse side of invoice or packing slip for additional terms and conditions of sale.

SIGMA-ALDRICH

sigma-aldrich.com

SAFETY DATA SHEET

according to Regulation (EC) No. 1907/2006
Version 5.1 Revision Date 29.04.2014
Print Date 15.08.2017
GENERIC EU MSDS - NO COUNTRY SPECIFIC DATA - NO OEL DATA

SECTION 1: Identification of the substance/mixture and of the company/undertaking

1.1   Product identifiers

Product name   :   Phenothiazine

Product Number   :   88580
Brand   :   Sigma-Aldrich
REACH No.   :   A registration number is not available for this substance as the substance
                            or its uses are exempted from registration, the annual tonnage does not
                            require a registration or the registration is envisaged for a later
                            registration deadline.
CAS-No.   :   92-84-2

1.2   Relevant identified uses of the substance or mixture and uses advised against

Identified uses   :   Laboratory chemicals, Manufacture of substances

1.3   Details of the supplier of the safety data sheet

Company   :   Sigma-Aldrich BVBA
                             Brusselsesteenweg 288
                             B-3090 OVERIJSE

Telephone   :   +32 3 899 1301
Fax   :   +32 3 899 1311
E-mail address   :   eurtechserv@sial.com

1.4   Emergency telephone number

Emergency Phone #   :   +(32) 28 083237 (CHEMTREC)
                                 070 245245 (Anti-poison centre)

SECTION 2: Hazards identification

2.1   Classification of the substance or mixture

Classification according to Regulation (EC) No 1272/2008
Acute toxicity, Oral (Category 4), H302
Skin sensitisation (Category 1), H317
Specific target organ toxicity - repeated exposure, Oral (Category 2), Blood, H373
Chronic aquatic toxicity (Category 3), H412

For the full text of the H-Statements mentioned in this Section, see Section 16.

Classification according to EU Directives 67/548/EEC or 1999/45/EC
Xn   Harmful   R22, R43, R48/22, R52/53

For the full text of the R-phrases mentioned in this Section, see Section 16.

2.2   Label elements

Labelling according Regulation (EC) No 1272/2008
Pictogram

Signal word   Warning

Hazard statement(s)
H302   Harmful if swallowed.

H317	May cause an allergic skin reaction.
H373	May cause damage to organs (Blood) through prolonged or repeated exposure if swallowed.
H412	Harmful to aquatic life with long lasting effects.

Precautionary statement(s)

| P273 | Avoid release to the environment. |
| P280 | Wear protective gloves. |

| Supplemental Hazard Statements | none |

2.3 **Other hazards** - none

SECTION 3: Composition/information on ingredients

3.1 **Substances**

Formula	:	$C_{12}H_9NS$
Molecular Weight	:	199,27 g/mol
CAS-No.	:	92-84-2
EC-No.	:	202-196-5

Hazardous ingredients according to Regulation (EC) No 1272/2008

Component			Classification	Concentration
Phenothiazine				
CAS-No. EC-No.	92-84-2 202-196-5		Acute Tox. 4; Skin Sens. 1; STOT RE 2; Aquatic Chronic 3; H302, H317, H373, H412	<= 100 %

Hazardous ingredients according to Directive 1999/45/EC

Component			Classification	Concentration
Phenothiazine				
CAS-No. EC-No.	92-84-2 202-196-5		Xn, R22 - R43 - R48/22 - R52/53	<= 100 %

For the full text of the H-Statements and R-Phrases mentioned in this Section, see Section 16

SECTION 4: First aid measures

4.1 **Description of first aid measures**

General advice
Consult a physician. Show this safety data sheet to the doctor in attendance.

If inhaled
If breathed in, move person into fresh air. If not breathing, give artificial respiration. Consult a physician.

In case of skin contact
Wash off with soap and plenty of water. Consult a physician.

In case of eye contact
Flush eyes with water as a precaution.

If swallowed
Never give anything by mouth to an unconscious person. Rinse mouth with water. Consult a physician.

4.2 **Most important symptoms and effects, both acute and delayed**
The most important known symptoms and effects are described in the labelling (see section 2.2) and/or in section 11

4.3 **Indication of any immediate medical attention and special treatment needed**
no data available

SECTION 5: Firefighting measures

5.1   Extinguishing media

Suitable extinguishing media
Use water spray, alcohol-resistant foam, dry chemical or carbon dioxide.

5.2   Special hazards arising from the substance or mixture
Carbon oxides, nitrogen oxides (NOx), Sulphur oxides

5.3   Advice for firefighters
Wear self contained breathing apparatus for fire fighting if necessary.

5.4   Further information
no data available

SECTION 6: Accidental release measures

6.1   Personal precautions, protective equipment and emergency procedures
Use personal protective equipment. Avoid dust formation. Avoid breathing vapours, mist or gas. Ensure adequate ventilation. Evacuate personnel to safe areas. Avoid breathing dust.
For personal protection see section 8.

6.2   Environmental precautions
Prevent further leakage or spillage if safe to do so. Do not let product enter drains. Discharge into the environment must be avoided.

6.3   Methods and materials for containment and cleaning up
Pick up and arrange disposal without creating dust. Sweep up and shovel. Keep in suitable, closed containers for disposal.

6.4   Reference to other sections
For disposal see section 13.

SECTION 7: Handling and storage

7.1   Precautions for safe handling
Avoid contact with skin and eyes. Avoid formation of dust and aerosols.
Provide appropriate exhaust ventilation at places where dust is formed.
For precautions see section 2.2.

7.2   Conditions for safe storage, including any incompatibilities
Store in cool place. Keep container tightly closed in a dry and well-ventilated place.

7.3   Specific end use(s)
Apart from the uses mentioned in section 1.2 no other specific uses are stipulated

SECTION 8: Exposure controls/personal protection

8.1   Control parameters

Components with workplace control parameters

8.2   Exposure controls

Appropriate engineering controls
Handle in accordance with good industrial hygiene and safety practice. Wash hands before breaks and at the end of workday.

Personal protective equipment

Eye/face protection
Face shield and safety glasses Use equipment for eye protection tested and approved under appropriate government standards such as NIOSH (US) or EN 166(EU).

Skin protection
Handle with gloves. Gloves must be inspected prior to use. Use proper glove removal technique (without touching glove's outer surface) to avoid skin contact with this product. Dispose of contaminated gloves after use in accordance with applicable laws and good laboratory practices. Wash and dry hands.

The selected protective gloves have to satisfy the specifications of EU Directive 89/686/EEC and the standard EN 374 derived from it.

Full contact
Material: Nitrile rubber
Minimum layer thickness: 0,11 mm
Break through time: 480 min
Material tested:Dermatril® (KCL 740 / Aldrich Z677272, Size M)

Splash contact
Material: Nitrile rubber
Minimum layer thickness: 0,11 mm
Break through time: 480 min
Material tested:Dermatril® (KCL 740 / Aldrich Z677272, Size M)

data source: KCL GmbH, D-36124 Eichenzell, phone +49 (0)6659 87300, e-mail sales@kcl.de, test method: EN374
If used in solution, or mixed with other substances, and under conditions which differ from EN 374, contact the supplier of the CE approved gloves. This recommendation is advisory only and must be evaluated by an industrial hygienist and safety officer familiar with the specific situation of anticipated use by our customers. It should not be construed as offering an approval for any specific use scenario.

Body Protection
Complete suit protecting against chemicals, The type of protective equipment must be selected according to the concentration and amount of the dangerous substance at the specific workplace.

Respiratory protection
For nuisance exposures use type P95 (US) or type P1 (EU EN 143) particle respirator.For higher level protection use type OV/AG/P99 (US) or type ABEK-P2 (EU EN 143) respirator cartridges. Use respirators and components tested and approved under appropriate government standards such as NIOSH (US) or CEN (EU).

Control of environmental exposure
Prevent further leakage or spillage if safe to do so. Do not let product enter drains. Discharge into the environment must be avoided.

SECTION 9: Physical and chemical properties

9.1   Information on basic physical and chemical properties

a)	Appearance	Form: pellets Colour: light yellow
b)	Odour	odourless
c)	Odour Threshold	no data available
d)	pH	7 at 10 g/l at 20 °C
e)	Melting point/freezing point	Melting point/range: 182 - 187 °C - lit. Melting point/range: 183 - 187 °C
f)	Initial boiling point and boiling range	371 °C - lit.
g)	Flash point	no data available
h)	Evapouration rate	no data available
i)	Flammability (solid, gas)	The product is not flammable. - Flammability (solids)
j)	Upper/lower	no data available

flammability or
explosive limits

k)	Vapour pressure	53 hPa at 290 °C
l)	Vapour density	no data available
m)	Relative density	no data available
n)	Water solubility	0,127 g/l at 23 °C - OECD Test Guideline 105 - slightly soluble
o)	Partition coefficient: n-octanol/water	log Pow: ca.3,78 at 25 °C
p)	Auto-ignition temperature	397 °C at 1.013 hPa
q)	Decomposition temperature	> 250 °C -
r)	Viscosity	no data available
s)	Explosive properties	no data available
t)	Oxidizing properties	no data available

9.2   Other safety information

Bulk density   0,65 g/l

SECTION 10: Stability and reactivity

10.1   Reactivity
no data available

10.2   Chemical stability
Stable under recommended storage conditions.

10.3   Possibility of hazardous reactions
no data available

10.4   Conditions to avoid
no data available

10.5   Incompatible materials
Strong oxidizing agents

10.6   Hazardous decomposition products
Other decomposition products - no data available
In the event of fire: see section 5

SECTION 11: Toxicological information

11.1   Information on toxicological effects

Acute toxicity
LD50 Oral - rat - male and female - 1.370 mg/kg

LD50 Dermal - rat - male and female - > 2.000 mg/kg
(OECD Test Guideline 402)

Skin corrosion/irritation
Skin - rabbit
Result: No skin irritation - 4 h
(OECD Test Guideline 404)

Serious eye damage/eye irritation
Eyes - rabbit
Result: No eye irritation
(OECD Test Guideline 405)

Respiratory or skin sensitisation
Causes photosensitivity. Exposure to light can result in allergic reactions resulting in dermatologic lesions, which can vary from sunburnlike responses to edematous, vesiculated lesions, or bullae

Maximisation Test - guinea pig
May cause sensitisation by skin contact.
(OECD Test Guideline 406)

Germ cell mutagenicity
Ames test
S. typhimurium
Result: negative

rat - male
Result: negative

Carcinogenicity

IARC: No component of this product present at levels greater than or equal to 0.1% is identified as probable, possible or confirmed human carcinogen by IARC.

Reproductive toxicity

Reproductive toxicity - rat - Oral
Effects on Fertility: Post-implantation mortality (e.g., dead and/or resorbed implants per total number of implants).

Specific target organ toxicity - single exposure
no data available

Specific target organ toxicity - repeated exposure
Oral - May cause damage to organs through prolonged or repeated exposure. - Blood

Aspiration hazard
no data available

Additional Information
RTECS: SN5075000

anemia, Discoloration of the skin.

SECTION 12: Ecological information

12.1 Toxicity

Toxicity to fish	static test LC50 - Oncorhynchus mykiss (rainbow trout) - 70,7 mg/l - 96 h (OECD Test Guideline 203)
Toxicity to daphnia and other aquatic invertebrates	static test EC50 - Daphnia magna (Water flea) - 11,92 mg/l - 48 h (OECD Test Guideline 202)
Toxicity to algae	static test EC50 - Desmodesmus subspicatus (green algae) - > 100 mg/l - 72 h (OECD Test Guideline 201)
Toxicity to bacteria	Respiration inhibition IC50 - Sludge Treatment - > 100 mg/l - 3 h (OECD Test Guideline 209)

12.2 Persistence and degradability
Biodegradability	aerobic Result: 0 % - Not readily biodegradable. (OECD Test Guideline 301D)
Chemical Oxygen Demand (COD)	2.337 mg/g

12.3 Bioaccumulative potential
Bioaccumulation	Cyprinus carpio (Carp) - 56 d

at 25 °C - 0,02 mg/l

Bioconcentration factor (BCF): 127 - 660

12.4   Mobility in soil
no data available

12.5   Results of PBT and vPvB assessment
PBT/vPvB assessment not available as chemical safety assessment not required/not conducted

12.6   Other adverse effects
Harmful to aquatic life with long lasting effects.

Additional ecological   no data available
information

Dissolved organic   8 mg/g
carbon (DOC)

SECTION 13: Disposal considerations

13.1   Waste treatment methods

Product
Offer surplus and non-recyclable solutions to a licensed disposal company. Dissolve or mix the material with a combustible solvent and burn in a chemical incinerator equipped with an afterburner and scrubber.

Contaminated packaging
Dispose of as unused product.

SECTION 14: Transport information

14.1   UN number
ADR/RID: -   IMDG: -   IATA: -

14.2   UN proper shipping name
ADR/RID: Not dangerous goods
IMDG: Not dangerous goods
IATA: Not dangerous goods

14.3   Transport hazard class(es)
ADR/RID: -   IMDG: -   IATA: -

14.4   Packaging group
ADR/RID: -   IMDG: -   IATA: -

14.5   Environmental hazards
ADR/RID: no   IMDG Marine pollutant: no   IATA: no

14.6   Special precautions for user
no data available

SECTION 15: Regulatory information

This safety datasheet complies with the requirements of Regulation (EC) No. 1907/2006.

15.1   Safety, health and environmental regulations/legislation specific for the substance or mixture

no data available

15.2   Chemical Safety Assessment
For this product a chemical safety assessment was not carried out

SECTION 16: Other information

Full text of H-Statements referred to under sections 2 and 3.

Acute Tox.	Acute toxicity
Aquatic Chronic	Chronic aquatic toxicity
H302	Harmful if swallowed.
H317	May cause an allergic skin reaction.
H373	May cause damage to organs through prolonged or repeated exposure if swallowed.
H412	Harmful to aquatic life with long lasting effects.
Skin Sens.	Skin sensitisation
STOT RE	Specific target organ toxicity - repeated exposure

Full text of R-phrases referred to under sections 2 and 3

Xn	Harmful
R22	Harmful if swallowed.
R43	May cause sensitisation by skin contact.
R48/22	Harmful: danger of serious damage to health by prolonged exposure if swallowed.
R52/53	Harmful to aquatic organisms, may cause long-term adverse effects in the aquatic environment.

Further information

SIGMA-ALDRICH

SAFETY DATA SHEET

SECTION 1: Identification of the substance/mixture and of the company/undertaking

1.1 Product identifiers

Product name : **Phosphoric acid, 85%**

Product Number	:	P5811
Brand	:	Sigma
REACH No.	:	A registration number is not available for this substance as the substance or its uses are exempted from registration, the annual tonnage does not require a registration or the registration is envisaged for a later registration deadline.
CAS-No.	:	7664-38-2

1.2 Relevant identified uses of the substance or mixture and uses advised against

Identified uses : Laboratory chemicals, Manufacture of substances

1.3 Details of the supplier of the safety data sheet

Company	:	Sigma-Aldrich BVBA
		Brusselsesteenweg 288
		B-3090 OVERIJSE
Telephone	:	+32 3 899 1301
Fax	:	+32 3 899 1311
E-mail address	:	eurtechserv@sial.com

1.4 Emergency telephone number

Emergency Phone #	:	+(32) 28 083237 (CHEMTREC)
		070 245245 (Anti-poison centre)

SECTION 2: Hazards identification

2.1 Classification of the substance or mixture

Classification according to Regulation (EC) No 1272/2008
Corrosive to metals (Category 1), H290
Skin corrosion (Category 1B), H314

For the full text of the H-Statements mentioned in this Section, see Section 16.

Classification according to EU Directives 67/548/EEC or 1999/45/EC

C	Corrosive		R34

For the full text of the R-phrases mentioned in this Section, see Section 16.

2.2 Label elements

Labelling according Regulation (EC) No 1272/2008
Pictogram

Signal word   Danger

Hazard statement(s)
H290	May be corrosive to metals.
H314	Causes severe skin burns and eye damage.

Precautionary statement(s)

P280	Wear protective gloves/ protective clothing/ eye protection/ face protection.
P305 + P351 + P338	IF IN EYES: Rinse cautiously with water for several minutes. Remove contact lenses, if present and easy to do. Continue rinsing.
P310	Immediately call a POISON CENTER or doctor/ physician.

Supplemental Hazard   none
Statements

According to European Directive 67/548/EEC as amended.
Hazard symbol(s)   C   Corrosive

R-phrase(s)
R34   Causes burns.

S-phrase(s)
S26   In case of contact with eyes, rinse immediately with plenty of water and
                           seek medical advice.
S45   In case of accident or if you feel unwell, seek medical advice immediately
                           (show the label where possible).

2.3   Other hazards - none

SECTION 3: Composition/information on ingredients

3.2   Mixtures

Synonyms	:	Orthophosphoric acid
Formula	:	H_3O_4P
Molecular Weight	:	98,00 g/mol

Hazardous ingredients according to Regulation (EC) No 1272/2008

Component			Classification	Concentration
Phosphoric acid				
CAS-No.	7664-38-2		Met. Corr. 1; Skin Corr. 1B; H290, H314	50 - 100 %
EC-No.	231-633-2			
Index-No.	015-011-00-6			

Hazardous ingredients according to Directive 1999/45/EC

Component			Classification	Concentration
Phosphoric acid				
CAS-No.	7664-38-2		C, R34	50 - 100 %
EC-No.	231-633-2			
Index-No.	015-011-00-6			

For the full text of the H-Statements and R-Phrases mentioned in this Section, see Section 16

SECTION 4: First aid measures

4.1   Description of first aid measures

General advice
Consult a physician. Show this safety data sheet to the doctor in attendance.

If inhaled
If breathed in, move person into fresh air. If not breathing, give artificial respiration. Consult a physician.

In case of skin contact
Take off contaminated clothing and shoes immediately. Wash off with soap and plenty of water. Consult a physician.

In case of eye contact
Rinse thoroughly with plenty of water for at least 15 minutes and consult a physician.

If swallowed
Do NOT induce vomiting. Never give anything by mouth to an unconscious person. Rinse mouth with water. Consult a physician.

4.2   Most important symptoms and effects, both acute and delayed
The most important known symptoms and effects are described in the labelling (see section 2.2) and/or in section 11

4.3   Indication of any immediate medical attention and special treatment needed
no data available

SECTION 5: Firefighting measures

5.1   Extinguishing media

Suitable extinguishing media
Use water spray, alcohol-resistant foam, dry chemical or carbon dioxide.

5.2   Special hazards arising from the substance or mixture
Thermal decomposition may produce toxic fumes of phosphorus oxides and/or phosphine
Oxides of phosphorus

5.3   Advice for firefighters
Wear self contained breathing apparatus for fire fighting if necessary.

5.4   Further information
no data available

SECTION 6: Accidental release measures

6.1   Personal precautions, protective equipment and emergency procedures
Wear respiratory protection. Avoid breathing vapours, mist or gas. Ensure adequate ventilation. Evacuate personnel to safe areas.
For personal protection see section 8.

6.2   Environmental precautions
Do not let product enter drains.

6.3   Methods and materials for containment and cleaning up
Soak up with inert absorbent material and dispose of as hazardous waste. Keep in suitable, closed containers for disposal.

6.4   Reference to other sections
For disposal see section 13.

SECTION 7: Handling and storage

7.1   Precautions for safe handling
Avoid inhalation of vapour or mist.
For precautions see section 2.2.

7.2   Conditions for safe storage, including any incompatibilities
Store in cool place. Keep container tightly closed in a dry and well-ventilated place. Containers which are opened must be carefully resealed and kept upright to prevent leakage.

7.3   Specific end use(s)
Apart from the uses mentioned in section 1.2 no other specific uses are stipulated

SECTION 8: Exposure controls/personal protection

8.1   Control parameters

Components with workplace control parameters

8.2   Exposure controls

Appropriate engineering controls
Handle in accordance with good industrial hygiene and safety practice. Wash hands before breaks and at the end of workday.

Personal protective equipment

Eye/face protection
Tightly fitting safety goggles. Faceshield (8-inch minimum). Use equipment for eye protection tested and approved under appropriate government standards such as NIOSH (US) or EN 166(EU).

Skin protection
Handle with gloves. Gloves must be inspected prior to use. Use proper glove removal technique (without touching glove's outer surface) to avoid skin contact with this product. Dispose of contaminated gloves after use in accordance with applicable laws and good laboratory practices. Wash and dry hands.

The selected protective gloves have to satisfy the specifications of EU Directive 89/686/EEC and the standard EN 374 derived from it.

Full contact
Material: Nitrile rubber
Minimum layer thickness: 0,11 mm
Break through time: 480 min
Material tested:Dermatril® (KCL 740 / Aldrich Z677272, Size M)

Splash contact
Material: Nitrile rubber
Minimum layer thickness: 0,11 mm
Break through time: 480 min
Material tested:Dermatril® (KCL 740 / Aldrich Z677272, Size M)

data source: KCL GmbH, D-36124 Eichenzell, phone +49 (0)6659 87300, e-mail sales@kcl.de, test method: EN374
If used in solution, or mixed with other substances, and under conditions which differ from EN 374, contact the supplier of the CE approved gloves. This recommendation is advisory only and must be evaluated by an industrial hygienist and safety officer familiar with the specific situation of anticipated use by our customers. It should not be construed as offering an approval for any specific use scenario.

Body Protection
Complete suit protecting against chemicals, The type of protective equipment must be selected according to the concentration and amount of the dangerous substance at the specific workplace.

Respiratory protection
Where risk assessment shows air-purifying respirators are appropriate use a full-face respirator with multi-purpose combination (US) or type ABEK (EN 14387) respirator cartridges as a backup to engineering controls. If the respirator is the sole means of protection, use a full-face supplied air respirator. Use respirators and components tested and approved under appropriate government standards such as NIOSH (US) or CEN (EU).

Control of environmental exposure
Do not let product enter drains.

SECTION 9: Physical and chemical properties

9.1   Information on basic physical and chemical properties

a)	Appearance	Form: liquid, clear
b)	Odour	no data available
c)	Odour Threshold	no data available
d)	pH	no data available
e)	Melting point/freezing point	Melting point/range: 40 °C - lit.
f)	Initial boiling point and boiling range	158 °C - lit.
g)	Flash point	no data available
h)	Evapouration rate	no data available
i)	Flammability (solid, gas)	no data available
j)	Upper/lower flammability or explosive limits	no data available
k)	Vapour pressure	no data available
l)	Vapour density	no data available
m)	Relative density	1,685 g/cm3 at 25 °C
n)	Water solubility	no data available
o)	Partition coefficient: n-octanol/water	no data available
p)	Auto-ignition temperature	no data available
q)	Decomposition temperature	no data available
r)	Viscosity	no data available
s)	Explosive properties	no data available
t)	Oxidizing properties	no data available

9.2   Other safety information
no data available

SECTION 10: Stability and reactivity

10.1   Reactivity
no data available

10.2   Chemical stability
Stable under recommended storage conditions.

10.3   Possibility of hazardous reactions
no data available

10.4   Conditions to avoid
no data available

10.5   Incompatible materials
Strong bases, Powdered metals

10.6   Hazardous decomposition products
Other decomposition products - no data available

In the event of fire: see section 5

SECTION 11: Toxicological information

11.1   Information on toxicological effects

Acute toxicity
no data available

Skin corrosion/irritation
no data available

Serious eye damage/eye irritation
no data available

Respiratory or skin sensitisation
no data available

Germ cell mutagenicity
no data available

Carcinogenicity

IARC: No component of this product present at levels greater than or equal to 0.1% is identified as
             probable, possible or confirmed human carcinogen by IARC.

Reproductive toxicity
no data available

Specific target organ toxicity - single exposure
no data available

Specific target organ toxicity - repeated exposure
no data available

Aspiration hazard
no data available

Additional Information
RTECS: Not available

burning sensation, Cough, wheezing, laryngitis, Shortness of breath, spasm, inflammation and edema of
the larynx, spasm, inflammation and edema of the bronchi, pneumonitis, pulmonary edema, Material is
extremely destructive to tissue of the mucous membranes and upper respiratory tract, eyes, and skin.

SECTION 12: Ecological information

12.1   Toxicity
no data available

12.2   Persistence and degradability
no data available

12.3   Bioaccumulative potential
no data available

12.4   Mobility in soil
no data available

12.5   Results of PBT and vPvB assessment
PBT/vPvB assessment not available as chemical safety assessment not required/not conducted

12.6   Other adverse effects
no data available

SECTION 13: Disposal considerations

13.1   Waste treatment methods

Product
Offer surplus and non-recyclable solutions to a licensed disposal company.

Contaminated packaging
Dispose of as unused product.

SECTION 14: Transport information

14.1   UN number
ADR/RID: 1805   IMDG: 1805   IATA: 1805

14.2   UN proper shipping name
ADR/RID: PHOSPHORIC ACID SOLUTION
IMDG: PHOSPHORIC ACID SOLUTION
IATA: Phosphoric acid, solution

14.3   Transport hazard class(es)
ADR/RID: 8   IMDG: 8   IATA: 8

14.4   Packaging group
ADR/RID: III   IMDG: III   IATA: III

14.5   Environmental hazards
ADR/RID: no   IMDG Marine pollutant: no   IATA: no

14.6   Special precautions for user
no data available

SECTION 15: Regulatory information

This safety datasheet complies with the requirements of Regulation (EC) No. 1907/2006.

15.1   Safety, health and environmental regulations/legislation specific for the substance or mixture

no data available

15.2   Chemical Safety Assessment
For this product a chemical safety assessment was not carried out

SECTION 16: Other information

Full text of H-Statements referred to under sections 2 and 3.

H290   May be corrosive to metals.
H314   Causes severe skin burns and eye damage.
Met. Corr.   Corrosive to metals
Skin Corr.   Skin corrosion

Full text of R-phrases referred to under sections 2 and 3

C   Corrosive
R34   Causes burns.

Further information
Copyright 2014 Sigma-Aldrich Co. LLC. License granted to make unlimited paper copies for internal use only.
The above information is believed to be correct but does not purport to be all inclusive and shall be used only as a guide. The information in this document is based on the present state of our knowledge and is applicable to the product with regard to appropriate safety precautions. It does not represent any guarantee of the properties of the product. Sigma-Aldrich Corporation and its Affiliates shall not be held

liable for any damage resulting from handling or from contact with the above product. See www.sigma-aldrich.com and/or the reverse side of invoice or packing slip for additional terms and conditions of sale.

SIGMA-ALDRICH

sigma-aldrich.com

SAFETY DATA SHEET

according to Regulation (EC) No. 453/2010
Version 5.8 Revision Date 26.11.2015
Print Date 15.08.2017
GENERIC EU MSDS - NO COUNTRY SPECIFIC DATA - NO OEL DATA

SECTION 1: Identification of the substance/mixture and of the company/undertaking

1.1 Product identifiers

Product name : **Triphenyl phosphite**

Product Number : T84654
Brand : Aldrich
REACH No. : A registration number is not available for this substance as the substance or its uses are exempted from registration, the annual tonnage does not require a registration or the registration is envisaged for a later registration deadline.
CAS-No. : 101-02-0

1.2 Relevant identified uses of the substance or mixture and uses advised against

Identified uses : Laboratory chemicals, Manufacture of substances

1.3 Details of the supplier of the safety data sheet

Company : Sigma-Aldrich BVBA
Brusselsesteenweg 288
B-3090 OVERIJSE

Telephone : +32 3 899 1301
Fax : +32 3 899 1311
E-mail address : eurtechserv@sial.com

1.4 Emergency telephone number

Emergency Phone # +(32) 28 083237 (CHEMTREC)
070 245245 (Anti-poison centre)

SECTION 2: Hazards identification

2.1 Classification of the substance or mixture

Classification according to Regulation (EC) No 1272/2008
Acute toxicity, Oral (Category 4), H302
Skin irritation (Category 2), H315
Eye irritation (Category 2), H319
Skin sensitisation (Category 1), H317
Acute aquatic toxicity (Category 1), H400
Chronic aquatic toxicity (Category 1), H410

For the full text of the H-Statements mentioned in this Section, see Section 16.

2.2 Label elements

Labelling according Regulation (EC) No 1272/2008
Pictogram

Signal word Warning

Hazard statement(s)

H302	Harmful if swallowed.
H315	Causes skin irritation.
H317	May cause an allergic skin reaction.
H319	Causes serious eye irritation.
H410	Very toxic to aquatic life with long lasting effects.

Precautionary statement(s)

P280	Wear protective gloves.
P301 + P312 + P330	IF SWALLOWED: Call a POISON CENTER or doctor/ physician if you feel unwell. Rinse mouth.
P305 + P351 + P338	IF IN EYES: Rinse cautiously with water for several minutes. Remove contact lenses, if present and easy to do. Continue rinsing.

Supplemental Hazard   none
Statements

2.3   Other hazards

This substance/mixture contains no components considered to be either persistent, bioaccumulative and toxic (PBT), or very persistent and very bioaccumulative (vPvB) at levels of 0.1% or higher.

SECTION 3: Composition/information on ingredients

3.1   Substances

Formula	:	$C_{18}H_{15}O_3P$
Molecular weight	:	310,28 g/mol
CAS-No.	:	101-02-0

Hazardous ingredients according to Regulation (EC) No 1272/2008

Component			Classification	Concentration
Triphenyl phosphite				
CAS-No.	101-02-0		Acute Tox. 4; Skin Irrit. 2; Eye Irrit. 2; Skin Sens. 1; Aquatic Acute 1; Aquatic Chronic 1; H302, H315, H319, H317, H400, H410 Concentration limits: >= 5 %: Skin Irrit. 2, H315; >= 5 %: Eye Irrit. 2, H319; M-Factor - Aquatic Acute: 10	<= 100 %
EC-No.	202-908-4			
Index-No.	015-105-00-7			
Phenol				
CAS-No.	108-95-2		Acute Tox. 3; Skin Corr. 1B; Muta. 2; STOT RE 2; Aquatic Chronic 2; H301, H331, H311, H314, H341, H373, H411 Concentration limits: >= 3 %: Skin Corr. 1B, H314; 1 - < 3 %: Skin Irrit. 2, H315; 1 - < 3 %: Eye Irrit. 2, H319;	>= 0,25 - < 1 %
EC-No.	203-632-7			
Index-No.	604-001-00-2			

For the full text of the H-Statements mentioned in this Section, see Section 16.

SECTION 4: First aid measures

4.1   Description of first aid measures

General advice

Consult a physician. Show this safety data sheet to the doctor in attendance.

If inhaled
If breathed in, move person into fresh air. If not breathing, give artificial respiration. Consult a physician.

In case of skin contact
Wash off with soap and plenty of water. Consult a physician.

In case of eye contact
Rinse thoroughly with plenty of water for at least 15 minutes and consult a physician.

If swallowed
Never give anything by mouth to an unconscious person. Rinse mouth with water. Consult a physician.

4.2   Most important symptoms and effects, both acute and delayed
The most important known symptoms and effects are described in the labelling (see section 2.2) and/or in section 11

4.3   Indication of any immediate medical attention and special treatment needed
No data available

SECTION 5: Firefighting measures

5.1   Extinguishing media

Suitable extinguishing media
Use water spray, alcohol-resistant foam, dry chemical or carbon dioxide.

5.2   Special hazards arising from the substance or mixture
Carbon oxides, Oxides of phosphorus

5.3   Advice for firefighters
Wear self-contained breathing apparatus for firefighting if necessary.

5.4   Further information
No data available

SECTION 6: Accidental release measures

6.1   Personal precautions, protective equipment and emergency procedures
Use personal protective equipment. Avoid breathing vapours, mist or gas. Ensure adequate ventilation. For personal protection see section 8.

6.2   Environmental precautions
Prevent further leakage or spillage if safe to do so. Do not let product enter drains. Discharge into the environment must be avoided.

6.3   Methods and materials for containment and cleaning up
Soak up with inert absorbent material and dispose of as hazardous waste. Keep in suitable, closed containers for disposal.

6.4   Reference to other sections
For disposal see section 13.

SECTION 7: Handling and storage

7.1   Precautions for safe handling
Avoid contact with skin and eyes. Avoid inhalation of vapour or mist.
For precautions see section 2.2.

7.2   Conditions for safe storage, including any incompatibilities
Store in cool place. Keep container tightly closed in a dry and well-ventilated place. Containers which are opened must be carefully resealed and kept upright to prevent leakage.

Moisture sensitive.
Storage class (TRGS 510): Combustible liquids

7.3   Specific end use(s)
Apart from the uses mentioned in section 1.2 no other specific uses are stipulated

SECTION 8: Exposure controls/personal protection

8.1   Control parameters

     Components with workplace control parameters

8.2   Exposure controls

     Appropriate engineering controls
Handle in accordance with good industrial hygiene and safety practice. Wash hands before breaks and at the end of workday.

     Personal protective equipment

        Eye/face protection
Face shield and safety glasses Use equipment for eye protection tested and approved under appropriate government standards such as NIOSH (US) or EN 166(EU).

        Skin protection
Handle with gloves. Gloves must be inspected prior to use. Use proper glove removal technique (without touching glove's outer surface) to avoid skin contact with this product. Dispose of contaminated gloves after use in accordance with applicable laws and good laboratory practices. Wash and dry hands.

The selected protective gloves have to satisfy the specifications of EU Directive 89/686/EEC and the standard EN 374 derived from it.

Full contact
Material: Nitrile rubber
Minimum layer thickness: 0,4 mm
Break through time: 480 min
Material tested:Camatril® (KCL 730 / Aldrich Z677442, Size M)

Splash contact
Material: Nitrile rubber
Minimum layer thickness: 0,4 mm
Break through time: 480 min
Material tested:Camatril® (KCL 730 / Aldrich Z677442, Size M)

data source: KCL GmbH, D-36124 Eichenzell, phone +49 (0)6659 87300, e-mail sales@kcl.de, test method: EN374
If used in solution, or mixed with other substances, and under conditions which differ from EN 374, contact the supplier of the CE approved gloves. This recommendation is advisory only and must be evaluated by an industrial hygienist and safety officer familiar with the specific situation of anticipated use by our customers. It should not be construed as offering an approval for any specific use scenario.

        Body Protection
Complete suit protecting against chemicals, The type of protective equipment must be selected according to the concentration and amount of the dangerous substance at the specific workplace.

        Respiratory protection
Where risk assessment shows air-purifying respirators are appropriate use a full-face respirator with multi-purpose combination (US) or type ABEK (EN 14387) respirator cartridges as a backup to engineering controls. If the respirator is the sole means of protection, use a full-face supplied air respirator. Use respirators and components tested and approved under appropriate government standards such as NIOSH (US) or CEN (EU).

        Control of environmental exposure
Prevent further leakage or spillage if safe to do so. Do not let product enter drains. Discharge into the environment must be avoided.

SECTION 9: Physical and chemical properties

9.1   Information on basic physical and chemical properties

a)	Appearance	Form: liquid Colour: clear
b)	Odour	No data available
c)	Odour Threshold	No data available
d)	pH	No data available
e)	Melting point/freezing point	Melting point/range: 22 - 24 °C - lit.
f)	Initial boiling point and boiling range	360 °C - lit.
g)	Flash point	210 °C
h)	Evaporation rate	No data available
i)	Flammability (solid, gas)	No data available
j)	Upper/lower flammability or explosive limits	No data available
k)	Vapour pressure	>= 0,00 hPa at 25 °C
l)	Vapour density	No data available
m)	Relative density	1,184 g/mL at 25 °C
n)	Water solubility	No data available
o)	Partition coefficient: n-octanol/water	No data available
p)	Auto-ignition temperature	> 400 °C at 1.013,250 hPa
q)	Decomposition temperature	No data available
r)	Viscosity	17,7 mm2/s at 20 °C -
s)	Explosive properties	No data available
t)	Oxidizing properties	No data available

9.2   Other safety information
No data available

SECTION 10: Stability and reactivity

10.1   Reactivity
No data available

10.2   Chemical stability
Stable under recommended storage conditions.
Contains the following stabiliser(s):
Phenol (0,5 %)

10.3   Possibility of hazardous reactions
No data available

10.4   Conditions to avoid
No data available

10.5 Incompatible materials
No data available

10.6 Hazardous decomposition products
Other decomposition products - No data available
In the event of fire: see section 5

SECTION 11: Toxicological information

11.1 Information on toxicological effects

Acute toxicity
LD50 Oral - Rat - male - 1.590 mg/kg
(OECD Test Guideline 401)

LC50 Inhalation - Rat - male and female - 1 h - > 6,7 mg/l
(OECD Test Guideline 403)

LD50 Dermal - Rabbit - male and female - > 2.000 mg/kg
(OECD Test Guideline 402)

Skin corrosion/irritation
No data available

Serious eye damage/eye irritation
Eyes - Rabbit
Result: Irritating to eyes. - 7 d
(OECD Test Guideline 405)

Respiratory or skin sensitisation
 - Mouse
Result: May cause sensitisation by skin contact.
(OECD Test Guideline 429)

Germ cell mutagenicity
Ames test
Salmonella typhimurium
Result: negative

OECD Test Guideline 474
Mouse - male and female
Result: negative

Carcinogenicity

IARC: 3 - Group 3: Not classifiable as to its carcinogenicity to humans (Phenol)

Reproductive toxicity

No data available

Specific target organ toxicity - single exposure
No data available

Specific target organ toxicity - repeated exposure
No data available

Aspiration hazard
No data available

Additional Information

Repeated dose   Rat - male and female - Oral - NOAEL : 15 mg/kg
toxicity
RTECS: Not available

To the best of our knowledge, the chemical, physical, and toxicological properties have not been
thoroughly investigated.

SECTION 12: Ecological information

12.1 Toxicity
No data available

12.2 Persistence and degradability
Biodegradability   aerobic - Exposure time 28 d
                          Result: 0,14 % - Not readily biodegradable.
                          (OECD Test Guideline 301D)

12.3 Bioaccumulative potential
No data available

12.4 Mobility in soil
No data available

12.5 Results of PBT and vPvB assessment
This substance/mixture contains no components considered to be either persistent, bioaccumulative and toxic (PBT), or very persistent and very bioaccumulative (vPvB) at levels of 0.1% or higher.

12.6 Other adverse effects
Very toxic to aquatic life with long lasting effects.

SECTION 13: Disposal considerations

13.1 Waste treatment methods

Product
Offer surplus and non-recyclable solutions to a licensed disposal company.

Contaminated packaging
Dispose of as unused product.

SECTION 14: Transport information

14.1 UN number
ADR/RID: 3077   IMDG: 3077   IATA: 3077

14.2 UN proper shipping name
ADR/RID: ENVIRONMENTALLY HAZARDOUS SUBSTANCE, SOLID, N.O.S. (Triphenyl phosphite)
IMDG: ENVIRONMENTALLY HAZARDOUS SUBSTANCE, SOLID, N.O.S. (Triphenyl phosphite)
IATA: Environmentally hazardous substance, solid, n.o.s. (Triphenyl phosphite)

14.3 Transport hazard class(es)
ADR/RID: 9   IMDG: 9   IATA: 9

14.4 Packaging group
ADR/RID: III   IMDG: III   IATA: III

14.5 Environmental hazards
ADR/RID: yes   IMDG Marine pollutant: yes   IATA: yes

14.6 Special precautions for user

Further information
EHS-Mark required (ADR 2.2.9.1.10, IMDG code 2.10.3) for single packagings and combination packagings containing inner packagings with Dangerous Goods > 5L for liquids or > 5kg for solids.

SECTION 15: Regulatory information

This safety datasheet complies with the requirements of Regulation (EC) No. 453/2010.

15.1 Safety, health and environmental regulations/legislation specific for the substance or mixture

15.2 Chemical Safety Assessment

For this product a chemical safety assessment was not carried out

---

SECTION 16: Other information

Full text of H-Statements referred to under sections 2 and 3.

H301	Toxic if swallowed.
H302	Harmful if swallowed.
H311	Toxic in contact with skin.
H314	Causes severe skin burns and eye damage.
H315	Causes skin irritation.
H317	May cause an allergic skin reaction.
H319	Causes serious eye irritation.
H331	Toxic if inhaled.
H341	Suspected of causing genetic defects.
H373	May cause damage to organs through prolonged or repeated exposure.
H400	Very toxic to aquatic life.
H410	Very toxic to aquatic life with long lasting effects.
H411	Toxic to aquatic life with long lasting effects.

Further information

SIGMA-ALDRICH

sigma-aldrich.com

SAFETY DATA SHEET

according to Regulation (EC) No. 453/2010
Version 5.2 Revision Date 03.12.2015
Print Date 15.08.2017
GENERIC EU MSDS - NO COUNTRY SPECIFIC DATA - NO OEL DATA

SECTION 1: Identification of the substance/mixture and of the company/undertaking

1.1   Product identifiers

Product name   :   2-Butanone

Product Number	:	443468
Brand	:	Sigma-Aldrich
Index-No.	:	606-002-00-3
REACH No.	:	A registration number is not available for this substance as the substance or its uses are exempted from registration, the annual tonnage does not require a registration or the registration is envisaged for a later registration deadline.
CAS-No.	:	78-93-3

1.2   Relevant identified uses of the substance or mixture and uses advised against

Identified uses   :   Laboratory chemicals, Manufacture of substances

1.3   Details of the supplier of the safety data sheet

Company	:	Sigma-Aldrich BVBA Brusselsesteenweg 288 B-3090 OVERIJSE
Telephone	:	+32 3 899 1301
Fax	:	+32 3 899 1311
E-mail address	:	eurtechserv@sial.com

1.4   Emergency telephone number

Emergency Phone #   +(32) 28 083237 (CHEMTREC)
                                       070 245245 (Anti-poison centre)

SECTION 2: Hazards identification

2.1   Classification of the substance or mixture

Classification according to Regulation (EC) No 1272/2008
Flammable liquids (Category 2), H225
Eye irritation (Category 2), H319
Specific target organ toxicity - single exposure (Category 3), Central nervous system, H336

For the full text of the H-Statements mentioned in this Section, see Section 16.

2.2   Label elements

Labelling according Regulation (EC) No 1272/2008
Pictogram

Signal word   Danger

Hazard statement(s)
H225   Highly flammable liquid and vapour.
H319   Causes serious eye irritation.

| H336 | May cause drowsiness or dizziness. |

Precautionary statement(s)

P210	Keep away from heat, hot surfaces, sparks, open flames and other ignition sources. No smoking.
P305 + P351 + P338	IF IN EYES: Rinse cautiously with water for several minutes. Remove contact lenses, if present and easy to do. Continue rinsing.
P370 + P378	In case of fire: Use dry powder or dry sand to extinguish.
P403 + P235	Store in a well-ventilated place. Keep cool.

Supplemental Hazard information (EU)

| EUH066 | Repeated exposure may cause skin dryness or cracking. |

2.3   Other hazards

This substance/mixture contains no components considered to be either persistent, bioaccumulative and toxic (PBT), or very persistent and very bioaccumulative (vPvB) at levels of 0.1% or higher.

SECTION 3: Composition/information on ingredients

3.1   Substances

Synonyms	:	Methyl ethyl ketone
		MEK
		Ethyl methyl ketone

Formula	:	C_4H_8O
Molecular weight	:	72,11 g/mol
CAS-No.	:	78-93-3
EC-No.	:	201-159-0
Index-No.	:	606-002-00-3

Hazardous ingredients according to Regulation (EC) No 1272/2008

Component			Classification	Concentration
Ethyl methyl ketone				
CAS-No.	78-93-3		Flam. Liq. 2; Eye Irrit. 2; STOT SE 3; H225, H319, H336	<= 100 %
EC-No.	201-159-0			
Index-No.	606-002-00-3			

For the full text of the H-Statements mentioned in this Section, see Section 16.

SECTION 4: First aid measures

4.1   Description of first aid measures

General advice
Consult a physician. Show this safety data sheet to the doctor in attendance.

If inhaled
If breathed in, move person into fresh air. If not breathing, give artificial respiration. Consult a physician.

In case of skin contact
Wash off with soap and plenty of water. Consult a physician.

In case of eye contact
Rinse thoroughly with plenty of water for at least 15 minutes and consult a physician.

If swallowed
Do NOT induce vomiting. Never give anything by mouth to an unconscious person. Rinse mouth with water. Consult a physician.

4.2 Most important symptoms and effects, both acute and delayed
The most important known symptoms and effects are described in the labelling (see section 2.2) and/or in section 11

4.3 Indication of any immediate medical attention and special treatment needed
No data available

SECTION 5: Firefighting measures

5.1 Extinguishing media

Suitable extinguishing media
Use water spray, alcohol-resistant foam, dry chemical or carbon dioxide.

5.2 Special hazards arising from the substance or mixture
Carbon oxides
Flash back possible over considerable distance., Container explosion may occur under fire conditions.

5.3 Advice for firefighters
Wear self-contained breathing apparatus for firefighting if necessary.

5.4 Further information
Use water spray to cool unopened containers.

SECTION 6: Accidental release measures

6.1 Personal precautions, protective equipment and emergency procedures
Use personal protective equipment. Avoid breathing vapours, mist or gas. Ensure adequate ventilation. Remove all sources of ignition. Evacuate personnel to safe areas. Beware of vapours accumulating to form explosive concentrations. Vapours can accumulate in low areas.
For personal protection see section 8.

6.2 Environmental precautions
Prevent further leakage or spillage if safe to do so. Do not let product enter drains.

6.3 Methods and materials for containment and cleaning up
Contain spillage, and then collect with an electrically protected vacuum cleaner or by wet-brushing and place in container for disposal according to local regulations (see section 13).

6.4 Reference to other sections
For disposal see section 13.

SECTION 7: Handling and storage

7.1 Precautions for safe handling
Avoid contact with skin and eyes. Avoid inhalation of vapour or mist.
Keep away from sources of ignition - No smoking.Take measures to prevent the build up of electrostatic charge.
For precautions see section 2.2.

7.2 Conditions for safe storage, including any incompatibilities
Store under inert gas. Store in cool place. Keep container tightly closed in a dry and well-ventilated place. Containers which are opened must be carefully resealed and kept upright to prevent leakage.

Hygroscopic.

7.3 Specific end use(s)
Apart from the uses mentioned in section 1.2 no other specific uses are stipulated

SECTION 8: Exposure controls/personal protection

8.1 **Control parameters**

Components with workplace control parameters

8.2 **Exposure controls**

Appropriate engineering controls
Handle in accordance with good industrial hygiene and safety practice. Wash hands before breaks and at the end of workday.

Personal protective equipment

Eye/face protection
Face shield and safety glasses Use equipment for eye protection tested and approved under appropriate government standards such as NIOSH (US) or EN 166(EU).

Skin protection
Handle with gloves. Gloves must be inspected prior to use. Use proper glove removal technique (without touching glove's outer surface) to avoid skin contact with this product. Dispose of contaminated gloves after use in accordance with applicable laws and good laboratory practices. Wash and dry hands.

The selected protective gloves have to satisfy the specifications of EU Directive 89/686/EEC and the standard EN 374 derived from it.

Splash contact
Material: butyl-rubber
Minimum layer thickness: 0,3 mm
Break through time: 292 min
Material tested:Butoject® (KCL 897 / Aldrich Z677647, Size M)

data source: KCL GmbH, D-36124 Eichenzell, phone +49 (0)6659 87300, e-mail sales@kcl.de, test method: EN374
If used in solution, or mixed with other substances, and under conditions which differ from EN 374, contact the supplier of the CE approved gloves. This recommendation is advisory only and must be evaluated by an industrial hygienist and safety officer familiar with the specific situation of anticipated use by our customers. It should not be construed as offering an approval for any specific use scenario.

Body Protection
Impervious clothing, Flame retardant antistatic protective clothing., The type of protective equipment must be selected according to the concentration and amount of the dangerous substance at the specific workplace.

Respiratory protection
Where risk assessment shows air-purifying respirators are appropriate use a full-face respirator with multi-purpose combination (US) or type ABEK (EN 14387) respirator cartridges as a backup to engineering controls. If the respirator is the sole means of protection, use a full-face supplied air respirator. Use respirators and components tested and approved under appropriate government standards such as NIOSH (US) or CEN (EU).

Control of environmental exposure
Prevent further leakage or spillage if safe to do so. Do not let product enter drains.

SECTION 9: Physical and chemical properties

9.1 **Information on basic physical and chemical properties**

a)	Appearance	Form: liquid, clear Colour: colourless
b)	Odour	No data available
c)	Odour Threshold	No data available

d)	pH	No data available
e)	Melting point/freezing point	-87 °C
f)	Initial boiling point and boiling range	80 °C - lit.
g)	Flash point	-3 °C - closed cup
h)	Evaporation rate	No data available
i)	Flammability (solid, gas)	No data available
j)	Upper/lower flammability or explosive limits	Upper explosion limit: 10,1 %(V) Lower explosion limit: 1,8 %(V)
k)	Vapour pressure	95 hPa at 20 °C
l)	Vapour density	2,49 - (Air = 1.0)
m)	Relative density	0,805 g/mL at 25 °C
n)	Water solubility	soluble
o)	Partition coefficient: n-octanol/water	log Pow: 0,29
p)	Auto-ignition temperature	No data available
q)	Decomposition temperature	No data available
r)	Viscosity	No data available
s)	Explosive properties	No data available
t)	Oxidizing properties	No data available

9.2   Other safety information

Surface tension	24,6 mN/m at 20 °C
Relative vapour density	2,49 - (Air = 1.0)

SECTION 10: Stability and reactivity

10.1   Reactivity
No data available

10.2   Chemical stability
Stable under recommended storage conditions.

10.3   Possibility of hazardous reactions
No data available

10.4   Conditions to avoid
Exposure to moisture
Heat, flames and sparks. Extremes of temperature and direct sunlight.

10.5   Incompatible materials
Oxidizing agents, Strong reducing agents

10.6   Hazardous decomposition products
Other decomposition products - No data available
In the event of fire: see section 5

SECTION 11: Toxicological information

11.1   Information on toxicological effects

Acute toxicity
LD50 Oral - Rat - 2.737 mg/kg

LC50 Inhalation - Mouse - 4 h - 32.000 mg/m3

LC50 Inhalation - Mammal - 38.000 mg/m3

LD50 Dermal - Rabbit - 6.480 mg/kg

Skin corrosion/irritation
Skin - Rabbit
Result: No skin irritation
(OECD Test Guideline 404)

Serious eye damage/eye irritation
Eyes - Rabbit
Result: Irritating to eyes.
(OECD Test Guideline 405)

Respiratory or skin sensitisation
No data available

Germ cell mutagenicity
No data available

Carcinogenicity

IARC: No component of this product present at levels greater than or equal to 0.1% is identified as
            probable, possible or confirmed human carcinogen by IARC.

Reproductive toxicity
No data available

Specific target organ toxicity - single exposure
May cause drowsiness or dizziness.

Specific target organ toxicity - repeated exposure
No data available

Aspiration hazard
No data available

Additional Information
RTECS: EL6475000

Central nervous system depression, Gastrointestinal disturbance, narcosis

Liver - Irregularities - Based on Human Evidence

SECTION 12: Ecological information

12.1   Toxicity

Toxicity to fish	mortality NOEC - Cyprinodon variegatus (sheepshead minnow) - 400 mg/l - 96 h
	LC50 - Pimephales promelas (fathead minnow) - 3.130 - 3.320 mg/l - 96 h
Toxicity to daphnia and other aquatic invertebrates	LC50 - Daphnia magna (Water flea) - > 520 mg/l - 48 h
	EC50 - Daphnia magna (Water flea) - 7.060 mg/l - 24 h

12.2   Persistence and degradability
No data available

12.3 Bioaccumulative potential
No data available

12.4 Mobility in soil
No data available

12.5 Results of PBT and vPvB assessment
This substance/mixture contains no components considered to be either persistent, bioaccumulative and toxic (PBT), or very persistent and very bioaccumulative (vPvB) at levels of 0.1% or higher.

12.6 Other adverse effects

No data available

SECTION 13: Disposal considerations

13.1 Waste treatment methods

Product
Burn in a chemical incinerator equipped with an afterburner and scrubber but exert extra care in igniting as this material is highly flammable. Offer surplus and non-recyclable solutions to a licensed disposal company.

Contaminated packaging
Dispose of as unused product.

SECTION 14: Transport information

14.1 UN number
ADR/RID: 1193   IMDG: 1193   IATA: 1193

14.2 UN proper shipping name
ADR/RID: ETHYL METHYL KETONE
IMDG: ETHYL METHYL KETONE
IATA: Ethyl methyl ketone

14.3 Transport hazard class(es)
ADR/RID: 3   IMDG: 3   IATA: 3

14.4 Packaging group
ADR/RID: II   IMDG: II   IATA: II

14.5 Environmental hazards
ADR/RID: no   IMDG Marine pollutant: no   IATA: no

14.6 Special precautions for user
No data available

SECTION 15: Regulatory information

This safety datasheet complies with the requirements of Regulation (EC) No. 453/2010.

15.1 Safety, health and environmental regulations/legislation specific for the substance or mixture

15.2 Chemical Safety Assessment
For this product a chemical safety assessment was not carried out

---

SECTION 16: Other information

Full text of H-Statements referred to under sections 2 and 3.

EUH066	Repeated exposure may cause skin dryness or cracking.
H225	Highly flammable liquid and vapour.
H319	Causes serious eye irritation.
H336	May cause drowsiness or dizziness.

Further information

SIGMA-ALDRICH

SAFETY DATA SHEET

SECTION 1: Identification of the substance/mixture and of the company/undertaking

1.1   Product identifiers

Product name   :   Butylated hydroxytoluene

Product Number   :   W218405
Brand   :   Aldrich
REACH No.   :   A registration number is not available for this substance as the substance
                                              or its uses are exempted from registration, the annual tonnage does not
                                              require a registration or the registration is envisaged for a later
                                              registration deadline.
CAS-No.   :   128-37-0

1.2   Relevant identified uses of the substance or mixture and uses advised against

Identified uses   :   Laboratory chemicals, Manufacture of substances

1.3   Details of the supplier of the safety data sheet

Company   :   Sigma-Aldrich BVBA
                                             Brusselsesteenweg 288
                                             B-3090 OVERIJSE

Telephone   :   +32 3 899 1301
Fax   :   +32 3 899 1311
E-mail address   :   eurtechserv@sial.com

1.4   Emergency telephone number

Emergency Phone #   :   +(32) 28 083237 (CHEMTREC)
                                             070 245245 (Anti-poison centre)

SECTION 2: Hazards identification

2.1   Classification of the substance or mixture

Classification according to Regulation (EC) No 1272/2008
Acute aquatic toxicity (Category 1), H400
Chronic aquatic toxicity (Category 1), H410

For the full text of the H-Statements mentioned in this Section, see Section 16.

Classification according to EU Directives 67/548/EEC or 1999/45/EC

N	Dangerous for the environment	R50/53

For the full text of the R-phrases mentioned in this Section, see Section 16.

2.2   Label elements

Labelling according Regulation (EC) No 1272/2008
Pictogram

Signal word   Warning

Hazard statement(s)
H410   Very toxic to aquatic life with long lasting effects.

Precautionary statement(s)
P273	Avoid release to the environment.
P501	Dispose of contents/ container to an approved waste disposal plant.

Supplemental Hazard   none
Statements

2.3   **Other hazards** - none

SECTION 3: Composition/information on ingredients

3.1   **Substances**

Synonyms	:	2,6-Di-tert-butyl-4-methylphenol
		BHT
		DBPC
		2,6-Di-tert-butyl-p-cresol
		Butylhydroxytoluene
		Butylated hydroxytoluene

Formula	:	$C_{15}H_{24}O$
Molecular Weight	:	220,35 g/mol
CAS-No.	:	128-37-0
EC-No.	:	204-881-4

Hazardous ingredients according to Regulation (EC) No 1272/2008

Component		Classification	Concentration
2,6-di-tert-Butyl-p-cresol			
CAS-No.	128-37-0	Aquatic Acute 1; Aquatic	<= 100 %
EC-No.	204-881-4	Chronic 1; H410	

Hazardous ingredients according to Directive 1999/45/EC

Component		Classification	Concentration
2,6-di-tert-Butyl-p-cresol			
CAS-No.	128-37-0	N, R50/53	<= 100 %
EC-No.	204-881-4		

For the full text of the H-Statements and R-Phrases mentioned in this Section, see Section 16

SECTION 4: First aid measures

4.1   **Description of first aid measures**

General advice
Consult a physician. Show this safety data sheet to the doctor in attendance.

If inhaled
If breathed in, move person into fresh air. If not breathing, give artificial respiration. Consult a physician.

In case of skin contact
Wash off with soap and plenty of water. Consult a physician.

In case of eye contact
Flush eyes with water as a precaution.

If swallowed
Never give anything by mouth to an unconscious person. Rinse mouth with water. Consult a physician.

4.2   **Most important symptoms and effects, both acute and delayed**
The most important known symptoms and effects are described in the labelling (see section 2.2) and/or in section 11

4.3 **Indication of any immediate medical attention and special treatment needed**
no data available

SECTION 5: Firefighting measures

5.1 **Extinguishing media**

Suitable extinguishing media
Use water spray, alcohol-resistant foam, dry chemical or carbon dioxide.

5.2 **Special hazards arising from the substance or mixture**
Carbon oxides

5.3 **Advice for firefighters**
Wear self contained breathing apparatus for fire fighting if necessary.

5.4 **Further information**
no data available

SECTION 6: Accidental release measures

6.1 **Personal precautions, protective equipment and emergency procedures**
Avoid dust formation. Avoid breathing vapours, mist or gas. Ensure adequate ventilation.
For personal protection see section 8.

6.2 **Environmental precautions**
Prevent further leakage or spillage if safe to do so. Do not let product enter drains. Discharge into the environment must be avoided.

6.3 **Methods and materials for containment and cleaning up**
Pick up and arrange disposal without creating dust. Sweep up and shovel. Keep in suitable, closed containers for disposal.

6.4 **Reference to other sections**
For disposal see section 13.

SECTION 7: Handling and storage

7.1 **Precautions for safe handling**
Provide appropriate exhaust ventilation at places where dust is formed.
For precautions see section 2.2.

7.2 **Conditions for safe storage, including any incompatibilities**
Store in cool place. Keep container tightly closed in a dry and well-ventilated place.

7.3 **Specific end use(s)**
Apart from the uses mentioned in section 1.2 no other specific uses are stipulated

---

SECTION 8: Exposure controls/personal protection

8.1 **Control parameters**

Components with workplace control parameters

8.2 **Exposure controls**

Appropriate engineering controls
Handle in accordance with good industrial hygiene and safety practice. Wash hands before breaks and at the end of workday.

Personal protective equipment

Eye/face protection
Use equipment for eye protection tested and approved under appropriate government standards such as NIOSH (US) or EN 166(EU).

Skin protection

Handle with gloves. Gloves must be inspected prior to use. Use proper glove removal technique (without touching glove's outer surface) to avoid skin contact with this product. Dispose of contaminated gloves after use in accordance with applicable laws and good laboratory practices. Wash and dry hands.

The selected protective gloves have to satisfy the specifications of EU Directive 89/686/EEC and the standard EN 374 derived from it.

Full contact
Material: Nitrile rubber
Minimum layer thickness: 0,11 mm
Break through time: 480 min
Material tested:Dermatril® (KCL 740 / Aldrich Z677272, Size M)

Splash contact
Material: Nitrile rubber
Minimum layer thickness: 0,11 mm
Break through time: 480 min
Material tested:Dermatril® (KCL 740 / Aldrich Z677272, Size M)

data source: KCL GmbH, D-36124 Eichenzell, phone +49 (0)6659 87300, e-mail sales@kcl.de, test method: EN374
If used in solution, or mixed with other substances, and under conditions which differ from EN 374, contact the supplier of the CE approved gloves. This recommendation is advisory only and must be evaluated by an industrial hygienist and safety officer familiar with the specific situation of anticipated use by our customers. It should not be construed as offering an approval for any specific use scenario.

Body Protection

Choose body protection in relation to its type, to the concentration and amount of dangerous substances, and to the specific work-place., The type of protective equipment must be selected according to the concentration and amount of the dangerous substance at the specific workplace.

Respiratory protection

Respiratory protection is not required. Where protection from nuisance levels of dusts are desired, use type N95 (US) or type P1 (EN 143) dust masks. Use respirators and components tested and approved under appropriate government standards such as NIOSH (US) or CEN (EU).

Control of environmental exposure

Prevent further leakage or spillage if safe to do so. Do not let product enter drains. Discharge into the environment must be avoided.

SECTION 9: Physical and chemical properties

9.1   Information on basic physical and chemical properties

a)	Appearance	Form: crystalline Colour: white
b)	Odour	no data available
c)	Odour Threshold	no data available
d)	pH	no data available
e)	Melting point/freezing point	Melting point/range: 69 - 73 °C - lit.
f)	Initial boiling point and boiling range	265 °C - lit.
g)	Flash point	127,0 °C - closed cup
h)	Evapouration rate	no data available
i)	Flammability (solid, gas)	no data available
j)	Upper/lower	no data available

	flammability or explosive limits	
k)	Vapour pressure	0,01 hPa at 20,0 °C
l)	Vapour density	no data available
m)	Relative density	1,05 g/cm3 at 20 °C
n)	Water solubility	0,0004 g/l at 20 °C - slightly soluble
o)	Partition coefficient: n-octanol/water	log Pow: 5,1
p)	Auto-ignition temperature	470,0 °C
q)	Decomposition temperature	no data available
r)	Viscosity	3,47 mm2/s at 80 °C -
s)	Explosive properties	no data available
t)	Oxidizing properties	no data available

9.2   Other safety information

Solubility in other solvents	Toluene - soluble Methanol - soluble Acetone - soluble
Dissociation constant	12,2

SECTION 10: Stability and reactivity

10.1   Reactivity
no data available

10.2   Chemical stability
Stable under recommended storage conditions.

10.3   Possibility of hazardous reactions
no data available

10.4   Conditions to avoid
no data available

10.5   Incompatible materials
Acid chlorides, Acid anhydrides, Oxidizing agents, Bases, Brass, Copper

10.6   Hazardous decomposition products
Other decomposition products - no data available
In the event of fire: see section 5

SECTION 11: Toxicological information

11.1   Information on toxicological effects

Acute toxicity
LD50 Oral - rat - male and female - > 6.000 mg/kg
(OECD Test Guideline 401)

LD50 Dermal - rat - male and female - > 2.000 mg/kg
(OECD Test Guideline 402)

Skin corrosion/irritation
no data available

Serious eye damage/eye irritation
Eyes - rabbit
Result: No eye irritation
(Read-across (Analogy))

Respiratory or skin sensitisation
no data available

Germ cell mutagenicity
Ames test
S. typhimurium
Result: negative

mouse - male and female
Result: negative

Carcinogenicity

This product is or contains a component that is not classifiable as to its carcinogenicity based on its IARC, ACGIH, NTP, or EPA classification.

IARC: 3 - Group 3: Not classifiable as to its carcinogenicity to humans (2,6-di-tert-Butyl-p-cresol)

Reproductive toxicity
no data available

Specific target organ toxicity - single exposure
no data available

Specific target organ toxicity - repeated exposure
no data available

Aspiration hazard
no data available

Additional Information

Repeated dose toxicity - rat - male and female - Oral - No observed adverse effect level - 25 mg/kg
RTECS: GO7875000

To the best of our knowledge, the chemical, physical, and toxicological properties have not been thoroughly investigated.

SECTION 12: Ecological information

12.1 Toxicity

Toxicity to fish	LC50 - Oryzias latipes - 5,3 mg/l - 48 h
Toxicity to daphnia and other aquatic invertebrates	static test EC50 - Daphnia magna (Water flea) - 0,48 mg/l - 48 h (OECD Test Guideline 202)
Toxicity to bacteria	Growth inhibition EC50 - Protozoa - 1,7 mg/l - 24 h

12.2 Persistence and degradability
no data available

12.3 Bioaccumulative potential
no data available

12.4 Mobility in soil
no data available

12.5 Results of PBT and vPvB assessment
PBT/vPvB assessment not available as chemical safety assessment not required/not conducted

12.6 Other adverse effects
Very toxic to aquatic life with long lasting effects.

SECTION 13: Disposal considerations

13.1 Waste treatment methods

Product
Offer surplus and non-recyclable solutions to a licensed disposal company. Dissolve or mix the material with a combustible solvent and burn in a chemical incinerator equipped with an afterburner and scrubber.

Contaminated packaging
Dispose of as unused product.

SECTION 14: Transport information

14.1 UN number
ADR/RID: 3077   IMDG: 3077   IATA: 3077

14.2 UN proper shipping name
ADR/RID: ENVIRONMENTALLY HAZARDOUS SUBSTANCE, SOLID, N.O.S. (2,6-di-tert-Butyl-p-cresol)
IMDG: ENVIRONMENTALLY HAZARDOUS SUBSTANCE, SOLID, N.O.S. (2,6-di-tert-Butyl-p-cresol)
IATA: Environmentally hazardous substance, solid, n.o.s. (2,6-di-tert-Butyl-p-cresol)

14.3 Transport hazard class(es)
ADR/RID: 9   IMDG: 9   IATA: 9

14.4 Packaging group
ADR/RID: III   IMDG: III   IATA: III

14.5 Environmental hazards
ADR/RID: yes   IMDG Marine pollutant: yes   IATA: yes

14.6 Special precautions for user

Further information
EHS-Mark required (ADR 2.2.9.1.10, IMDG code 2.10.3) for single packagings and combination packagings containing inner packagings with Dangerous Goods > 5L for liquids or > 5kg for solids.

SECTION 15: Regulatory information

This safety datasheet complies with the requirements of Regulation (EC) No. 1907/2006.

15.1 Safety, health and environmental regulations/legislation specific for the substance or mixture

no data available

15.2 Chemical Safety Assessment
For this product a chemical safety assessment was not carried out

SECTION 16: Other information

Full text of H-Statements referred to under sections 2 and 3.

Aquatic Acute	Acute aquatic toxicity
Aquatic Chronic	Chronic aquatic toxicity
H400	Very toxic to aquatic life.
H410	Very toxic to aquatic life with long lasting effects.

Full text of R-phrases referred to under sections 2 and 3

N	Dangerous for the environment
R50/53	Very toxic to aquatic organisms, may cause long-term adverse effects in the aquatic environment.

Further information

SIGMA-ALDRICH

SAFETY DATA SHEET

1. IDENTIFICATION OF THE SUBSTANCE/MIXTURE AND OF THE COMPANY/UNDERTAKING

1.1 Product identifiers

Product name : **Bismuth neodecanoate**

Product Number : 544132
Brand : Aldrich
CAS-No. : 34364-26-6

1.2 Relevant identified uses of the substance or mixture and uses advised against

Identified uses : Laboratory chemicals, Manufacture of substances

1.3 Details of the supplier of the safety data sheet

Company : Sigma-Aldrich BVBA
Brusselsesteenweg 288
B-3090 OVERIJSE

Telephone : +32 3 899 1301
Fax : +32 3 899 1311
E-mail address : eurtechserv@sial.com

1.4 Emergency telephone number

Emergency Phone # : +(32) 28 083237 (CHEMTREC)
070 245245 (Anti-poison centre)

2. HAZARDS IDENTIFICATION

2.1 Classification of the substance or mixture

Not a hazardous substance or mixture according to Regulation (EC) No. 1272/2008.
This substance is not classified as dangerous according to Directive 67/548/EEC.

2.2 Label elements

The product does not need to be labelled in accordance with EC directives or respective national laws.

2.3 Other hazards - none

3. COMPOSITION/INFORMATION ON INGREDIENTS

3.1 Substances
Formula : $C_{30}H_{57}BiO_6$
Molecular Weight : 722,75 g/mol

4. FIRST AID MEASURES

4.1 Description of first aid measures

If inhaled
If breathed in, move person into fresh air. If not breathing, give artificial respiration.

In case of skin contact
Wash off with soap and plenty of water.

In case of eye contact
Flush eyes with water as a precaution.

If swallowed
Never give anything by mouth to an unconscious person. Rinse mouth with water.

4.2   Most important symptoms and effects, both acute and delayed

4.3   Indication of any immediate medical attention and special treatment needed
no data available

---

5.   FIREFIGHTING MEASURES

5.1   Extinguishing media

Suitable extinguishing media
Use water spray, alcohol-resistant foam, dry chemical or carbon dioxide.

5.2   Special hazards arising from the substance or mixture
Carbon oxides, Bismuth oxides

5.3   Advice for firefighters
Wear self contained breathing apparatus for fire fighting if necessary.

5.4   Further information
no data available

---

6.   ACCIDENTAL RELEASE MEASURES

6.1   Personal precautions, protective equipment and emergency procedures
Avoid breathing vapors, mist or gas.

6.2   Environmental precautions
Do not let product enter drains.

6.3   Methods and materials for containment and cleaning up
Keep in suitable, closed containers for disposal.

6.4   Reference to other sections
For disposal see section 13.

---

7.   HANDLING AND STORAGE

7.1   Precautions for safe handling
Normal measures for preventive fire protection.

7.2   Conditions for safe storage, including any incompatibilities
Store in cool place. Keep container tightly closed in a dry and well-ventilated place. Containers which are opened must be carefully resealed and kept upright to prevent leakage.

7.3   Specific end uses
no data available

---

8.   EXPOSURE CONTROLS/PERSONAL PROTECTION

8.1   Control parameters

Components with workplace control parameters

8.2   Exposure controls

Appropriate engineering controls
General industrial hygiene practice.

Personal protective equipment

Eye/face protection
Use equipment for eye protection tested and approved under appropriate government standards such as NIOSH (US) or EN 166(EU).

Skin protection
Handle with gloves. Gloves must be inspected prior to use. Use proper glove removal technique (without touching glove's outer surface) to avoid skin contact with this product. Dispose of

contaminated gloves after use in accordance with applicable laws and good laboratory practices. Wash and dry hands.

The selected protective gloves have to satisfy the specifications of EU Directive 89/686/EEC and the standard EN 374 derived from it.

Body Protection
impervious clothing, The type of protective equipment must be selected according to the concentration and amount of the dangerous substance at the specific workplace.

Respiratory protection
Respiratory protection not required. For nuisance exposures use type OV/AG (US) or type ABEK (EU EN 14387) respirator cartridges. Use respirators and components tested and approved under appropriate government standards such as NIOSH (US) or CEN (EU).

9. PHYSICAL AND CHEMICAL PROPERTIES

9.1 Information on basic physical and chemical properties

a)	Appearance	Form: liquid Colour: light yellow
b)	Odour	no data available
c)	Odour Threshold	no data available
d)	pH	no data available
e)	Melting point/freezing point	no data available
f)	Initial boiling point and boiling range	300 °C
g)	Flash point	> 110,00 °C - closed cup
h)	Evaporation rate	no data available
i)	Flammability (solid, gas)	no data available
j)	Upper/lower flammability or explosive limits	no data available
k)	Vapour pressure	no data available
l)	Vapour density	no data available
m)	Relative density	1,145 g/mL at 25 °C
n)	Water solubility	no data available
o)	Partition coefficient: n-octanol/water	no data available
p)	Autoignition temperature	no data available
q)	Decomposition temperature	no data available
r)	Viscosity	no data available
s)	Explosive properties	no data available
t)	Oxidizing properties	no data available

9.2 Other safety information
no data available

10. STABILITY AND REACTIVITY

10.1 Reactivity
no data available

10.2 Chemical stability
no data available

10.3 Possibility of hazardous reactions
no data available

10.4 Conditions to avoid
no data available

10.5 Incompatible materials
Strong oxidizing agents

10.6 Hazardous decomposition products
Other decomposition products - no data available

11. TOXICOLOGICAL INFORMATION

11.1 Information on toxicological effects

Acute toxicity
no data available

Skin corrosion/irritation
no data available

Serious eye damage/eye irritation
no data available

Respiratory or skin sensitization
no data available

Germ cell mutagenicity
no data available

Carcinogenicity

IARC: No component of this product present at levels greater than or equal to 0.1% is identified as
           probable, possible or confirmed human carcinogen by IARC.

Reproductive toxicity
no data available

Specific target organ toxicity - single exposure
no data available

Specific target organ toxicity - repeated exposure
no data available

Aspiration hazard
no data available

Potential health effects

Inhalation	May be harmful if inhaled. May cause respiratory tract irritation.
Ingestion	May be harmful if swallowed.
Skin	May be harmful if absorbed through skin. May cause skin irritation.
Eyes	May cause eye irritation.

Additional Information
RTECS: Not available

12. ECOLOGICAL INFORMATION

12.1 Toxicity
no data available

12.2 Persistence and degradability
no data available

12.3 Bioaccumulative potential
no data available

12.4 Mobility in soil
no data available

12.5 Results of PBT and vPvB assessment
no data available

12.6 Other adverse effects
no data available

13. DISPOSAL CONSIDERATIONS

13.1 Waste treatment methods

Product
Offer surplus and non-recyclable solutions to a licensed disposal company.

Contaminated packaging
Dispose of as unused product.

14. TRANSPORT INFORMATION

14.1 UN number
ADR/RID: -   IMDG: -   IATA: -

14.2 UN proper shipping name
ADR/RID: Not dangerous goods
IMDG: Not dangerous goods
IATA: Not dangerous goods

14.3 Transport hazard class(es)
ADR/RID: -   IMDG: -   IATA: -

14.4 Packaging group
ADR/RID: -   IMDG: -   IATA: -

14.5 Environmental hazards
ADR/RID: no   IMDG Marine pollutant: no   IATA: no

14.6 Special precautions for user
no data available

15. REGULATORY INFORMATION

This safety datasheet complies with the requirements of Regulation (EC) No. 1907/2006.

15.1 Safety, health and environmental regulations/legislation specific for the substance or mixture
no data available

15.2 Chemical Safety Assessment
no data available

16. OTHER INFORMATION

Further information
Copyright 2012 Sigma-Aldrich Co. LLC. License granted to make unlimited paper copies for internal use only.
The above information is believed to be correct but does not purport to be all inclusive and shall be used only as a guide. The information in this document is based on the present state of our knowledge and is applicable to the product with regard to appropriate safety precautions. It does not represent any guarantee of the properties of the product. Sigma-Aldrich Corporation and its Affiliates shall not be held liable for any damage resulting from handling or from contact with the above product. See www.sigma-aldrich.com and/or the reverse side of invoice or packing slip for additional terms and conditions of sale.

SAFETY DATA SHEET

Revision date 2017-03-30

Revision number 3.05

1. IDENTIFICATION OF THE SUBSTANCE/MIXTURE AND OF THE COMPANY/UNDERTAKING

1.1 Product identifier

Product name	BISOMER® PEA 6
Product code	745785
Synonyms	None

1.2 Relevant identified uses of the substance or mixture and uses advised against

Recommended use [RU]	Monomer for special polymers
Uses advised against	None known

1.3 Details of the supplier of the safety data sheet

Supplier
GEO Specialty Chemicals UK Ltd
Charleston Road, Hardley, Hythe
Southampton, Hampshire SO45 3ZG
United Kingdom
Phone: +44 (0)23 80894666
Fax No: +44 (0)23 80243113

Responsibility Statement   For further information, please contact **safety-data-sheet-fp@geosc.com**

1.4 Emergency telephone number

Emergency telephone   24 Hour Emergency Phone Number
GEO Specialty Chemicals UK Ltd
+44 (0)23 80891806

2. HAZARDS IDENTIFICATION

2.1 Classification of the substance or mixture

Classification according to Regulation (EC) No. 1272/2008 [CLP]

Skin Corrosion/Irritation	Category 2
Serious eye damage/eye irritation	Category 2
Skin sensitization	Category 1

2.2 Label elements

Labeling according to Regulation (EC) No. 1272/2008 [CLP]

_____

Signal word WARNING

Hazard statements
H315 - Causes skin irritation
H317 - May cause an allergic skin reaction
H319 - Causes serious eye irritation

Precautionary statements
P262 - Do not get in eyes, on skin, or on clothing
P280 - Wear protective gloves/protective clothing/eye protection/face protection
P303 + P361 + P353 - IF ON SKIN (or hair): Remove/Take off immediately all contaminated clothing. Rinse skin with water/shower
P305 + P351 + P338 - IF IN EYES: Rinse cautiously with water for several minutes. Remove contact lenses, if present and easy to do. Continue rinsing

Special labeling of certain preparations Contains 4-Methoxyphenol. May produce an allergic reaction

2.3 Other Information

None known

3. COMPOSITION/INFORMATION ON INGREDIENTS

3.1 Substances

Component	EU EINECS	weight-%	Classification according to Regulation (EC) No. 1272/2008 [CLP]	(REACh) Regulation (EC 1907/2006)
Acrylate oligomers	Not applicable	> 65 - < 80%	Not Classified as Hazardous	In compliance
Polyethylene Glycol 25322-68-3	Not applicable	> 15 - < 25%	Not Classified as Hazardous	In compliance
Acrylic acid, 2-hydroxyethyl ester 818-61-1	212-454-9	< 8%	Acute Tox. 3 (H311) Skin Corr. 1B (H314) Skin Sens. 1 (H317) Aquatic Acute 1 (H400)	In compliance
4-Methoxyphenol 150-76-5	205-769-8	<= 0.15%	Acute Tox. 4 (H302) Eye Irrit. 2 (H319) Skin Sens. 1 (H317) Repr. 2 (H361d) Aquatic Chronic 3 (H412)	In compliance

For the full text of the H-Statements mentioned in this Section, see Section 16.

3.2 Mixtures

Not applicable

4. FIRST AID MEASURES

4.1 Description of first aid measures

General advice
In case of adverse health effects seek medical advice.

_____

_____

Eye contact
Remove contact lenses, if worn. Immediately flush with plenty of water for at least 10 minutes, holding eyelids apart to ensure flushing of the entire surface. Seek medical advice immediately.

Skin contact
Rinse with running water and soap. Remove contaminated clothing and shoes.

Ingestion
Rinse mouth with water, then drink one or two glasses of water. Do NOT induce vomiting. Never give anything by mouth to an unconscious person. If vomiting should occur spontaneously, keep airway clear. Get medical attention.

Inhalation
Remove to fresh air. If not breathing, give artificial respiration. If breathing is difficult, give oxygen. Get medical attention.

4.2 Most important symptoms and effects, both acute and delayed

Most important symptoms and effects
No information available.

Chronic effects
Repeated or prolonged exposure may result in liver or kidney damage.

4.3 Indication of any immediate medical attention and special treatment needed

Note to physicians
Treat symptomatically.

5. FIRE-FIGHTING MEASURES

5.1 Extinguishing media

Suitable extinguishing media
Water spray jet, Alcohol-resistant foam, Extinguishing powder, Carbon dioxide.

Extinguishing media which must not be used for safety reasons
High pressure waterjet.

5.2 Special hazards arising from the substance or mixture

Special Hazard
Formation of toxic gases is possible during heating or in fires. The product may undergo spontaneous polymerization at high temperatures. Polymerization is exothermic and may cause damage to the container and/or release of thermal decomposition products.

5.3 Advice for firefighters

Special protective equipment for firefighters
Firefighters should wear self-contained breathing apparatus and full firefighting turnout gear.

Firefighting measures
Cool exposed containers with water spray after extinguishing fire.

6. ACCIDENTAL RELEASE MEASURES

6.1 Personal precautions, protective equipment and emergency procedures

Personal precautions
Wear suitable protective clothing and gloves.

6.2 Environmental precautions

_____

_____

Environmental precautions
Do not empty into drains/surface water/ground water. Inform authorities in the event of product spillage to water courses or sewage systems.

6.3 Methods and material for containment and cleaning up

Methods for cleaning up
Remove with liquid-absorbing material (sand, peat, sawdust). Dispose of contaminated material as waste according to Section 13.

6.4 Reference to other sections

See Section 12 for additional Ecological Information

7. HANDLING AND STORAGE

7.1 Precautions for safe handling

Advice on safe handling
Avoid contact with eyes, skin and clothing
Avoid breathing vapor or mist
Use only in well-ventilated areas
Personal protective equipment comprising: suitable protective gloves, safety goggles and protective clothing.
Wash thoroughly after handling
Ensure that eyewash stations and safety showers are close to the workstation location

7.2 Conditions for safe storage, including any incompatibilities

Technical measures and storage conditions
The product is stabilized against spontaneous polymerization before delivery. However, if the permissible storage time or storage temperature are greatly exceeded the product may polymerize.
Keep only in the original container in a cool, well-ventilated place
Store at temperatures not exceeding 25 °C/ 77 °F
Store in a dry place. Store away from direct heat or sunlight.
Tanks should preferably contain no dead spaces where the product can be trapped and polymerize. Internal structural members should therefore be kept to a minimum and tanks should be welded.
Storage tank vents, especially those fitted with flame arrestors, should be inspected regularly for polymer fouling which can arise from vapor phase polymerization.
Do not store together with reductants.
Do not store together with oxidants.

7.3 Specific end use(s)

Specific use(s)
 Not applicable

8. EXPOSURE CONTROLS/PERSONAL PROTECTION

8.1 Control parameters

Occupational exposure limit value

Component	European Union	United Kingdom	Spain	Germany	Turkey
Polyethylene Glycol 25322-68-3	NAV	NAV	NAV	TWA: 1000 mg/m³ (average molecular weight 200-600, inhalable fraction) Peak: 8000 mg/m³ (average molecular weight 200-600, inhalable fraction)	NAV
4-Methoxyphenol 150-76-5	NAV	NAV	TWA: 5 mg/m³ sensitizer	NAV	NAV

_____

_____

Component	Ireland	France	Italy	Portugal
4-Methoxyphenol 150-76-5	TWA: 5 mg/m³	TWA: 5 mg/m³	NAV	TWA: 5 mg/m³

Component	Austria	Belgium	Switzerland	Poland
Polyethylene Glycol 25322-68-3	STEL 4000 mg/m³ TWA: 1000 mg/m³	NAV	TWA: 1000 ppm	NAV
4-Methoxyphenol 150-76-5	STEL 10 mg/m³ TWA: 5 mg/m³	TWA: 5 mg/m³	NAV	TWA: 5 mg/m³ Skin

Component	Finland	Norway	Denmark	Netherlands
4-Methoxyphenol 150-76-5	NAV	STEL: 10 mg/m³ TWA: 5 mg/m³	TWA: 5 mg/m³	NAV

Biological limit values

Component	European Union	United Kingdom	Spain	Germany	Turkey
Polyethylene Glycol 25322-68-3	NAV	NAV	NAV	NAV	NAV
4-Methoxyphenol 150-76-5	NAV	NAV	NAV	NAV	NAV

Legend
NAV - Not available

8.2 Exposure controls

Personal Protective Equipment

Eye/face Protection
If splashes are likely to occur: Chemical Goggles.

Hand Protection
Polychloroprene gloves. Coating thickness 1.1 mm. Level 5 > 240 min breakthrough time.

Skin and body protection
Wear suitable protective clothing.

Respiratory protection
Filter A2 is recommended in cases of prolonged exposure.

Other personal protection data
Eyewash fountains and safety showers must be easily accessible.

Hygiene measures
Handle in accordance with good industrial hygiene and safety practice.

Environmental exposure controls
No information available.

9. PHYSICAL AND CHEMICAL PROPERTIES

9.1 Information on basic physical and chemical properties

Physical state	liquid
Color	almost colorless
Appearance	clear
Odor	characteristic
Odor threshold	No information available

Property	Values	Remarks
pH	No information available	No information available

_____

_____

Melting / freezing point	No information available	No information available
Boiling point / boiling range	No information available	No information available
Flash point	> 100.0 °C / > 212 °F	CC (closed cup)
Evaporation rate	No information available	No information available
Flammability (solid, gas)	No information available	No information available
Flammability Limit in Air		
Upper flammability limit	No information available	No information available
Lower flammability limit	No information available	No information available
Vapor pressure	No information available	No information available
Vapor density	No information available	No information available
Specific gravity	No information available	No information available
Solubility (water)	Soluble	No information available
Solubility in other solvents	No information available	No information available
Partition coefficient: n-octanol/water	< 2.27	A8 92/69/EEC
Autoignition temperature	No information available	No information available
Decomposition temperature	No information available	No information available
Kinematic viscosity	No information available	No information available
Dynamic viscosity	No information available	No information available
Density	1.1220 g/cm^3	ASTM D 1298-99

9.2 Other information

Bulk Density	No information available
Explosive properties	Can polymerize violently.
Oxidizing properties	The substance or mixture is not classified as oxidizing.
Softening point	No information available
Molecular weight	336 g/mol
Volatile Organic Compound (VOC) content, wt.%	No information available
Percent Volatile, wt.%	No information available

10. STABILITY AND REACTIVITY

10.1 Reactivity

Reactivity
Polymerizes readily unless inhibited. Polymerization is highly exothermic and, if not controlled, may be violent.

10.2 Chemical stability

Chemical stability
Stable under normal conditions of handling, use and transportation. Periodic air sparging in storage will assist long term stability.

10.3 Possibility of hazardous reactions

_____

_____

Hazardous polymerization
May occur if inhibitor is depleted or if exposed to high temperature.

10.4 Conditions to avoid

Conditions to avoid
This product contains a peroxidation inhibitor. To maintain inhibitor activity, oxygen must not be eliminated from the
atmosphere above the product. Avoid radical forming substances (metal-ions, peroxides). Avoid heating. If prolonged
excursions above the recommended storage temperature occur, then the rate of inhibitor depletion could accelerate, leading to
an increased risk of polymerization. In these circumstances it is recommended that the inhibitor level be checked periodically
using ASTM procedure D 3125, and more inhibitor added if depletion is observed.

10.5 Incompatible materials

Materials to avoid
Reaction with reducing agents. Reaction with oxidants.

10.6 Hazardous decomposition products

Hazardous decomposition products
Carbon monoxide. Carbon dioxide. Irritating vapors.

11. TOXICOLOGICAL INFORMATION

11.1 Information on toxicological effects

Acute health hazard

Eye contact
Causes eye irritation.

Skin contact
Irritating to skin. May cause sensitization by skin contact.

Ingestion
May be harmful if swallowed.

Inhalation
Vapors may be irritating.

Acute toxicity

Oral LD50	> 2,000 mg/kg Method: OECD Test No. 401: Acute Oral Toxicity
Dermal LD50	> 2,000 mg/kg Method: OECD Test No. 402: Acute Dermal Toxicity
Inhalation LC50	No information available

Skin corrosion/irritation
Irritating (Experiment)

Serious eye damage/eye irritation
Irritating (analogy)

Sensitization
Dermal sensitization: sensitizing
Method: OECD Test No. 429: Skin Sensitization: Local Lymph Node Assay

Germ cell mutagenicity
No information available

_____

_____

Mutagenicity
 In vitro mutagenicity: not mutagenic
Method: Ames test

Carcinogenicity
No information available

Reproductive toxicity
No information available

Specific target organ toxicity - Single exposure
No information available

Specific target organ toxicity - Repeated exposure
No information available

Aspiration hazard
No information available

12. ECOLOGICAL INFORMATION

12.1 Toxicity

Acute aquatic toxicity

Fish	No information available
Crustacea	EC50 (48 hour) > 10 - <= 100
Algae/aquatic plants	No information available

12.2 Persistence and degradability

Persistence and degradability
No information available

Ultimate biodegradation
Good biodegradability. All organic substances contained in the product achieve > 60% BOD/COD or CO_2 liberation, or > 70% DOC reduction in tests for ease of degradability.

12.3 Bioaccumulative potential

Bioaccumulative potential
No information available

12.4 Mobility in soil

Mobility
No information available.

12.5 Results of PBT and vPvB assessment

PBT and vPvB assessment
No information available

12.6 Other adverse effects

Other information
No other ecological studies have been carried out on this product.

_____

_____

13. DISPOSAL CONSIDERATIONS

13.1 Waste treatment methods

Disposal of wastes
Waste incineration with the approval of the responsible local authority.

Contaminated packaging
Packaging that cannot be cleaned are to be disposed of in the same manner as the product. Disposal must be made according to official regulations.

14. TRANSPORT INFORMATION

US DOT Not regulated
14.1. UN number
14.2. UN proper shipping name
14.3. Transport hazard class(es)
14.4. Packing group
14.5. Environmental hazards
14.6. Special precautions for user

Land transport (ADR/RID) Not regulated
14.1. UN number
14.2. UN proper shipping name
14.3. Transport hazard class(es)
14.4. Packing group
14.5. Environmental hazards
14.6. Special precautions for user

Inland waterway transport (ADN) Not regulated
14.1. UN number
14.2. UN proper shipping name
14.3. Transport hazard class(es)
14.4. Packing group
14.5. Environmental hazards
14.6. Special precautions for user

Air transport (ICAO-TI / IATA-DGR) Not regulated
14.1. UN number
14.2. UN proper shipping name
14.3. Transport hazard class(es)
14.4. Packing group
14.5. Environmental hazards
14.6. Special precautions for user

Sea transport (IMDG) Not regulated
14.1. UN number
14.2. UN proper shipping name
14.3. Transport hazard class(es)
14.4. Packing group
14.5. Environmental hazards
14.6. Special precautions for user

14.7 Transport in bulk according to Annex II of MARPOL 73/78 and the IBC Code
Not applicable

_____

_____

15. REGULATORY INFORMATION

15.1 Safety, health and environmental regulations/legislation specific for the substance or mixture

International Inventories

Australia (AICS)
Some ingredients are not on the inventory.

Canada (DSL)
Some ingredients are not on the inventory.

Canada (NDSL)
Some ingredients are on the inventory.

China (IECSC)
All ingredients are on the inventory or exempt from listing

European Union (EINECS)
All ingredients are on the inventory or exempt from listing

European Union (ELINCS)
None of the ingredients are on the inventory.

Japan (ENCS)
All ingredients are on the inventory or exempt from listing

South Korea (KECL)
All ingredients are on the inventory or exempt from listing

Philippines (PICCS)
Some ingredients are not on the inventory.

United States (TSCA)
All ingredients are on the inventory or exempt from listing

Legend
 AICS - Australian Inventory of Chemical Substances
 DSL/NDSL - Canadian Domestic Substances List/Non-Domestic Substances List
 IECSC - China Inventory of Existing Chemical Substances
 EINECS/ELINCS - European Inventory of Existing Commercial Chemical Substances/EU List of Notified Chemical Substances
 ENCS - Japan Existing and New Chemical Substances
 KECL - Korean Existing and Evaluated Chemical Substances
 PICCS - Philippines Inventory of Chemicals and Chemical Substances
 TSCA - United States Toxic Substances Control Act Section 8(b) Inventory

15.2 Chemical Safety Report

No information available.

16. OTHER INFORMATION

Product code   745785

Revision date   2017-03-30

Full text of H-Statements referred to under sections 2 and 3
H315 - Causes skin irritation
H317 - May cause an allergic skin reaction
H319 - Causes serious eye irritation
H302 - Harmful if swallowed
H311 - Toxic in contact with skin

_____

_____

H314 - Causes severe skin burns and eye damage
H361d - Suspected of damaging the unborn child
H400 - Very toxic to aquatic life
H412 - Harmful to aquatic life with long lasting effects

Key or legend to abbreviations and acronyms used in the safety data sheet
NAV - Not available

This safety data sheet complies with the requirements of: Regulation (EC) No. 1907/2006.

Additional information
BISOMER® is a registered trademark of GEO Specialty Chemicals UK Ltd.

Disclaimer
The information provided in this Safety Data Sheet is correct to the best of our knowledge, information and belief at the date of its publication. The information given is designed only as a guidance for safe handling, use, processing, storage, transportation, disposal and release and is not to be considered a warranty or quality specification. The information relates only to the specific material designated and may not be valid for such material used in combination with any other materials or in any process, unless specified in the text.

_____